



Universidad  
Politécnica  
de Cartagena



**PROGRAMA DE DOCTORADO EN ENERGÍAS RENOVABLES Y EFICIENCIA ENERGÉTICA**

**TESIS DOCTORAL**

**CARACTERIZACIÓN EXPERIMENTAL Y MODELADO NUMÉRICO DE  
UNA INSTALACIÓN PARA LA GENERACIÓN DE ACS CON BOMBA  
DE CALOR**

Presentada por Mohammed Reda Haddouche para optar  
al grado de Doctor  
por la Universidad Politécnica de Cartagena

Dirigida por:  
Dr. Fernando Illán Gómez

Codirigida por:  
Dr. Francisco Javier Sánchez Velasco

Cartagena, 2022



Universidad  
Politécnica  
de Cartagena



**DOCTORAL PROGRAMME IN RENEWABLE ENERGIES AND ENERGY EFFICIENCY**

**PhD THESIS**

**EXPERIMENTAL CHARACTERIZATION AND NUMERICAL MODELLING OF AN  
INSTALLATION FOR THE GENERATION OF DOMESTIC HOT WATER WITH HEAT  
PUMP**

Presented by Mohammed Reda Haddouche  
to the Technical University of Cartagena in fulfilment of  
the thesis requirement for the award of PhD

Supervisor:  
Dr. Fernando Illán Gómez

Co-supervisor:  
Dr. Francisco Javier Sánchez Velasco

Cartagena, 2022

## **Thanks**

I would like to address my sincere thanks to my family, my father, my mother and my brothers, Zakaria and Abdelhadi for their support all the time

Also, to all My professors of the laboratory “Calor y frío” of the UPCT University who were of precious help to me

And also, the members of the jury for agreeing to evaluate my work

## **Abstract**

In this thesis, the energetic efficiency of a trans-critical CO<sub>2</sub> heat pump coupled to a hot water storage tank for domestic hot water production is characterized and analyzed under the European standard EN16147. An experimental facility is set up in order to realize the tests mentioned in the standard and determine the thermodynamic performance of the heat pump and the energetic performance of the domestic hot water generation system. The tests conditions of this study were performed according the European standard EN16147 conditions. In the beginning, two configurations of the heat pump, with and without internal heat exchanger were studied under the same operating conditions to show the impact of the internal heat exchanger on the thermodynamic performance of the CO<sub>2</sub> heat pump. The results showed that the introduction of an internal heat exchanger give better thermodynamic performance. The global COP of the cycles with and without internal heat exchanger had the value of 3.28 and 3.14 respectively, which means that the global COP of the system is enhanced of about 4.42% by adding the internal heat exchanger. Then, three main tests were realized under the standard's conditions: the heating step, the cooling step, and the load profile step. The heating process of the storage tank was effectuated under various gas cooler flowrate conditions and various evaporator inlet temperature with objective to determine and characterize the time evolution of the COP of the heat pump and analyze the thermo-hydraulic performance of the stratification within the storage tank under these operating conditions. results showed that the gas cooler flowrate plays important role on the thermal stratification inside the storage tank. Lower gas cooler flowrates give better stratification, and better COP. The extraction process and the cooling process also are performed and analyzed under the 3XL extraction profile conditions. The results of the extraction process according to the 3XL profile, show that the heat pump starts up after the fourth extraction and the heating process of this step take time of 6 hours until the storage tank heated up again to 60 °C, and global COP of 2.89 is obtained. The characterization of the cooling process of the storage tank was performed under three extraction flowrates. Results show that, as the extraction flowrate increases, the cooling time decreases. In addition, a new numerical model of a stratified storage tank was developed and discretized using the finite difference method for the use in numerical simulation using TRNSYS software. The comparison of the numerical results with the results obtained from the experimental set up showed a good agreement.





## Resumen

En esta tesis, la eficiencia energética de una bomba de calor trans-crítica de CO<sub>2</sub> acoplada a un tanque de almacenamiento de agua caliente para la producción de agua caliente sanitaria se caracteriza y analiza bajo la norma europea EN16147. Se desarrolló una instalación experimental para realizar los ensayos mencionados en la norma y determinar el rendimiento termodinámico de la bomba de calor y el rendimiento energético del sistema de generación de agua caliente sanitaria. Las condiciones de los ensayos de este estudio se realizaron según las condiciones de la norma europea EN16147. Al principio, se estudiaron dos configuraciones de la bomba de calor, con y sin intercambiador de calor interno bajo las mismas condiciones de funcionamiento para mostrar el impacto del intercambiador de calor interno en el rendimiento termodinámico de la bomba de calor de CO<sub>2</sub>. Los resultados mostraron que la introducción de un intercambiador de calor interno da un mejor rendimiento termodinámico. El COP global de los ciclos con y sin intercambiador de calor interno tenía el valor de 3.28 y 3.14 respectivamente, lo que significa que el COP global del sistema se mejora de aproximadamente 4.42% al agregar el intercambiador de calor interno. Luego, se realizaron tres pruebas principales bajo las condiciones del estándar: el paso de calentamiento, el paso de enfriamiento y el paso del perfil de carga. El proceso de calentamiento del tanque de almacenamiento se llevó a cabo bajo varias condiciones de caudal de gas cooler y varias temperaturas de entrada del evaporador con el objetivo de determinar y caracterizar la evolución temporal del COP de la bomba de calor y analizar el rendimiento termo-hidráulico de la estratificación dentro del tanque de almacenamiento bajo estas condiciones de operación. Los resultados mostraron que el caudal del gas cooler tiene un impacto importante en la estratificación térmica dentro del tanque de almacenamiento. Los caudales más bajos del gas cooler dan una mejor estratificación y un mejor COP. El proceso de extracción y el proceso de enfriamiento también se realizan y analizan bajo las condiciones de perfil de extracción 3XL. Los resultados del proceso de extracción según el perfil 3XL, muestran que la bomba de calor se pone en marcha tras la cuarta extracción y el proceso de calentamiento de este ensayo tarda 6 horas hasta que el tanque de almacenamiento se calienta de nuevo a 60 °C, y se obtiene un COP global de 2,89. La caracterización del proceso de enfriamiento del tanque de almacenamiento se realizó bajo tres caudales de extracción. Los resultados muestran que, a medida que aumenta el caudal de extracción, el tiempo de enfriamiento disminuye. Además, se desarrolló y discretizó un nuevo modelo numérico

de un tanque de almacenamiento estratificado utilizando el método de diferencia finita para su uso en simulación numérica utilizando el software TRNSYS. La comparación de los resultados numéricos con los resultados obtenidos de la configuración experimental mostró una buena concordancia.

## Contents:

Thanks .....	i
Abstract .....	iii
Contents .....	vii
List of figures .....	xi
List of tables .....	xv
Nomenclatures .....	xvii
<b>Introduction</b> .....	23
<b>Chapter I: State of the art</b>	
I.1. Introduction.....	27
I.2. Refrigerants.....	27
I.2.1. Pure inorganic substances.....	27
I.2.2. Hydrocarbons.....	27
I.2.3. Halogenated hydrocarbons.....	28
I.2.3.1. Chlorofluorocarbons (CFC) .....	28
I.2.3.2. Hydrochlorofluorocarbons (HCFC) .....	28
I.2.3.3. Hydrofluorocarbons (HFC) .....	28
I.2.4. Toxicity classification of refrigerants.....	28
I.2.4.1. Group A.....	28
I.2.4.2. Group B.....	28
I.2.5. Flammability classification of refrigerants.....	29
I.2.5.1. Group 1.....	29
I.2.5.2. Group 2.....	29
I.2.5.3. Group 3.....	29
I.3. CO <sub>2</sub> as refrigerant.....	30
I.4. CO <sub>2</sub> heat pump.....	30
I.5. Storage tank.....	31
I.6. State of the art water-water heat pumps for industrial or domestic hot water production systems.....	32
I.6.1. Studies and analysis of the CO <sub>2</sub> heat pump technology.....	32
I.6.2. Studies and analysis of the stratification and DHW storage tank.....	39
I.6.3. Technics to enhance the thermal stratification with storage tanks.....	41
I.6.3.1. Baffles.....	42

I.6.3.2. Tank shape.....	44
I.6.3.3. Heat exchanger.....	45
I.6.3.4. Stratification pipes (stratification enhancer).....	46
I.6.3.5. Diffusers and deflectors.....	47

## **Chapter II: Description of the test facility**

II.1. Introduction.....	51
II.2. The standard EN16147.....	51
II.2.1. [Step A & B]: Stabilization and test preparation.....	52
II.2.2. [Step C]: Determination the water heating time.....	52
II.2.3. [Step D]: Determination Energy absorbed in steady state.....	53
II.2.4. [Step E]: Extraction profiles.....	53
II.2.5. [Step F] Water cooling.....	55
II.3. Description of the test facility.....	55
II.3.1. CO2 Heat pump.....	55
II.3.1.1. Compressor.....	57
II.3.1.2. Gas Cooler.....	57
II.3.1.3. Evaporator.....	59
II.3.1.4. Internal heat exchanger (IHX).....	60
II.3.2. Water loop.....	61
II.3.2.1. Water pumps.....	62
II.3.2.2. Three-ways valve.....	63
II.3.2.3. Flow meter.....	63
II.3.2.4. Regulating valve.....	64
II.3.2.5. Cypex Valve.....	64
II.3.2.6. Thermal storage tank.....	65
II.3.3. Stratified storage tank.....	65
II.3.3.1. Hot water storage tank.....	65
II.3.3.2. Cold-water storage tank.....	67
II.3.3.3. PID Controller.....	68
II.3.3.4 Temperature measurement.....	70
II.3.3. Data acquisition.....	71
II.3.3.1. NI 9263.....	71
II.3.3.2. NI 9207.....	72

II.3.3.3. NI 9482.....	73
II.3.3.4. NI 9216.....	73
II.3.3.5. Temperature control.....	74
II.4. Test Steps.....	75
II.4.1. [Step A, B]: Preparation.....	75
II.4.2. [Step C]: Determination the water heating time.....	76
II.4.3. [Step E]: Extraction profiles.....	78
II.4.4. [Step F] water cooling.....	80

### **Chapter III: Results and discussions**

III.1 Introduction.....	85
III.2. Heating Process (Step C).....	85
III.2.1. Impact of the Internal Heat Exchanger (IHX).....	86
III.2.2 Impact of the gas cooler flowrate.....	89
III.2.2.1. Thermodynamic performance of the CO2 heat pump.....	106
III.2.2.2. Thermal stratification and temperature distribution analysis.....	109
III.2.3. Impact of the evaporator inlet temperature.....	118
III.3. Extraction process (step E).....	123
III.4. Cooling process (Step F).....	127

### **Chapter IV: Numerical model of stratified storage tank**

I.1. Introduction.....	133
I.2. Thermal stratification.....	133
I.3. Stratified storage tank models.....	137
I.3.1. Stratified fluid storage tank (Type 4).....	137
I.3.2. Plug flow Tank (Type 38).....	138
I.3.3. Stratified storage tank model (Type 60).....	139
I.4. Development of a new model: Present model (Type 269).....	140
I.5. Model validation.....	145
<b>Conclusion</b> .....	155
Acknowledgement .....	157
Annex I .....	159
References.....	161



## List of figures:

Figure I.1: schematic diagram and P-h diagram of a CO <sub>2</sub> trans-critical heat pump.....	31
Figure I.2: Schematic diagram of a stratified storage tank.....	32
Figure I.3: Configuration of CO <sub>2</sub> heat pump water heating system.....	33
Figure I.4: Schematic diagram of the trans-critical CO <sub>2</sub> heat pump heating system.....	34
Figure I.5: Test facility of the two CO <sub>2</sub> heat pump configurations studied.....	34
Figure I.6: Schematic of the air source CO <sub>2</sub> heat pump water heater.....	35
Figure I.7: Schematic diagram of the CO <sub>2</sub> heat pump prototype.....	35
Figure I.8: The configuration of the CO <sub>2</sub> heat pump system.....	36
Figure I.9: Schematic diagram of the air source CO <sub>2</sub> heat pump water heater...	37
Figure I.10: Schematic diagram of the air source heat pump.....	37
Figure I.11: Schematic diagram of Experimental Setup studied.....	38
Figure I.12: Schematic diagrams of the configurations studied.....	38
Figure I.13: Geometries used to investigate the thermal stratification in storage tanks.....	39
Figure I.14: Experimental set-up.....	41
Figure I.15: Different inlet devices of a stratified storage tank.....	41
Figure I.16: Inlet devices of the storage tank studied	42
Figure I.17: Shapes and geometries of the baffles to enhance thermal stratification.....	43
Figure I.18: Obstacles and their shapes used.....	43
Figure I.19: Storage tank geometries.....	44
Figure I.20: Hot water tank geometries and their insulation studied.....	45
Figure I.21: Hot water storage tank with mantle heat exchanger.....	45
Figure I.22: Stratification pipe.....	46
Figure I.23: Stratifier made of three compound inlet pipes.....	47
Figure I.24: Elbow and diffuser inlet devices.....	47
Figure I.25: Configurations of the storage tank with different flat plat's orientations.....	48
Figure II.1: Stages of the test.....	52
Figure II.2: Illustration of the test method.....	54



Figure II.3: Schematic diagram of the CO <sub>2</sub> heat pump.....	56
Figure II.4: Dorin CO <sub>2</sub> compressor.....	57
Figure II.5: Schematic diagram of the Gas cooler Swep B16.....	58
Figure II.6: Schematic diagram of the evaporator Swep BX8T.....	59
Figure II.7: Schematic diagram of the IHX Swep B17.....	60
Figure II.8: Schematic diagram of the water loop.....	61
Figure II.9: Baxi pumps.....	62
Figure II.10: Danfoss Three-ways valve.....	63
Figure II.11: Siemens SITRANS fm mag 5100 w flow meter.....	63
Figure II.12: Sauter Three-ways valve.....	64
Figure II.13: Cypex Valve.....	64
Figure II.14: Schematic diagram of the storage tank.....	65
Figure II.15: RTD sensors support.....	66
Figure II.16: Schematic diagram of the hot water storage tank.....	66
Figure II.17: Cold-water storage tank.....	67
Figure II.18: Virtual PID controller.....	68
Figure II.19: LabView program of the PID controller.....	69
Figure II.20: Temperature of the storage tank controlled by the PID controller.....	69
Figure II.21: RTD PT100 sensor.....	70
Figure II.22: LabView program of the Temperature measurement.....	70
Figure II.23: National Instrument Compact DAQ.....	71
Figure II.24: National instrument NI 9263.....	72
Figure II.25: National instrument NI 9207.....	72
Figure II.26: National instrument NI 9482.....	73
Figure II.27: National instrument NI 9216.....	74
Figure II.28: LabView program of the compressor control.....	75
Figure II.29: Water cycle of the test preparation.....	76
Figure II.30: Water cycle of the step C.....	77
Figure II.31: LabView program of the Step C.....	77
Figure II.32: LabView program of the compressor control.....	78
Figure II.33: LabView program of the Step E.....	79

Figure II.34: Water cycle of the step E.....	80
Figure II.35: LabVIEW program of the step F.....	81
Figure II.36: LabVIEW program of the elapsed time of the step F.....	81
Figure III.1: Schematic diagram of the two configurations of the trans-critical CO2 heat pump.....	87
Figure III.2: Instantaneous COP of the heat pump with and without IHX	88
Figure III.3: T-s diagrams comparing the heat pump with and without the IHX.....	88
Figure III.4: Schematic diagram of the test facility.....	89
Figure III.5: Temperature evolution of the 10 RTD sensors in function of time and for different gas cooler flowrate values.....	91
Figure III.6: Temperature distribution of the topper RTD sensor in function of time and for different gas cooler flowrate values.....	92
Figure III.7: Evolution of the instantaneous COP in function of time for different gas cooler flowrate cases.....	94
Figure III.8: Comparison of temperature evolution at different heights of the hot water storage tank and the instantaneous COP for the case of lowest and highest gas cooler flowrate.....	95
Figure III.9: Evolution of the global COP and the energy stored for different gas cooler flowrate cases studied.....	96
Figure III.10: Tank energy efficiency ( $E^*$ ) of every stratification layer for different gas cooler flowrates.....	99
Figure III.11: Total energy efficiency for different gas cooler flowrates.....	100
Figure III.12: Stratification number and dimensionless temperature of the top ( $T^* 1$ ) and the bottom ( $T^* 10$ ) of the storage tank for different gas cooler flowrates in function of dimensionless time.....	103
Figure III.13: stratification number (STR) for different gas cooler flowrates	104
Figure III.14: Richardson number (Ri) for different gas cooler flowrate.....	105
Figure III.15: T-s diagram of different gas cooler flowrate.....	106
Figure III.16: Comparison of the T-s diagram in the beginning and the end of the heating process of the lowest and highest gas cooler flowrate.....	108
Figure III.17: Temperature distribution in function of the tank height for different gas cooler flowrates.....	111

Figure III.18: Temperature distribution in function of the tank height for different instant of the heating process (every one hour).....	115
Figure III.19: Temperature evolution in function of time of the lowest gas cooler flowrate (0.083 kg·s <sup>-1</sup> ).....	116
Figure III.20: Temperature evolution of the 10 RTD sensors in function of time and for different evaporator inlet temperature values.....	119
Figure III.21: Temperature distribution of the topper RTD sensors in function of time and for different evaporator inlet temperature values.....	120
Figure III.22: Evolution of the instantaneous COP in function of time for different evaporator inlet temperature cases.....	120
Figure III.23: Evolution of the global COP for different evaporator inlet temperature.....	121
Figure III.24: T-s diagram of different evaporator inlet temperature.....	122
Figure III.25: Temperature evolution in the storage tank with function of time of the 10 RTD sensors.....	123
Figure III.26: Temperature evolution of the hot water storage tank outlet and the extraction flowrate.....	124
Figure III.27: Temperature of the inlet temperature.....	125
Figure III.28: Energy extracted of the of the hot water in every extraction.....	125
Figure III.29: Theoretical COP in function of time of heating process of the E step.....	126
Figure III.30: Temperature evolution of the storage tank in function of time of the cooling process (extraction flowrate 0.8 kg·s <sup>-1</sup> ).....	127
Figure III.31: Temperature evolution of the storage tank in function of time of the cooling process (extraction flowrate 0.4 kg·s <sup>-1</sup> ).....	128
Figure III.32: Temperature evolution of the storage tank in function of time of the cooling process (extraction flowrate of 0.1 kg·s <sup>-1</sup> ).....	129
Figure III.33: Temperature evolution highest part of the storage tank in function of time of the cooling process.....	130
Figure IV.1: Schematic diagram of a stratified storage tank.....	133
Figure IV.2: Schematic diagram of stratified storage tank model.....	135
Figure IV.3: Schematic diagram of thermal storage tank.....	136
Figure IV.4: Stratified fluid storage tank model.....	137

Figure IV.5: Plug flow Tank model.....	138
Figure IV.6: Schematic diagram of the present model (Type 269).....	140
Figure IV.7: Schematic diagram of the heat transfer phenomena based on the thermal resistance of system.....	141
Figure IV.8: Energy balance of the node 1 (top).....	143
Figure IV.9: Energy balance of the central nodes.....	143
Figure IV.10: Energy balance of the last node (bottom).....	144
Figure IV.11: TRNSYS program of the Step C.....	145
Figure IV.12: Comparison of the temperature evolution of the heating process.....	146
Figure IV.13: Impact of the node number on the stratification formation (Type 269).....	147
Figure IV.14: Comparison of the temperature evolution of the cooling process. a) comparison of 10 different layers. b) Top and the bottom temperatures.....	148
Figure IV.15: Temperature evolution of the step E for both numerical and experimental results.....	149
Figure IV.16: Temperature evolution of three sensors for Type 4 model and the present model (Type269).....	150

## List of tables

Table I.1: Refrigerants classification.....	29
Table II.1: Geometric characteristic of the gas Cooler.....	58
Table II.2: Geometric characteristic of the evaporator.....	59
Table III.1: Test conditions considered at the evaporator in the study.....	85
Table III.2: The COP and the energy stored in the storage tank.....	96
Table III.3: Extraction profile of 3XL.....	123
Table III.4: Cooling process elapsed time.....	130
Table IV.1: Cooling time for both numerical and experimental.....	149



## Nomenclature

$C_p$	Specific heat	$(\text{kJ}\cdot\text{kg}^{-1}\cdot\text{K}^{-1})$
$D$	Inner diameter of the tank	(m)
$E$	Energy	(kJ)
$E^*$	Partial Energy efficiency	(-)
$ET$	Total energy efficiency	(-)
$g$	Gravity	$(\text{m}\cdot\text{s}^{-2})$
$H$	Height	(m)
$H^*$	Dimensionless height	(-)
$h$	Convective heat transfer coefficient	$(\text{W}\cdot\text{m}^{-2}\cdot\text{K}^{-1})$
$k$	Conductivity	$(\text{W}\cdot\text{m}^{-1}\cdot\text{K}^{-1})$
$L$	Height	(m)
$\dot{m}$	Mass flowrate	$(\text{kg}\cdot\text{s}^{-1})$
$m, M$	Mass	(kg)
$N$	Number of layers	(-)
$Nu$	Nusselt number	(-)
$Pr$	Prandtl number	(-)
$Q$	Thermal power	(kW)
$Ra$	Rayleigh	(-)
$Ri$	Richardson number	(-)
$S$	Surface	$(\text{m}^2)$
$s$	Entropy	$(\text{kJ}\cdot\text{kg}^{-1}\cdot\text{K}^{-1})$
$T$	Temperature	(°C)
$T^*$	Dimensionless temperature	(-)
$t$	Time	(s), (min), (h)
$t^*$	Dimensionless time	(-)
$V$	Volume	$(\text{m}^3)$
$v$	Velocity	$(\text{m}\cdot\text{s}^{-1})$
$\dot{W}$	Electric power	(kW)

## Greek letters

$\alpha$	thermal diffusivity	( $\text{m}^2 \cdot \text{s}$ )
$\beta$	Volume expansion coefficient	( $\text{K}^{-1}$ )
$\Delta T$	Temperature difference	( $^{\circ}\text{C}$ )
$\rho$	Density	( $\text{kg} \cdot \text{m}^{-3}$ )
$\mu$	Dynamic viscosity	( $\text{kg} \cdot \text{m}^{-1} \cdot \text{s}^{-1}$ )
$\xi$	Dimensionless filling time	(-)

## Subscripts

amb	Ambient
c	Cold
comp	Compressor
cw	Cold water
evap	Evaporator
GC	Gas Cooler
h	Hot
hw	Hot water
<i>i</i>	Layer number
inst	Instantaneous
<i>j</i>	Iteration time
m	Medium
ref	Reference
tap	Amount of energy extracted
w	wall

## Abbreviations

CFC	Chlorofluorocarbons
COP	Coefficient Of Performance
DHW	Domestic Hot Water
EEV	Electronic Expansion Valve
HCFC	Hydrochlorofluorocarbons
HFC	Hydrofluorocarbons
GC	Gas Cooler
GWP	Global Warming Potential

HP	Heat pump
HVAC	Heating, Ventilation and Air-Conditioning
IHX	Internal Heat Exchanger
ODP	Ozone Depletion Potential
PCM	Phase Changing Material
STR	Stratification
ppm	Parts Per Million
RTD	Resistance Temperature Detector





# Introduction



**R**enewable energy promotion and energy efficiency improvement are probably the most important steps to achieve the sustainable energy policy goals. Heat pumps have become increasingly important in the world as a technology to improve energy efficiency and reduce CO<sub>2</sub> emissions. The use of CO<sub>2</sub> heat pumps for residential and industrial hot water production has seen an increasing development regarding its energetic and environmental benefits.

Nowadays, the heat pump is considered to be one of the most economical and ecological technology to meet the energy needs for heating and air conditioning applicable to both renovation and new construction for all building sectors regarding its economic, and sustainable energy supply as well as environmental and climate protection which are important challenges of the 21<sup>st</sup> century.

Currently, refrigeration and air conditioning technologies are forced to use more environmentally friendly refrigerants in their installations. Carbon dioxide CO<sub>2</sub> (R744) seems to have the desired characteristics. CO<sub>2</sub> is a substance that can be found in the environment and costs less than other fluids. It also has no risks to be used as refrigerant.

Despite the abundance of investigations devoted to both, the study of heat pumps for DHW generation, and the study of the thermal stratification inside a hot water storage tank, there are very few studies dedicated to the analysis of the overall performance of the system when a heat pump is coupled with a storage tank together in a DHW production system. This thesis is devoted to study the coupling between a CO<sub>2</sub> heat pump and a hot water storage tank and the overall performance and efficiency of the system. With the aim to analyze and determine the performance and the energy efficiency of the domestic hot water (DHW) production system by means of heat pumps with electrically driven compressors, the European standard UNE-EN16147 is a norm that specifies the test methods. In this thesis it is analyzed a domestic hot water production system using a trans-critical CO<sub>2</sub> heat pump under the European Standard EN16147 conditions experimentally and numerically.

For this an experimental set-up is mounted and it consist of a trans critical CO<sub>2</sub> heat pump and stratified storage tanks in order to realize the tests following the standard norm procedures and analyze the energetic performance of the system and the behavior of the stratification phenomenon. Also, for further investigation of domestic hot water

production system, a numerical model of a stratified storage tank is developed and used in TRNSYS to perform the numerical simulations.

A series of tests are conducted in order to analyze the thermodynamic performance of the heat pump and the thermo-hydraulic performance of the stratified storage tank. The test procedures mentioned in the standard are based on several steps, and it is designed to determine the energy efficiency and the performance of the water heater heat pump for DHW production.

This thesis consists of four chapters that describe and explain the test procedures following the standard norm conditions.

In this first chapter, a brief state of art describing the heat pumps and the heat source that can be used as well as the refrigerants is presented. Also, a series of previous numerical and experimental works conducted by researchers in this domain are analyzed.

The second chapter describes the experimental set-up of the test procedures and the installation elements of the heat pump and the DHW production system. As well as the test steps of the standard. In this chapter, the heating process and the cooling process of the stratified storage tank are described, and the extraction test is described and illustrated with LabVIEW programs of every step of the test procedure.

The third chapter discusses the results of the test procedures of the heating and cooling processes. Here various parameters of the heat pump as the inlet temperature of the evaporator, the flowrate of the gas cooler, and other parameters are studied under the same operating conditions. The energetic performance of the heat pump and the domestic hot water production system are reported. In addition, the thermo-hydraulic behavior of the stratified storage tank under these conditions is discussed.

The fourth chapter of this thesis explains a stratified storage tank model developed in FORTRAN in order to use it in TRNSYS. This model is developed taking into account the heat losses to the ambient depending on the temperatures. The objective of this model is to develop a model more accurate than that of TRNSYS library. The validation of this model and the numerical simulation are conducted using TRNSYS. Also, the numerical discretization and its procedure are described and illustrated.

# Chapter I



## I.1. Introduction

Ensuring a reliable, economic, and sustainable energy supply as well as environmental and climate protection are important challenges of the 21<sup>st</sup> century. Renewable energy and improving energy efficiency are the most important steps to achieve these goals of energy policy. Heat pumps have become increasingly important in the world as a technology to improve energy efficiency and reduce CO<sub>2</sub> emissions. The use of CO<sub>2</sub> heat pumps for residential and industrial hot water production has seen a great development due to its energetic and environmental benefits [1-3].

## I.2. Refrigerants

In this section it will be briefly classified the refrigerants usually used in heat pumps. A refrigerant is a substance which evolves in the refrigeration circuit. Refrigerants have the particularity of having a very low evaporation temperature, under atmospheric pressure. This thermodynamic property makes it possible to produce cold and heat. Refrigerants can be classified by the principal categories as follow [4]:

### I.2.1. Pure inorganic substances

The most representative refrigerants of this category are: water H<sub>2</sub>O (R-718), Ammonia NH<sub>3</sub> (R-717) and the dioxide-carbon CO<sub>2</sub> (R-744). Nowadays NH<sub>3</sub> is employed as a refrigerant in industrial installations because of its potential flammability and its toxicity. Ammonia is a colorless gas with a pungent smell. In acute exposure, this gas immediately causes irritation to the lungs and eyes. On the contrary CO<sub>2</sub> is non-flammable and it is considered non-toxic. Besides it has a very low greenhouse warming potential (GWP=1). These properties have risen the interest of CO<sub>2</sub> as a potential refrigerant in the building sector.

### I.2.2. Hydrocarbons

The principal refrigerants of this category are the Butane (R-600), isobutane (R-600a), propane (R-290), Cyclopropane (RC-270) propylene (R-1270) etc.... The components of this category refrigerants are flammable, which make it dangerous of employment. Usually, the isobutane is used as refrigerant in case of low quantity.



### **I.2.3. Halogenated hydrocarbons**

In this category it can be encountered the refrigerants most commonly used. Some of them are currently in phasing-out period or they are forbidden especially due to environmental protection reasons. It can find three subcategories of this type of refrigerants:

#### **I.2.3.1. Chlorofluorocarbons (CFC)**

These were the most used as refrigerants in the past. They have been substituted by chlorine or fluorine hydrocarbons. They have a high ozone depletion potential (ODP) and therefore they have the potential to destroy the atmospheric ozone layer.

#### **I.2.3.2. Hydrochlorofluorocarbons (HCFC)**

This is the second generation of halogenated hydrocarbons used as refrigerants. They are chemical compounds made up of chlorine, fluorine, hydrogen, and carbon. They have a middle ozone depletion potential.

#### **I.2.3.3. Hydrofluorocarbons (HFC)**

HFCs are composed of fluorine, hydrogen, and carbon. They are the third generation of halogenated hydrocarbons used as refrigerants. Currently used in new installations (pure or as a mixture). They have null or very low ODP and therefore they don't pose a danger to the ozone layer, but they can contribute to the greenhouse effect.

According to its toxicity and flammability the refrigerant can be classified as follows:

### **I.2.4. Toxicity classification of refrigerants**

There are two groups A and B:

#### **I.2.4.1. Group A**

For which there is no evidence of refrigerant toxicity for concentrations less than or equal to 400 ppm.

#### **I.2.4.2. Group B**

For which there is evidence of toxicity for concentrations below 400 ppm.

### I.2.5. Flammability classification of refrigerants

There are three groups 1, 2 and 3

#### I.2.5.1. Group 1

The refrigerant does not allow flame propagation in air at 21 °C and 101 kPa.

#### I.2.5.2. Group 2

The refrigerant has a lower flammability limit greater than  $0.10 \text{ kg}\cdot\text{m}^{-3}$  at 21 °C and 101 kPa and a heat of combustion less than  $19 \text{ kJ}\cdot\text{kg}^{-1}$ .

#### I.2.5.3. Group 3

The refrigerant is highly flammable with a lower flammability limit less than or equal to  $0.10 \text{ kg}\cdot\text{m}^{-3}$  at 21 °C and 101 kPa and a heat of combustion greater than or equal to  $19 \text{ kJ}\cdot\text{kg}^{-1}$ .

The classification of the refrigerants is symbolized and classified according to the flammability and toxicity as shown in the table I.1:

Table I.1: Refrigerants classification.

	Weakly toxic	Strongly toxic
Highly flammable	A3	B3
Flammable	A2	B2
Non-flammable	A1	B1

### **I.3. CO<sub>2</sub> as refrigerant**

Currently, refrigeration and air conditioning players are forced to use more environmentally friendly refrigerants in their installations. Among the solutions developed for new refrigeration technologies, Carbon dioxide CO<sub>2</sub> (R-744) seems to have the desired characteristics. CO<sub>2</sub> is a substance that can be found in the environment and costs less than other fluids. It therefore constitutes a sustainable solution. It also has no risks by using this fluid as refrigerant, the CO<sub>2</sub> is non-flammable, non-corrosive, non-toxic and non-explosive. Also, it has other properties that make the CO<sub>2</sub> a great refrigerant.

It has a low specific volume. This allows the installation to be compact and it is compatible with all materials also, CO<sub>2</sub> is perfectly miscible with compressor oil.

The CO<sub>2</sub> has an environmental impact very low compared to other refrigerants, on ozone, its depletion potential is zero (ODP = 0) and on greenhouse effect, its global warming potential is 1 (GWP = 1) [4].

The only inconvenient of this refrigerant is that the operating pressure to phase change of CO<sub>2</sub> is high, reaching 100 bar and above. In addition, if CO<sub>2</sub> take contact with humidity, it changes to carbonic acid and becomes corrosive.

### **I.4. CO<sub>2</sub> heat pump**

As described, the use of CO<sub>2</sub> as a refrigerant has a great energetic and environmental benefit [5]. Thanks to its friendly environmental characteristics, CO<sub>2</sub> heat pumps have experienced a boost in the markets of refrigeration, air conditioning and domestic hot water production. CO<sub>2</sub> has a remarkable particularity in these thermodynamic properties which distinguishes it from other refrigerants, its critical temperature is very low (31°C) on the other hand its critical pressure is much higher (73.77 bars) than that of other refrigerants, under these conditions it is difficult to condense CO<sub>2</sub> for operation at relatively high ambient temperature. So, the heat transfer no longer takes place by condensation but by cooling the gas in the supercritical state, the low-pressure part of the cycle remaining subcritical. For this the condenser is replaced by a gas cooler as shown in figure I.1.

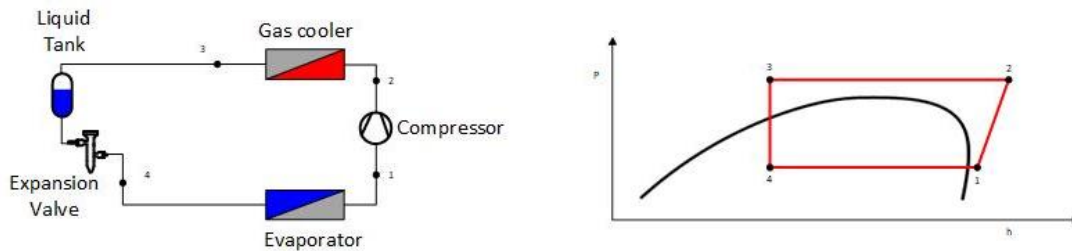


Figure I.1: Schematic diagram and P-h diagram of a CO<sub>2</sub> trans-critical heat pump

The heat absorption by the refrigerants at the evaporator in the subcritical region is similar in both cycles. However, the heat rejection process takes place in two different regions. For the conventional heat pump, the refrigerant rejects heat by condensation at constant temperature at the condenser. For CO<sub>2</sub>, the heat rejection at the gas cooler takes place without condensation with a temperature that decreases throughout the exchange process. Also, the pressure difference between the evaporator and the gas cooler is much higher in a trans-critical cycle compared to a conventional cycle.

In the supercritical region, the outlet temperature of the gas cooler is independent of pressure. Several researchers have indicated that there is an optimum gas cooler pressure for a given cooling temperature [6]. This optimum gas cooler pressure would provide the maximum COP of the system and must be found in each specific configuration and/or operating condition. CO<sub>2</sub> heat pumps have seen a wide range of domestic and industrial applications [6-9].

## I.5. Storage tank

A special tank design is highly required in the hot water production technology. Stratified storage tanks are the key elements to satisfy this need (figure I.2), in order to minimize mixing and conductive heat transfer between the hot and cold water during the dynamic periods [10].

Thermal stratification is a natural phenomenon that occurs in a thermal storage tank, and it consists in forming of horizontal layers at different temperature such way that the layer's temperature is always higher than that of the bellow one. The main idea of using a stratified storage tank in hot water production is the objective to secure a high temperature to the user and lower temperature outgoing to the heat source. The

thermocline is a transient region that separates the hot and cold regions, and also has an energetic benefit to avoid mixing.

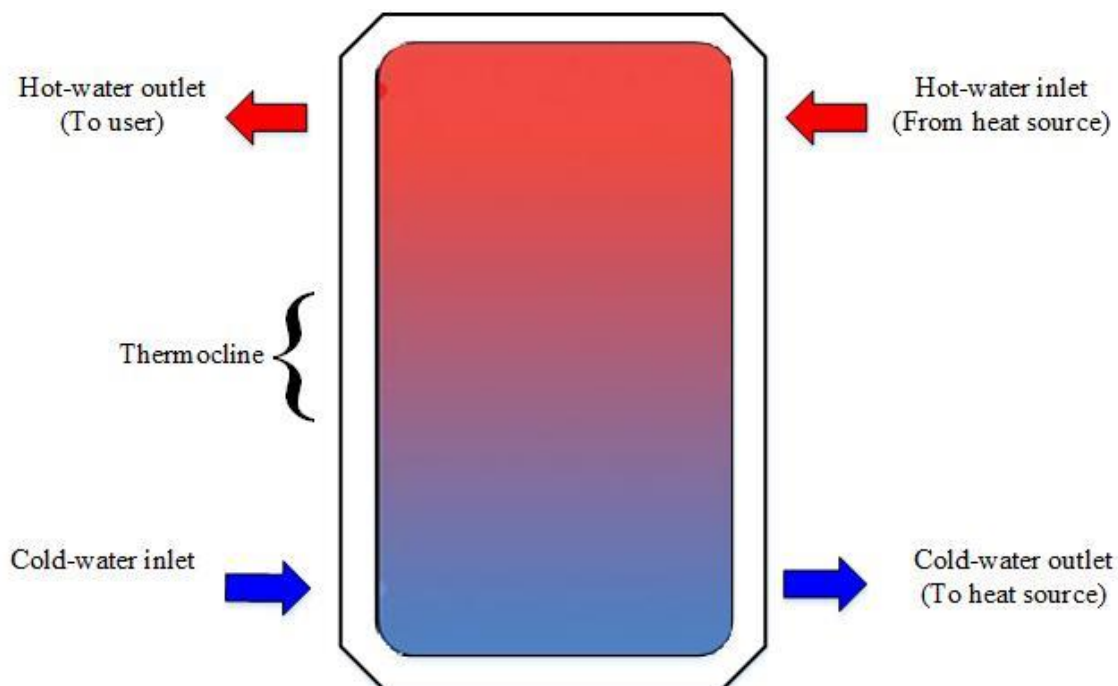


Figure I.2: Schematic diagram of a stratified storage tank

## I.6. State of the art water-water heat pumps for industrial or domestic hot water production systems

### I.6.1. Studies and analysis of the CO<sub>2</sub> heat pump technology

In such system of industrial or domestic hot water production, heat pumps and stratified storage tanks are primordial elements of the systems. Many researchers and engineers focus on the thermodynamic performance of the heat pump [11] and the heat transfer behavior of the storage tank [12]. Ma Liangdong et al. [13] investigated experimentally the effect of the operating parameters on the heating performance of a serially cascaded wastewater source heat pump. Heat pumps working with CO<sub>2</sub> are one of the most efficient heating generators for DHW using A1 refrigerants. Due to its low critical point (critical temperature of 31 °C), CO<sub>2</sub> is mainly used in heat pumps water heaters with trans-critical cycles. The use of these types of cycles allows CO<sub>2</sub> heat pumps to provide high COP values for heating water from very low inlet water temperatures as the heat transfer at the hot sink is performed with sensible energy (not latent energy) also at the refrigerant side of the heat exchanger, what increases its efficiency [14]. In contrast to subcritical cycles,

in trans-critical cycles, the pressure at which the heat is transferred to the heat sink is not directly conditioned by the temperature of that sink. Thus, there exists an optimal operating pressure that depends on the specific working conditions of the heat pump [6,16]. Many authors have studied the optimal design and configurations to obtain high efficient CO<sub>2</sub> trans-critical heat pumps both experimentally and theoretically [17-19]. To assist in the design process of new models, it is a key issue not only to develop numerical models that permit the characterization of this type of hot water production system but also to provide ad-hoc experimental data to validate those models. Yokoyama et al. [19] analyzed numerically the influence of the hot water demand on the performance of a CO<sub>2</sub> heat pump.

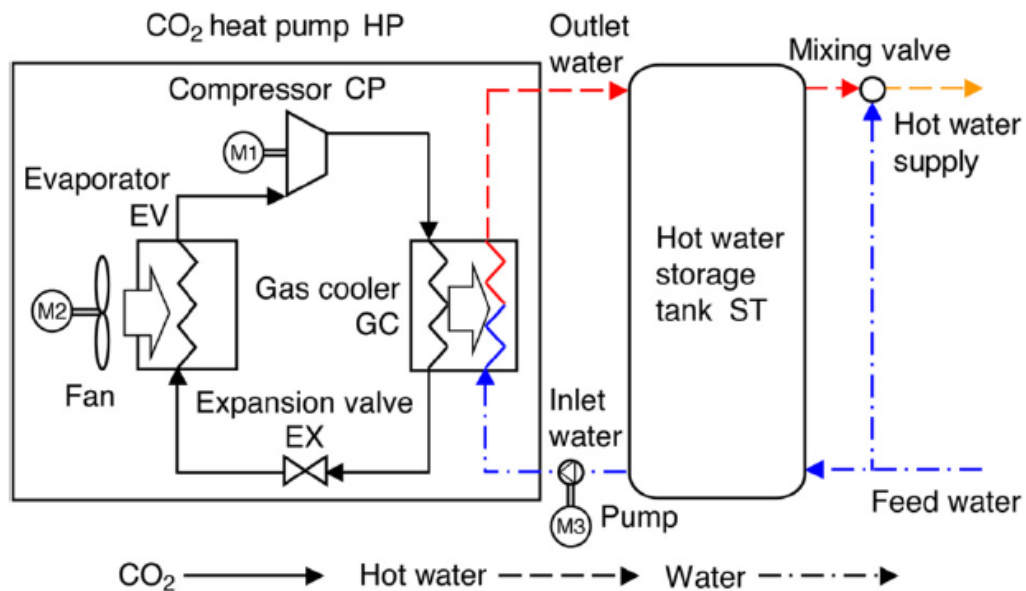


Figure I.3: Configuration of CO<sub>2</sub> heat pump water heating system [19]

They concluded that the daily change in the hot water demand does not significantly affect the daily average system efficiencies.

Zhihua Wang et al. [20] analyzed numerically the performance of a CO<sub>2</sub> heat pump for residential heating system using TRNSYS. In their work they proposed a trans-critical CO<sub>2</sub> heat pump unit integrated with two thermal energy storage containing phase change materials (PCMs).

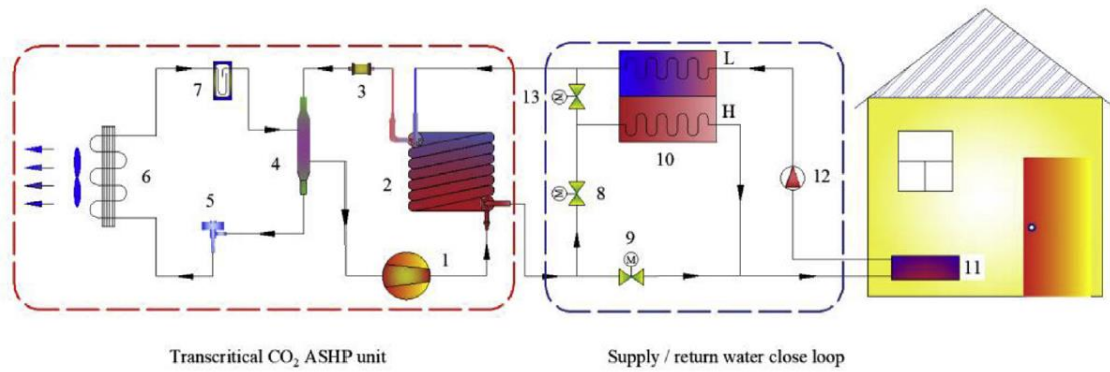
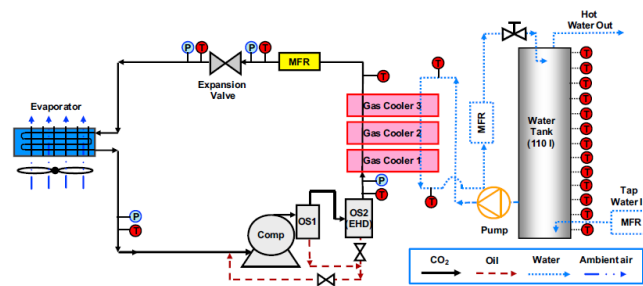


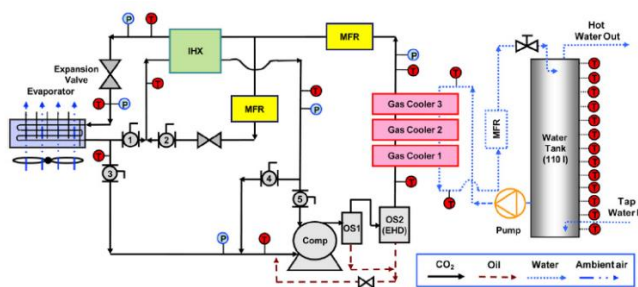
Figure I.4: Schematic diagram of the trans-critical CO<sub>2</sub> heat pump heating system [20]

Their results showed that the heating capacity and energy consumption of the proposed system were decreased by 21 and 24%, respectively, in comparison with the baseline system using water.

Nicholas Fernandez et al. [21] investigated the effect of the environmental conditions on the COP of a CO<sub>2</sub> heat pump water heater and they compared a two-stage cycle with an internal heat exchanger and a cycle with a suction line heat exchanger to baseline cycle (without IHX).



a) Baseline cycle



b) two-stage IHX cycle

Figure I.5: Test facility of the two CO<sub>2</sub> heat pump configurations studied [21]

They concluded that increasing ambient temperature increases the overall COP, and by using a suction line heat exchanger they obtained an increase in the COP by up to 7.9 % with respect to the baseline cycle under the same conditions.

Bin Hu et al. [22] studied experimentally an air-source trans-critical CO<sub>2</sub> heat pump water heater under different working conditions.

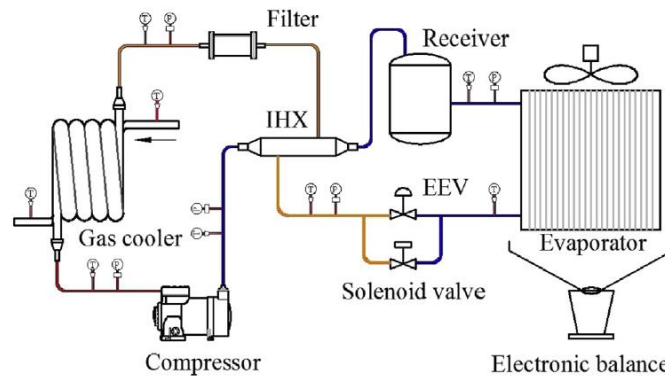


Figure I.6: Schematic of the air source CO<sub>2</sub> heat pump water heater [22]

Their results show that the higher hot water temperature can be reached by decreasing the inlet water flow rate or increasing the water inlet temperature.

Feng Cao et al [23] studied experimentally the influence of IHX on the air source trans-critical CO<sub>2</sub> heat pump water heater.

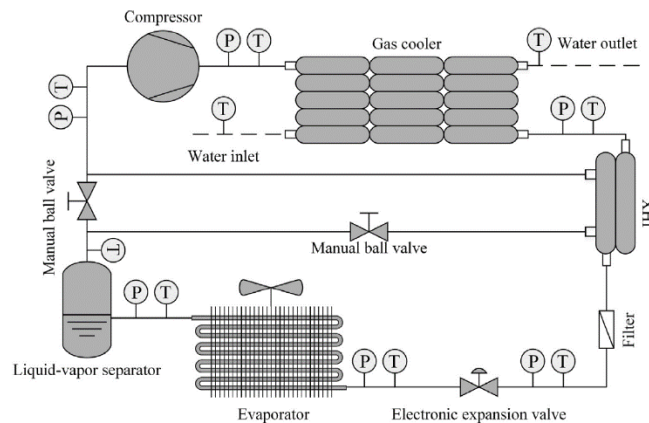


Figure I.7: Schematic diagram of the CO<sub>2</sub> heat pump prototype [23]

They concluded that the total exergy destruction and the product exergy increased with the application of IHX, and the exergy efficiency of system reduced in all working conditions. Also, the reliability of the heat pump system might also be enhanced by the



reduced optimal discharge pressure that could be due to decrease of the ambient temperature, the increase of the water inlet temperature and the increase of the water outlet temperature.

Sung Goo Kim et al [24] investigated numerically and experimentally the influence of a heat exchanger on the performance of a trans-critical CO<sub>2</sub> cycle. They found that the geometrical parameters of the internal heat exchanger affect the mass flow rate of refrigerant. Moreover, they found that the compressor power consumption decreases with the increase of the length of the heat exchanger whereas the COP of the CO<sub>2</sub> cycle is improved.

Ji Wang et al [25] presented a study of trans-critical CO<sub>2</sub> heat pump system with a flash gas bypass technic and they simulated the optimal COPs for heating, cooling and combined performance considering the interstage pressure, discharge pressure and gas cooler outlet temperature.

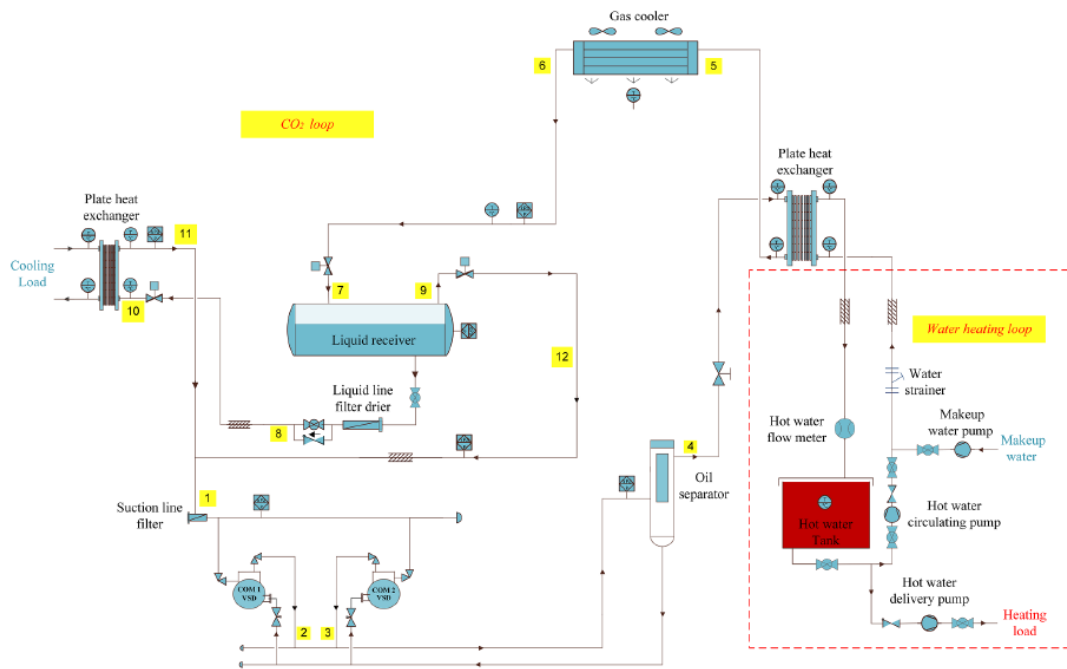


Figure I.8: The configuration of the CO<sub>2</sub> heat pump system [25]

They reported that the optimal combined COPs generally decrease from 3.84 to 3.68 (with the interstage pressure from 29.65 bar to 53.60 bar) and the optimal combined COP of 4.27 occurs at the same pressure and the optimal heating COP of 2.63 is achieved while the optimal cooling COP of 1.66 occurs.

Yikai Wang et al [26] studied experimentally an air source trans-critical CO<sub>2</sub> heat pump water heater and its cost, based on the Chinese standard operating conditions.

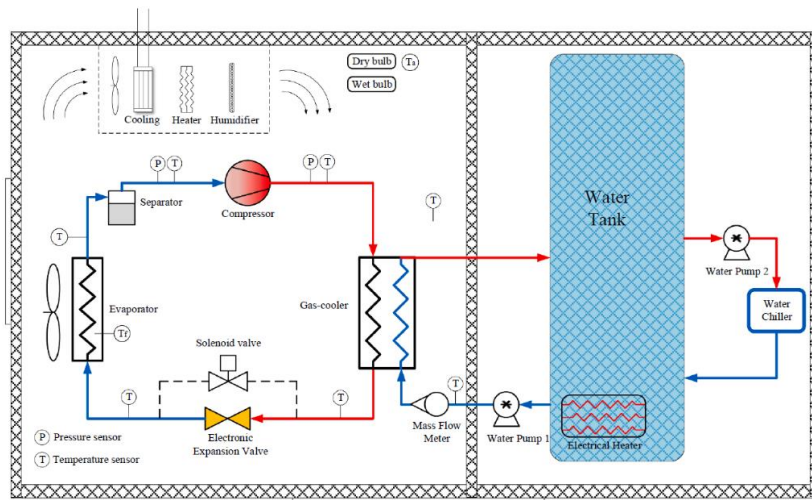


Figure I.9: Schematic diagram of the air source CO<sub>2</sub> heat pump water heater [26]

They concluded that the heating capacity and the COP of microchannel heat exchanger system were respectively improved by 16.5%-37.3% and 16.3%–22.6% compared with the baseline fin-and-tube heat exchanger system. Also, the primary energy consumption of the microchannel heat exchanger system is reduced.

Kashif Nawaz et al [27] studied and analyzed a CO<sub>2</sub> heat pump water heater performance considering water supply temperature, water circulation rate, tank stratification. Also, they compared the performance of CO<sub>2</sub> heat pump system with that of a similar system using R-134a as the refrigerant.

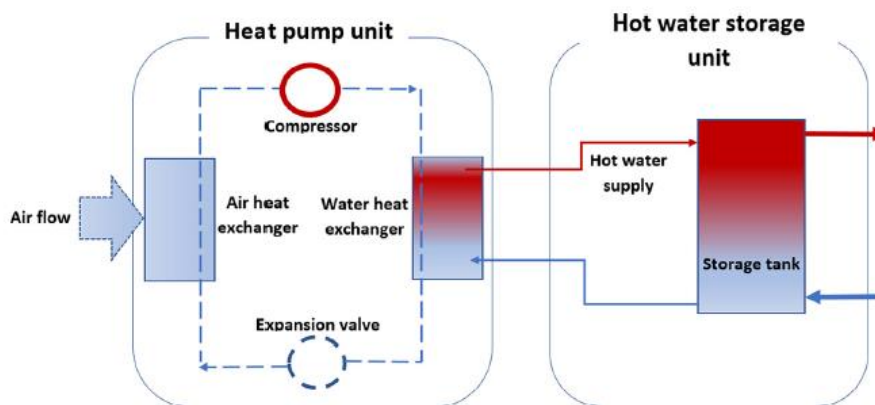


Figure I.10: Schematic diagram of the air source heat pump [27]

They concluded that the system was highly sensitive to the water circulation rate and has a direct impact on the stratification and the system efficiency also the set point for water supply temperature had a significant impact on the system performance. They showed that the system is improved for both the CO<sub>2</sub> and R-134a systems when the set point temperature was decreased.

Fang Liu et al [28,29] investigated experimentally the CO<sub>2</sub> heat pump system performances with simultaneous cooling and heating thermal storage tanks.

They found that the optimum system performance for a CO<sub>2</sub> heat pump system for both cooling and heating thermal storage can be achieved by adjusting the compressor frequency, expansion valve opening and cold/hot water flow rates for thermal storage tank.

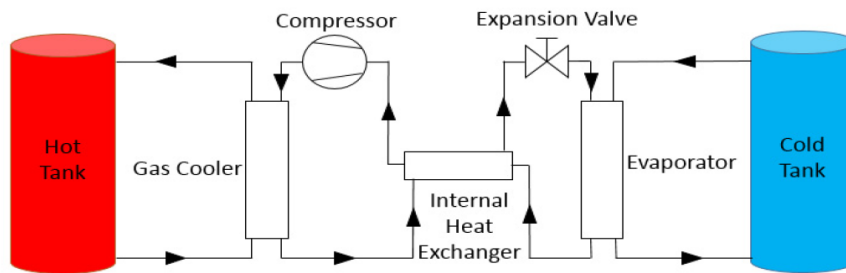


Figure I.11: Schematic diagram of Experimental Setup studied [28]

F. Illán-Gómez et al [14] studied experimentally different configurations of CO<sub>2</sub> heat pump for DHW production under the same operating conditions. Also, they evaluated the influence of different parameters, such as the high pressure, the superheating, the IHX effectiveness, and the heat exchangers area.

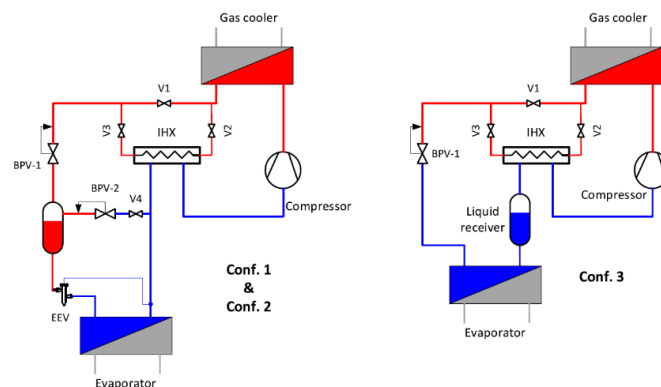


Figure I.12: Schematic diagrams of the configurations studied [14]

The showed that the use of a IHX is always beneficial and improve the thermal performance of the system, as well as it exchange-surface increases, better system performance is obtained. Even if the gas cooler temperature increases or the evaporation temperature decreases.

### I.6.2. Studies and analysis of the stratification and DHW storage tank

Besides the heat pump efficiency, there are other factors that influence the energy efficiency of a hot water production system. Thermal stratification plays an important role on the efficiency of the energy system [30]. It is usually employed in domestic hot water storage tanks [31, 32], and it is highly recommended for heat pumps water heaters in order to maintain a high energy performance [21].

The temperature distribution in a stratified storage tank depends mainly on its geometry, in fact the factor height-width plays an important role in the stratification formation and stability. The form and the disposition are also an important parameter that can be taken in consideration [33 - 35].

Azharul Karim et al [35] investigated numerically the performance of a stratified storage tank for heating and cooling applications. They analyzed the mixing and thermocline behaviors of the stratified storage tank in function of inlet velocity, the temperature difference between the inlet water and stored water and the tank aspect ratio. For this, five different tank geometries were examined in their study.

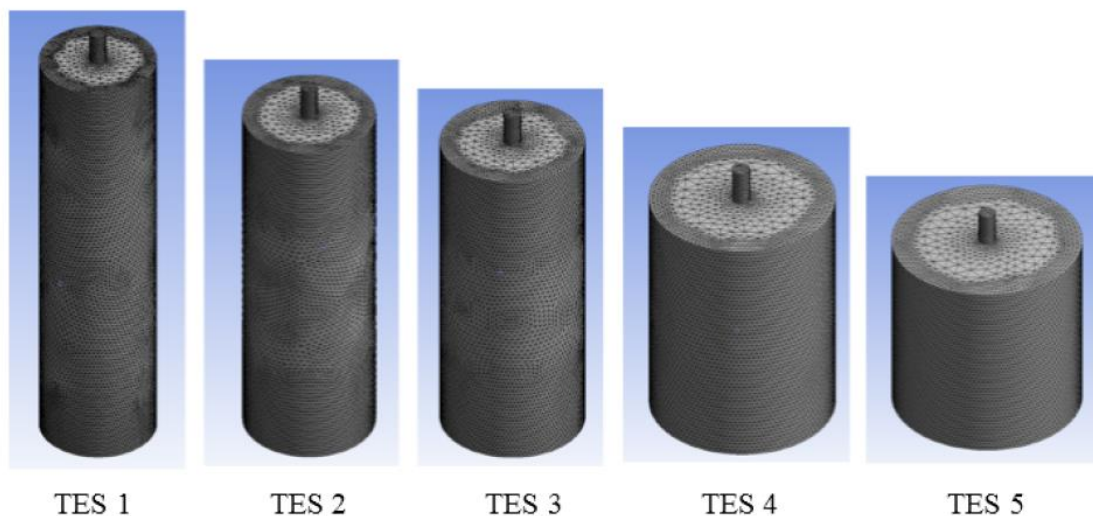


Figure I.13: Geometries used to investigate the thermal stratification in storage tanks [35]

They reported that higher inlet velocities increase the mixing of water for lower aspect ratio, contrarily to higher aspect ratio of the tank. Also, higher temperature differences between the inlet and the stored water reduce mixing because of greater density differences between layers. Other aspects that can affect the thermal performance of the tank are the position of the inlet and the outlet ports, and the duration of the filling or discharging of the tank.

Darci et al. [36] presented a numerical analysis of laminar natural convections of a horizontal cylindrical storage tank. They concluded that the stratification degree increased as the heat loss increased, and the presence of the baffle plate allows the formation of temperature profiles with a better thermal stratification. The inlet jet at the top of the tank has a great signification and the inlet jet temperature inside the storage tank leads to a greater thermal stratification.

Simon Ievers and Wenxian Lin [37] investigated numerically using CFD three-dimensional transient model fluid dynamics within the thermal energy storage tanks. They analyzed the effects of the aspect ratio, outlet and inlet flowrate, and the positions of the inlet and the outlet ports. They reported that as the aspect ratio of the storage tank increases, the degree of thermal stratification increases. Also, the flowrate and the positions of the inlet and the outlet ports have a great impact on the thermal performance of the storage tank.

Gao et al. [38] studied experimentally and numerically different geometries of a central hole baffle plate to improve and characterize the thermal stratification of a DHW storage tank during the charging process. They performed an optimization process based on the Richardson number of the system as a representative descriptor of the stratification and provided a plate geometry and location as well as an inlet velocity that maximized the tank stratification.

Wang et al. [39] experimentally investigated the effect of the inclusion of PCM balls on the thermal stratification of a hot water storage tank.

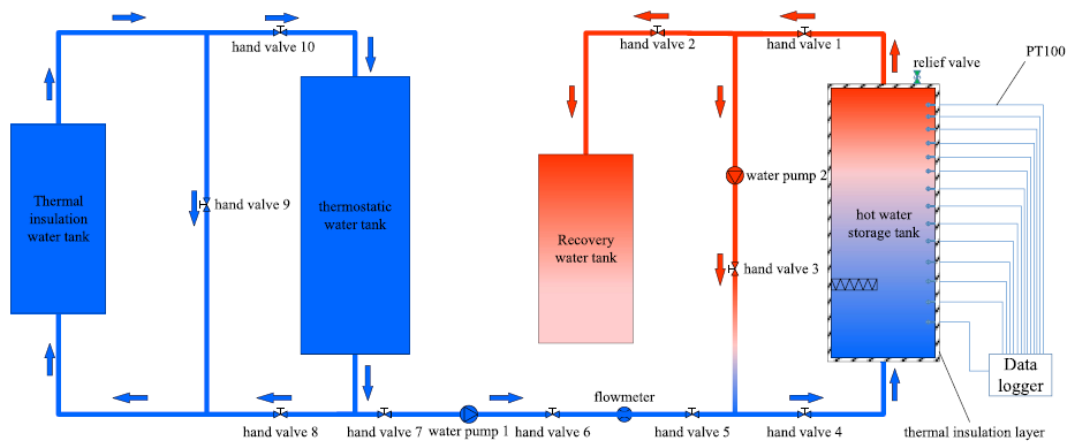


Figure I.14: Experimental set-up [39]

They found that, for a fixed inlet flow rate, an improvement of the thermal stratification was achieved as the positions of the balls became closer to the inlet.

### I.6.3. Technics to enhance the thermal stratification with storage tanks

With the aim to enhance the thermal stratification of the storage system, numerous methods have been proposed for the improvement of thermal stratification in water storages as baffles, separators and controlled variable inlet of the jet (figure I.15) [40-42].

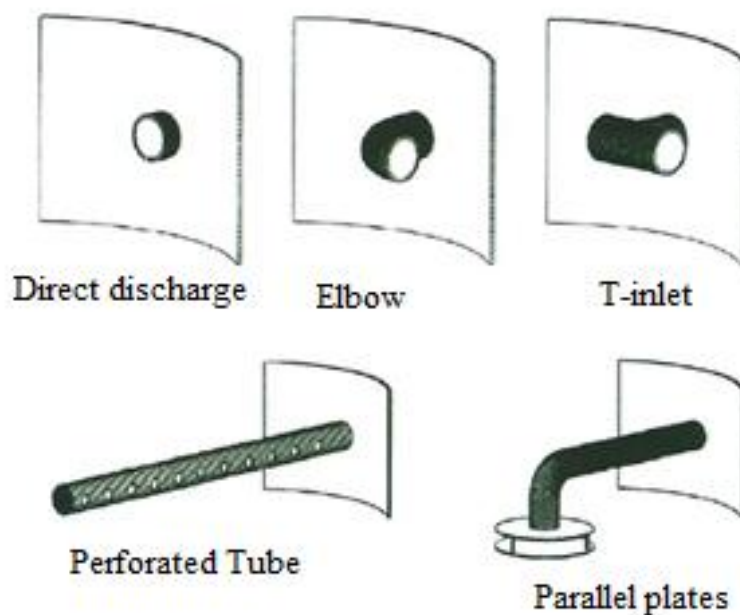


Figure I.15: Different inlet devices of a stratified storage tank [42]

Chandra and Matuska [43] presented a numerical study using CFD of the stratification performance in DHW storage tanks. They analyzed the impact that three types of inlet devices (perforated inlet, slotted inlet, and simple inlet) had in the stratification process.

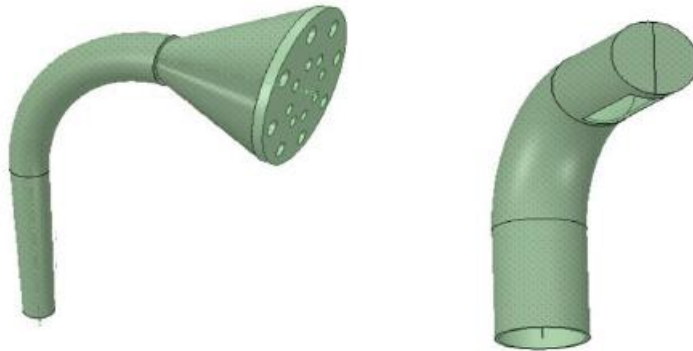


Figure I.16: Inlet devices of the storage tank studied [43]

They found that all devices performed similarly at low flow rate and high temperature difference between mean storage and water inlet ( $\Delta T$ ), whereas at high flow rate and low  $\Delta T$  (typical conditions in heat pumps application) the slotted inlet performed better than the others.

Saïf Ed-Dîn Fertahi [44] presented a review of experimental and numerical studies on thermal Stratified storage tanks. They highlighted the different component of a stratified storage tank like auxiliary heater, mechanisms with different geometries and designs to enhance the stratification within the storage tanks, also, different numerical models are presented.

#### **I.6.3.1. Baffles**

Baffles are a type of obstacles located inside the tank in order to minimize the mixing. Necdet Altuntop et al. [45] analyzed the effect of obstacles on thermal stratification in hot water storage tanks and they presented various shapes and geometries with different dispositions.



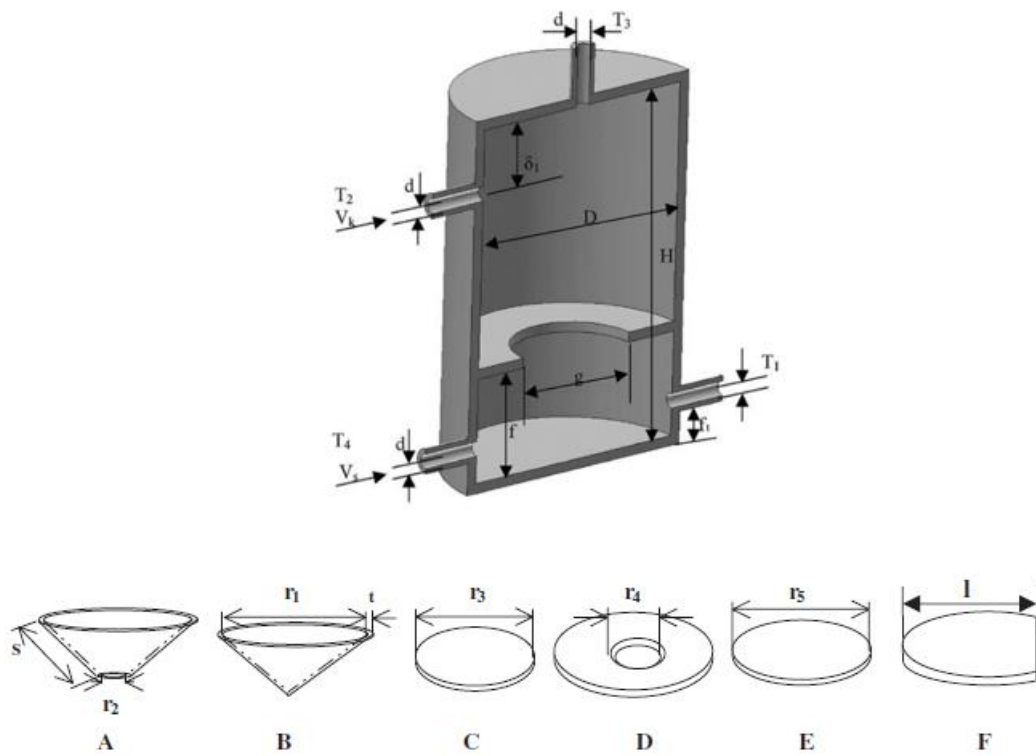


Figure I.17: Shapes and geometries of the baffles to enhance thermal stratification [45]

Dogan Erdemir and Necdet Altuntop [46] presented four types of obstacles to improve the thermal stratification inside a vertical hot water storage tank.

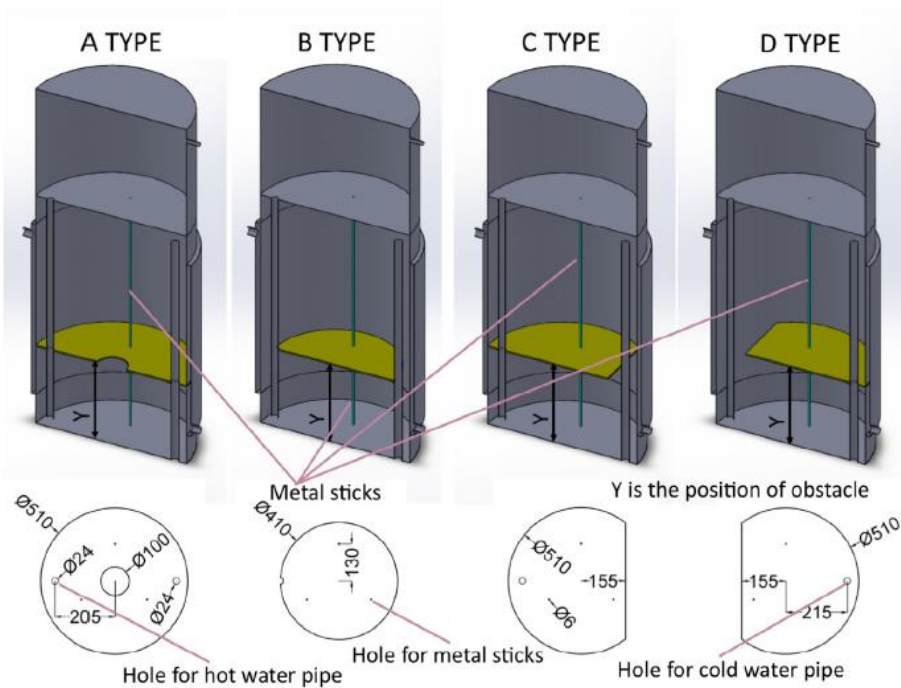


Figure I.18: obstacles and their shapes used [46]



The main conclusion is that the obstacle in tank provides the best thermal stratification in the tank in all the considered cases.

### I.6.3.2. Tank shape

Angui Li et al. [47] investigated numerically the influences of thermal storage tank structures on the temperature stratification, heat storage capacity and the thermal characteristics of three shapes of thermal storage tanks.

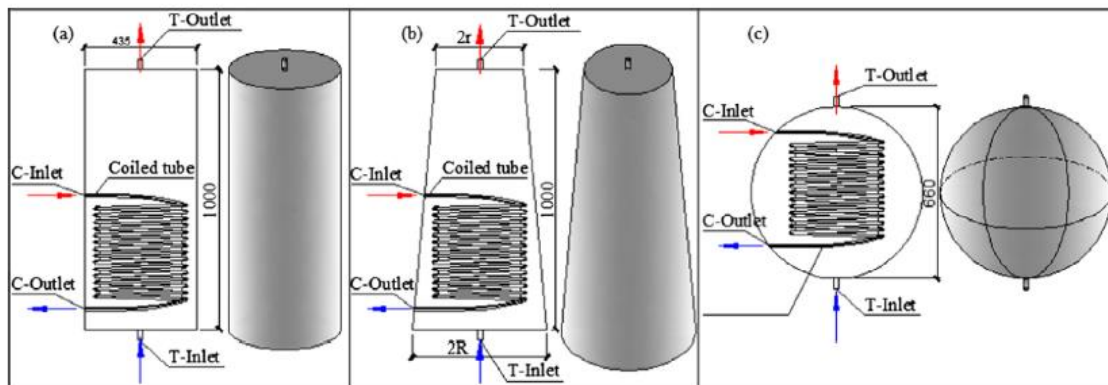


Figure I.19: Storage tank geometries [47]

They reported that the temperature stratification of the circular truncated cone tanks was better compared to the other tanks, especially, when the radius ratio was 0.450, and the temperature stratification of the spherical tank was the worst. Also, the charging efficiency of the circular truncated cone tanks was always higher compared to the other tanks. Taking circular truncated cone water tanks as the research object, as the radius ratio decreased, there was a better thermal stratification in the tank, but the charging efficiency was reduced.

Burak Kurşun [48] presented a numerical investigation of thermal stratification with storage tank comparing cylindrical and rectangular with truncated cone and pyramid shaped insulation geometry as shown in the figure I.20. He analyzed different values of insulation thicknesses and tank aspect ratios.

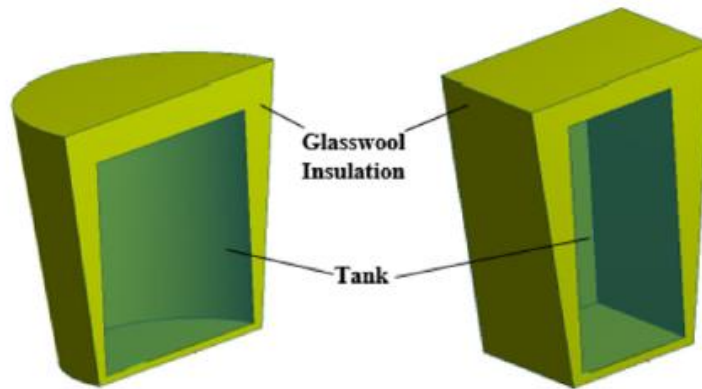


Figure I.20: Hot water tank geometries and their insulation studied [48]

His results showed that when truncated cone and pyramid shaped insulation geometries were used, the amount of heat transfer at the bottom of the tank increased and the average water temperature decreased. In addition, the increase in the thickness of the insulation towards the top of the tank prevented the water temperature drop in the top region of the tank. In general, this geometry of insulation enhances the thermal stratification of the tank.

### I.6.3.3. Heat exchanger

Mevlut Arslan and Atila Abir Igci [49] presented thermal performance analysis of a vertical hot water storage tank with a mantle heat exchanger.

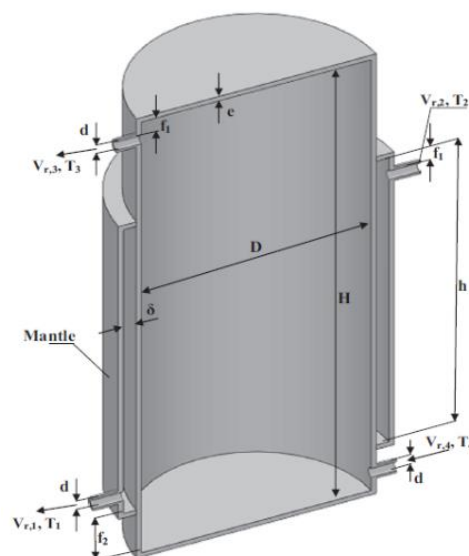


Figure I.21: Hot water storage tank with mantle heat exchanger [49]

They concluded that the use of the mantle heat exchanger enhances the thermal stratification of the storage tank in in the case of higher flowrate of the hot fluid throughout the mantle

#### I.6.3.4. Stratification pipes (stratification enhancer)

Stratification enhancer are pipes installed inside the storage tank that can be work depending on the pressure difference between the storage tank and the pipe [50,51] or depending on the temperature of the tank, and it injects the water entering the tank in the layer temperature closest and slowest rate possible [42,50]

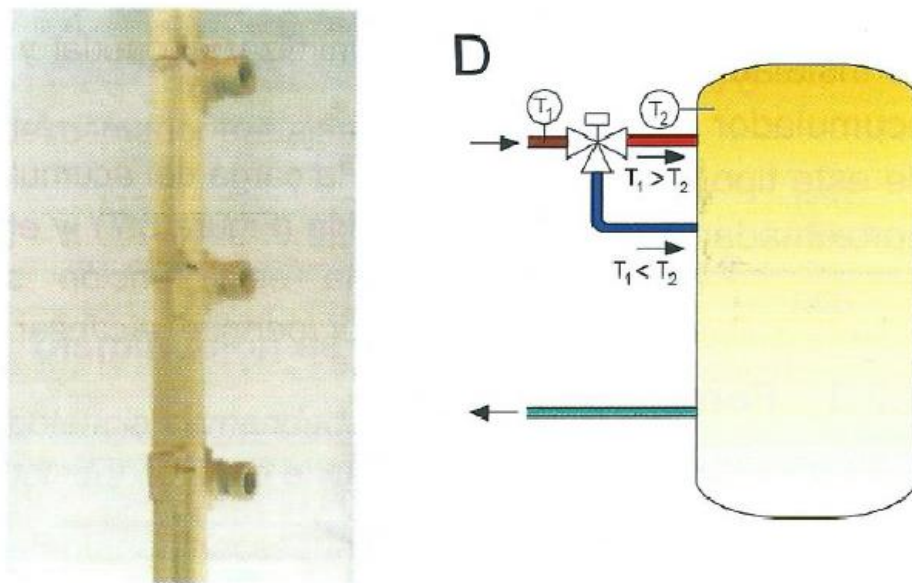


Figure I.22: Stratification pipe [42]

Stefan el al [51] presented a theoretical and experimental study of an inlet stratifier for thermal storage tanks. They investigated experimentally a rigid stratifier and also a numerical study using CFD. The stratifier consists of a tube installed inside the storage tank with three circular openings.

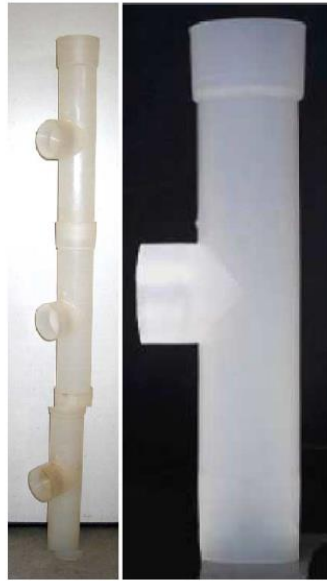


Figure I.23: Stratifier made of three compound inlet pipes [51]

#### I.6.3.5. Diffusers and deflectors

Eugenio García-Marí et al. [52] investigated experimentally the integration of a new inlet device that enhances thermal stratification during charging in a hot water storage tank. This device is a sintered bronze conical diffuser (SBCD) and compared the results with the conventional inlet elbow as shown in the figure.



Figure I.24: Elbow and diffuser inlet devices [52]

They concluded that a greater degree of stratification is reached when the conical diffuser is used as an inlet device comparing with the inlet elbow, a greater flow gives a greater degree of water mixing during thermal charging of the tank.

T. Bouhal et al. [53] presented a numerical model using CFD to optimize the thermal stratification in hot water storage tanks for domestic applications. They studied the thermal performance of a cylindrical storage tank using a flat plate inside the tank (figure I.23), and they investigated the distribution of the flat plates, the geometrical parameters, the positions, and the angle of inclination. They simulated numerically the flow characteristics and the thermal stratification performance during charging and discharging phases for two vertical storage tanks configurations. From their analysis they found that the tank with two plates located at the middle and top is the optimum case, and the tank with a  $30^\circ$  tilted plate is offering the best performance.

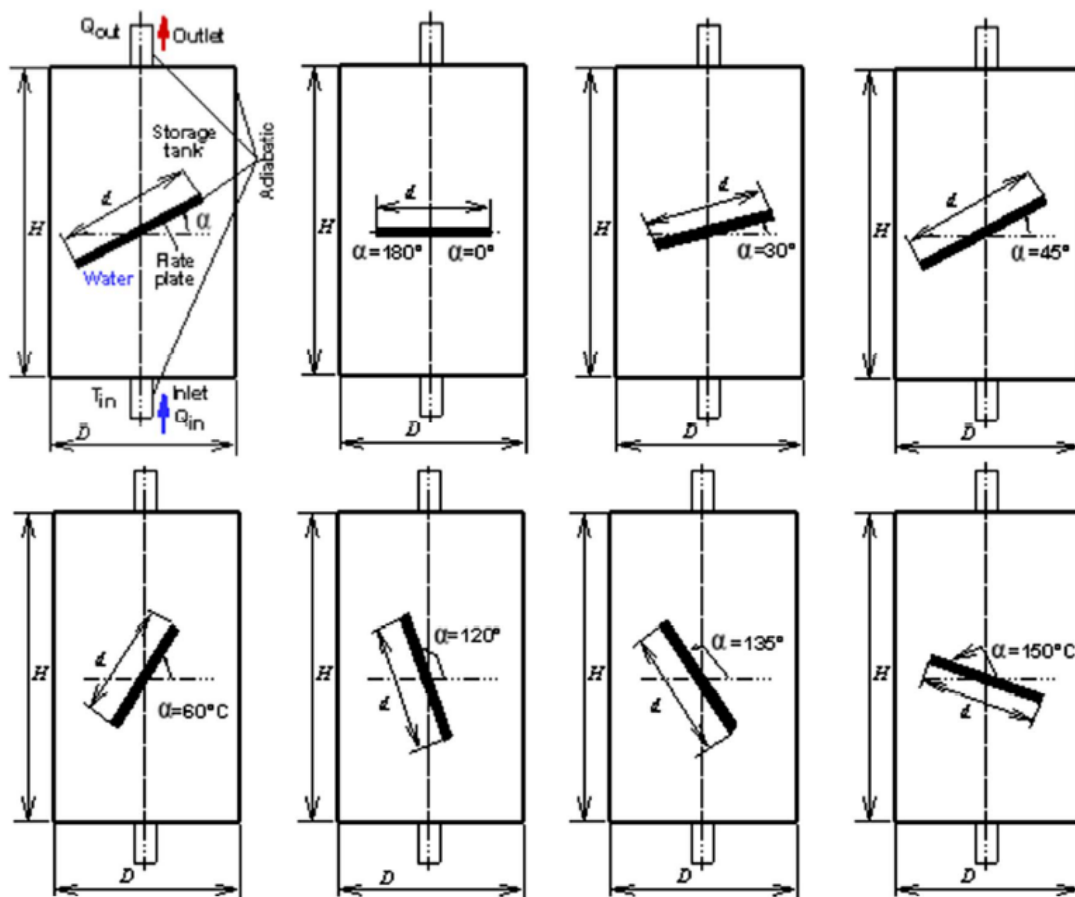


Figure I.25: Configurations of the storage tank with different flat plat's orientations [53]

# Chapter II



### II.1. Introduction

This chapter describes the experimental facility developed with the aim to perform the test procedure specified in the European Standard EN16147 in order to determine the performance and the energy efficiency of the domestic hot water production system by means of heat pumps with electrically driven compressors. The chapter begins with a review of the Standard EN16147 explaining the test steps, then, a description of the test set-up of the installation and its components, finally the LabVIEW programs of all test steps are illustrated.

### II.2. The standard EN16147 [54]

The European Standard EN16147 is a norm that specifies the test methods to determine the performance and the energy efficiency of the domestic hot water production system by means of heat pumps with electrically driven compressors. The test methods of this standard are based on several steps [54]. A test series are carried out to investigate the thermodynamic performance of the heat pump under various operating conditions. The test consists of different steps and are as follow:

- Step A: Stabilization
- Step B: filling the accumulation tank and prepare the test set-up.
- Step C: Determination the water heating time.
- Step D: Determination of the energy absorbed in the steady state.
- Step E: Water extraction-
- Step F. Determination of cooling time.

It can be seen that the steps A and B are the test preparation. The tests from C to F are carried out to determine the energy efficiency and the performance of the water heater heat pump for domestic hot water production as indicated in Figure II.1.



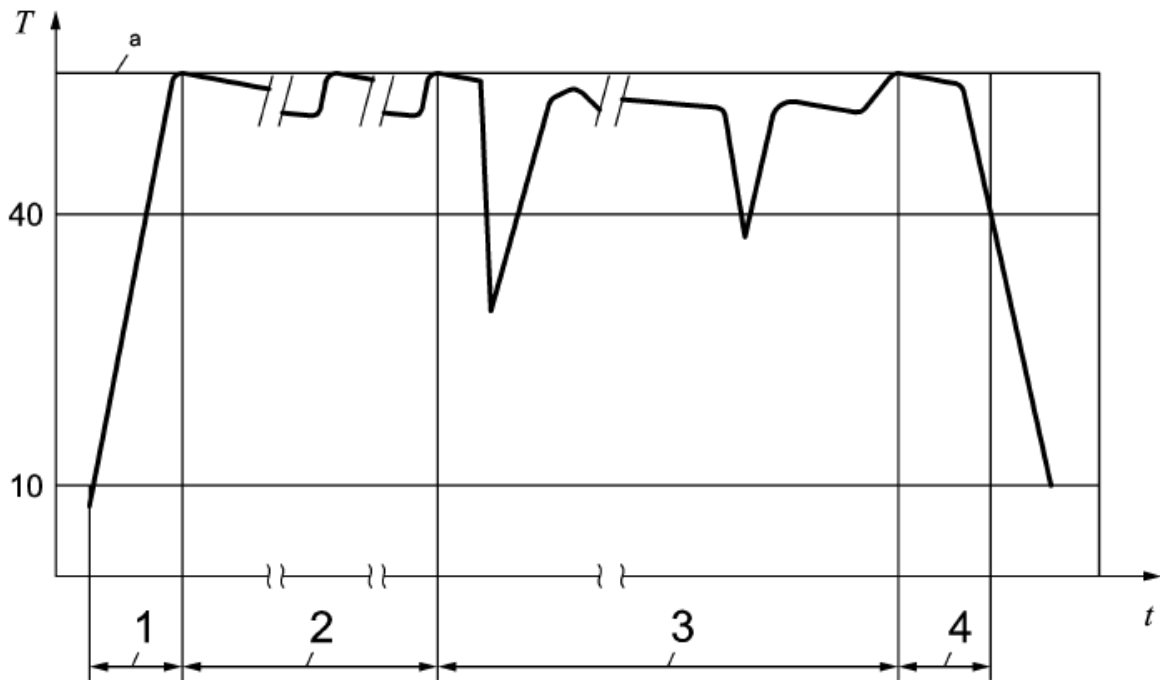


Figure II.1: Stages of the test [54]

Figure II.1 shows the stages of the test and it consist of 4 main steps beside the preparation steps. The stretch 1, represent the filling and heating test (step C). Stretch 2, represent the steady state performance (step D). Stretch 3, represents the extraction test (step E) and the final stretch 4, represents the cooling test (step F).

As it indicated above the test is a series of steps where every final condition of a step is the initial condition of the following step, and each individual stage can be performed independently.

### II.2.1. [Step A & B]: Stabilization and test preparation

As indicated during these tests the facility is prepared for the following steps. Step A is for system stabilization and Step B for filling the accumulation tank and prepare the test set-up.

### II.2.2. [Step C]: Determination the water heating time

In this step, the storage tank must be filled with cold water. Cold water must circulate in the accumulation tank until the outlet temperature is equal to the inlet temperature, within the allowed variation limit  $\pm 0.2$  K.

This step consists of determining the time necessary  $T_h$  to heat the stored water from the initial condition (Temperature of the cold water equal to 10 °C) to the first compressor stop caused by the tank thermostat, when the tank temperature reaches the temperature of 60 °C. The hot water temperature of 60 °C is not mentioned in the standard norm, but usually, in domestic hot water production system, the temperature of the hot water is 60 °C.

### II.2.3. [Step D]: Determination Energy absorbed in steady state

When the thermostat stops the heat pump after the step C, the system continues working without hot water flow for a specified number of complete cycles. The test must be carried out for a period of 48 h or less if there are 6 starts / stops cycles. This way the energy absorbed by the system to maintain the temperature level in the storage tank is evaluated.

### II.2.4. [Step E]: Extraction profiles

The test of this step starts by the last stop of the heat pump when the storage tank temperature's reaches the value of 60 °C.

In this step the hot water depends on the extraction profile chosen for the test (Annex 1). The extractions of the hot water begin at a specific time and stop when the energy consumed reaches the value mentioned in the profile in kWh and it is defined as follow:

$$Q_{tap} = \frac{1}{3600} \int_0^{t_{tap}} \dot{m} \cdot C_p \cdot (T_{hw} - T_{cw}) dt \quad (II.1)$$

Where:

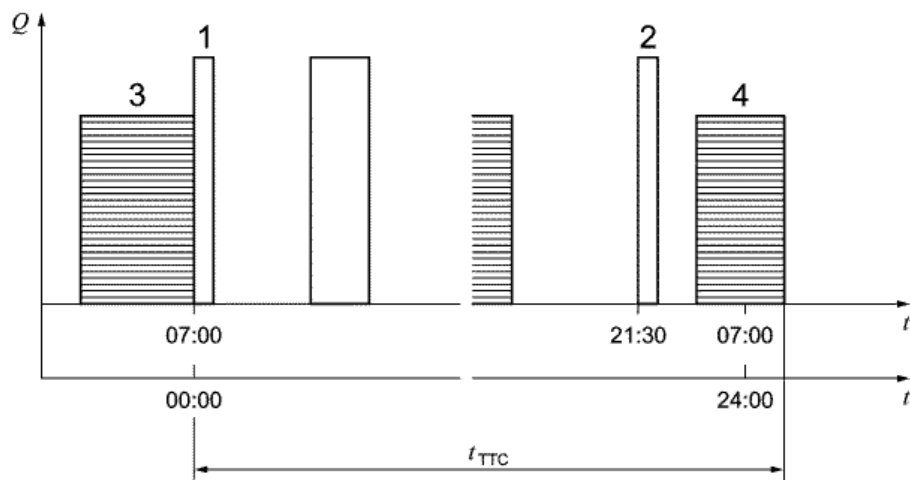
$T_{hw} - T_{cw}$  : is the temperature difference of the hot water and the cold water at the inlet and the outlet of the storage tank respectively in K.

$\dot{m}$  : is the flow rate of the extraction of the hot water in  $\text{kg}\cdot\text{s}^{-1}$ .

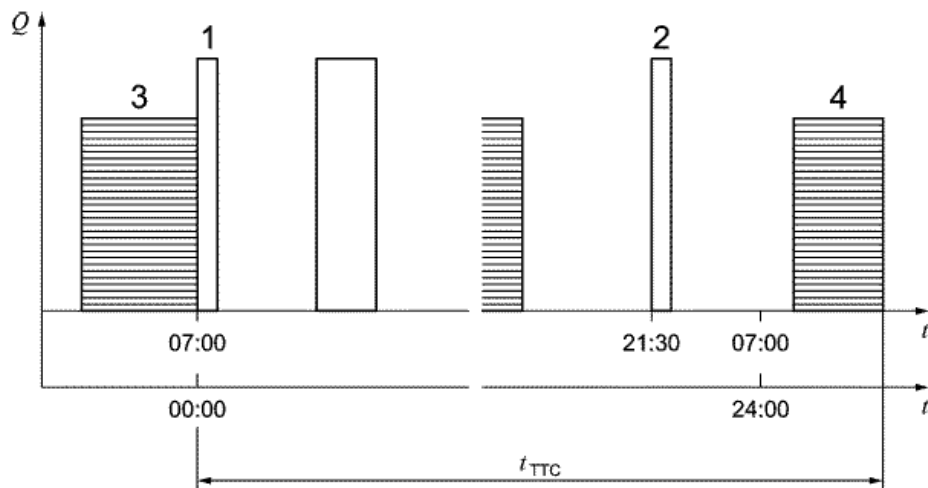
$C_p$  : is the specific heat of the fluid, in  $\text{kJ}\cdot\text{kg}^{-1}\cdot\text{K}^{-1}$ .

$t_{tap}$ : is the duration of the extraction in s.

This test step terminates at the last stop of the heat pump if the duration of the extraction profile is greater than or equal to 24 hours. If the heat pump does not work within 24 hours after the start of the test, it is extended until the heat pump starts and stops again as shown in the Figure II.2.



- a) Illustration of the test where the heat pump is still running after the extraction profile



- b) Illustration of the test where the heat pump is off at the end of the extraction profile

Figure II.2: Illustration of the test method [54]

### II.2.5. [Step F] Water cooling

This step begins with the stop of the compressor, at the end of the last hot water extraction of the step E.

This test step begins with the extraction of the hot water with the maximum flow rate mentioned in the extraction profile chosen until the temperature in the storage tank reaches 40°C and determinates the energy consumed during the extraction and the extracted volume.

## II.3. Description of the test facility

In order to realize the test mentioned in this standard and analyze it, a test set-up is built in the laboratory using a water heater CO<sub>2</sub> heat pump and 4 storage tanks as shown in the Figure II.3

The test facility consists of a combination of a CO<sub>2</sub> heat pump, the water circuit and the water tank in which the hot water produced will be stored.

### II.3.1. CO<sub>2</sub> Heat pump

CO<sub>2</sub> heat pumps are heat pumps using carbon dioxide R-744 as refrigerant, and it is a natural gas, non-polluting and non-toxic.

Figure II.3 shows the test facility's schematic diagram of the heat pump used in the laboratory to realize the tests described above under the standard's conditions. It is constructed to be capable to work and produce heat at different conditions and different configurations. For more information about the CO<sub>2</sub> heat pump, Víctor Francisco [55] in his thesis studied experimentally and numerically the optimum pressure of this installation and he presented a brief description of the installation and the data acquisition used, and it can be useful as a reference for further information about the equipment.

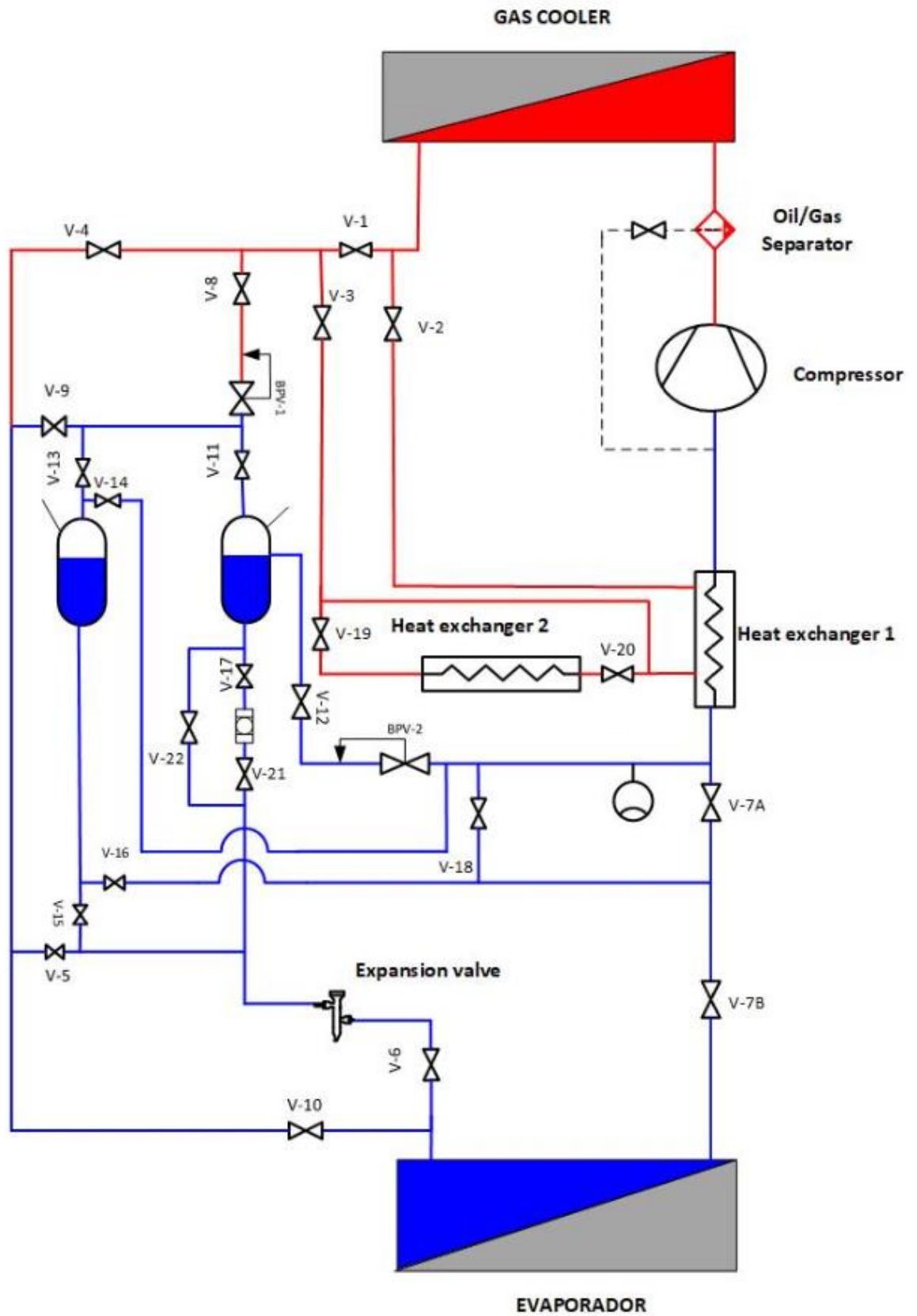


Figure II.3: Schematic diagram of the CO<sub>2</sub> heat pump

The CO<sub>2</sub> heat pump consists of four principal elements and other various elements.

### II.3.1.1. Compressor

The compressor is one of the principal elements of a CO<sub>2</sub> heat pump and it is situated between the low-pressure and high-pressure zones. It uses an electrical source of energy to produce work. The refrigerant at low pressure and low temperature is compressed in order to increase its pressure and its temperature. Dorin offers different type of CO<sub>2</sub> compressor (figure II.4) [56], a CD300H semi-hermetic compressor is used in this test facility.



Figure II.4: Dorin CO<sub>2</sub> compressor [56]

### II.3.1.2. Gas Cooler

In a CO<sub>2</sub> heat pump the condenser is replaced by a gas cooler heat exchanger and this is due to the non-phase change in a CO<sub>2</sub> heat pumps, in the contrary, a traditional heat pump which use another refrigerant a condenser is used. The condenser or the gas cooler in heat pump system is the element in which the refrigerant exchanges and releases heat.

Swep provides wide variety of heat exchanger (figureII.5) [57]. Swep B16 is used in the test facility as a gas cooler, and it is designed, for one-phase applications and it consists of 34 plates, and it's made from 316 stainless steel plates and copper brazing corrugated channel plates with

a filler material between each plate. The maximum flow mentioned by the manufacturer is about  $16.9 \text{ m}^3 \cdot \text{h}^{-1}$

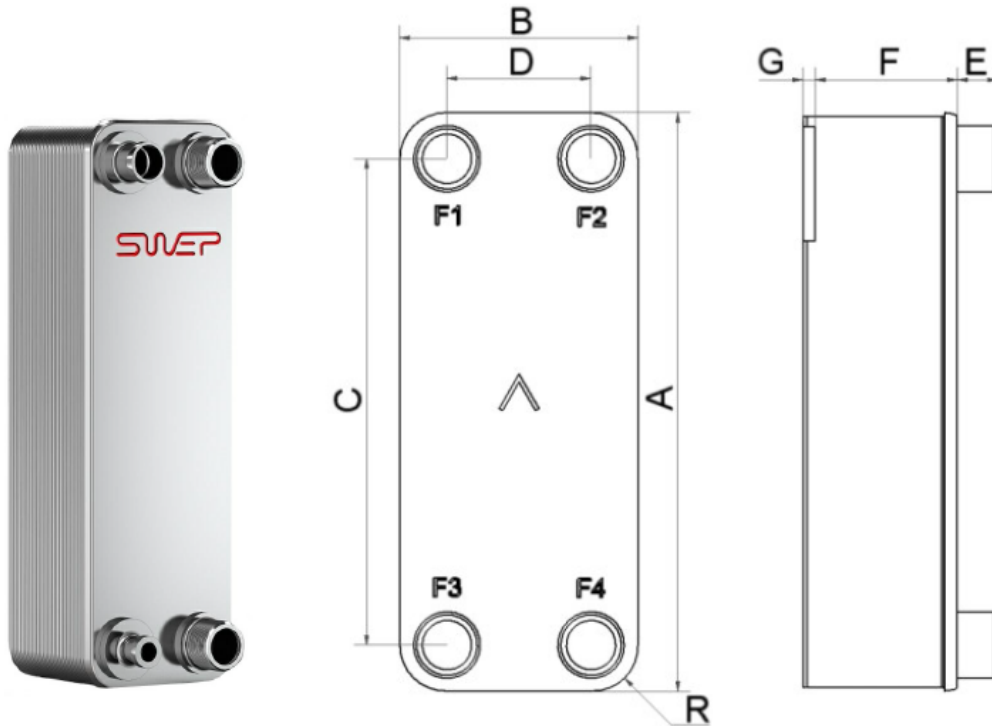


Figure II.5: Schematic diagram of the Gas cooler Swep B16 [57]

And the geometric characteristics are illustrated in the table II.1 below:

Table II.1: Geometric characteristic of the gas cooler [57].

	Dimensions (mm)
A	376
B	119
C	320
D	63
F	$4+2.24*(NP)$
G	6
R	23

### II.3.1.3. Evaporator

Swep BX8T is designed as an evaporator for the refrigeration and heat pumps applications (figure II.6) [58]. The evaporator is made from 316 stainless steel plates and copper brazing corrugated channel plates with a filler material between each plate. The maximum flow mentioned by the constructor is about  $4 \text{ m}^3 \cdot \text{h}^{-1}$ .

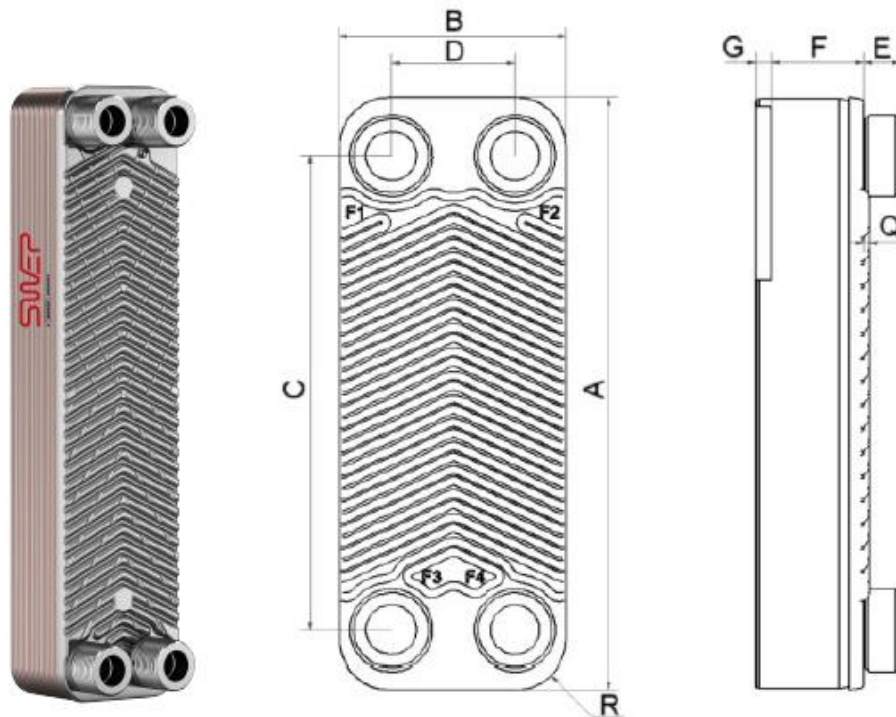


Figure II.6: Schematic diagram of the evaporator Swep BX8T [58]

And the geometric characteristics are illustrated in the table II.2 below:

Table II.2: Geometric characteristic of the evaporator [58].

	Dimensions (mm)
A	315
B	73
C	278
D	40
G	7
Q	2
R	16



II.3.1.4. Internal heat exchanger (IHX)

To improve the efficiency of the system, the use of an IHX is recommended. Swep also provide a heat exchanger adopted with this kind of heat pumps that have a high operating pressure (more than 140 bar) [59]. The SWEP B17 (figure II.7) is optimized for high heat pump capacities, and it is made from 316 stainless steel plates and copper brazing. The Brazed Plate Heat Exchanger (BPHE) is constructed as a plate package of corrugated channel plates with a filler material between each plate.

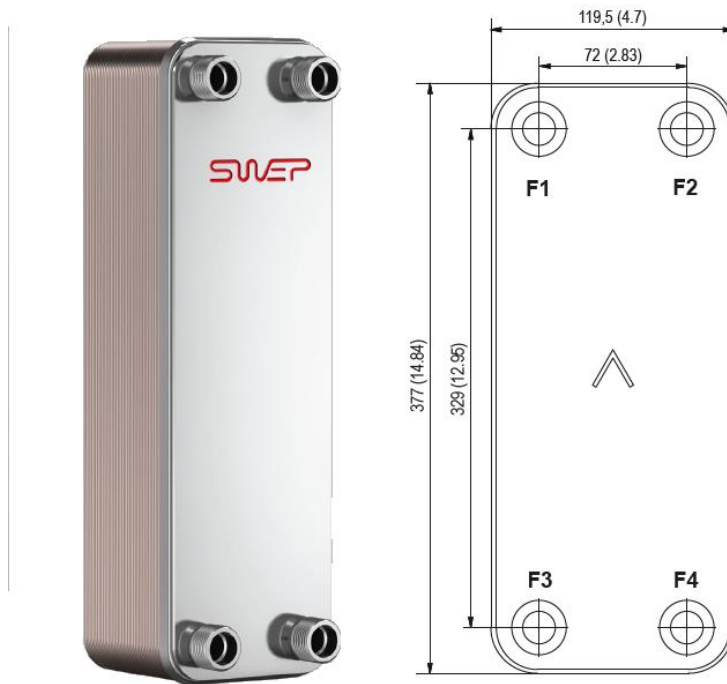


Figure II.7: Schematic diagram of the IHX Swep B17 [59]

### II.3.2. Water loop

Figure II.8 shows the schematic diagram of the water loop. The main elements of this cycle are the storage tanks, a refrigerator, pumps, and different type of valves. The water lines are identified through different names LA 1, LA2, LB1, LB2, LC1 and LC2 and its connection will be explained below during the test's description.

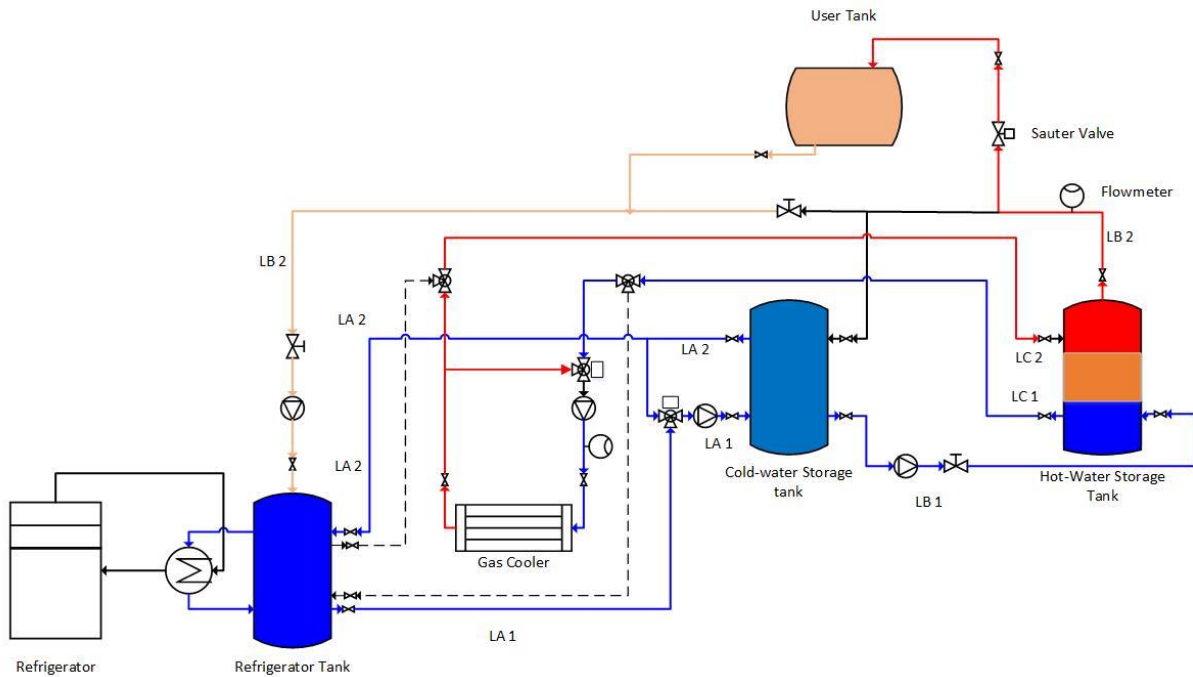


Figure II.8: Schematic diagram of the water loop

As seen in the schematic diagram of the water loop (figure II.8), there are four storage tanks: the cold-water storage tank, the hot-water storage tank, the refrigerator tank, and the user tank.

The refrigerator tank is the tank that contains water under 10 °C, it is always connected to a refrigerator, and it used to cool the water in the system.

The user tank is the tank in which the hot water extracted goes every extraction. It simulates the consumption of domestic hot water during the test as it stores the water extracted from the hot water storage tank.

The water loop system consists of various elements like tanks, pumps, valves, and other hydraulic elements.

### II.3.2.1. Water pumps

There are various pumps in the water loop system [60]:

Baxi Quantum Eco 40 (figure II.9.a) is a circulation pump used in the installation to secure the water flow at demands (line LB1. in figure II.8)

Another Baxi Quantum Eco1025 (figure II.9.b) water pumps is a small pump used in the recirculation of the cold-water storage tank in order to maintain it at the initial temperatures (line LB2 in figure II.8).



a) Baxi Quantum Eco 40



b) Baxi Quantum Eco1025

Figure II.9: Baxi pumps [60]

### II.3.2.2. Three-ways valve

A Danfoss three-way valve is installed with a regulator motor, and it is controlled by a PID controller. This valve is installed between the inlet and outlet of the same cold-water storage tank (between line LA1 and line LA2 in figure II.8), in order to maintain it at a desired temperature.



Figure II.10: Danfoss Three-ways valve

### II.3.2.3. Flow meter [61]

A Siemens SITRANS fm mag5100w (figure II.11) flow meter is used to measure the flow rate of the water extracted.



Figure II.11: Siemens SITRANS fm mag 5100 w flow meter [61]

### II.3.2.4. Regulating valve

A Sauter valve is used in the outlet pipeline of the hot-water storage tank to maintain a desired value of flowrate. This valve is controlled by an electric motor as shown in the figure II.12. The main objective of this valve is open or close to increase or decrease the flow rate at demand.



Figure II.12: Sauter Three-ways valve

### II.3.2.5. Cypex Valve

This valve is an electro-valve, and it works Boolean. It receives an analogical control signal in order to open or close the valve completely and spontaneously.



Figure II.13: Cypex Valve

### II.3.2.6. Thermal storage tank

Two stratified storage tanks are installed in the facility; both are stratified storage tanks Lapesa GX800-RB of 772L [62].

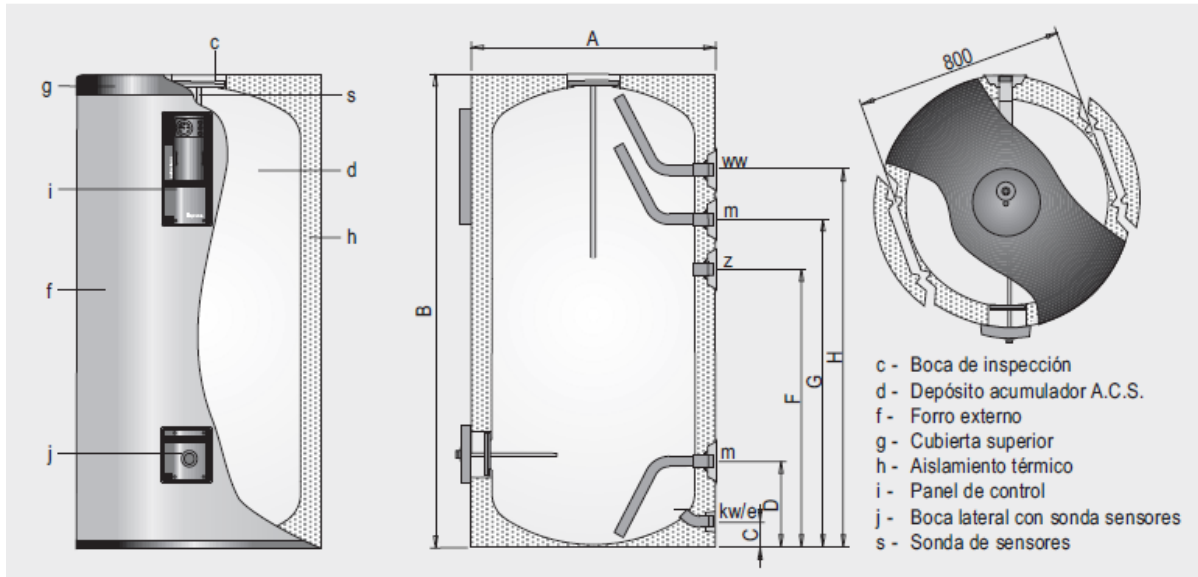


Figure II.14: Schematic diagram of the storage tank [62]

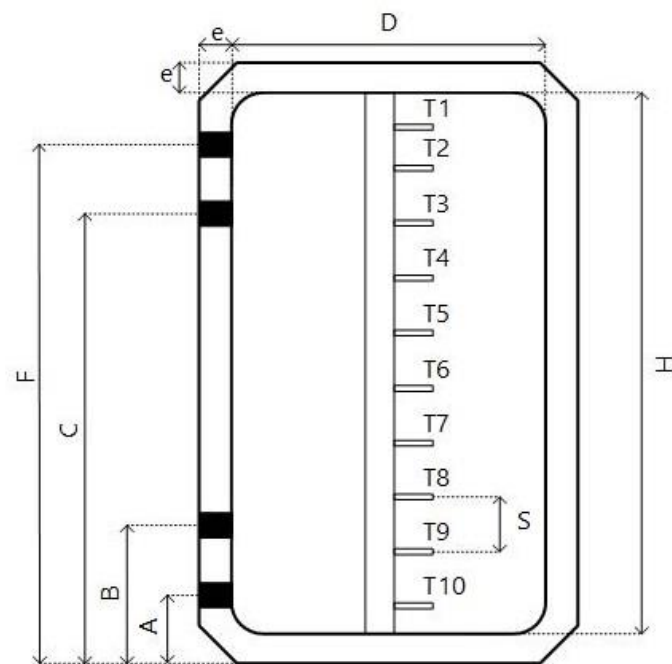
### II.3.3. Stratified storage tank

#### II.3.3.1. Hot water storage tank

The hot-water storage tank is the most important element of the system. A stratified storage tank is the key element, and it is highly recommended in a domestic hot water production system, in which the hot water generated by the heat pump will be stored, it is not only for water storage but also for thermal efficiency of the whole system. Therefore, the stratification has an important role in the performance of the energy storage system. This tank has 10 temperature sensors installed in its central axis (figure II.15 and figure II.16). In the objective to measure the temperature in different regions inside the tank and analyze the stratification of the hot water, and two temperature sensors are installed at the inlet and the outlet of the tank.



Figure II.15: RTD sensors support



- H : Height = 1.68m
- D : Diameter = 0.79 m
- e : Thickness = 0.08 m
- A : Height of the outlet 1 = 0.1 m
- B : Height of the Inlet 1 = 0.33 m
- C : Height of the Inlet 2 = 1.07 m
- F : Height of the outlet 2 = 1.47 m
- S : distance between sensors =  $H/10$

Figure II.16: Schematic diagram of the hot water storage tank

### II.3.3.2. Cold-water storage tank

The cold-water storage tank must be always at the temperature of 10°C. For this reason, a three-ways valve with an electrical motor is installed between the inlet and the outlet of the tank and it is controlled by a PID controller. The purpose of this tank is preparing and maintains the water at the initial conditions as mentioned in the standard.

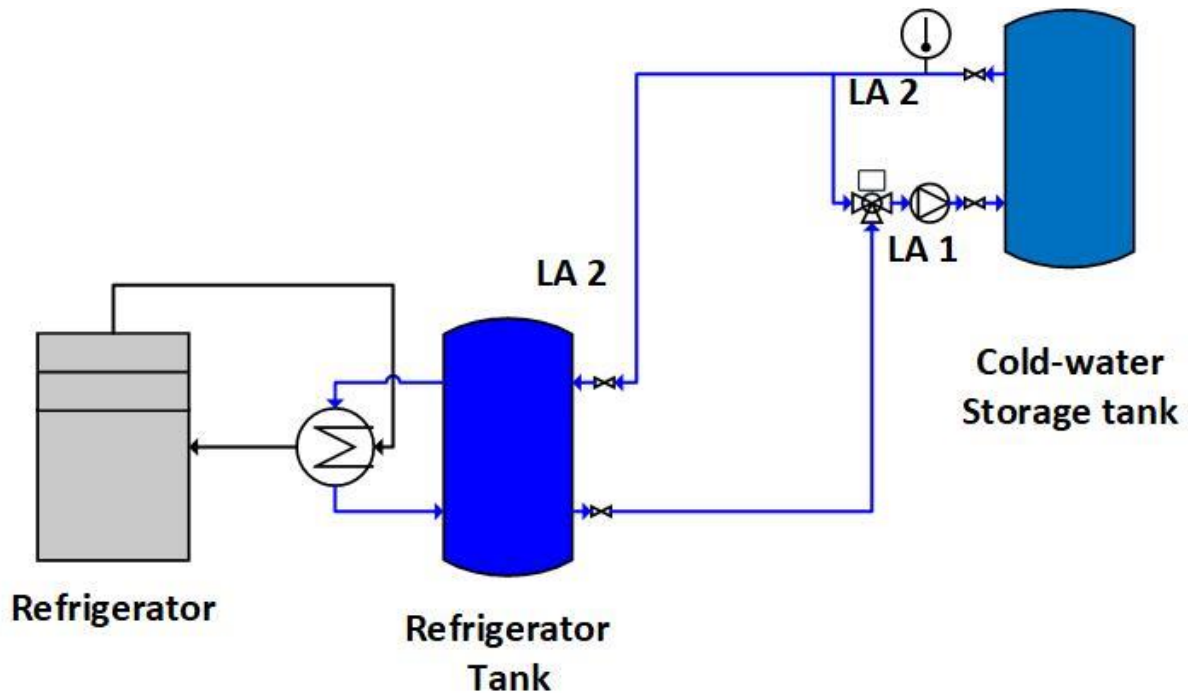


Figure II.17: Cold-water storage tank

Figure II.17 shows the schematic diagram of the cold water and its control system. In order to maintain the water at the initial condition (10 °C), an RTD sensor is placed at the outlet of the tank and a three-ways valve is connected at the inlet of the same tank. The three ways-valve has electric motor, and it is controlled by a PID controller.

This tank is connected to another tank (refrigerator tank) which contains water below 10°C. For this, it is also connected to a refrigerator by means a heat exchanger.

The three ways-valve connects between the refrigerator tank and the cold-water storage tank. The RTD sensor measures the temperature of the tank and send a control signal by mean of a control card in order to open the loop or close the loop and recirculate the water in the tank.



### II.3.3.3. PID Controller

A closed loop is used to control the tank's temperature at the outlet, and it is connected to the source tank with a control valve. A virtual PID have the same characteristics as a physical one. LabVIEW offers an option to set up a PID and it is described in figure II.18.

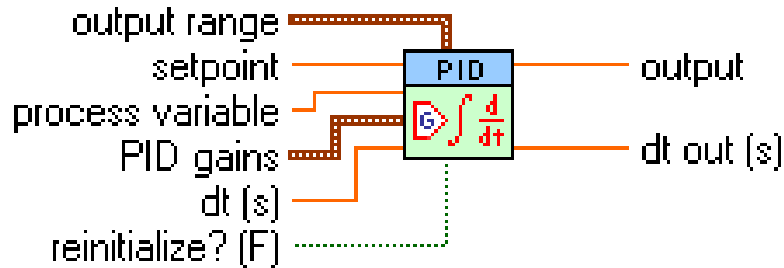


Figure II.18: Virtual PID controller

*Output range:* is the range in which coerce the control output.

*Setpoint:* is the desired value of the process variable being controlled.

*Process variable:* is the measured value of the process variable being controlled.

*PID gains:* are the proportional gain, integral time, and derivative time parameters of the controller.

*dt (s):* is the loop-cycle time.

*Output:* returns the control output of the PID algorithm that is applied to the control process.

The PID's program shown in figure II.19 measures the temperature (process variable), in this case is the cold storage tank's temperature, and if it is different than the desired value (set-point) a signal control (output range) from 0 to 10V is sent to the valve.

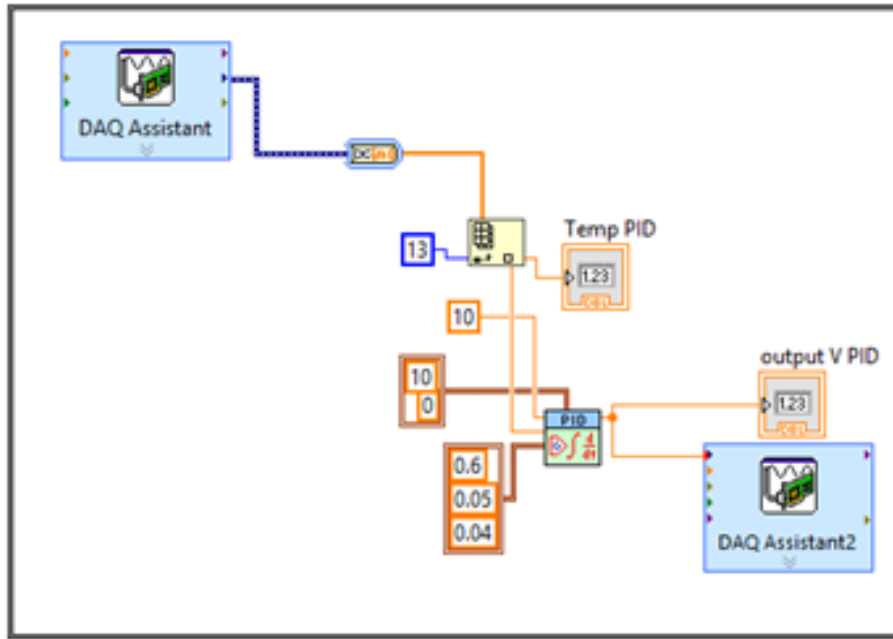


Figure II.19: LabView program of the PID controller

The role of the virtual PID controller is to maintain the cold water always at 10°C, when the temperature of the cold water is less than 10°C, the three-way valve closes the loop between the inlet and the outlet of the storage tank and the water circulates in the tank, if its temperature is greater than 10°C the three way-valve opens the loop, takes colder water (< 10 °C) and mixes it with the stored water until its temperature reaches 10 °C.

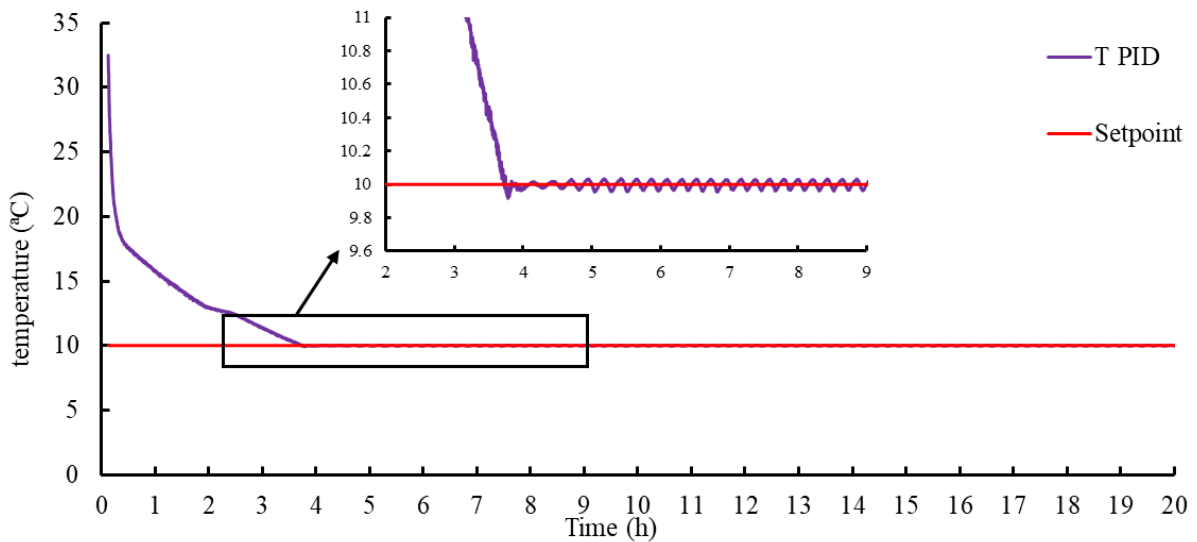


Figure II.20: Temperature of the storage tank controlled by the PID controller

### II.3.3.4 Temperature measurement

As mentioned above, the hot-water storage tank has 10 temperatures sensors installed in its central axis to measure the temperature inside the tank and analyze the stratification phenomenon and two sensors in order to measure the inlet and outlet temperature of the fluid.

All the temperature sensors are RTD PT100 figure II.21.



Figure II.21: RTD PT100 sensor

In the figure II.22 bellow shows the Data acquisition's LabView program of the temperatures using the DAQ Assistance tool.

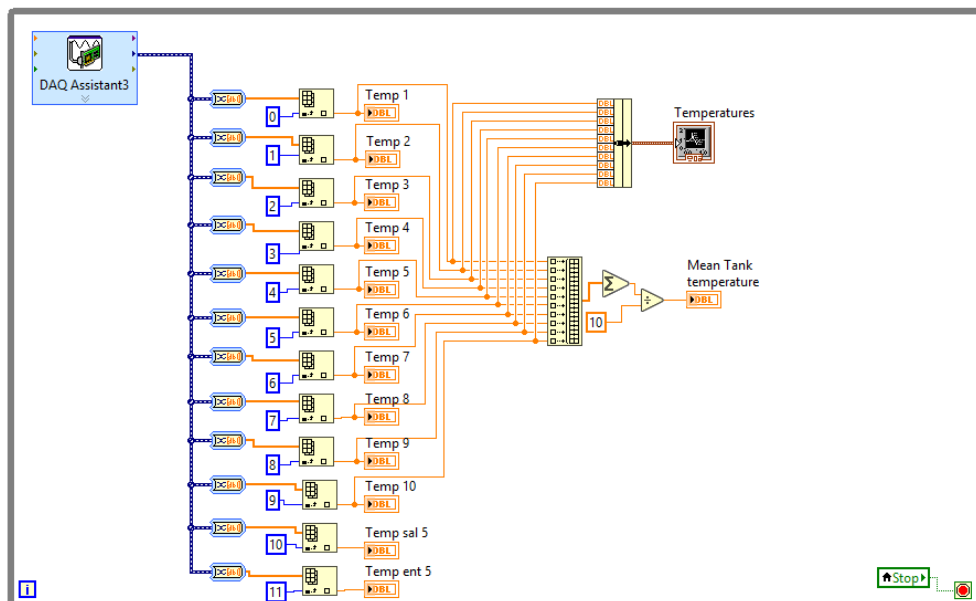


Figure II.22: LabView program of the Temperature measurement

### II.3.3. Data acquisition

In order to perform a high precision measurement and control all the devices in an installation, a high-quality device is needed. National instruments offer various type of control card in this field. National Instrument NI cDAQ 9189 and LabView software are used to control the test [63].



Figure II.23: National Instrument Compact DAQ [63]

The national instrument with 7 modules is used in our laboratory. There are two modules of temperature measurement, two relays, a voltage-current output-input and an analogue output.

#### II.3.3.1. NI 9263

The NI 9263 is an analogue output module, it has four analogue outputs with a range of  $\pm 10V$ . This module is used to control the valve motors of the three-ways valve and the regulating valve.



Figure II.24: National instrument NI 9263 (Voltage analogue outputs Module)

### II.3.3.2. NI 9207

The NI 9207 combination voltage and current input module and it has eight channels of  $\pm 20$  mA input and eight channels of  $\pm 10$  V input. This module is used to measure the flow rate by means of a current analogue input.



Figure II.25: National instrument NI 9207 (voltage and current analogue input module)

### II.3.3.3. NI 9482

The NI 9482 provides connections for four electromechanical relay channels. The relay here is used to control the regulating valve (Sauter Valve), the compressor, the gas cooler pump and the Cypex valve



Figure II.26: National instrument NI 9482 (relay)

### II.3.3.4. NI 9216

The NI 9216 RTD analogue input module provides eight channels and 24 bits of resolution for PT100 RTD measurements. The NI 9216 is compatible with 3- and 4-wire RTD measurements. It is clear that this module is used to measure the temperatures.



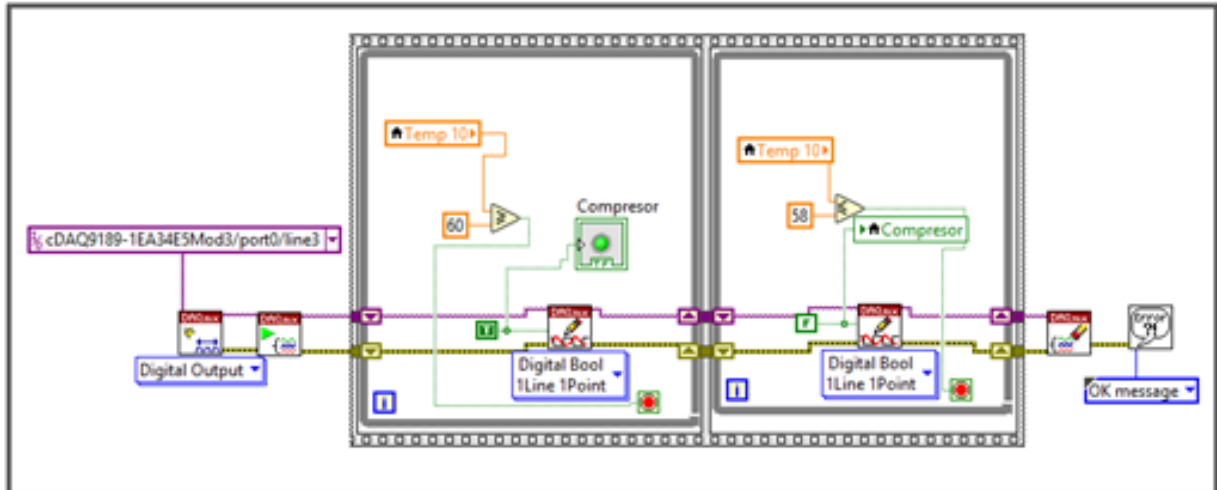


Figure II.28: LabView program of the compressor control

In the other hand the cold-water tank's temperature must be always equal to 10 °C. In this case a PID is used to perform this type of control.

## II.4. Test Steps

### II.4.1. [Step A, B]: Preparation

The steps A and B are the steps named stabilization and filling the accumulation tank and prepare the test set-up. Actually, the two first steps are the preparation of the step C, and the role here is to maintain the test set-up at the initial conditions mentioned in the standard [1].

In the first, the two storage tanks are connected, and the water circulates in both tanks until the temperature difference between the outlet and the inlet of the hot water storage tank is equal to  $\pm 0.2$  °C. Figure II.29 shows the circuit connection of the test facility for Steps A and B.



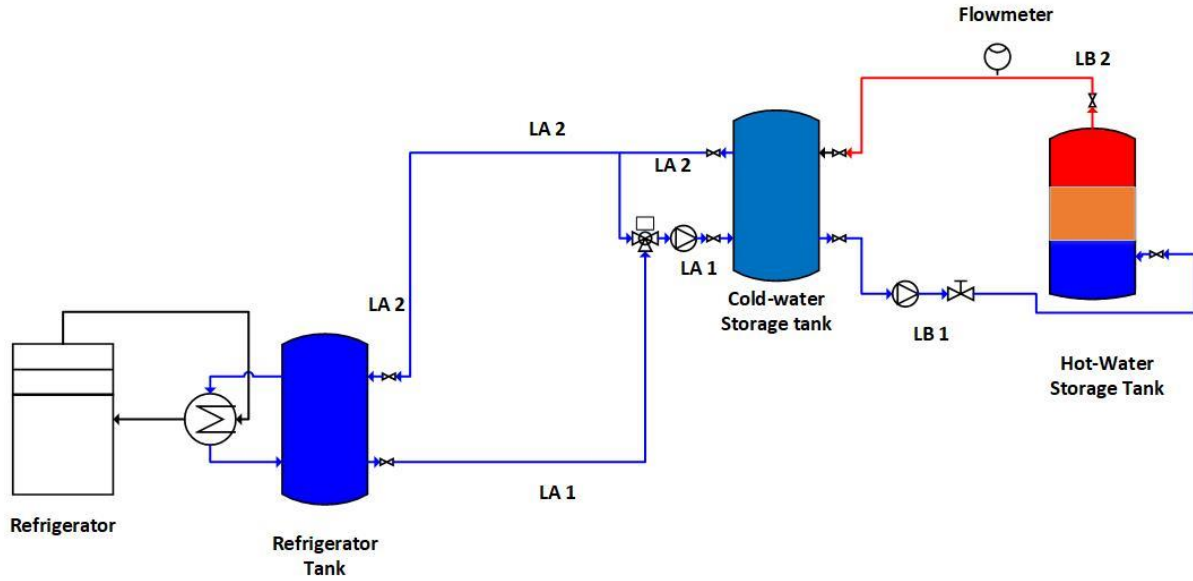


Figure II.29: Water cycle of the test preparation

#### II.4.2. [Step C]: Determination the water heating time

In the step C, the test consists of heating water from the initial temperature (10 °C) and heated it to 60 °C.

This step begins when the initial condition of the step A is accomplished. Once the initial conditions are established, the hot-water storage tank disconnects from the cold-water storage tank, and it is connected to the gas cooler, in order to heat it from this initial temperature condition.

At this step, the water is at 10 °C, the heating process begins by extracting the cold water from the bottom of the tank, sending it to the gas cooler where it is heated, and then, returning to the upper part of the same tank. Figure II.230 illustrates this process. This process continues until the temperature of the water reaches 60 °C.

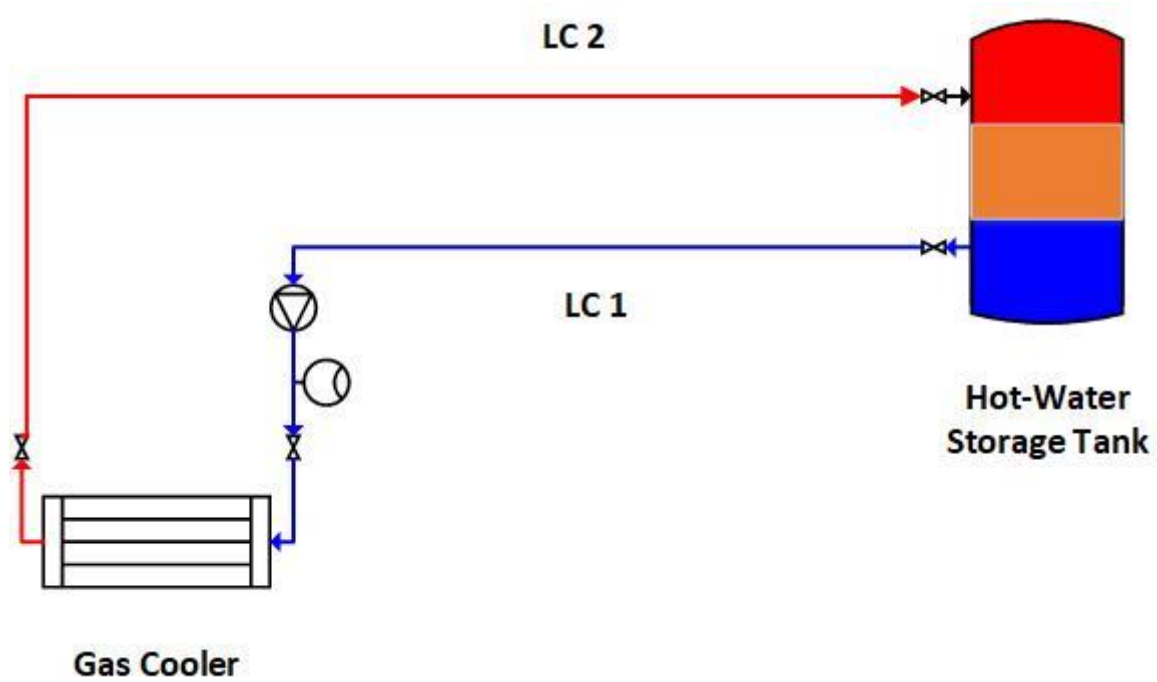


Figure II.30: Water cycle of the step C (water heating process)

Figure II.31 shows the LabView program used to control this step. In this program, the heat pump’s compressor is on, and the hot water tank is connected to the gas cooler. Once the temperature’s value of the upper RTD sensor reaches 60 °C, a control signal is sent to the water pump and the compressor of the heat pump in order to stop function and the valves of the tank to close.

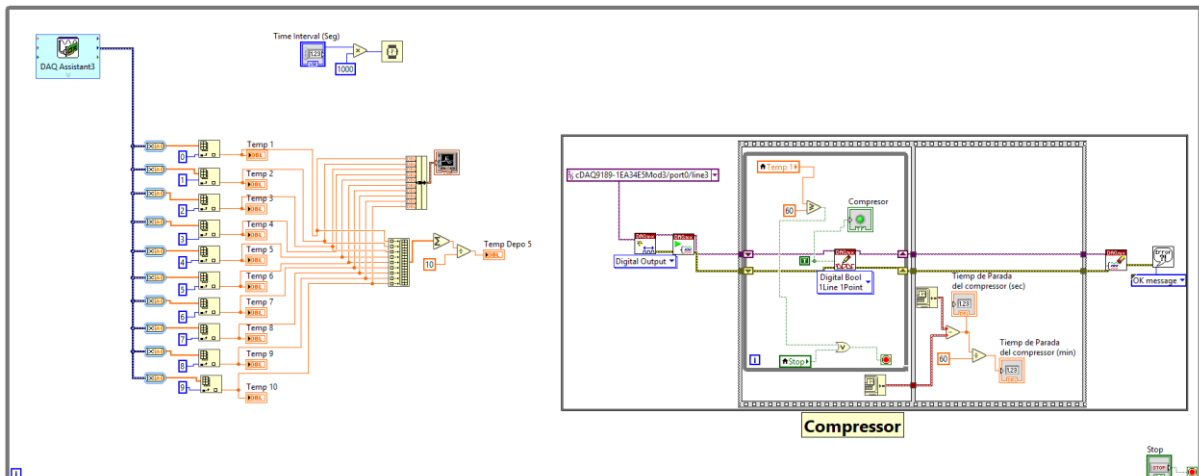


Figure II.31: LabView program of the Step C (water heating step)

Figure II.32 shows the sub-program that is used to control the compressor. During the heating process, the heat pump is on, once the temperature of the storage tank reaches 60 °C, a control signal is sent to the compressor and the water pumps, and the system stops working. In the same

sub-program, also the heating time is calculated, once the compressor stops, the sub program reports the time of the heating process.

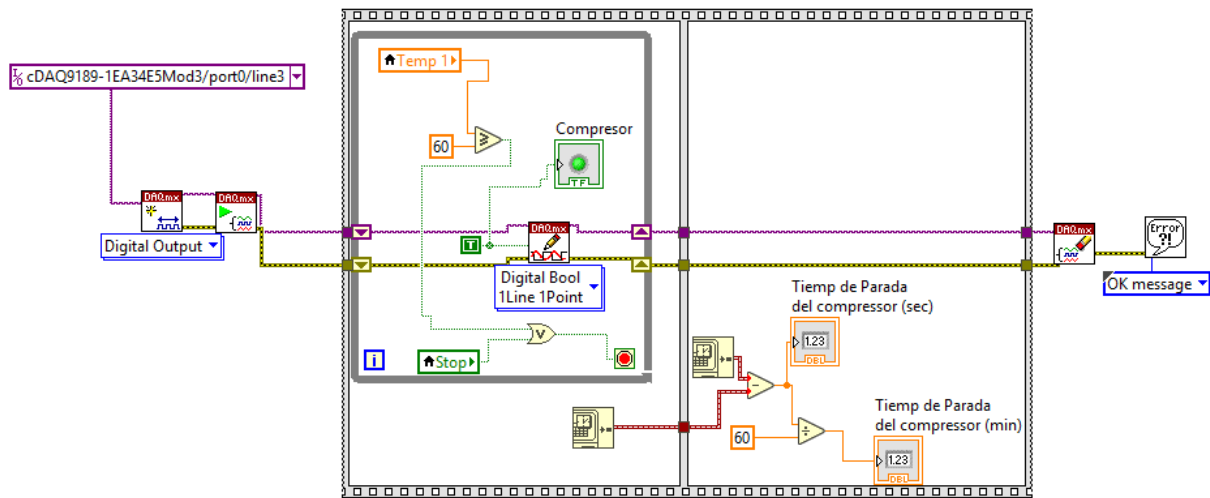


Figure II.32: LabView program of the compressor control

### II.4.3. [Step E]: Extraction profiles

The step E is the step most complicated of the test. This step begins when the hot-water storage tank is at the temperature of 60 °C.

According to the extraction profile and at a specific time, the user extracts an amount of hot water until the energy of hot water consumed is equal to the value mentioned in the extraction profile chosen of the standard. This process of extractions continues depending on the profile chosen in the standard norm.

As mentioned before, at the beginning of the test the hot-water storage tank is at 60 °C, which means that the heat pump's compressor is off. A sub-program is used here to control the temperature of the tank and to maintain the outlet of the hot water always at this temperature, because the hot water in each extraction must be always at 60 °C if it is possible, but never less than 40 °C. Therefore, when the temperature of the tank is equal to 60 °C the heat pump's compressor is off, and if this temperature is below 59 °C the compressor is on.

$$\text{Compressor} \begin{cases} \text{On, } temperature < 59 \text{ }^\circ\text{C} \\ \text{Off, } temperature \geq 60 \text{ }^\circ\text{C} \end{cases} \quad (\text{II.2})$$

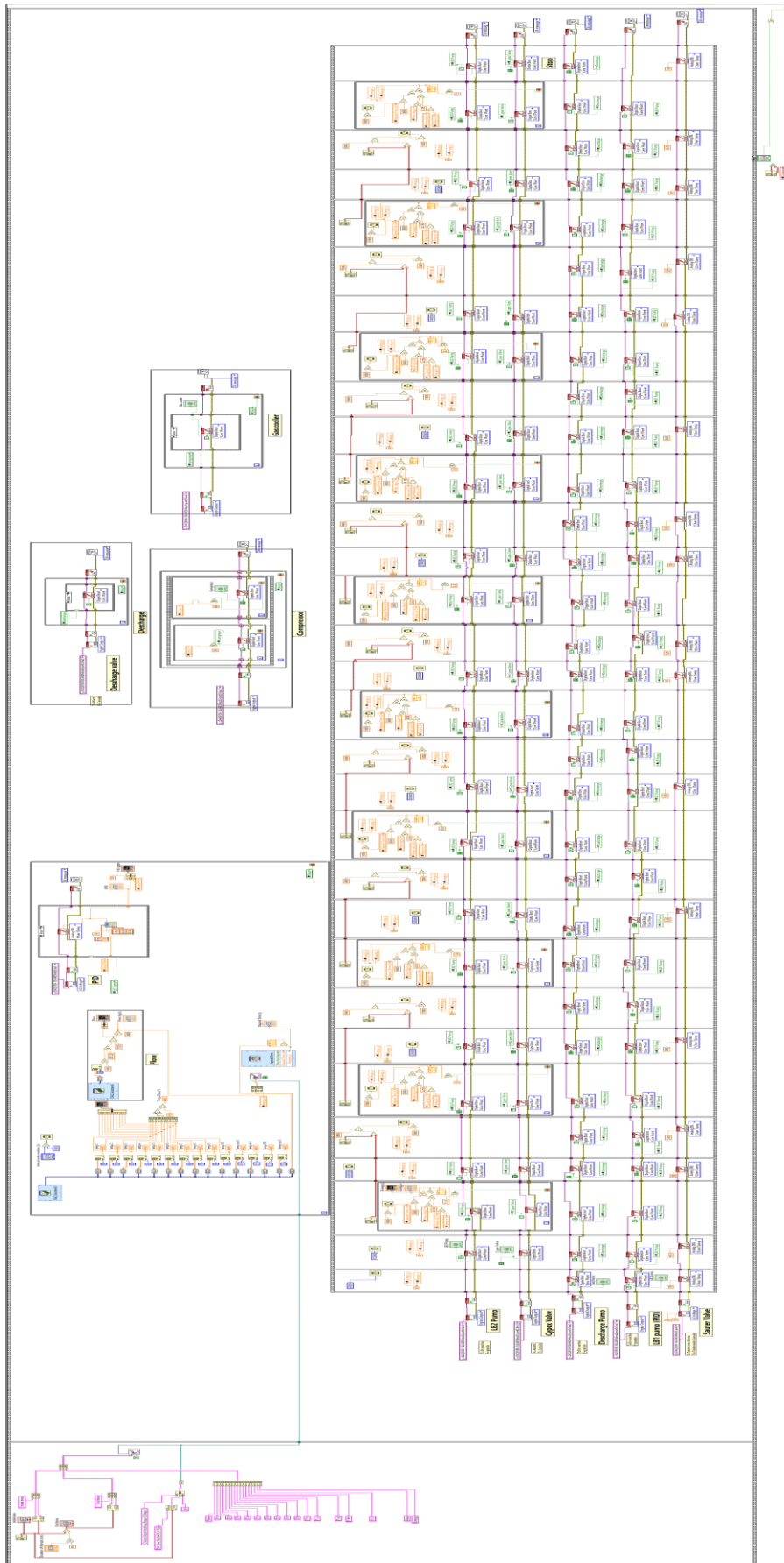


Figure II.33: LabView program of the Step E

In the test setup, the extraction pump is situated between the cold water and hot water storage tanks. At every extraction, the hot water extracted is replaced by cold water at 10 °C. The extraction of the hot water is from the top part of the storage tank and the cold water enters in the bottom part of the storage tank.

At the end of each extraction, the water extracted in the user tank must be returned to the refrigerator tank to be cooled.

At every extraction, the cold-water storage tank disconnects from the refrigerator tank by closing the three-ways valve and recirculates the water in the objective to maintain the water at 10 °C and prevent the temperature drop.

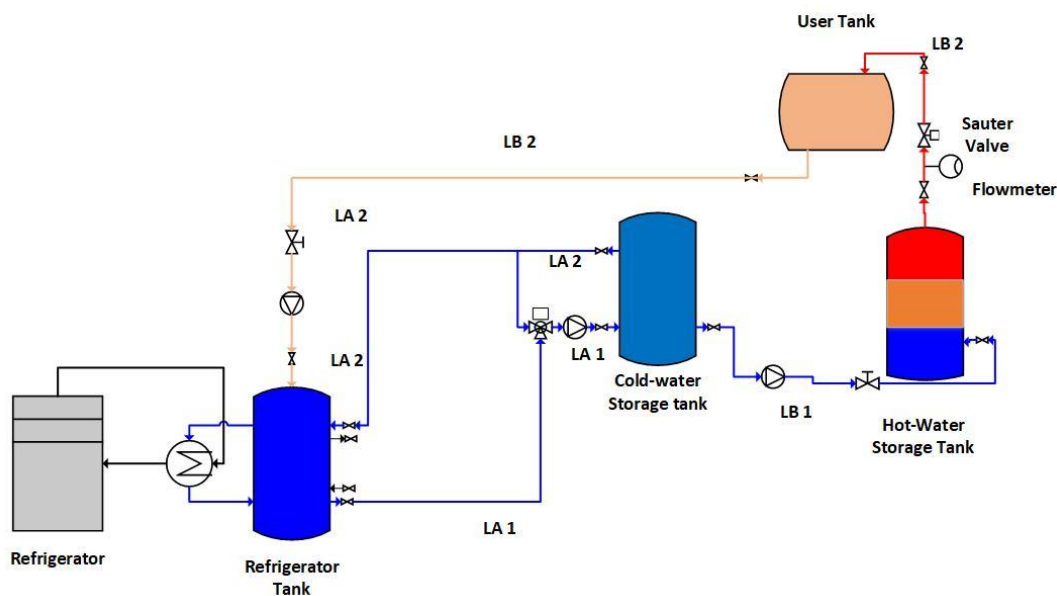


Figure II.34: Water cycle of the step E

### II.4.4. [Step F] water cooling

In this step the hot-water storage tank must be at 60 °C and the cold one at 10 °C and maintained at this temperature during all the step periods. This step consists of cooling the hot-water storage tank by pumping cold water at 10 °C with the maximum flow rate of the chosen profile (annex I) until the temperature of the hot-water decreases and reaches 40 °C. Figure II.35 and figure II.36 describe the test facility connection for this step and the control program used in this step.

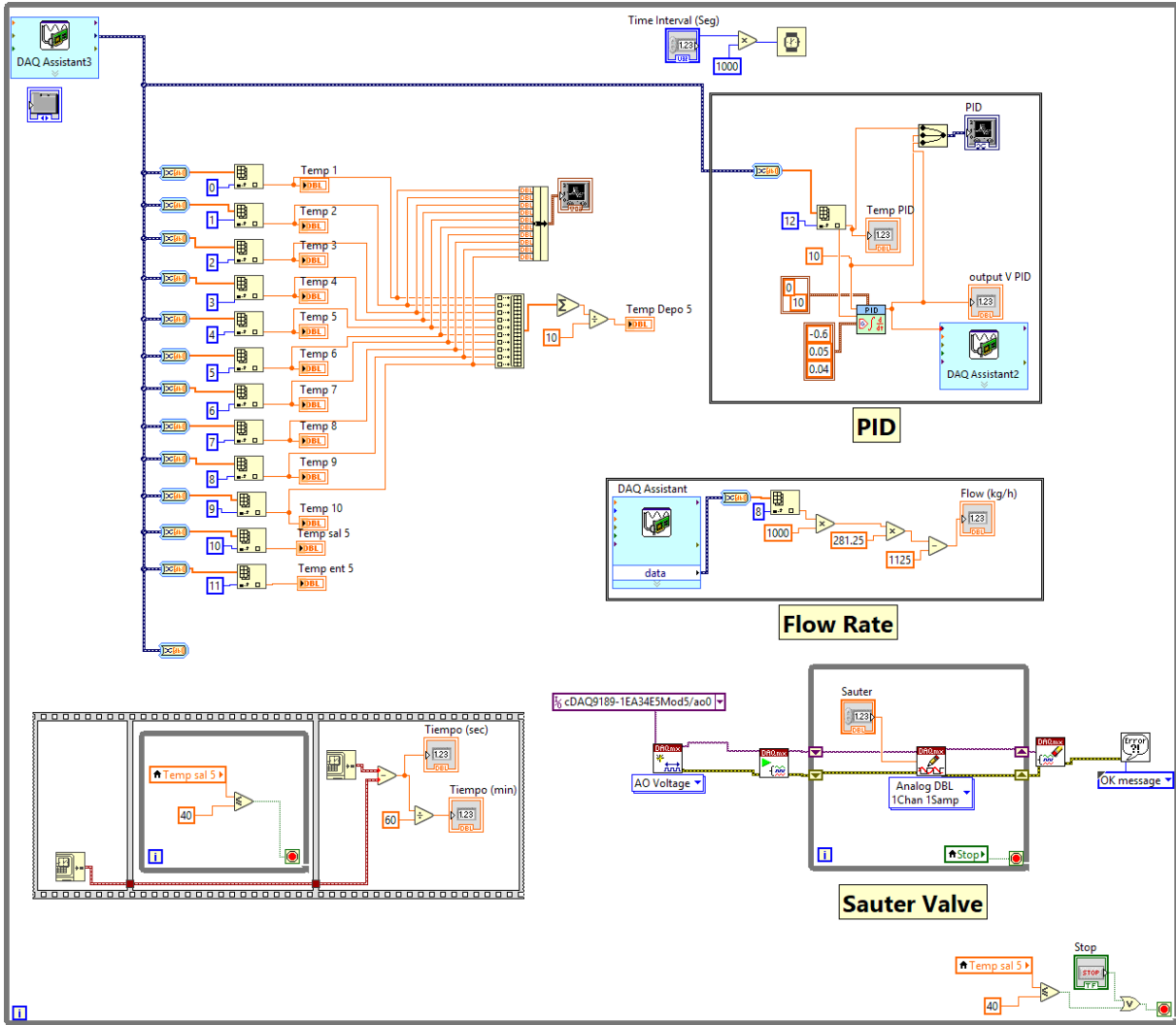


Figure II.35: LabVIEW program of the step F (cooling process)

This sub-program is used to calculate elapsed time of the cooling step (figure II.36).

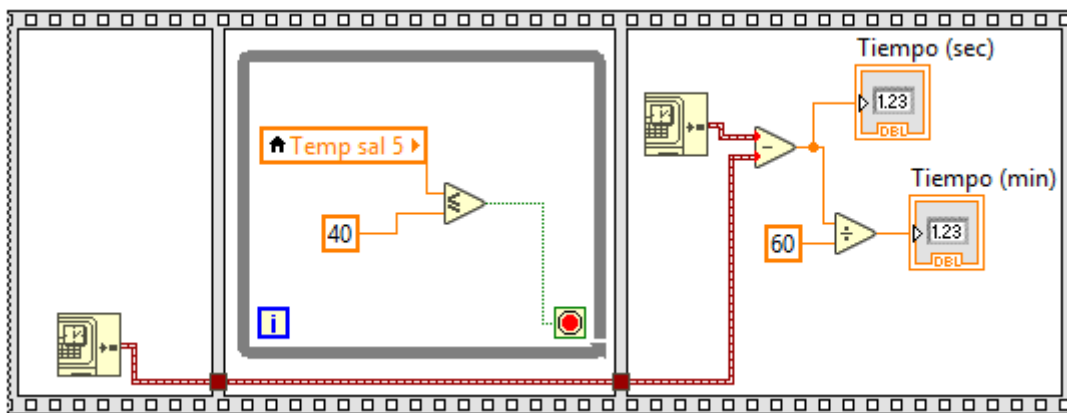


Figure II.36: LabVIEW program of the elapsed time of the step F



# Chapter III





### III.1 Introduction

The impact of various operating conditions and parameters on the thermodynamic performance of the heat pump and the thermos-hydraulic behavior of the storage tank under different operating conditions are studied in this chapter. The experimental results are analyzed and presented. The heating process (step C), the extraction process (Step E) and the cooling process (step F) of the EN 16417 standard are taken into account.

### III.2. Heating Process (Step C)

In this part of this chapter, the heating process is studied under different operating conditions with the objective to analyze the impact of the gas cooler flowrate, the inlet temperature of the evaporator, and the impact of the intermediate heat exchanger (IHX).

Table III.1 shows the test matrix considered, and it summarizes the test conditions considered in the evaporator and the gas cooler. 10 tests were conducted to analyze the energetic performance of the DHW production system developed during the heating process. In all the cases the tests included an IHX except the test number 6 that does not include an IHX.

Table III.1: Test conditions considered at the evaporator in the study.

Test N°	Evaporator			Gas Cooler
	Water inlet Temperature (°C)	Water outlet temperature (°C)	Water flowrate (kg·s <sup>-1</sup> )	Water flowrate (kg·s <sup>-1</sup> )
1	10	7	-	0.0833
2	10	7	-	0.1388
3	10	7	-	0.1944
4	10	7	-	0.25
5	10	7	-	0.3055
6 (Without IHX)	10	7	-	0.3055
7	5	-	0.544	0.3055
8	10	-	0.544	0.3055

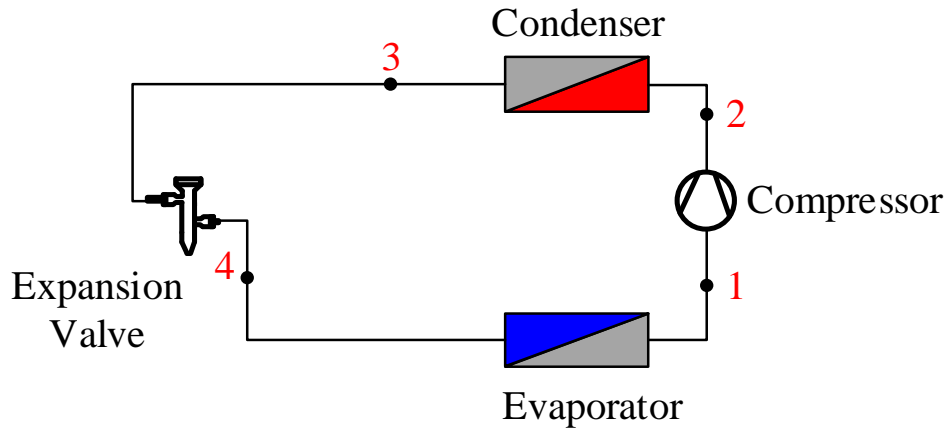
9	15	-	0.544	0.3055
10	20	-	0.544	0.3055

As previously indicated, the tests were designed following the procedure established at the EN 16147 standard. The tests included different inlet and outlet water temperatures and flowrates that were imposed constant during the tests. The inlet water temperature at the gas cooler was always 10 °C at the beginning of the test. There are two main parameters on which this study is focused: the flowrate in the gas cooler and the inlet temperature of the evaporator. The first six rows of the table are the tests where the evaporator conditions were constant, with an inlet and outlet temperature of 10 °C and 7 °C respectively, and the water flowrate at the gas cooler varied between 0.0833 kg·s<sup>-1</sup> and 0.305 kg·s<sup>-1</sup> with an increment of 0.055 kg·s<sup>-1</sup>. Tests 7 to 10 were performed with a fixed gas cooler flowrate of 0.305 kg·s<sup>-1</sup> and a fixed evaporator flowrate of 0.544 kg·s<sup>-1</sup>. These tests were performed at the maximum gas cooler flowrate that can be reached in the facility (0.305 kg·s<sup>-1</sup>). In this case, the inlet water temperature at the evaporator was imposed between 5 °C and 20 °C with an increment of 5 °C.

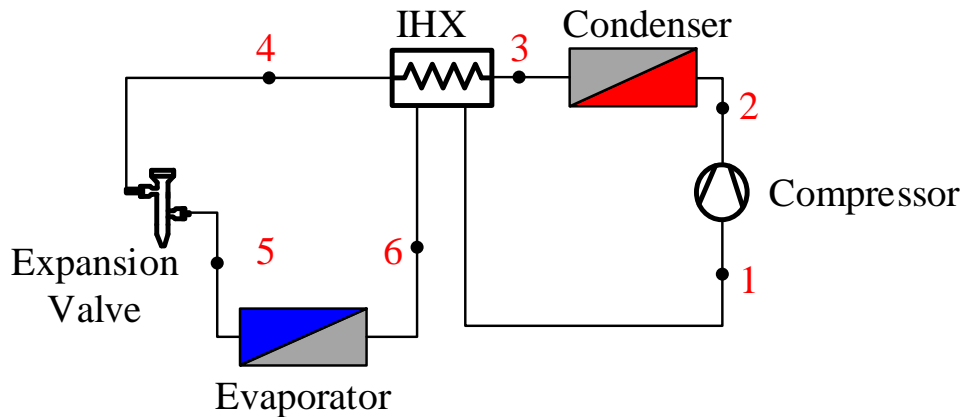
### **III.2.1. Impact of the Internal Heat Exchanger (IHX)**

To show the impact of the IHX on the performance of the heat pump, two configurations of heat pump cycle are taken into account and studied under the same conditions (the test number 5 and 6 of the table III.1).

This test is based on the step C of the standard, and it consists of heating the storage tank from the initial temperature of 10 °C until it reaches 60 °C. The evaporator parameters are taken as constant inlet and outlet temperature of 10 °C and 7 °C respectively. The gas cooler flowrate is constant for both tests and has a value of 0.305 kg·s<sup>-1</sup>.



a) Without IHX



b) With IHX

Figure III.1: Schematic diagram of the two configurations of the trans-critical CO<sub>2</sub> heat pump

Figure III.1 shows a schematic diagram of the two configurations studied. Figure III.1.a presents the schematic diagram of the heat pump cycle without the IHX (base cycle), and the Figure III.1.b represents the schematic diagram of the heat pump with an IHX. In the enhanced cycle (Figure III.1.b) an IHX is added to the base cycle between the outlet of the gas cooler and the inlet of the expansion valve, its main role is to superheat the refrigerant fluid (vapor state) at the inlet of the compressor and sub-cool the fluid (liquid state) at the outlet of the gas cooler and facilitate the expansion process.

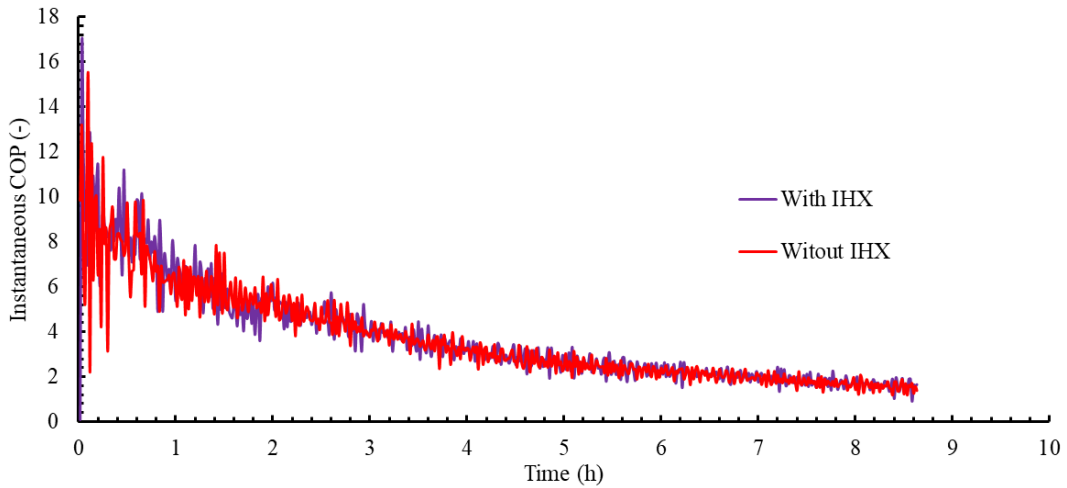


Figure III.2: Instantaneous COP of the heat pump with and without IHX

Figure III.2 presents the instantaneous COP of the system for both heat pump configurations (with and without the IHX). At the beginning of the heating process, the COP of the system in the case of the cycle with the IHX is better than that of the cycle without IHX, and then the COP of the system seems equal for both configurations. The global COP of the cycles with and without IHX has the value of 3.28 and 3.14 respectively, which means that the global COP of the system is enhanced of about 4.42% by adding the IHX.

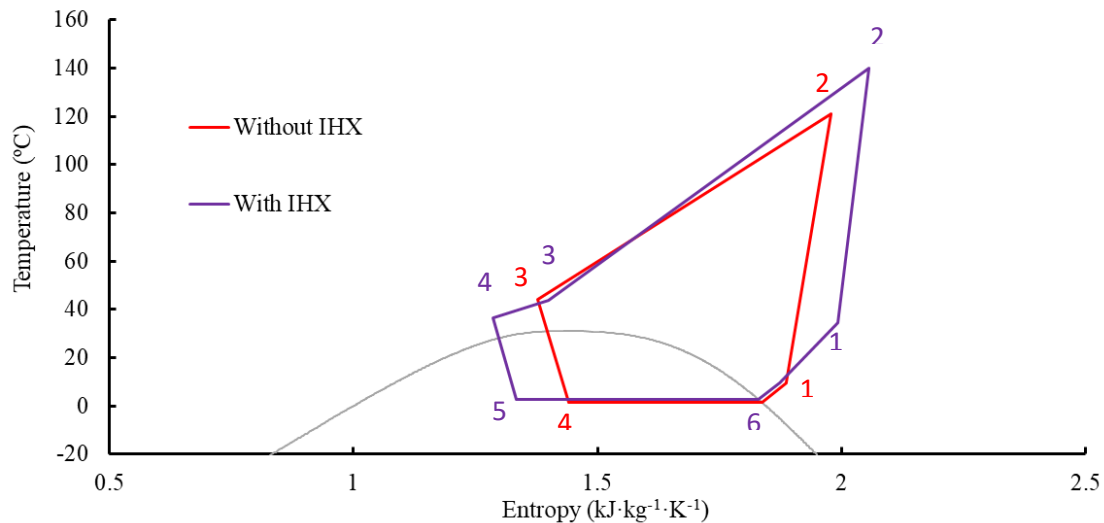


Figure III.3: T-s diagrams comparing the heat pump with and without the IHX

Figure III.3 shows the T-s diagram of the two heat pump configurations with and without IHX. It can be seen clearly that the heat released by the gas cooler is higher in the case of

the heat pumps with IHX, and this is the main reason of the higher COP obtained by the configuration with IHX and this means a high thermodynamic performance system.

### III.2.2 Impact of the gas cooler flowrate

Since the configuration of the heat pump with an IHX (figure III.4) gives higher thermodynamic performance, this configuration is chosen to perform the tests.

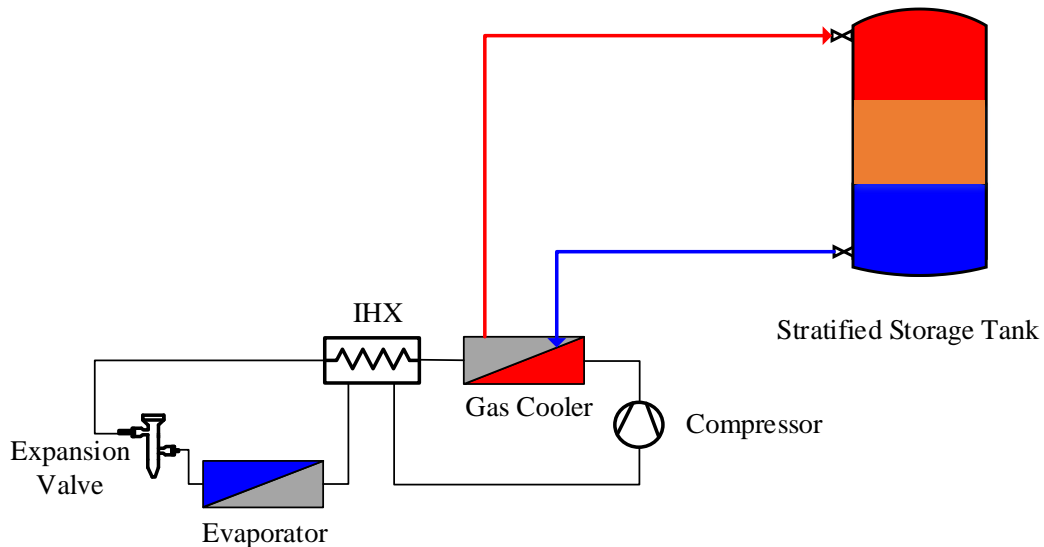
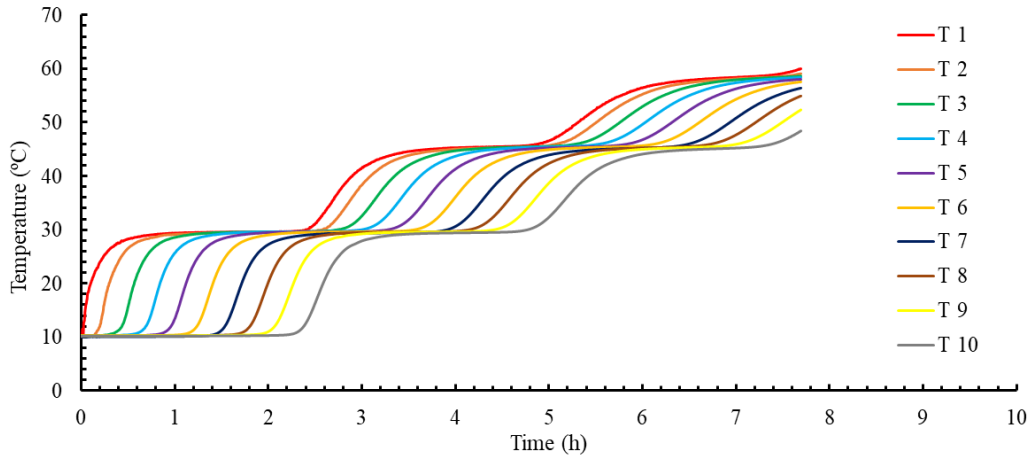
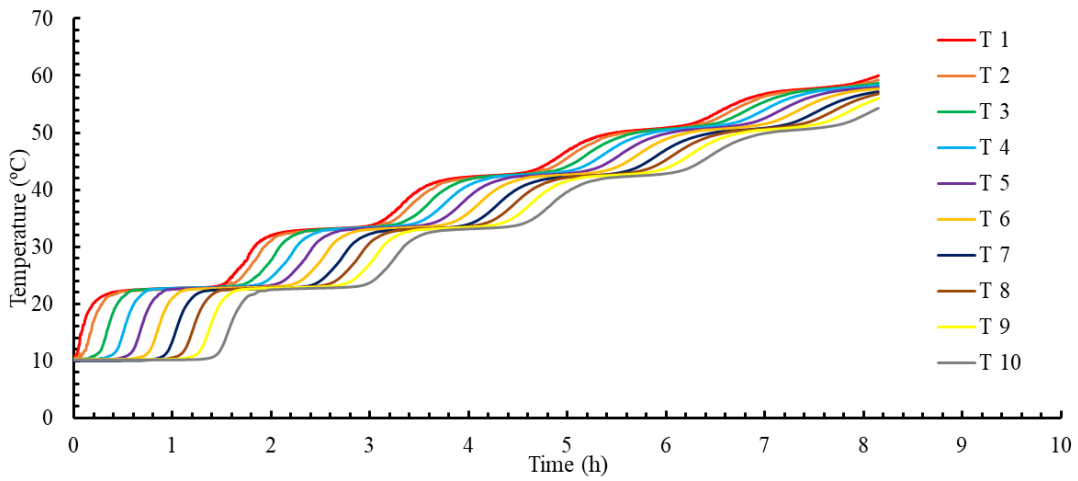


Figure III.4: Schematic diagram of the test facility

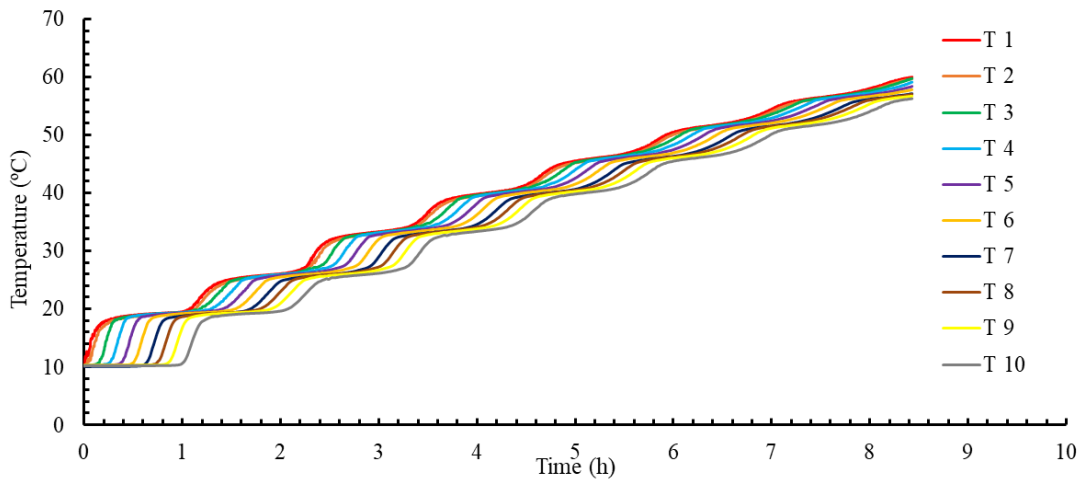
The gas cooler flowrate plays an important role not only on the thermodynamic performance of the heat pump but also on the thermal stratification inside the storage tank. In order to analyze the influence of the gas cooler flowrate, various tests are conducted considering that the operating conditions in the evaporator are taken as constants inlet and outlet temperature of 10 °C and 7 °C respectively. And the gas cooler flowrate varies between  $0.0833 \text{ kg}\cdot\text{s}^{-1}$  and  $3.055 \text{ kg}\cdot\text{s}^{-1}$  with an increment of  $0.055 \text{ kg}\cdot\text{s}^{-1}$ .



a) Gas cooler flowrate =  $0.083 \text{ kg}\cdot\text{s}^{-1}$



b) Gas cooler flowrate =  $0.138 \text{ kg}\cdot\text{s}^{-1}$



c) Gas cooler flowrate =  $0.194 \text{ kg}\cdot\text{s}^{-1}$

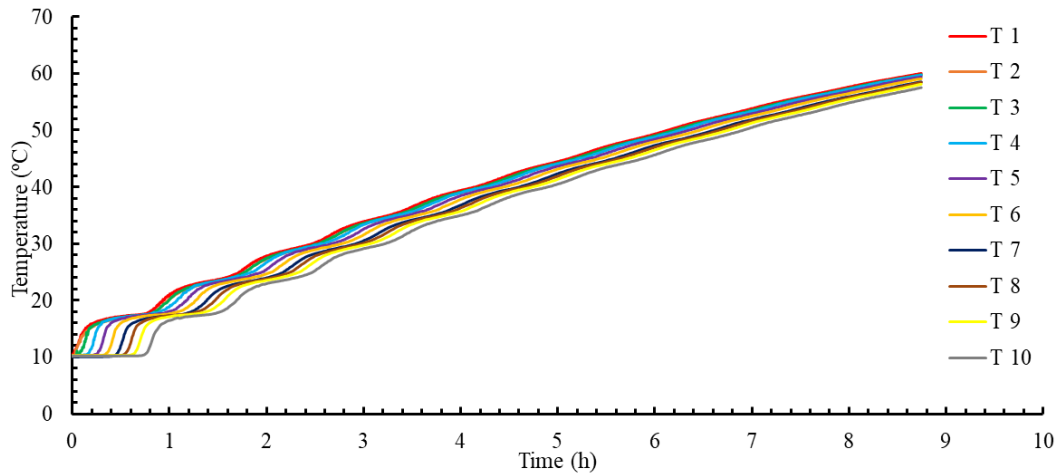
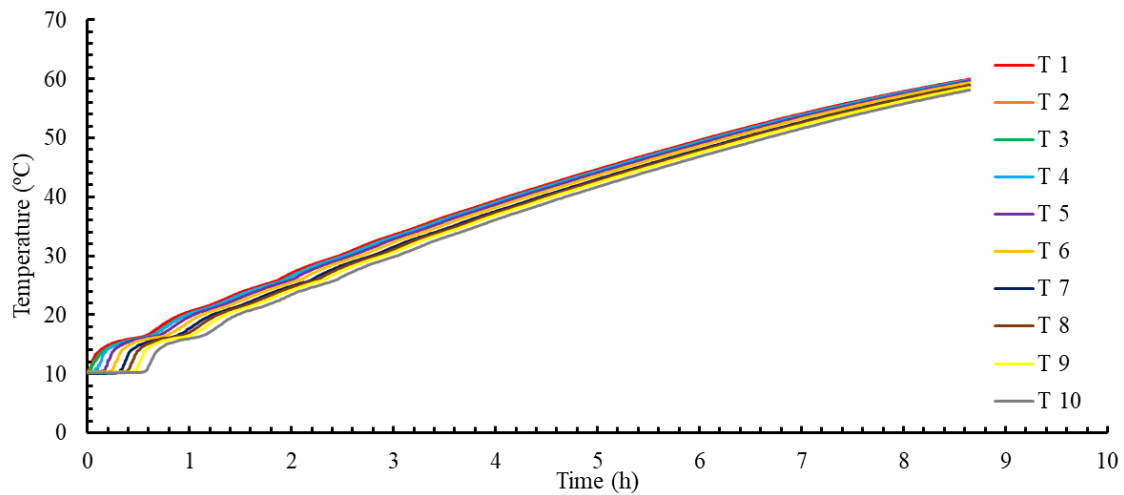
d) Gas cooler flowrate =  $0.25 \text{ kg}\cdot\text{s}^{-1}$ e) Gas cooler flowrate =  $0.305 \text{ kg}\cdot\text{s}^{-1}$ 

Figure III.5: Temperature evolution of the 10 RTD sensors in function of time and for different gas cooler flowrate values.

Figure III.5 shows the temperature evolution of the 10 RTD sensors in function of time and for different flowrate values during the heating process. From these figures, it can be seen that the temperature evolution inside the storage tank depends highly on the gas cooler flowrate. In the case of higher flowrate, the temperature of the entire tank begins to heat up from the beginning of the heating process and the storage tank has a homogenous temperature, the temperature increases with a continuous manner which means that there is no stratification in the storage tank. On the other hand, in the case of lower flowrate, the storage tank has different temperature at different heights, the



temperature of the top part is much higher than that of the lower one, the bottom part remains at the initial temperature until the top part heated up, for example, the temperature of the lowest layer remains at the initial temperature until the layer above it heated up, and then its temperature begins to increase.

It can be noticed also, as the flowrate increases the temperature gradient between the top and the bottom of the storage tank decreases, and this is due to the vertical velocity and the time required of the hot water to travel from the top (inlet) of the tank to the bottom of the storage tank.

During the heating process, and in the case of lowest flowrate the temperature evolution increases with a discontinued manner making stages. As the flowrate in the gas cooler increases, the traveling velocity inside the storage tank increases, and the temperature gradient between the top and the bottom of the storage tank decreases, and this can be translated as the heating capacity of the gas cooler at a specific flowrate. As the gas cooler flowrate increases the temperature on the storage tank is more homogenous and there is no stratification, resulting a higher energy accumulation in the storage tank.

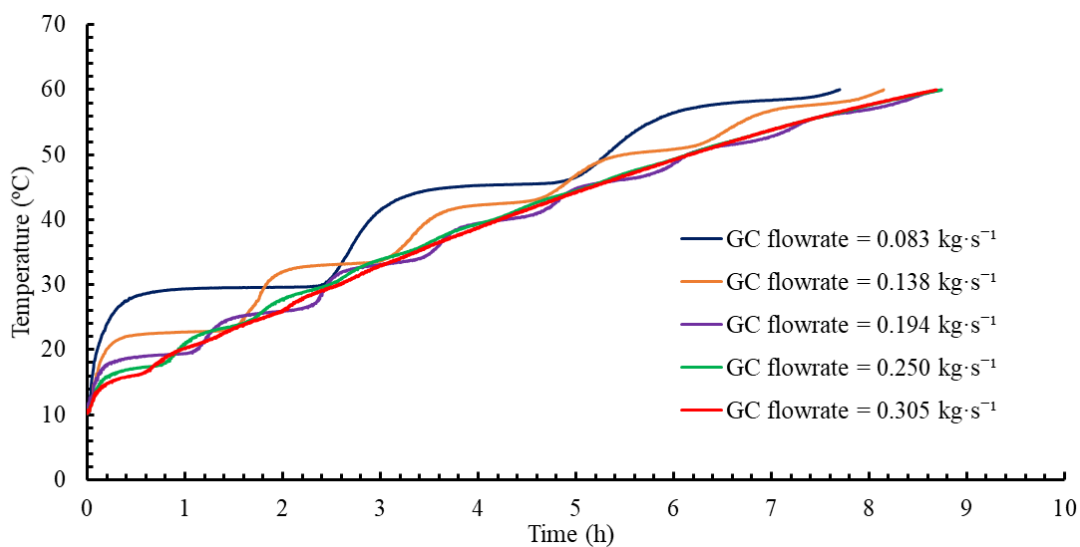


Figure III.6: Temperature distribution of the topper RTD sensor in function of time and for different gas cooler flowrate values.

Figure III.6 shows the temperature evolution of the upper part of the storage tank. Furthermore, the gas cooler flowrate has an impact not only on the stratification inside the storage tank, but also on the heating time of the heating process. In the case of lower

flowrate, the heating time is smaller than that of the higher flowrate but with a penalty of the energy stored.

In order to evaluate the thermodynamic performance of the heat pump, the COP is the suitable dimensionless number that can be used, and it is defined as the ratio of the energy released by the gas cooler to the energy consumed by the compressor (eq. III.1)

$$COP_{inst} = \frac{dE_{tank}(t)}{dE_{comp}(t)} \quad (III.1)$$

where  $dE_{comp}$  is the instantaneous electrical energy consumed by the compressor during the heating process in (kJ). (The energy of the recirculating pumps is neglected)

$dE_{tank}$  in kJ is obtained from:

$$dE_{tank}(t) = \int_0^H \frac{\pi D^2}{4} \cdot \rho \cdot C_p \cdot T_i(t) \cdot d\xi - \int_0^H \frac{\pi D^2}{4} \cdot \rho \cdot C_p \cdot T_i(t - dt) \cdot d\xi = \sum_{i=1}^{i=10} C_p \cdot dT_i(t) \cdot \Delta m \quad (III.2)$$

And  $dT_i(t) = T_i(t) - T_i(t-dt)$  is the temperature variation of the measured water temperature at height level  $i=i \cdot H/10$  of the tank during the heating lapse  $dt$ .

And the global COP is calculated as the following equation:

$$global\ COP = \frac{E_{tank}}{E_{comp}} = \frac{\int_0^H \frac{\pi D^2}{4} \cdot \rho \cdot C_p \cdot (T_i(t=t_{tank}) - T_i(t=0)) \cdot d\xi}{E_{comp}} = \frac{\sum_{i=1}^{i=10} C_p \cdot (T_i(t=t_{tank}) - T_i(t=0)) \cdot \Delta m}{E_{comp}} \quad (III.3)$$

where:

$\rho$  is the water density in  $kg \cdot m^{-3}$ .

$T_i(t=t_{tank}) - T_i(t=0)$  is the temperature variation of the measured water temperature at height level  $i=i \cdot H/10$  of the tank during the heating period.

$\Delta m$  : is one-tenth of the water mass of the tank (M) in kg ( $M/10$ ).

$C_p$  : is the specific heat of the hot water, in  $kJ \cdot kg^{-1} \cdot K^{-1}$ .

The instantaneous COP is obtained from Equation III.1 at each time step of the data acquisition process during the test. Finally, an averaged or accumulated COP can be obtained for each time  $t$  of the heating process by considering the energy consumed by

the compressor and the energy accumulated at the tank from the beginning of the test until instant  $t$ :

$$accumulated\ COP = \frac{E_{tank}(t)}{E_{comp}(t)} = \frac{\int_0^t \frac{\pi D^2}{4} \cdot \rho \cdot c_p \cdot (T_i(t) - T_i(t=0)) \cdot d\xi}{E_{comp}(t)} = \frac{\sum_{i=1}^{i=10} c_p \cdot (T_i(t) - T_i(t=0)) \cdot \Delta m}{E_{comp}(t)} \quad (III.4)$$

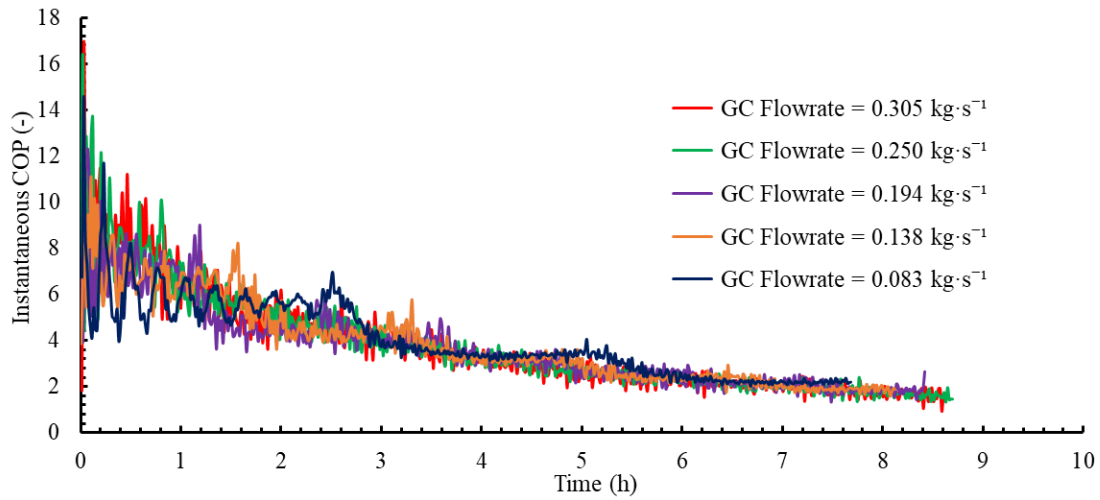
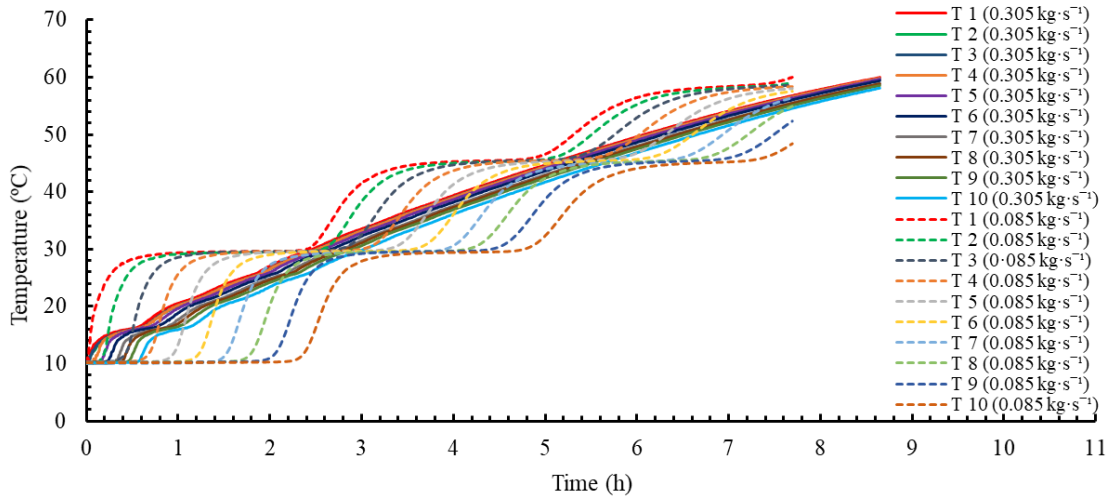


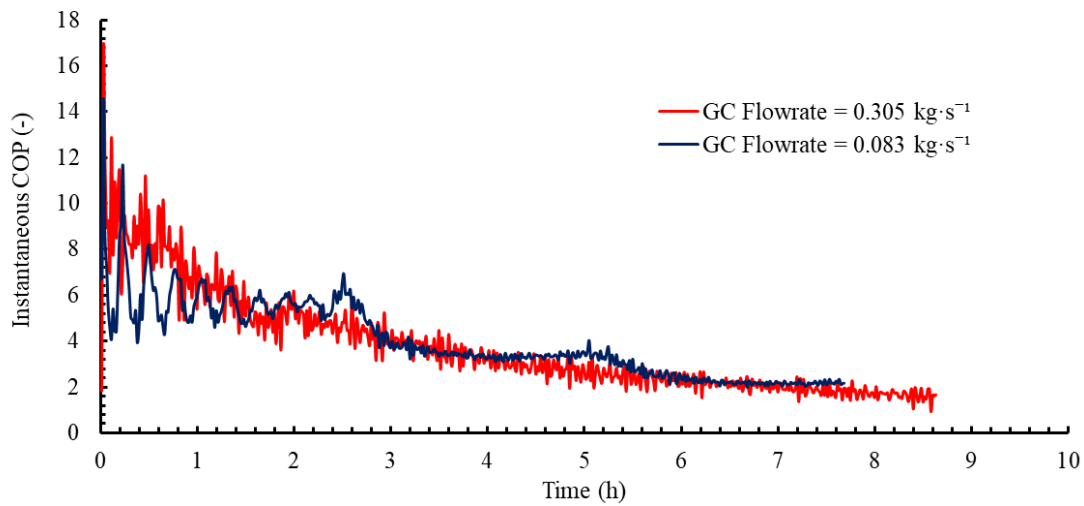
Figure III.7: Evolution of the instantaneous COP in function of time for different gas cooler flowrate cases.

Figure III.7 shows the evolution of the instantaneous COP in function of time for different gas cooler flowrate cases. The COP in the case of higher flowrates has initially a higher value and then it begins to decrease. Contrarily, in the case of the lowest flowrate, the COP of the system has the lowest value at the beginning of the heating process, also it can be seen the stages on the COP, and this is due to the inlet temperature of the gas cooler.

In the case of the lowest flowrates and in the first third of the heating time, the bottom of the tank remains at the initial temperature and has the lowest temperature resulting lower temperature at the inlet of the gas cooler which gives a higher COP. On the other hand, and in the case of higher flowrates, the hot water travels with a high vertical velocity inside the storage tank which make a homogeneous temperature in all the storage tank,



a) Temperature evolution at different heights of the hot water storage tank for the case of lowest and highest gas cooler flowrate



b) Instantaneous COP evolution for the lowest and highest gas cooler flow rate

Figure III.8: Comparison of temperature evolution at different heights of the hot water storage tank and the instantaneous COP for the case of lowest and highest gas cooler flowrate.

Figure III.8 a and b show a comparison of temperature evolution at different heights of the hot water storage tank for the case of the lowest and the highest gas cooler flowrate. This figure explains and clearly shows the impact of the gas cooler flowrate on the thermal stratification of the storage tank and the thermodynamic performance of the heat pump. In a general word, the lower gas cooler flowrate gives better performance of the DHW production system.

The stratification has a positive impact on the thermodynamic performance of the heat pump which enhances the thermodynamic performance of the system, and it gives a higher COP in the case of lower flowrates, but it results in a lower amount of energy accumulated in the storage tank. Figure III.8 presents the global COP of the system (left axis) and the energy accumulated (right axis) for different gas cooler flowrates. The global COP of the system has a decreasing tendency with the increase of the gas cooler flowrate, in which the case of the lowest gas cooler flowrate ( $0.0833 \text{ kg}\cdot\text{s}^{-1}$ ) has the highest value of global COP 3.68 and the lowest value of the energy stored. Contrarily, in the highest gas cooler flowrate case ( $0.3055 \text{ kg}\cdot\text{s}^{-1}$ ), it has a lowest value of the global COP 3.28 with a high energy stored in the storage tank. Both, the COP of the system and the energy stored, depend highly on the gas cooler flowrate.

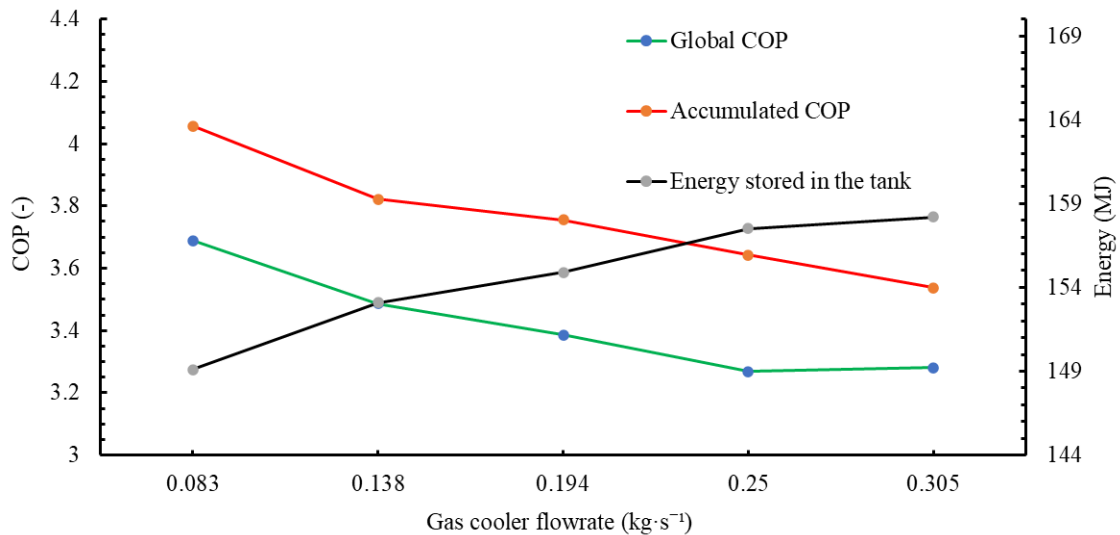


Figure III.9: Evolution of the global COP and the energy stored for different gas cooler flowrate cases studied

Table III.2: The COP and the energy stored in the storage tank.

Gas cooler flow rate $\text{kg}\cdot\text{s}^{-1}$	Global COP of the DHW production system	Accumulated COP of the $\text{CO}_2$ heat pump	Thermal energy storage $E_{\text{tank}}$ (MJ)
0.083	3.688	4.021	149.1
0.138	3.486	3.953	153.1
0.194	3.386	3.944	154.9
0.25	3.269	3.733	157.5
0.305	3.280	3.756	158.2

Table III.2 summarizes the results of the thermodynamic performance of the heat pump and the energy stored in the storage tank.

For more details of the energy accumulation analysis of the stratified storage tank, the energy stored by the storage tank in each horizontal layer are presented in the following figures. In this analysis a dimensionless parameter for time, temperature and the height are used. They are defined in the equations: III.5, III.6 and III.7.

$$t^* = \frac{t_{inst}}{t_{test}} \quad (III.5)$$

$$T^* = \frac{T_i}{T_{60}} \quad (III.6)$$

$$H^* = \frac{h_i}{H_{tank}} \quad (III.7)$$

The energy efficiency  $E^*$  [65] can be defined as the ratio of the actual measured energy accumulated to the energy accumulated in a perfectly stratified storage tank from the beginning of charging until the end of the test (eq. III.8). The energy efficiency is based on the first law of thermodynamic that can be useful to analyze the energy and the thermal stratification within the storage tank

$$E^* = \frac{Q_{exp}}{Q_{stratified}} \quad (III.8)$$

$$ET = \int_0^{t_{test}} \dot{m} \cdot c_p \cdot (T_{i+1} - T_i) dt \quad (III.9)$$

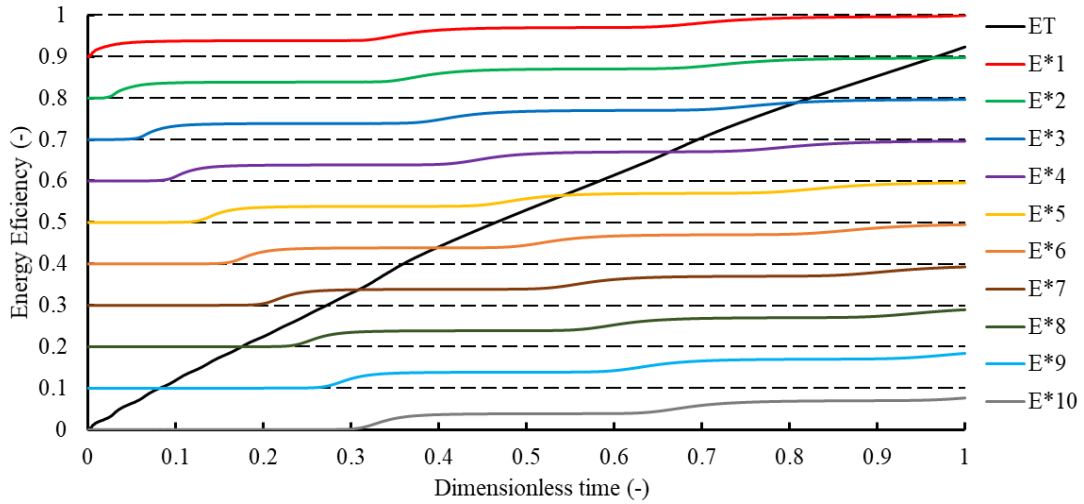
Where:

$$Q_{exp} = \int_0^{t_{test}} \dot{m} \cdot \rho \cdot c_p \cdot (T_{exp} - T_{cold}) dt \quad (III.10)$$

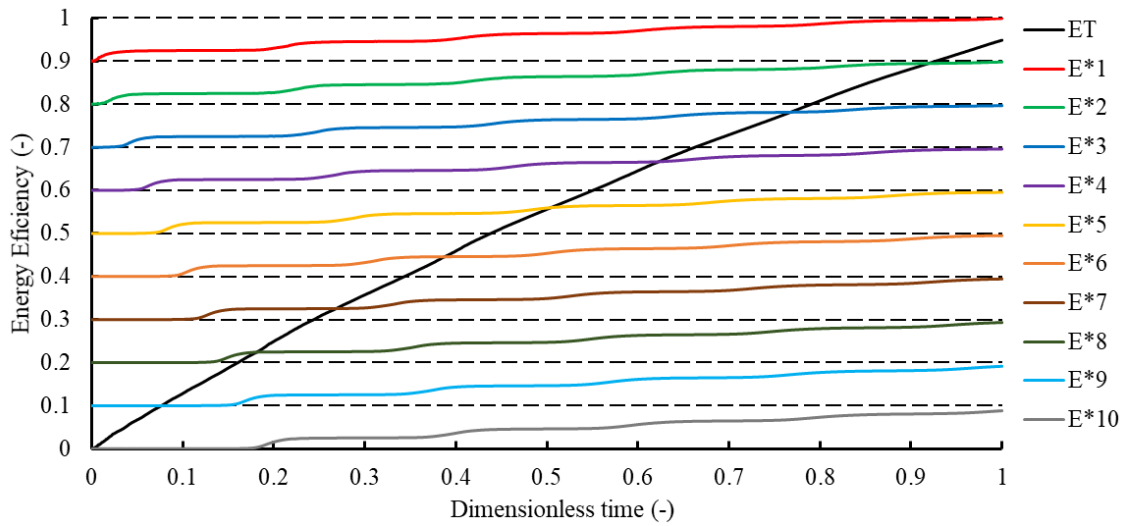
And,

$$Q_{stratified} = \int_0^{t_{test}} \dot{m} \cdot \rho \cdot c_p \cdot (T_{hot} - T_{cold}) dt \quad (III.11)$$

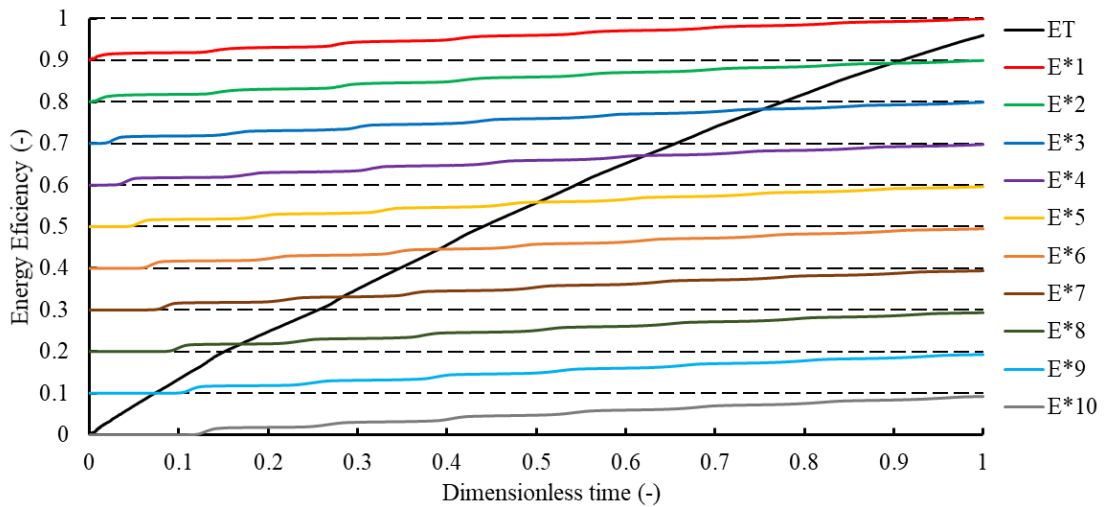
$T_{hot}$  and  $T_{cold}$  are the hot and cold temperature,  $T_{exp}$  is the temperature measured experimentally.  $T_{i+1}$  and  $T_i$  are the temperature of the layers at any instance.



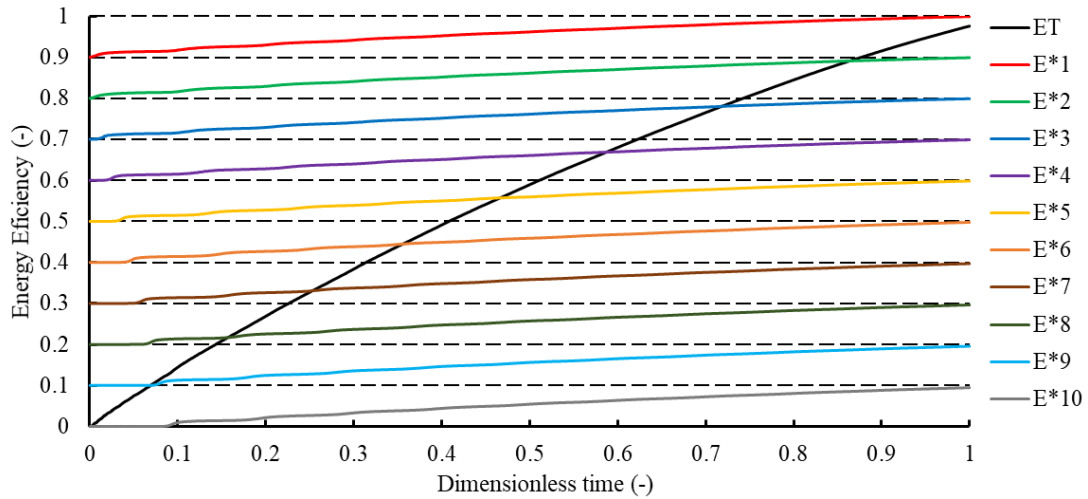
a) Gas cooler flowrate =  $0.083 \text{ kg}\cdot\text{s}^{-1}$



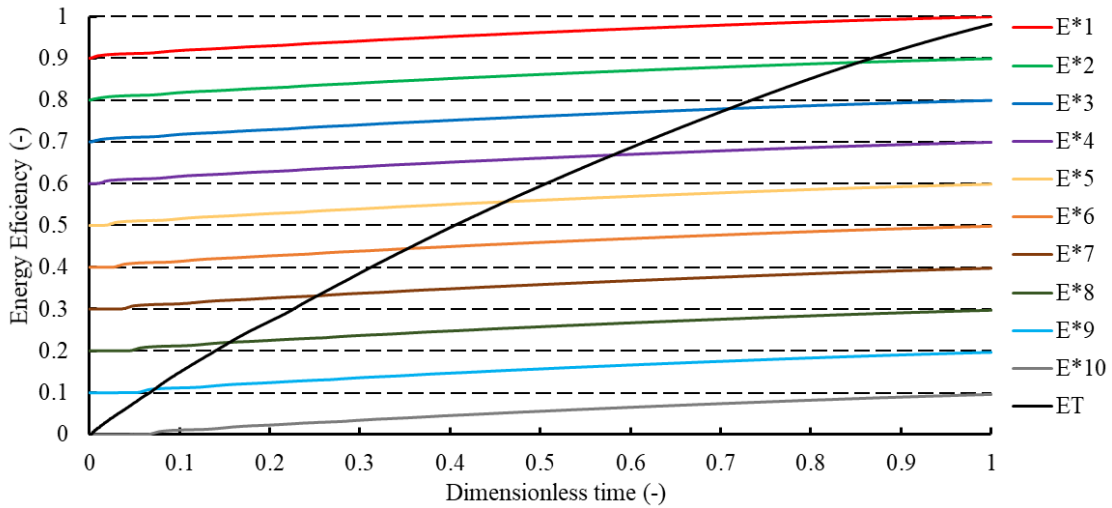
b) Gas cooler flowrate =  $0.138 \text{ kg}\cdot\text{s}^{-1}$



c) Gas cooler flowrate =  $0.194 \text{ kg}\cdot\text{s}^{-1}$



d) Gas cooler flowrate =  $0.25 \text{ kg}\cdot\text{s}^{-1}$



e) Gas cooler flowrate =  $0.305 \text{ kg}\cdot\text{s}^{-1}$

Figure III.10: Tank energy efficiency ( $E^*$ ) of every stratification layer for different gas cooler flowrates

Figure III.10 shows the tank energy efficiency ( $E^*$ ) of each stratification layer for different gas cooler flowrates. It can be seen that the tank energy efficiency increases with the increase of the dimensionless time for the 10 layers and for all gas cooler flowrate cases. In the case of lowest gas cooler flowrate ( $0.083 \text{ kg}\cdot\text{s}^{-1}$ ), in the lowest layer and at the beginning of the heating process, the tank energy efficiency is minimal and equal to 0, until the dimensionless time reaches about 1/3 of the total dimensionless time, and this is due to the temperature propagation inside the storage tank and at the end of the heating process, the total amount of the accumulated energy is only at the upper half of the storage tank. Therefore, in the case of higher gas cooler flowrates, the tank energy efficiency increases with the beginning of the heating process, and at the end of the heating process,



all the layers are collected almost the totality of the energy. The tank energy efficiency is higher in the case of the higher gas cooler flowrates than that of the lower gas cooler flowrates. For the cases studied, the energy accumulated in the case of highest gas cooler flowrate ( $0.305 \text{ kg}\cdot\text{s}^{-1}$ ) is 10% higher than that of the lowest gas cooler flowrate ( $0.083 \text{ kg}\cdot\text{s}^{-1}$ ).

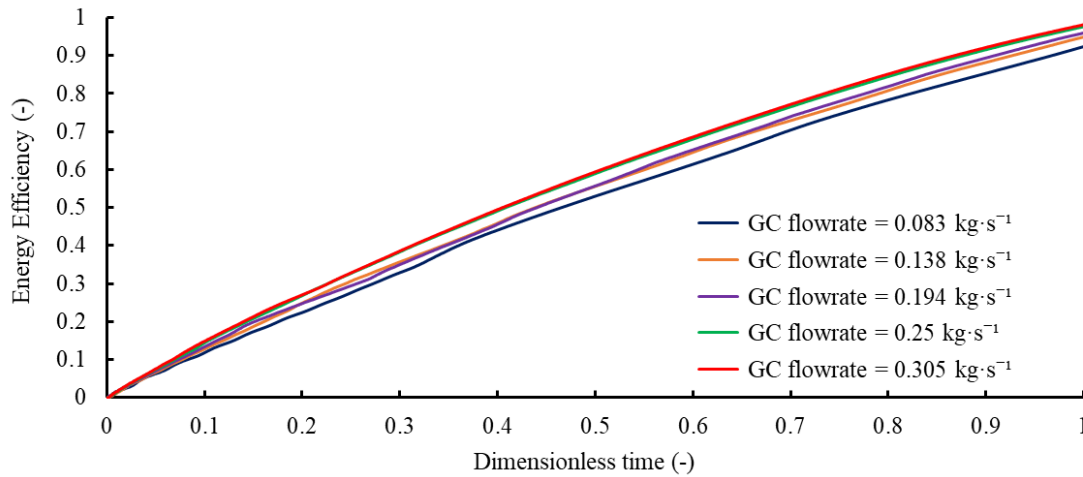


Figure III.11: Total energy efficiency (ET) for different gas cooler flowrates

Figure III.11 presents the energy efficiency of the storage tank as a function of dimensionless time for different gas cooler flowrate. This figure summarizes the energy efficiency of all gas cooler flowrate. From this figure it can be noticed that the energy efficiency of all cases increases with the increase of dimensionless time. The energy efficiency is higher in the case of higher gas cooler flowrate. The total energy stored in the storage tank is 10 % higher in the case of the highest gas cooler flowrate ( $0.305 \text{ kg}\cdot\text{s}^{-1}$ ) comparing to the lowest gas cooler flowrate ( $0.083 \text{ kg}\cdot\text{s}^{-1}$ ).

The stratification number (STR) is a suitable dimensionless tool to analyze the thermal stratification inside a storage tank, and it is defined as the ratio of the average temperature gradient at a determined instant to the average value of the maximum temperature gradient during the heating process. And its defined as [65]:

$$STR = \frac{\overline{\left(\frac{dT}{dy}\right)_t}}{\left(\frac{dT}{dy}\right)_t} \quad (\text{III.12})$$

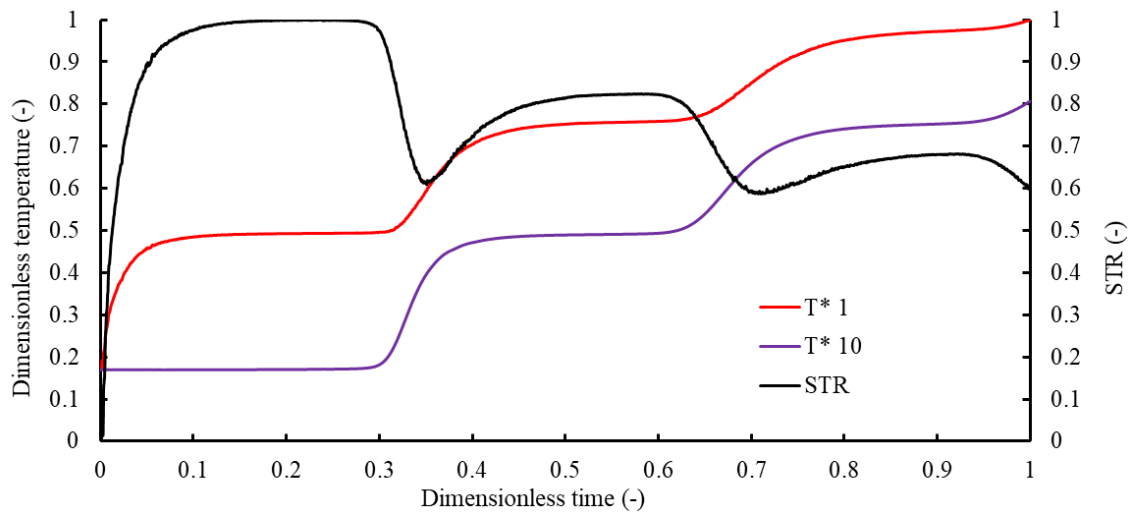
Where:

$$\overline{\left(\frac{dT}{dy}\right)}_t = \frac{1}{N-1} \left[ \sum_{i=1}^{N-1} \left( \frac{T_i - T_{i+1}}{\Delta h_i} \right) \right] \quad (\text{III.13})$$

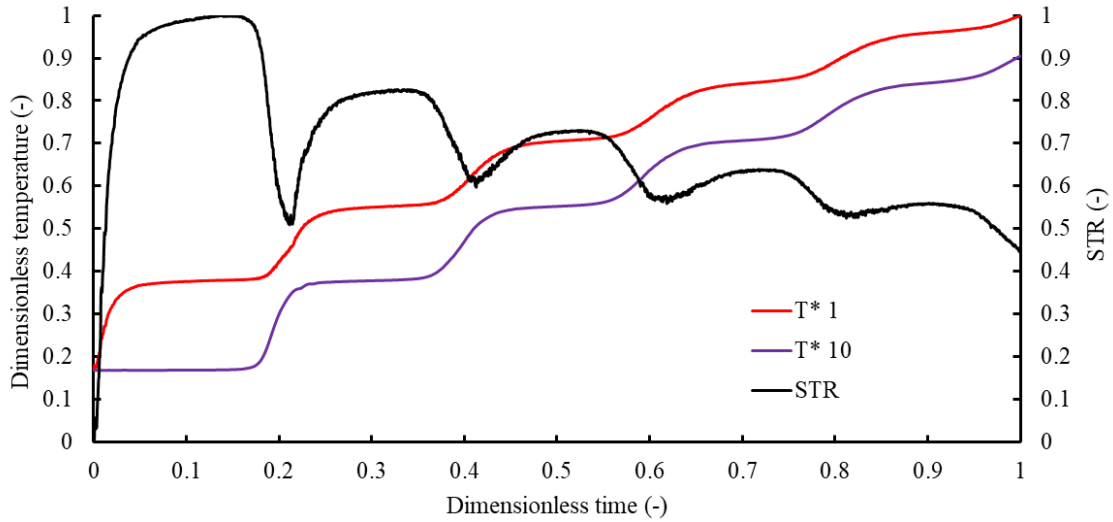
And;

$$\left(\frac{dT}{dy}\right)_t = \frac{\Delta T_{max}}{(N-1)\Delta h} \quad (\text{III.14})$$

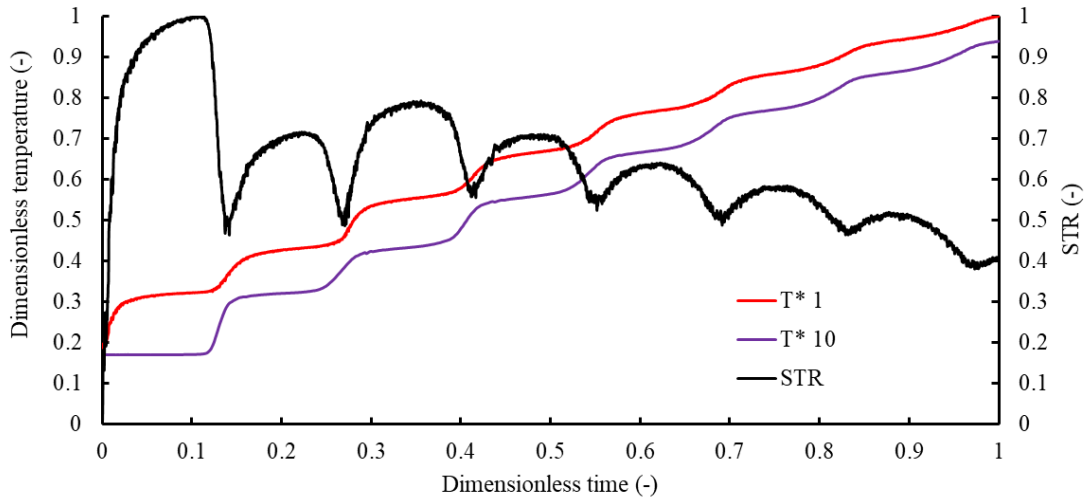
In the equation above, the  $N$  represents the nodes number (temperature sensors number equally spaced) within the tank.  $\Delta h$  is the nodes distance,  $\Delta T_{max}$  is the maximum temperature gradient between the top ( $T^* 1$ ) and the bottom ( $T^* 10$ ) of the storage tank.



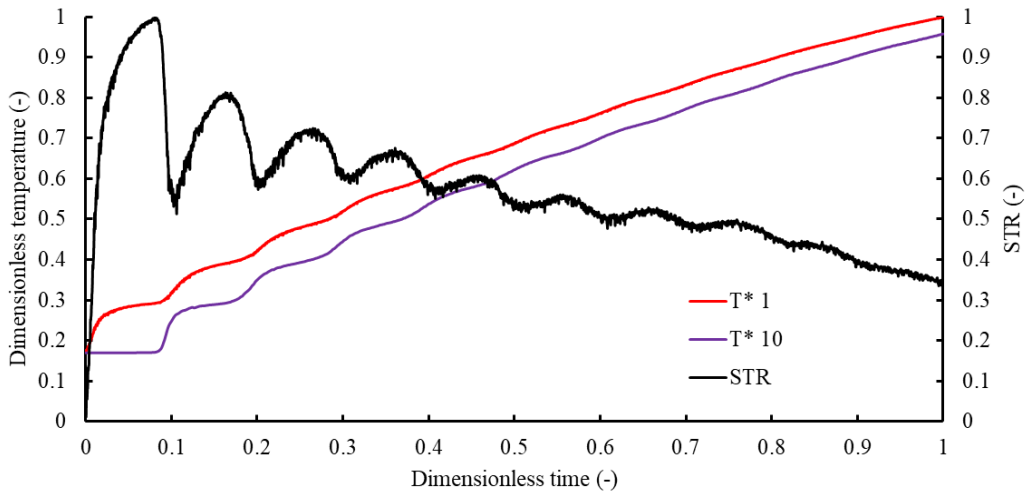
a) Gas cooler flowrate =  $0.083 \text{ kg}\cdot\text{s}^{-1}$



b) Gas cooler flowrate =  $0.138 \text{ kg}\cdot\text{s}^{-1}$



c) Gas cooler flowrate =  $0.194 \text{ kg}\cdot\text{s}^{-1}$



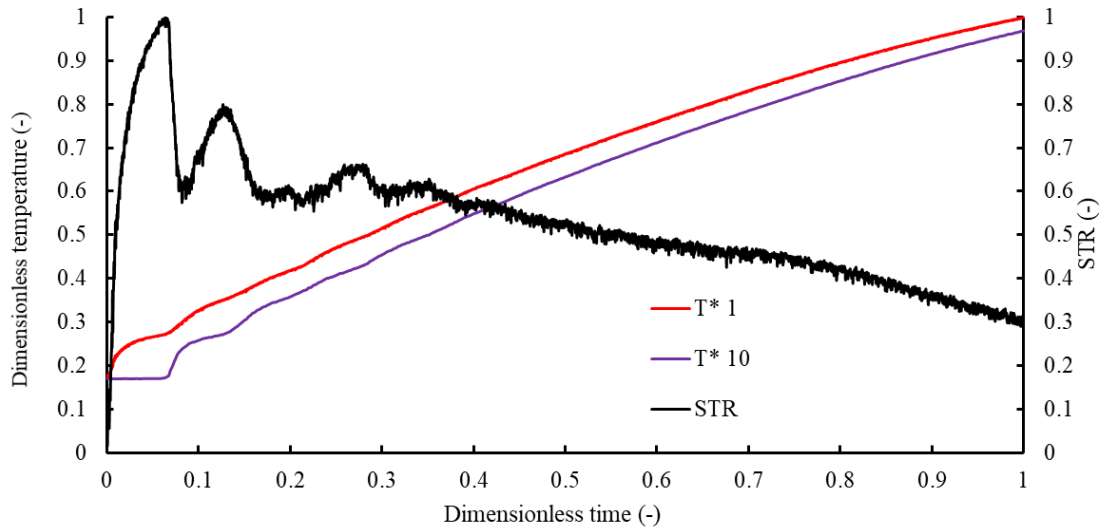
d) Gas cooler flowrate =  $0.25 \text{ kg}\cdot\text{s}^{-1}$ e) Gas cooler flowrate =  $0.305 \text{ kg}\cdot\text{s}^{-1}$ 

Figure III.12: Stratification number and dimensionless temperature of the top ( $T^* 1$ ) and the bottom ( $T^* 10$ ) of the storage tank for different gas cooler flowrates in function of dimensionless time

Figure III.12 shows the STR number and the dimensionless temperature in function of dimensionless time for five different gas cooler flowrates. From these figures, it can be seen that the stratification number depends mainly on the temperature gradient between the top and the bottom of the storage tank, the STR number has a higher value in the beginning of the heating process, and its value decreases with the decrease of the dimensionless time and dimensionless temperature gradient. The stratification number has a higher averaged value during the heating period in the case of lower gas cooler flowrate because of the low vertical velocity inside the storage tank and the low temperature propagation, which means a high stratification degree.

Figure III.13 compares the STR number evolution with dimensionless time for all gas cooler flowrate cases. It can be seen clearly that, as the gas cooler flowrate increases, the temperature gradient of the storage tank decreases, and this is due to the high velocity inside the storage tank, and this leads to a high velocity of the hot water to travel from the top part to the bottom part of the storage tank resulting a mixed and homogenous temperature and there is no stratification within the storage tank

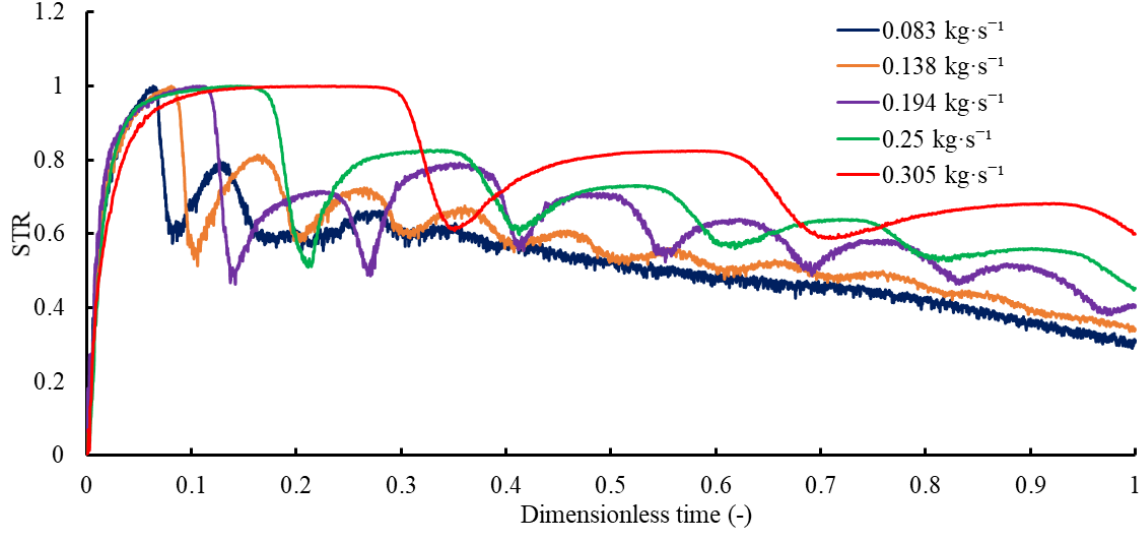


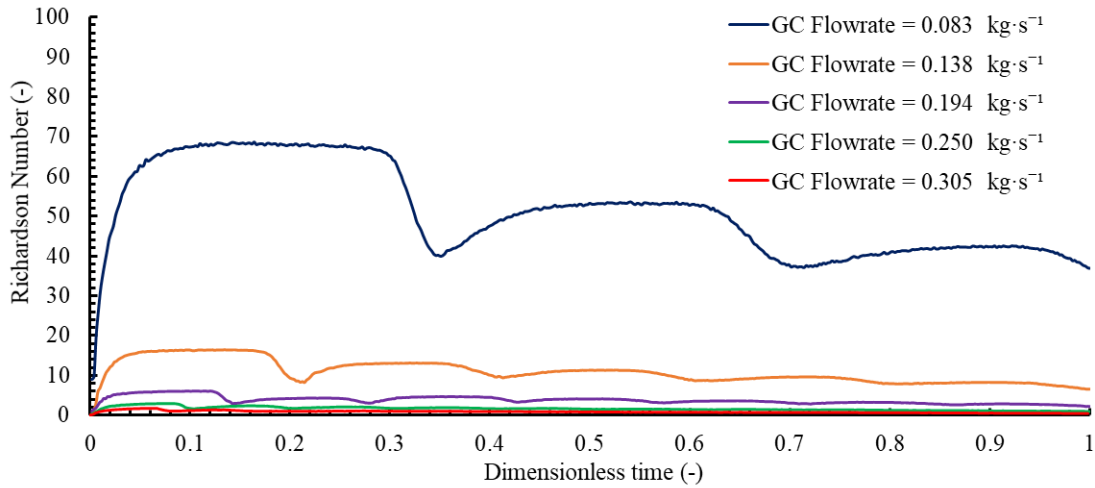
Figure III.13: Stratification number (STR) for different gas cooler flowrates

Also, the Richardson number is a suitable dimensionless number that characterizes the thermal stratification in the storage tank. Figure III.14.a shows the time-averaged Richardson number during the heating process for different gas cooler mass flow rates and Figure III.14.b shows the Ri evolution with time. In this case Richardson number (Ri) is defined as:

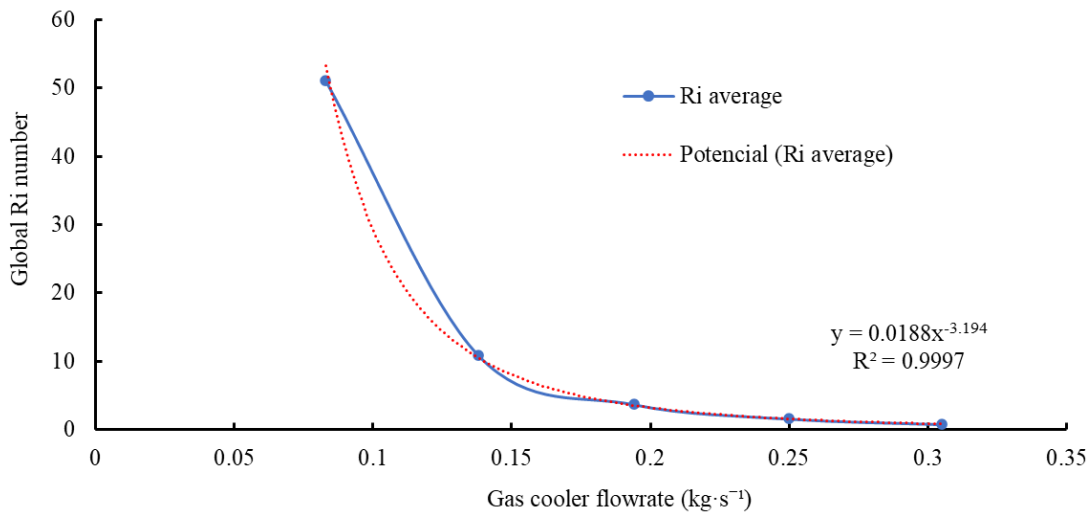
$$Ri = g \cdot H' \cdot (T_1 - T_{10}) / v_{in}^2 \quad (III.15)$$

Ri number describes the ratio of the buoyancy to the mixing force and is a usual descriptor of the stratification. A large Ri indicates a stratified storage tank whereas a small Ri means a mixed storage tank. Note that, we follow the definition of Richardson number of [39, 40] where  $H'$  represents the vertical distance between the inlet and outlet water ports of the tank,  $v_{in}$  is the inlet velocity of the water to the tank. The time-averaged Ri is calculated following the mean value theorem as (eq.III.16):

$$time - averaged Ri = \frac{1}{t_{tank}} \int_{t=0}^{t=t_{tank}} Ri^* \cdot dt \quad (III.16)$$



a) Time-averaged Richardson number (Ri) for different gas cooler flowrates



b) Richardson number (Ri) in function of gas cooler flowrates

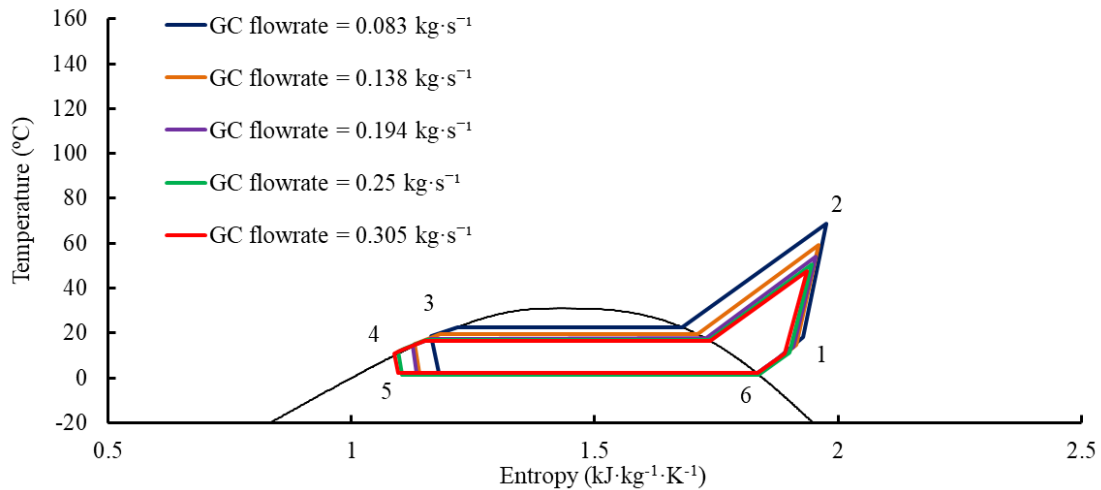
Figure III.14: Richardson number (Ri) for different gas cooler flowrate

For the case of a water flow rate of  $0.138 \text{ kg}\cdot\text{s}^{-1}$ , which corresponds to  $Ri \simeq 10$  the stratification is deficient (with a temperature gradient of  $\simeq 4 \text{ K/m}$ ), whereas for the case of  $0.083 \text{ kg}\cdot\text{s}^{-1}$  ( $Ri \simeq 40$ ) the stratification is better established (with a temperature gradient of  $\simeq 8 \text{ K/m}$ ). The region between  $Ri \simeq [10, 40]$  could be considered as a transition region where the flow regime evolves towards a stable, stratified regime. Under this perspective, the value of  $Ri \simeq 40$  should be understood as a minimum reference order of magnitude that maintains the stratification in the storage tank. Thus, when coupling a  $\text{CO}_2$  heat pump with a hot-water storage tank,  $H'$ ,  $d$ ,  $\dot{m}$ ,  $\dot{W}$  and COP must be selected to ensure a

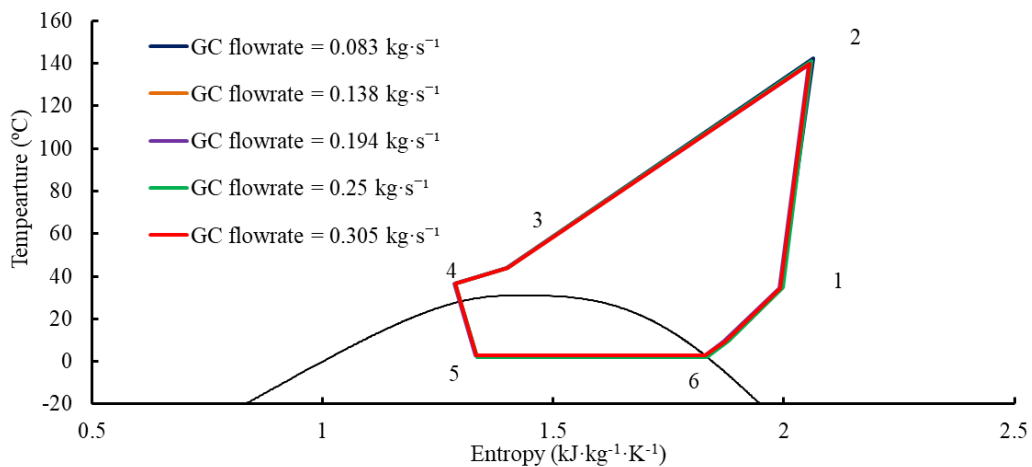
minimum order of magnitude of  $Ri \approx 40$ . Note that, during the estimation of the order of magnitude of the  $Ri$  in the design process of a DHW system,  $W$  and COP can be obtained from the reference values provided by the manufacturer of the heat pump. Once selected the tank and the heat pump, the gas cooler mass flow rate is the variable that can be changed by the control system and/or the user in order to promote stratification and improve the global COP of the system.

### III.2.2.1. Thermodynamic performance of the CO<sub>2</sub> heat pump

Also, for further analysis and more details of the thermodynamic performance of the heat pump, the T-s diagram of each case of gas cooler flowrate studied in this part are presented.



a) In the first hour of the heating process



b) In the last hour of the heating process

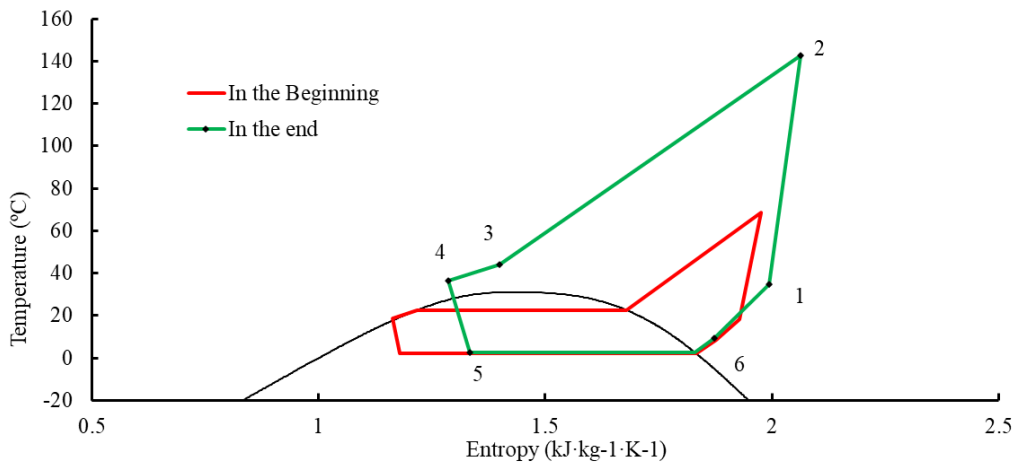
Figure III.15: T-s diagram of different gas cooler flowrate

In the case of the CO<sub>2</sub> heat pump used in the present study, the back-pressure electronic valve seeks for the optimal gas cooler pressure in the refrigerant side in order to maximize the COP of the heat pump. This control strategy permits the heat pump to work with a gas cooler pressure over or under the critical pressure of the CO<sub>2</sub>. As indicated in the test methodology section, during the tests it was logged the evolution of the working pressure of the refrigerant at the gas cooler with time, in order to evaluate whether the CO<sub>2</sub> heat pump was working with a trans-critical or a subcritical thermodynamic cycle. In the case of the trans-critical thermodynamic cycle (figure III.15.b), All the diagrams are superimposed because the system is working under the same working pressure and the gas cooler efficiency is optimum, so, the gas cooler flowrate has no impact on the cycle.

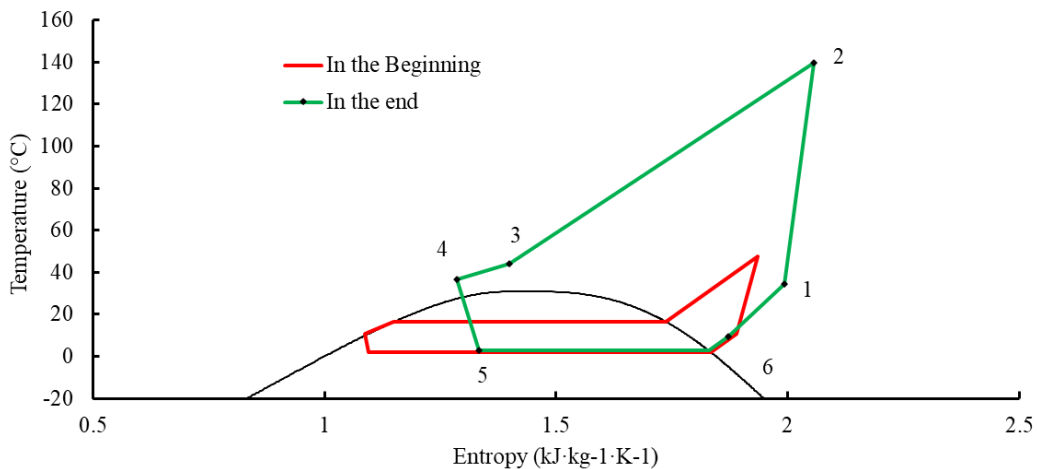
Figure III.16 shows the T-s working diagrams of the CO<sub>2</sub> heat pump for the case of test 1 and 5. These tests have a water mass flow rate at the gas cooler of 0.083 kg·s<sup>-1</sup> and 0.305 kg·s<sup>-1</sup>, respectively. In both cases it is shown two representative examples of the working cycle: one at the beginning of the heating test and another at the end of the heating test. In order to properly compare the operation mode of the heat pump, the cases selected for test 5 have a similar water temperature at the gas cooler inlet to that of the test 1. In the figure, the black line represents the thermodynamic states of the refrigerant (i.e. CO<sub>2</sub>) and the blue line represents thermodynamic states of the water at the gas cooler during the heating process. As shown, during the beginning of the heating process, the water temperature at the inlet of the gas cooler is relatively low and the heat pump works under a subcritical mode with a gas cooler optimal pressure at the refrigerant side below the critical pressure of the CO<sub>2</sub>. In this case there is a phase change of the CO<sub>2</sub>, and the gas cooler works as a condenser. This subcritical operational mode at the beginning of the heating process is found for all the water mass flow rate conditions tested. It is also found that the higher the mass flow rate, the lower gas cooler optimal pressure established: In the case of 0.083 kg·s<sup>-1</sup>, it is reached 60 bars, whereas the case of 0.305 kg·s<sup>-1</sup> it is reached 52 bars. This operational mode results in a lower pressure ratio and a lower power consumption at the compressor. Besides, the higher mass flowrate at the gas cooler of test 5 provides a lower gas cooler working pressure and an increase of 50% in the instantaneous heat pump COP when compared with test 1. Thus, in the case of the heat pump working under a subcritical operation mode it is recommended to set high water mass flowrates in order to maximize the COP of the DHW production system.



During the end of the heating process, the water temperature at the inlet of the gas cooler is higher and the heat pump works under a trans-critical mode with a gas cooler pressure at the refrigerant side over the critical pressure of the CO<sub>2</sub>. In this case the optimal working pressure at the gas cooler is much higher (around 105 bars) and the instantaneous COP of the heat pump is drastically reduced when compared to the subcritical operation mode. Moreover, the difference of the gas cooler working pressure between test 1 and 5 is considerably reduced to less than 0.7 bars (it is 105.6 bars in the case of 0.083 kg·s<sup>-1</sup>, and 105 bars in the case of 0.305 kg·s<sup>-1</sup>). This shows that the influence of the water mass flow rate at the gas cooler strongly influences the COP of the heat pump when it works under a subcritical cycle (with low inlet water temperatures at the gas cooler) whereas this influence of the water mass flow rate almost vanishes when the inlet temperature of the water at the gas cooler is relatively high, and the heat pump works under a trans-critical cycle.



a) Gas cooler flowrate = 0.083 kg·s<sup>-1</sup>



b) Gas cooler flowrate = 0.305 kg·s<sup>-1</sup>

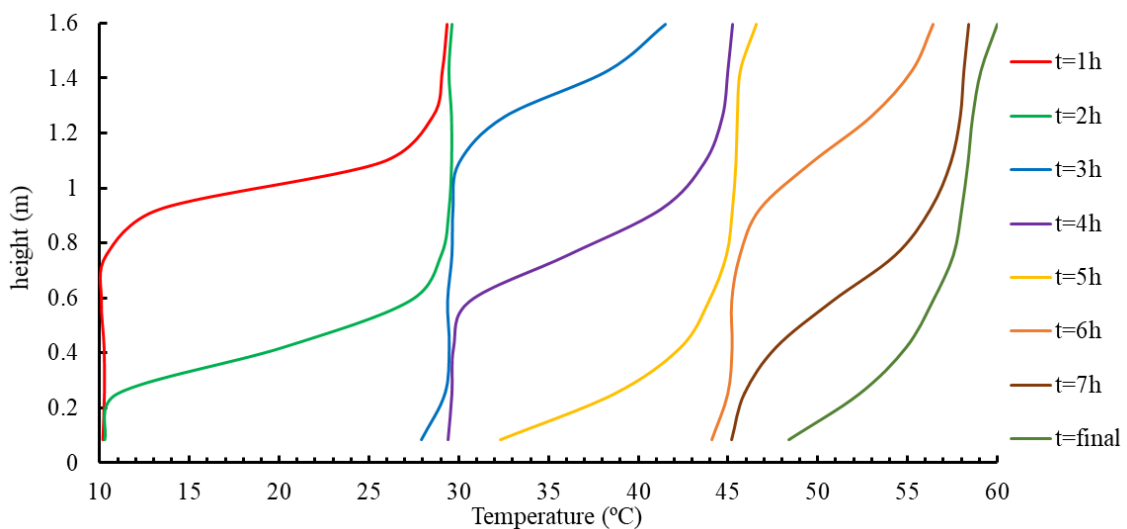
Figure III.16: Comparison of the T-s diagram in the beginning and the end of the heating process of the lowest and highest gas cooler flowrate.

All in all, it is found that in order to maximize the COP of the DHW production system, the heat pump should work with high mass flow rates when it operates under subcritical mode (in the beginning of the tank heating process when the water temperature at the bottom of the tank is low) and it should “switch” to low mass flow rates when it works under a trans-critical operation mode (during the rest of the tank heating process, when the water temperature at the bottom of the tank is higher). This change in the mass flow rate should be progressive as the heat pump evolves from subcritical towards trans-critical operation modes always seeking the maximization of COP of the DHW production system.

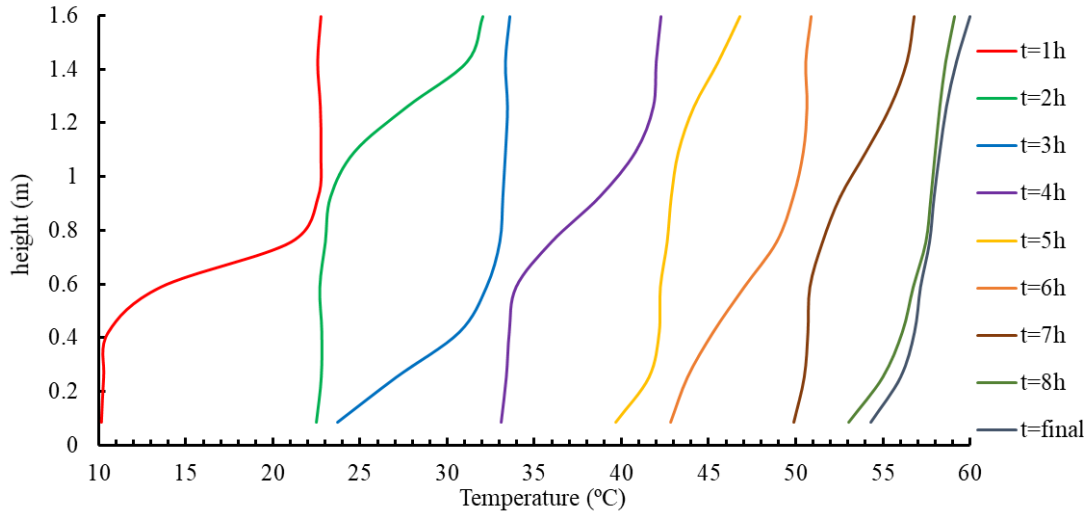
### III.2.2.2. Thermal stratification and temperature distribution analysis

Figure III.17 presents the temperature distribution in function of the tank height every one hour from the beginning of the . process for the five cases of the gas cooler flowrates. From these figures, it can be shown that the temperature distribution within the storage tank depends mainly on the gas cooler flowrate. At a specific gas cooler flowrate value, the temperature distribution in the storage tank varies with the height and time.

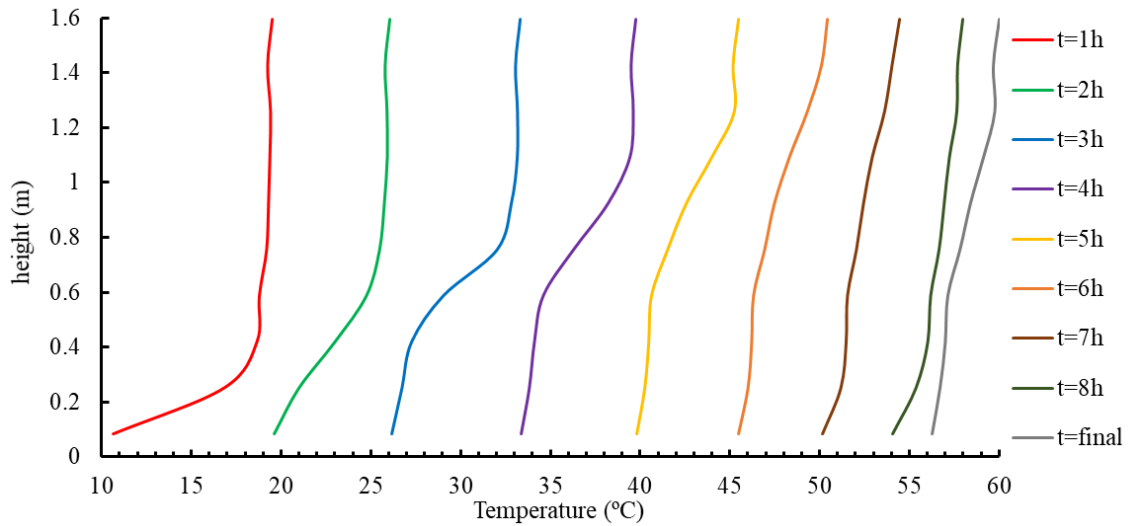
For lower gas cooler flowrates, the temperature in the upper part is always higher than that of the bottom. In the beginning of the heating process (first hour) the temperature gradient is higher, and it decreases with the increase of the time. Also, as the gas cooler flowrate increases the temperature gradient decreases resulting a homogeneous temperature.



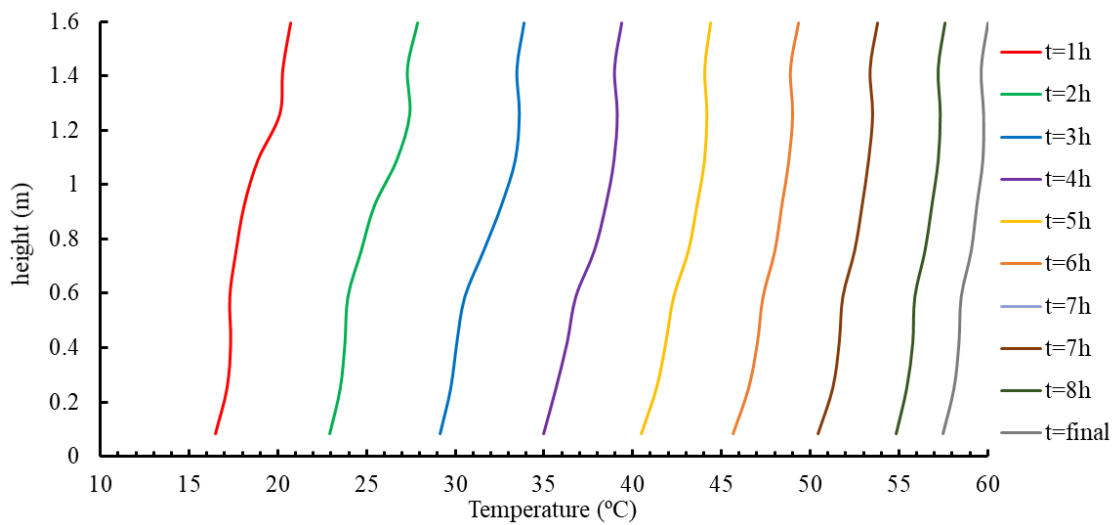
a) Gas cooler flowrate =  $0.083 \text{ kg}\cdot\text{s}^{-1}$



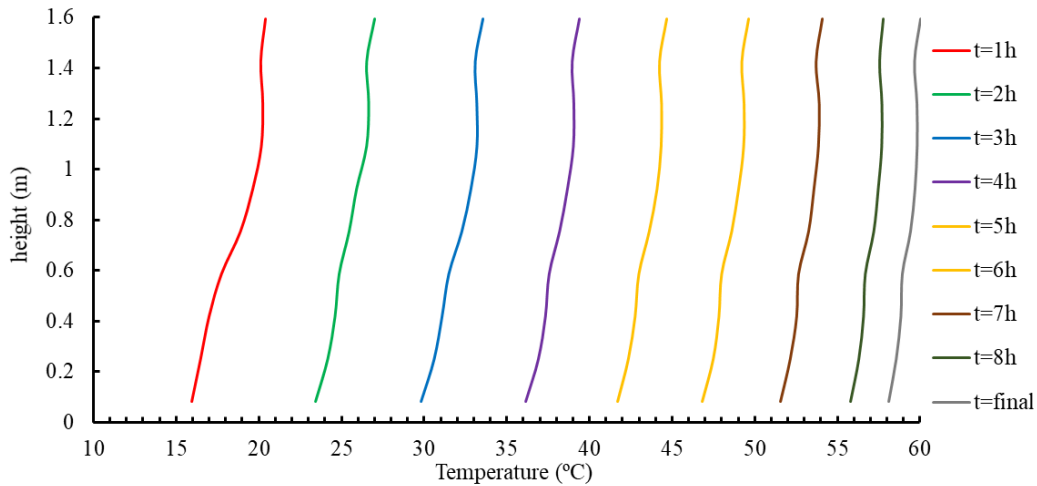
b) Gas cooler flowrate =  $0.138 \text{ kg}\cdot\text{s}^{-1}$



c) Gas cooler flowrate =  $0.194 \text{ kg}\cdot\text{s}^{-1}$



d) Gas cooler flowrate =  $0.25 \text{ kg}\cdot\text{s}^{-1}$

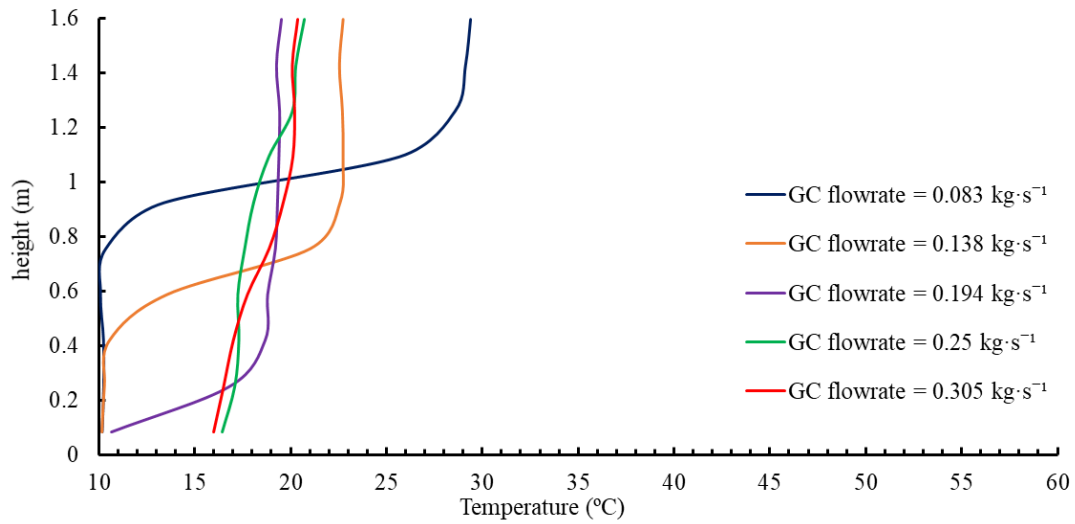


e) Gas cooler flowrate =  $0.305 \text{ kg}\cdot\text{s}^{-1}$

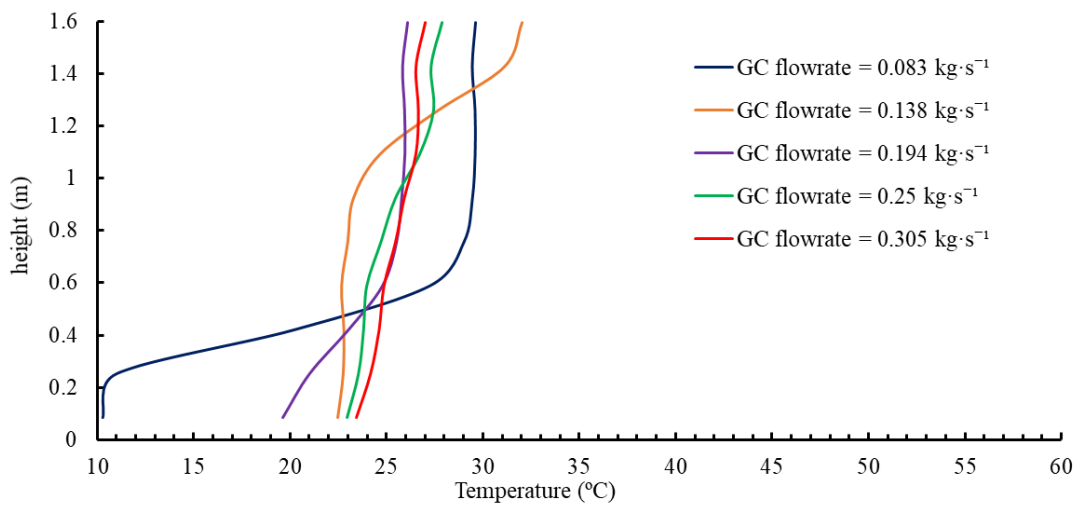
Figure III.17: Temperature distribution in function of the tank height for different gas cooler flowrates.

Furthermore, in the case of lower flowrates, the hot water entering the storage tank, travels with low velocity, which make the upper part of the storage tank hotter than that of the bottom resulting higher temperature gradient, and this is due to the elapsed time of the water in the gas cooler before entering the storage tank. Hence, lower gas cooler flowrates mean that the water remains more time in the gas cooler which make it heated up more. In addition, lower velocity minimizes turbulence, and it avoids the mixing of the water contained in the storage tank, resulting a well stratified tank.

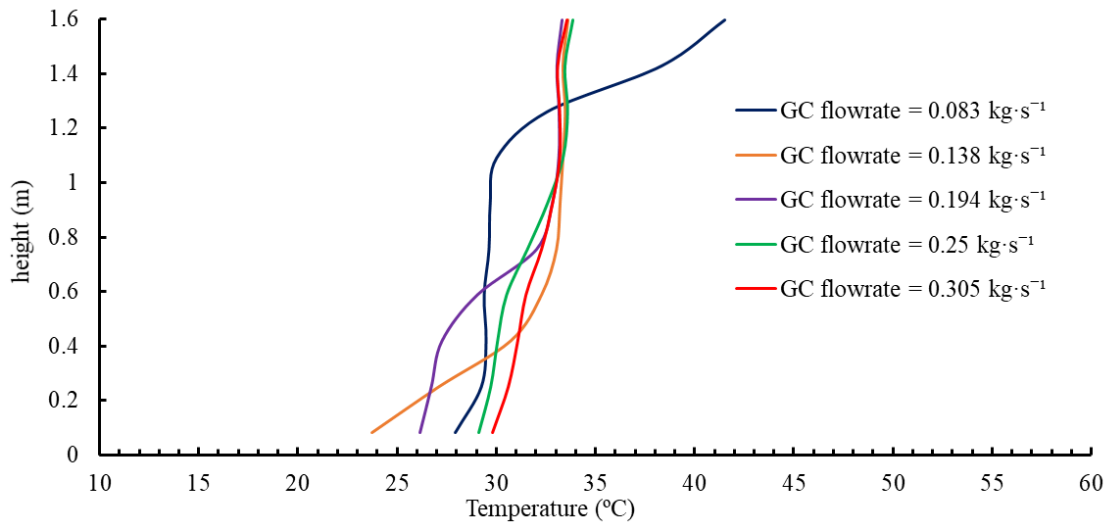
On the other hand, higher gas cooler flowrate gives a homogenous temperature distribution, and the absence of the thermal stratification is due to the mixing of the water contained in the storage tank because of the higher velocity. Also, higher gas cooler flowrates make the hot water to travel with higher velocity from the top to the bottom of the storage tank.



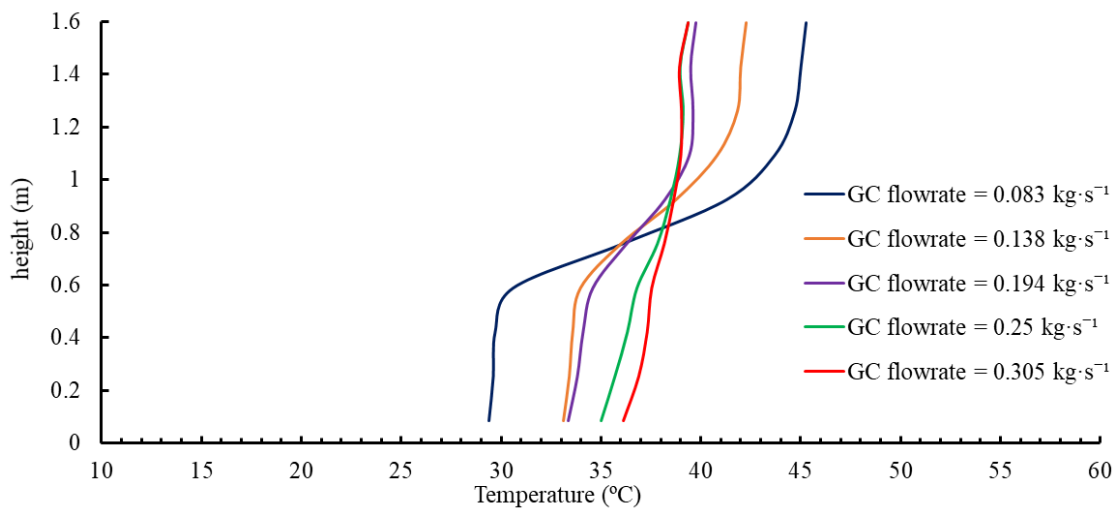
a) 1<sup>st</sup> hour



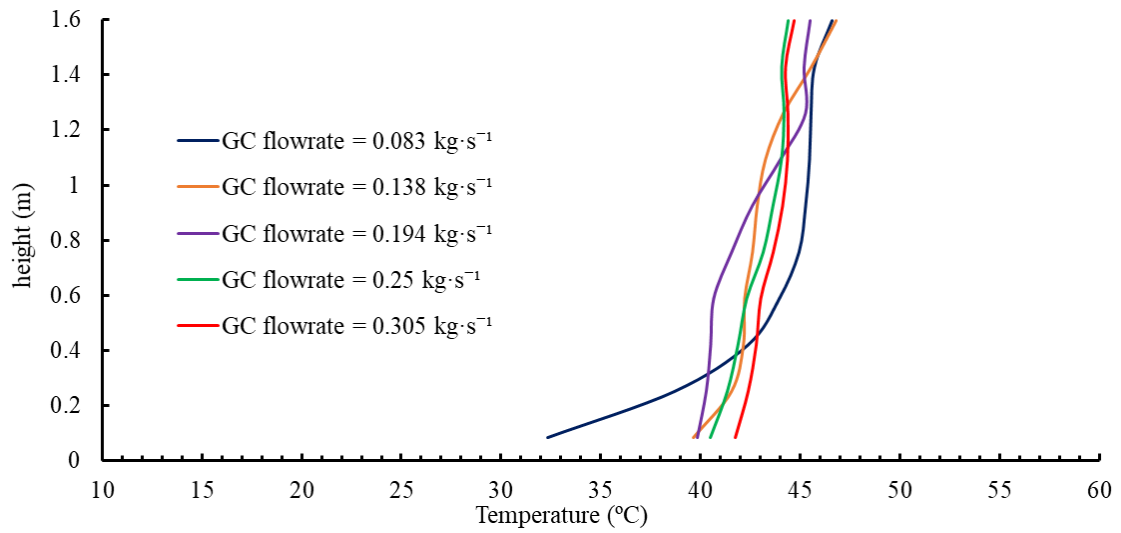
b) 2<sup>nd</sup> hour



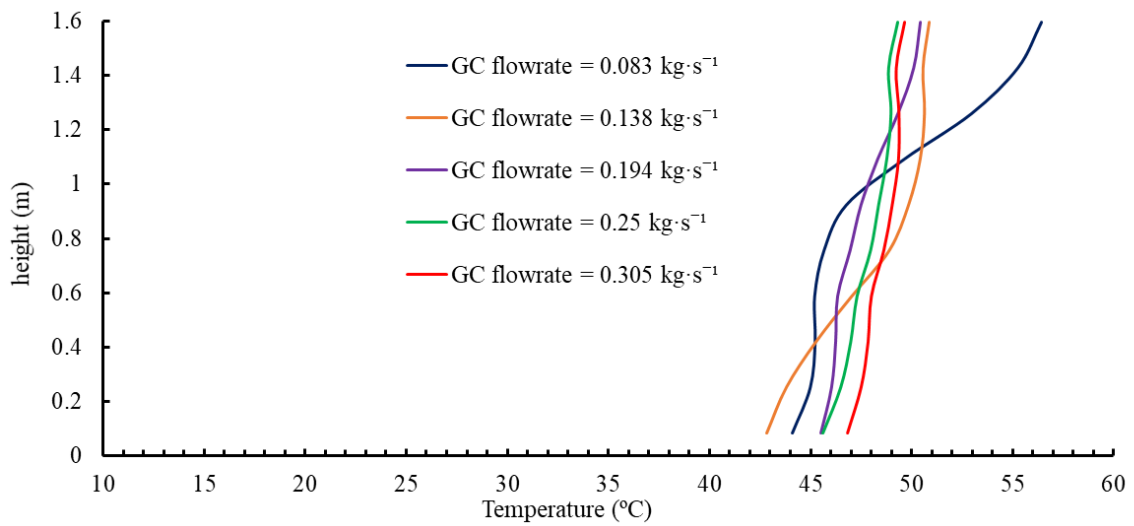
c) 3<sup>rd</sup> hour



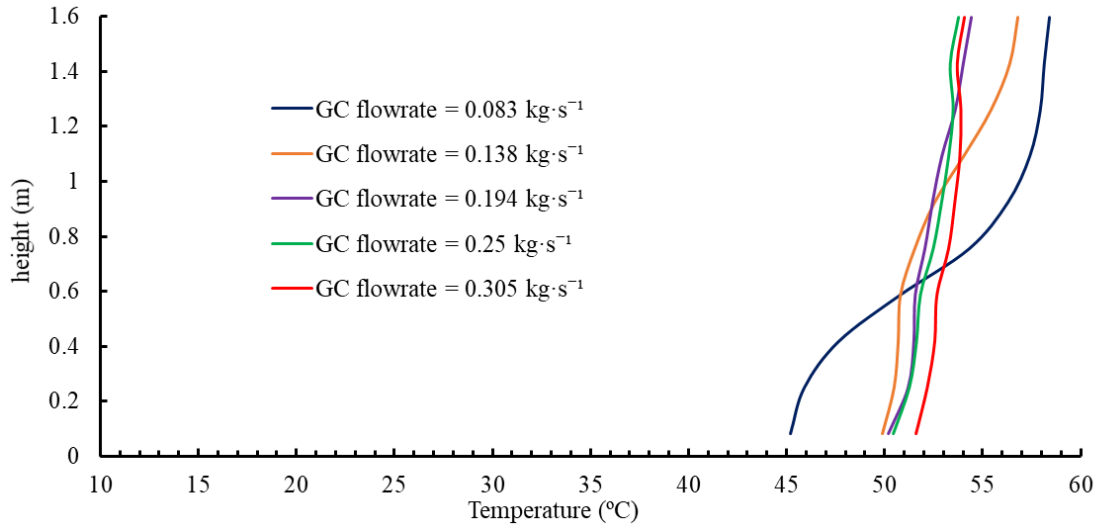
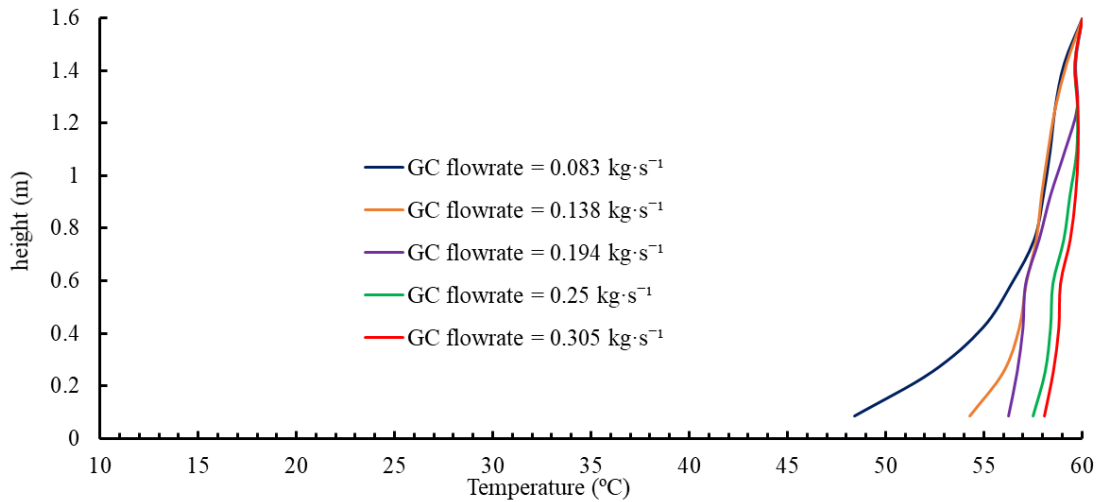
d) 4<sup>th</sup> hour



e) 5<sup>th</sup> hour



f) 6<sup>th</sup> hour

g) 7<sup>th</sup> hour

h) end of the tests

Figure III.18: Temperature distribution in function of the tank height for different instant of the heating process (every one hour)

To clarify and the stratification in the storage tank, the temperature distribution is represented in Figure III.18 as a function of the tank height for different gas cooler flowrates and in different moments. Note that the thermocline only appears in the lower gas cooler flowrates and in different moments. As the gas cooler flowrate increases the thermal stratification disappears, and the temperature distribution is homogenous.

In the case of lower flowrates, the thermocline has a thin width but a high temperature gradient, as the gas cooler flowrate increases the thermocline width increases and the



temperature gradient decreases until it disappears, and the temperature becomes homogenous in the tank.

For further comprehension of the thermal stratification phenomenon within the storage tank, it will be discussed the case of the lowest gas cooler flowrate ( $0.083 \text{ kg}\cdot\text{s}^{-1}$ ) as it is the most interesting to analyze in terms of performance of the thermal stratification and the thermocline notion.

In this case of gas cooler flowrate, the temperature evolution increases with a discontinued manner making stages, so, in this part we will study in detail only the first stage of heating process of the lowest gas cooler flowrate case as shown in figure III.19.

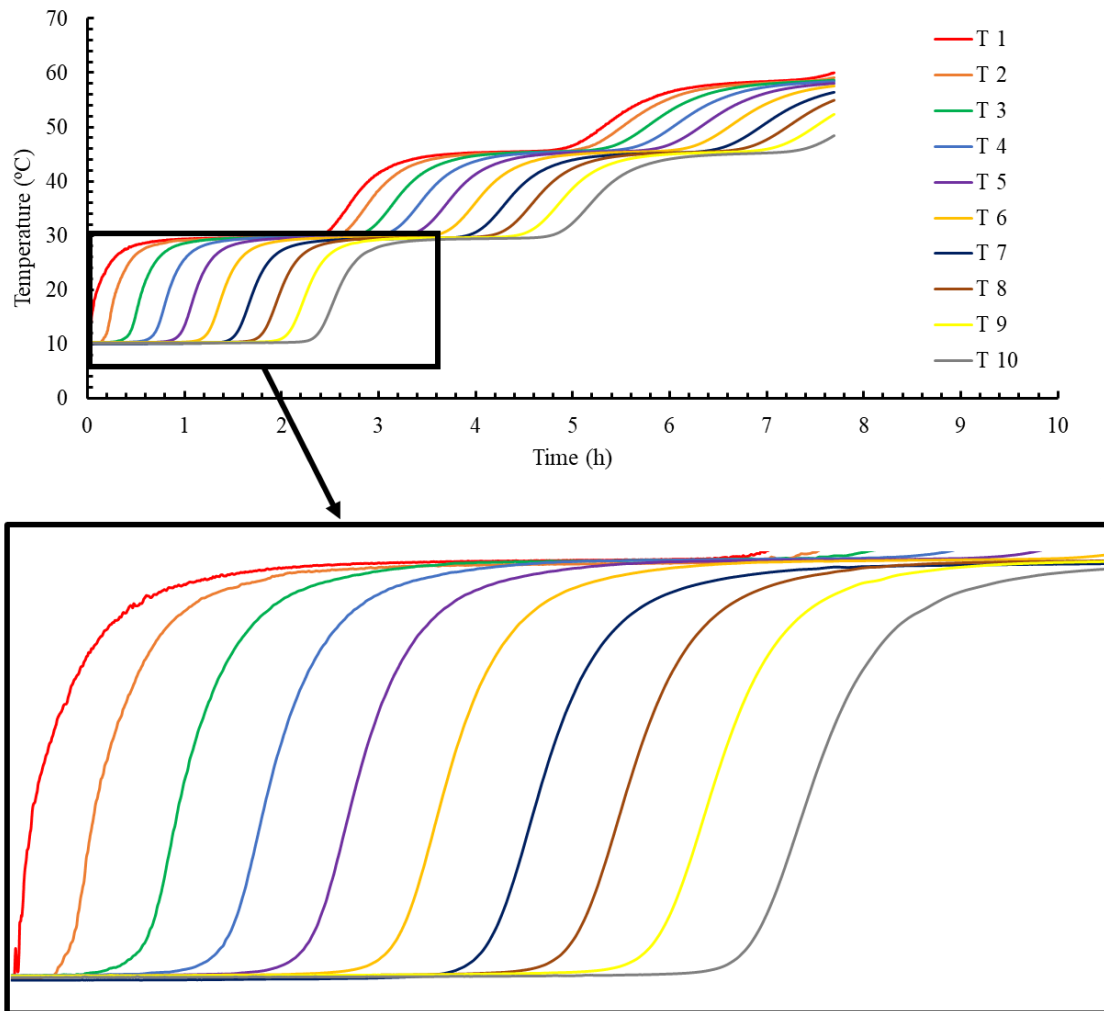
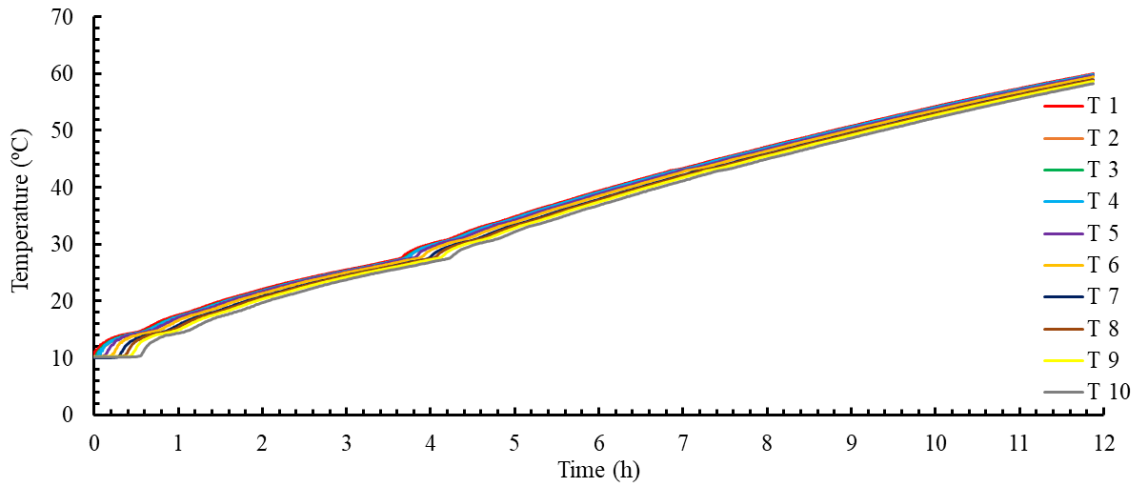


Figure III.19: Temperature evolution in function of time of the lowest gas cooler flowrate ( $0.083 \text{ kg}\cdot\text{s}^{-1}$ )

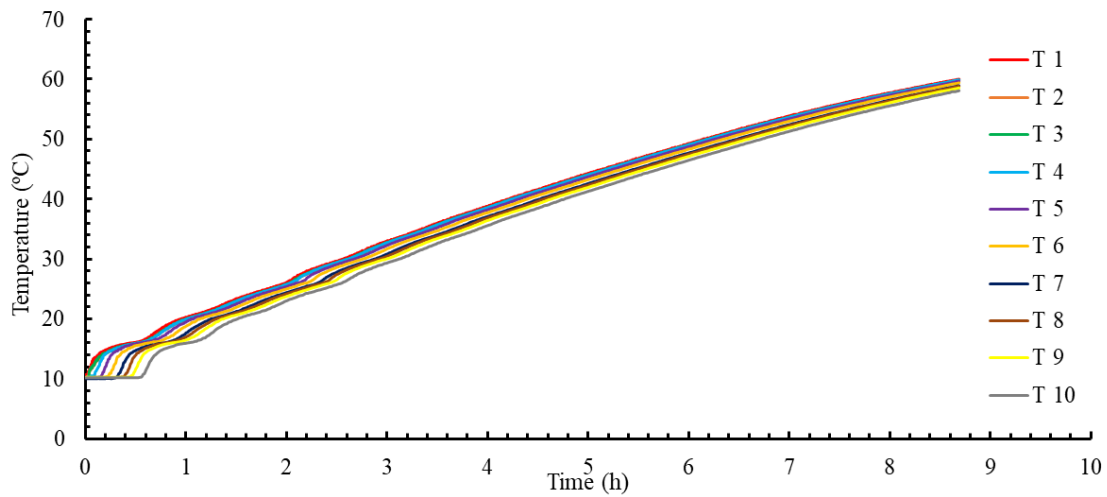
In the beginning of the heating process, the temperature of the highest part of the storage tank (T1) increases from the first instant of the test until it reaches the value of 32 °C, and the temperature of the lowest region (T10) remains at the initial temperature of 10 °C. This is because the hot water coming from the gas cooler enters in the upper part of the storage tank, and because of the low gas cooler flowrate, the hot water travels with a low velocity inside the storage tank, which makes the heating process at this gas cooler flowrate take place of stages.

### III.2.3. Impact of the evaporator inlet temperature

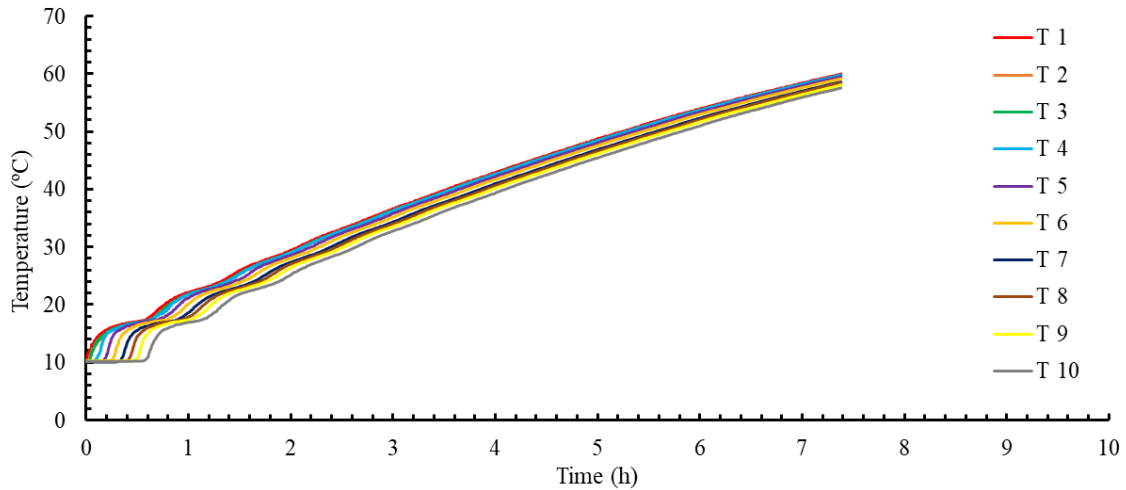
To analyse the impact of the inlet temperature of the evaporator ( $T_{in\ evap}$ ), tests 7 to 10 were performed by varying the inlet temperature in the evaporator between 5 °C and 20 °C with an increment of 5 °C, the operating conditions of the gas cooler are constant during the heating process (gas flowrate = 0.305 kg·s<sup>-1</sup>). The four tests are performed under the same operating conditions of the gas cooler.



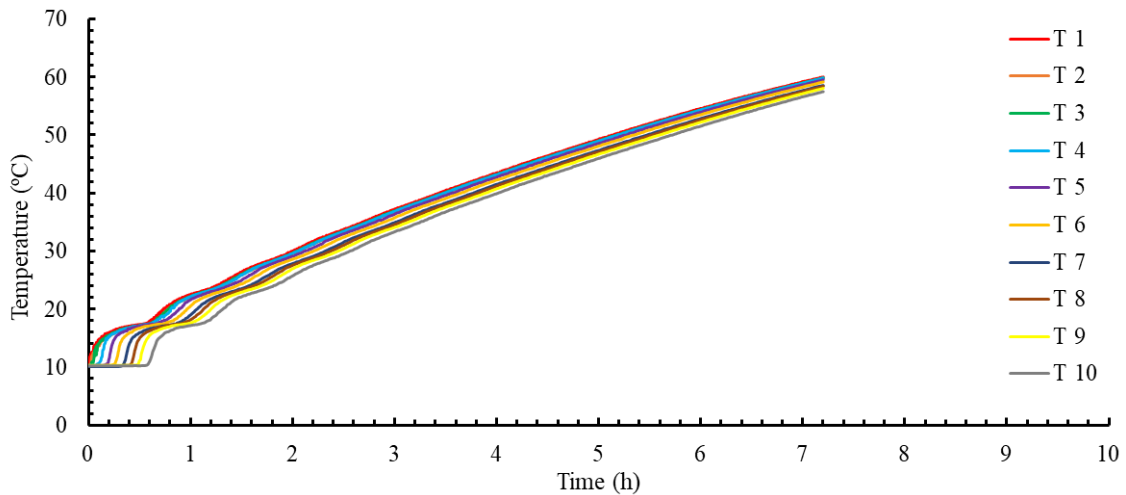
a) Evaporator inlet temperature = 5 °C



b) Evaporator inlet temperature = 10 °C



c) Evaporator inlet temperature = 15 °C



d) Evaporator inlet temperature = 20 °C

Figure III.20: Temperature evolution of the 10 RTD sensors in function of time and for different evaporator inlet temperature values.

Figure III.20 shows the temperature evolution of the 10 RTD sensors in function of time and for different evaporator inlet temperature values during the heating process. From these figures, it can be seen that the temperature evolution inside the storage tank not only depends on the gas cooler flowrate, but also, on the evaporator inlet temperature. The temperature of the storage tank increases with the increase of the time and the tank has a homogenous temperature, and it increases with a continuous manner which means that there is no stratification in the storage tank for all evaporator inlet temperature cases. So, that the evaporator inlet temperature affects only the thermodynamic performance of the

heat pump but not the thermal stratification within the storage tank because of the gas cooler flowrate condition.

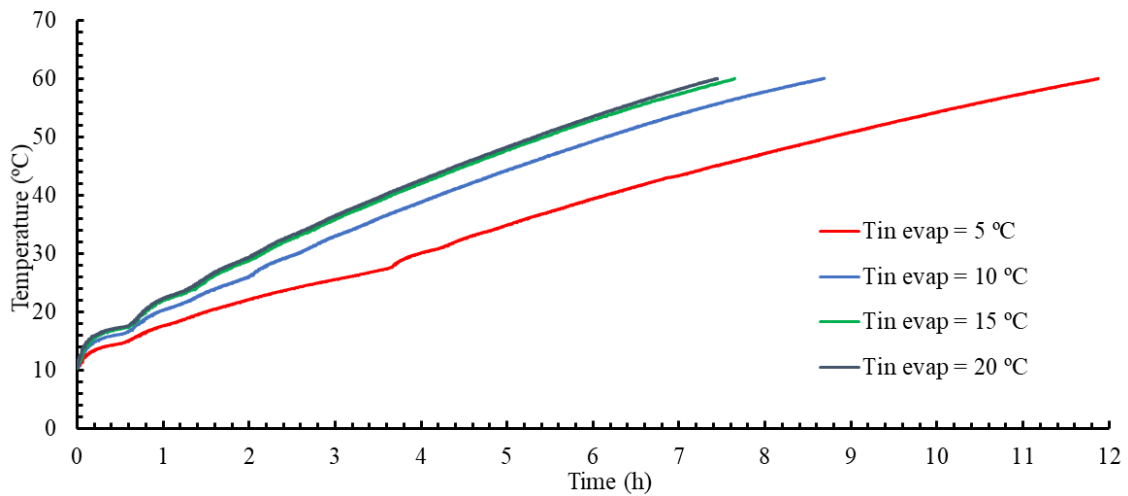


Figure III.21: Temperature distribution of the topper RTD sensors in function of time and for different evaporator inlet temperature values.

Actually, the evaporator inlet temperature has an impact on the heating time of the storage tank. Figure III.21 shows the temperature evolution of the topper RTD sensors in function of time and for different evaporator inlet temperature values. The heating time decreases by the increase of the evaporator inlet temperature. The heating time is about 12h and about 7h in the case of evaporator inlet temperature of 5 °C and 20 °C respectively

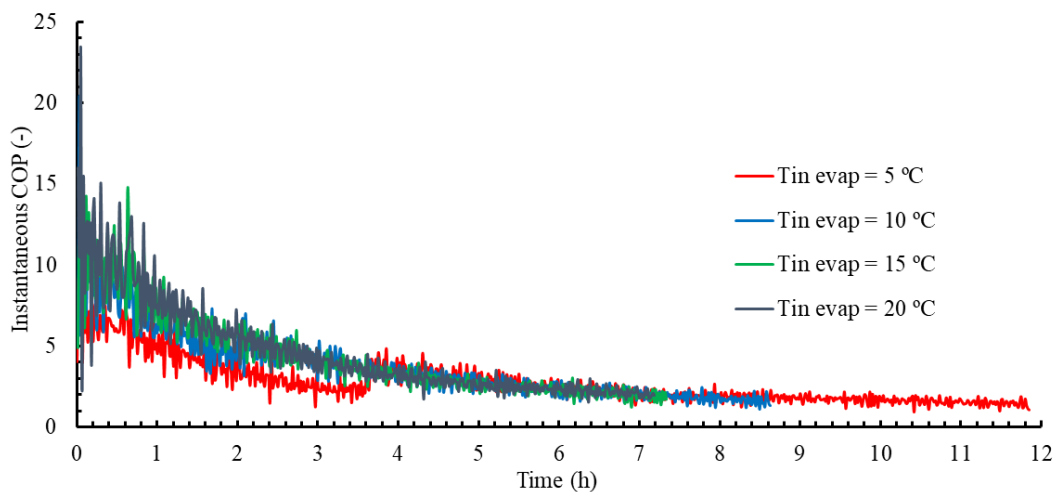


Figure III.22: Evolution of the instantaneous COP in function of time for different evaporator inlet temperature cases.

The heat pump performance is presented in Figure III.22. This figure shows the evolution of the instantaneous COP of the system as a function of time. It can be seen that the instantaneous COP decreases with the increase of time, and this is due to the increase of the inlet temperature to the gas cooler, hence, when the storage tank temperature increases, the inlet temperature in the gas cooler increase. Also, as the evaporator inlet temperature increase, the system performance increases, so, when the evaporator inlet temperature is higher, the system gives higher COP.

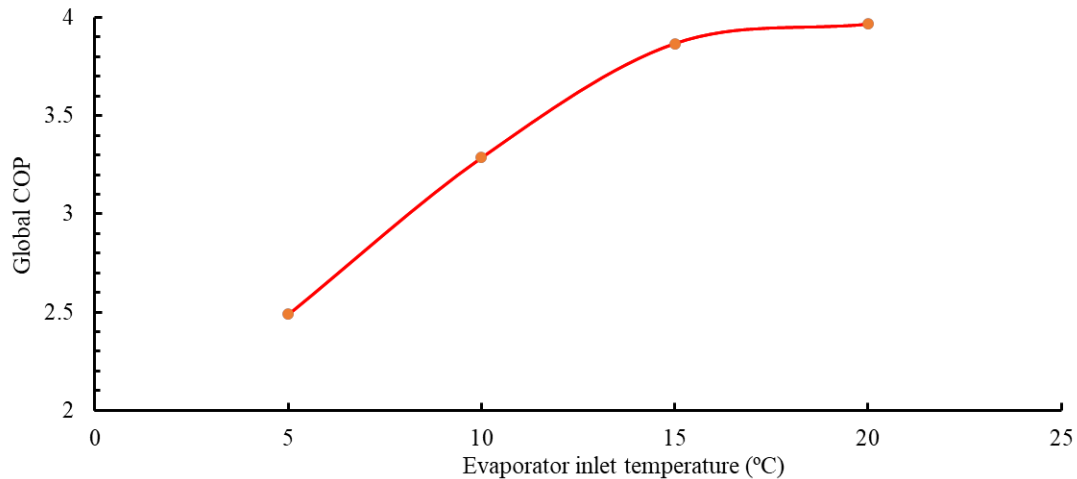
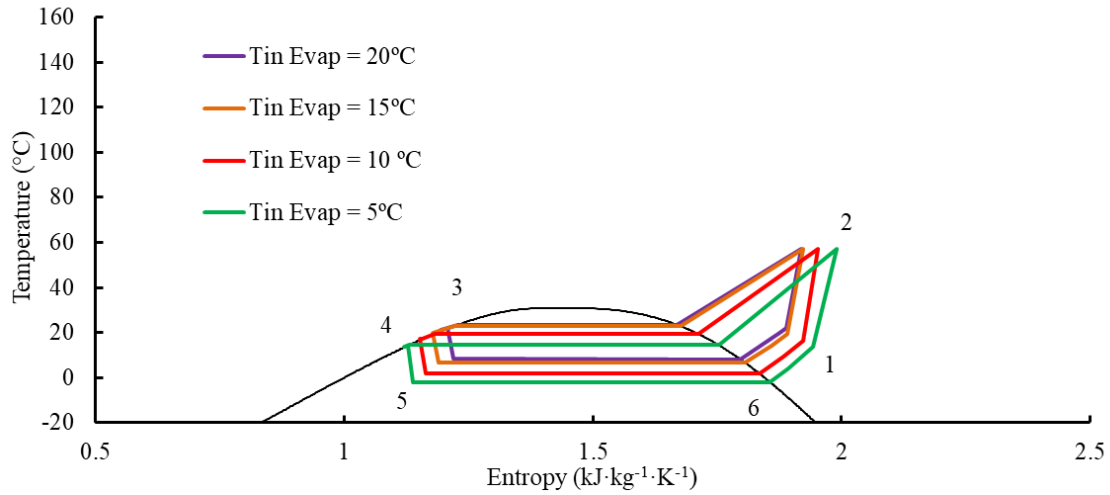
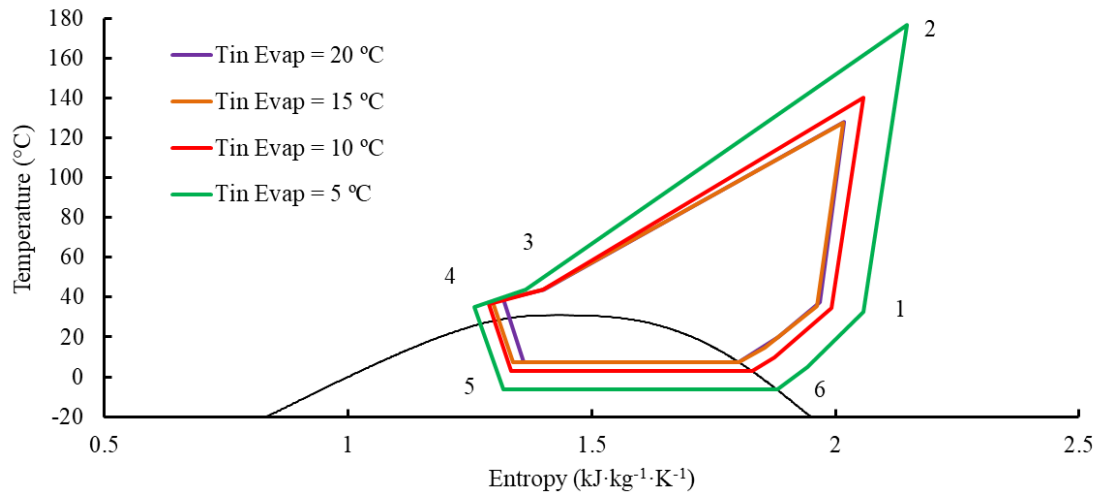


Figure III.23: Evolution of the global COP for different evaporator inlet temperature.

The thermodynamic performance of the heat pump and the energy stored by the system are presented in Figure III.23. The global COP of the system increases with the increase of the evaporator inlet temperature. In the case of lower evaporator inlet temperature, the heating process take time of about 12h to reach 60 °C which means that the compressor does more work consuming more electrical energy with time even if the energy stored is higher.



a) In the first hour of the heating process



b) In the last hour of the heating process

Figure III.24: T-s diagram of different evaporator inlet temperature.

Figure III.24 presents the T-s diagram of different evaporator inlet temperature in the beginning and the end of the heating process. As shown in the figure, as the inlet temperature of the evaporator decreases the work of the compressor increases and the compressor discharge temperature increases also. And for this reason, the COP of the system decreases as the evaporator inlet temperature decreases.

### III.3. Extraction process (step E)

The procedure of this test step is based on the extraction profile mentioned in the standard (annex I). As mentioned, the test consists of extracting the hot water at 60 °C, at a specified time following the extraction profile. In this test, the extraction profile of 3XL (table III.3) is chosen in order to realize the test and then analyze the thermodynamic performance of the heat pump and the thermohydraulic performance of the stratified storage tank. More details of test setup and the LabVIEW control program are explained in the chapter II.

Table III.3: Extraction profile of 3XL.

Time	$Q_{tap}$ (kWh)	Flow $Kg \cdot s^{-1}$	$T_m$ °C	$T_p$ °C
07:00	11.2	0.8	40	
08:01	5.04	0.4	25	
09:00	1.68	0.4	25	
10:30	0.84	0.4	10	40
11:45	1.68	0.4	25	
12:45	2.52	0.6	10	55
15:30	2.52	0.4	25	
18:30	3.36	0.4	25	
20.:30	5.88	0.6	10	55
21:30	12.04	0.8	40	

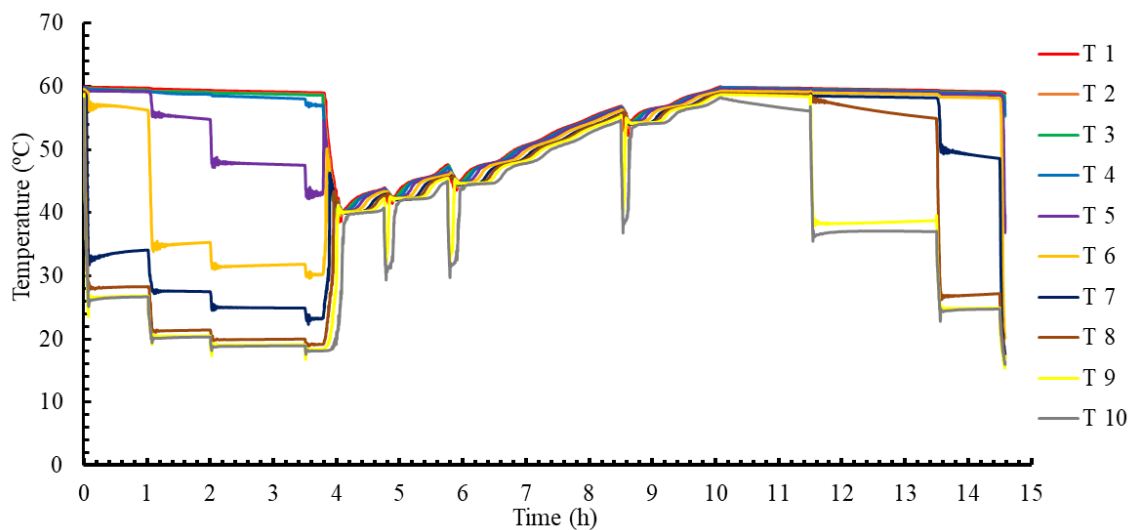


Figure III.25: Temperature evolution in the storage tank with function of time of the 10 RTD sensors.



Figure III.25 shows the temperature repartition in the storage tank during the extraction test. The first extraction begins with the beginning of the test, so the temperature of the bottom of the storage tank decreases rapidly because of the inlet of the cold water with temperature of 10 °C. It can be noticed also that the half upper part remains at the initial temperature of 60 °C and this due to the volume of the cold water entering to the hot water storage tank and also due to the stratification phenomenon. At the second extraction, the temperature of the bottom part still decreases because it was entering more cold water at 10 °C, but the upper part is still hot.

After the fourth extraction the temperature of the highest part of the storage tank decreases below 59 °C, so the heat pump starts up. The temperature of the storage tank homogenizes and decreases to a medium temperature and this is due to the water movement inside the storage tank. In fact, when the heat pump starts up, the gas cooler pump takes the cold water contained in the lower part of the hot water storage tank and heats it up, and then returns it to the upper part of the storage tank with a gas cooler flowrate of 0.305 kg·s<sup>-1</sup>, so, a destratification is resulted and the temperature of the hot water storage tank decreases and it homogenizes and then the heating process begins until the highest part reaches 60 °C. During the heating process of this test, three hot water extractions are realized, so the cold water at 10 °C enters the bottom part of the storage tank and this is why the temperature of the entire storage tank decreases at the extractions of the hot water.

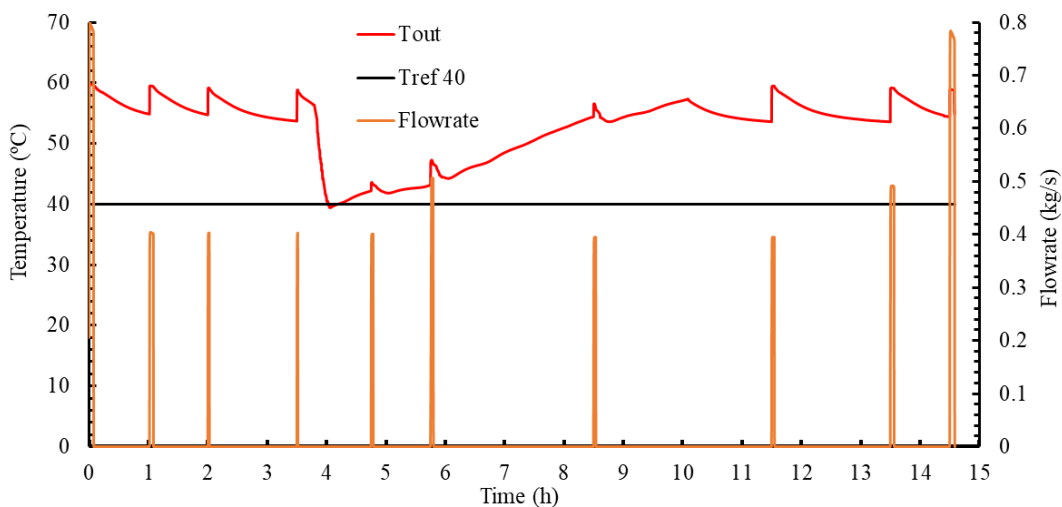


Figure III.26: Temperature evolution of the hot water storage tank outlet and the extraction flowrate.

Figure III.26 shows the temperature evolution of the outlet of the hot water storage tank during the test and the extraction flowrate. During the extraction, the temperature of the hot water at the outlet must be always higher than 40 °C, it can be seen clearly that the temperature is always higher than 40 °C in every extraction.

Also, the inlet temperature of the cold water inlet must be 10 °C. Figure III.27 presents the inlet temperature of the cold water to hot water storage tank at every extraction. From this figure it can be seen that inlet temperature is always 10 °C with a small error.

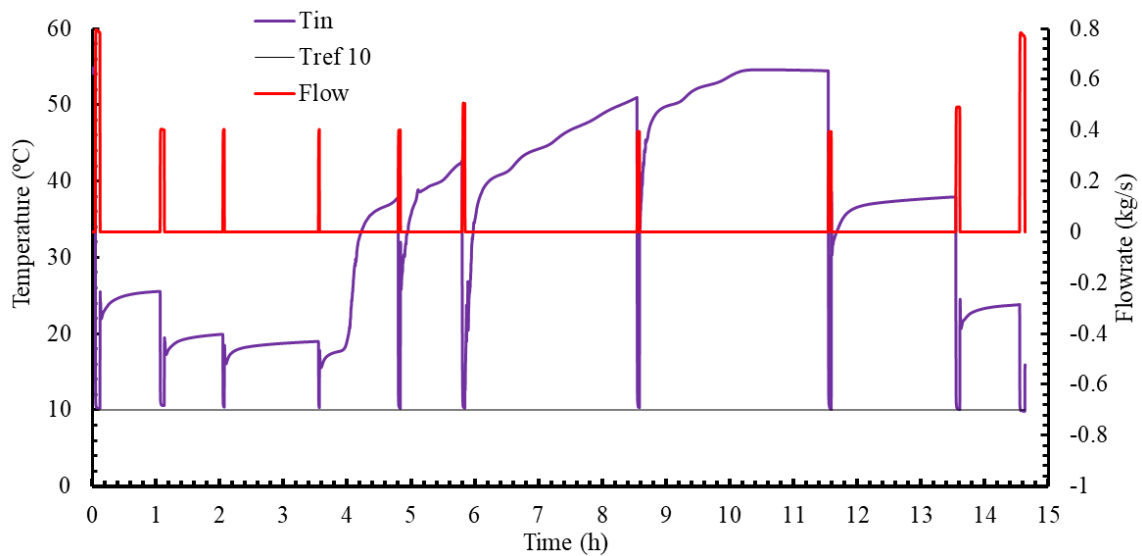


Figure III.27: Temperature of the inlet temperature

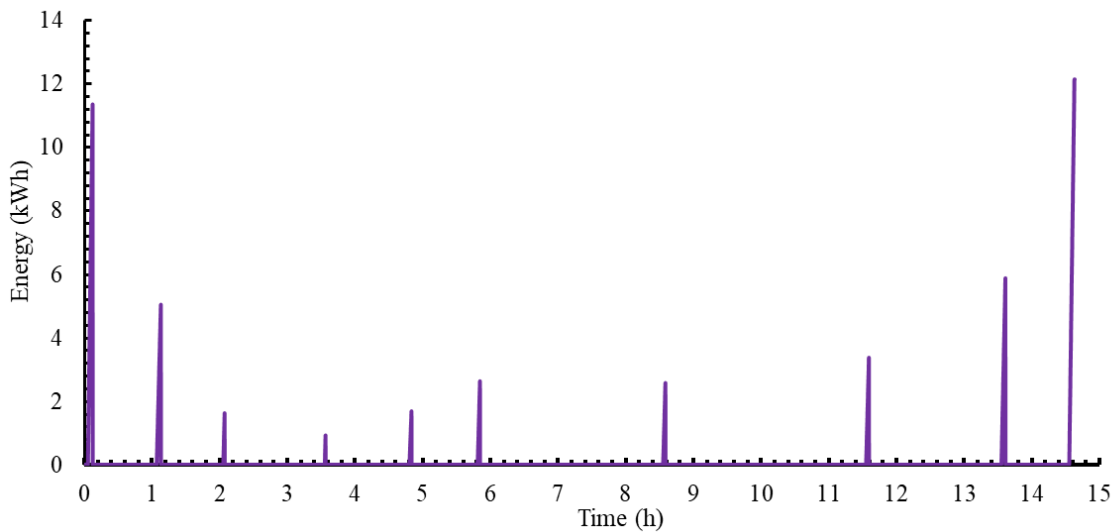


Figure III.28: Energy extracted of the of the hot water in every extraction

Figure III.28 shows the energy extracted in kWh of the hot water in every extraction. The extraction of the hot water begins at a specified moment according to the standard, once

the energy of the hot water extracted reaches the value mentioned in the extraction profile, the water pump stops and the valve closes.

The thermodynamic performance of the heat pump is also presented. As mentioned in the description the heat pump is off while the temperature of the highest region of the storage tank is higher than 59 °C, once this temperature is below 59 °C the heat pump starts up. Figure III.28 presents the theoretical COP as a function of time during the heating process of this test step. The theoretical COP is calculated according to the eq III.19.

$$COP_{th} = \frac{\int_0^{t_{test}} E_{GC}}{\int_0^{t_{test}} E_{comp}} \quad (III.19)$$

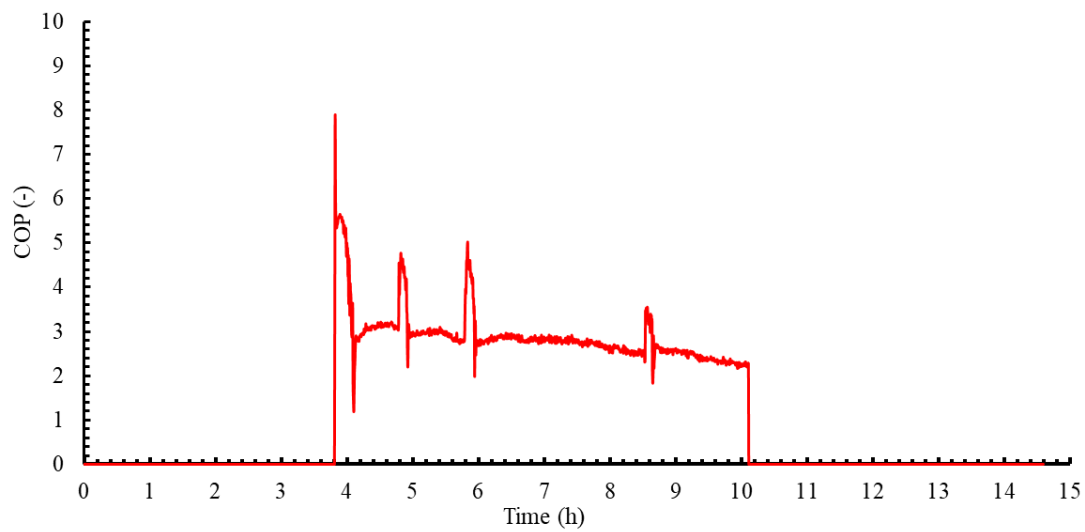
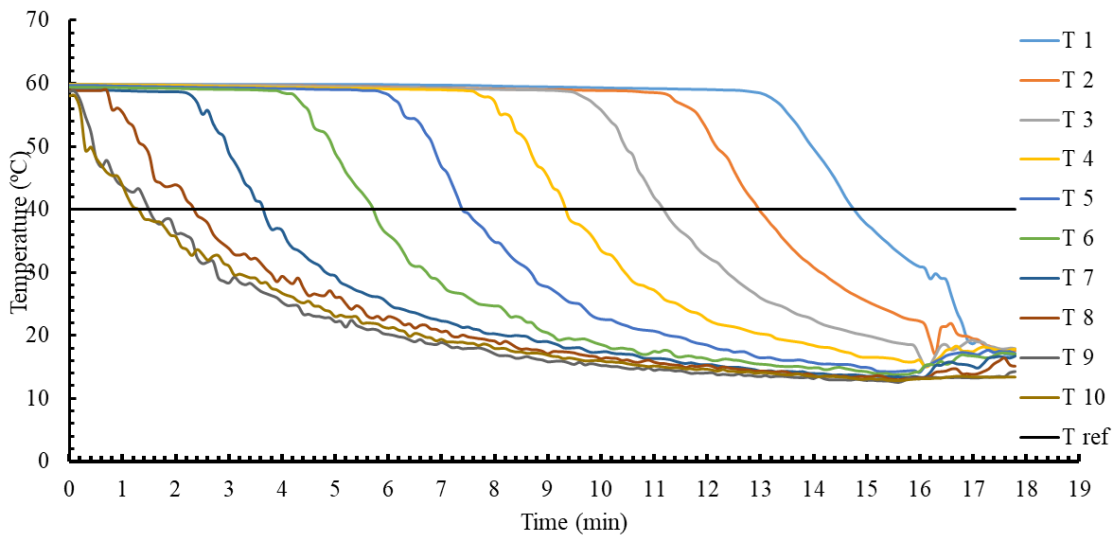


Figure III.29: Theoretical COP in function of time of heating process of the E step

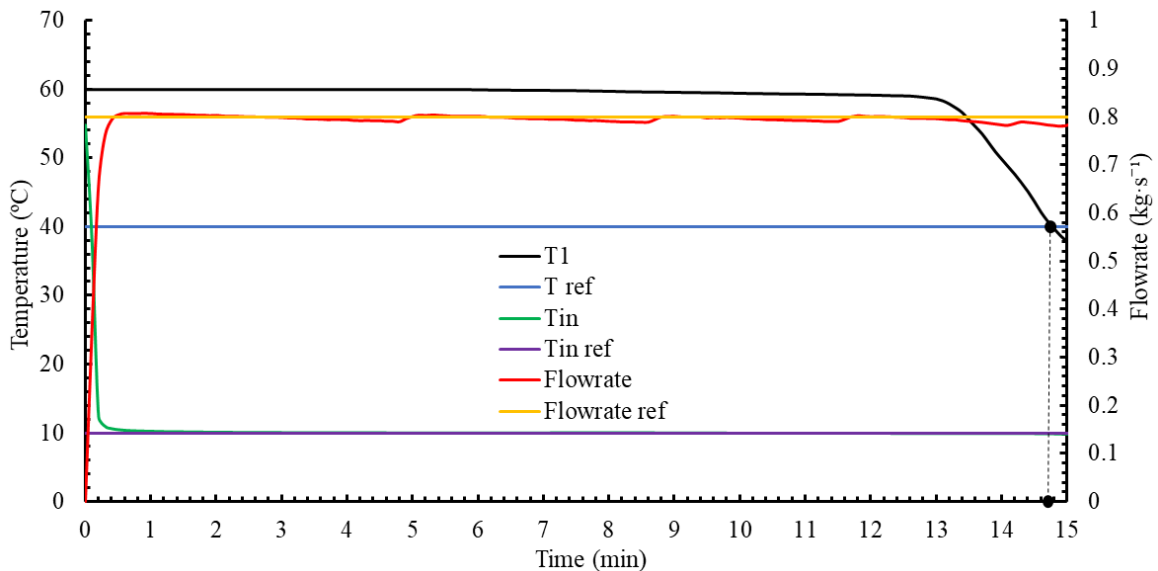
In figure III.29 the theoretical COP is represented in function of time during the extraction process. The COP is equal to 0 in the beginning and the end of this test step because the heat pump is off. Once the heat pump starts up the compressor consume electrical energy. The peaks in the figure refer to extraction moments. In those moments, the cold water enters the hot water storage tank at the bottom, and because the outlet port that extract water towards the gas cooler is situated at the bottom of the storage tank also, then, cold water at low temperature goes through the gas cooler, and as the gas cooler inlet temperature is lower, the COP increases, afterward the COP decreases because the water temperature homogenizes and increases inside the storage tank. In this period of the heating process of the step E, a global COP of 2.89 is resulted.

### III.4. Cooling process (Step F)

The test of the cooling process of the storage tank consists of extracting the hot water at a specific constant flowrate during the process until the temperature of the upper part of the tank decreases to 40 °C. Actually, the extracted hot water is replaced by the cold water at 10 °C, knowing that the extraction is from the top and the cold water enters at the bottom of the storage tank. Three extraction flowrates are investigated in this part: 0.1, 0.4 and 0.8 kg·s<sup>-1</sup>.

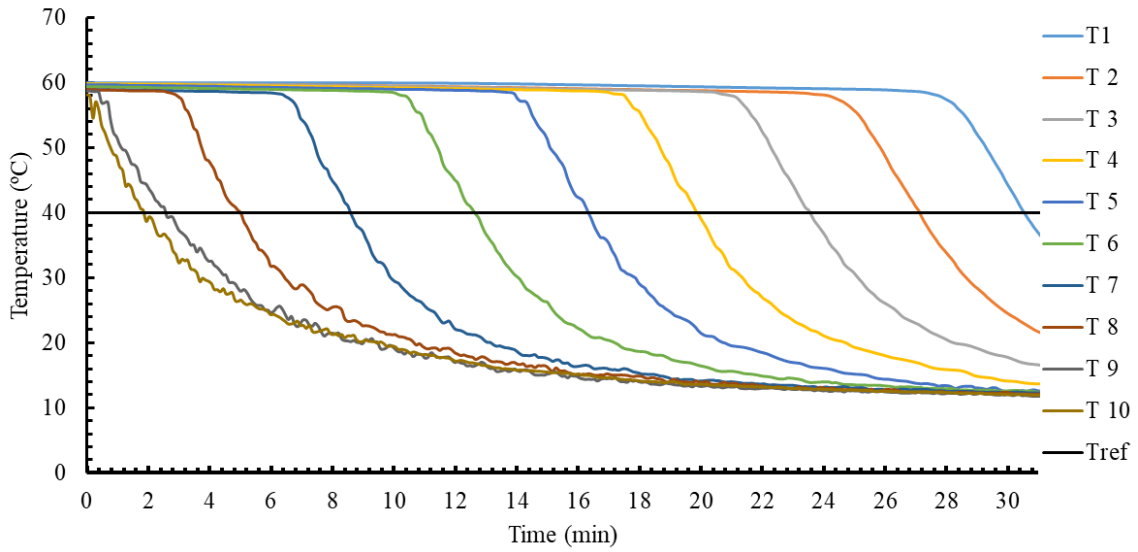


a) Temperature evolution of the 10 RTD sensors in function of time

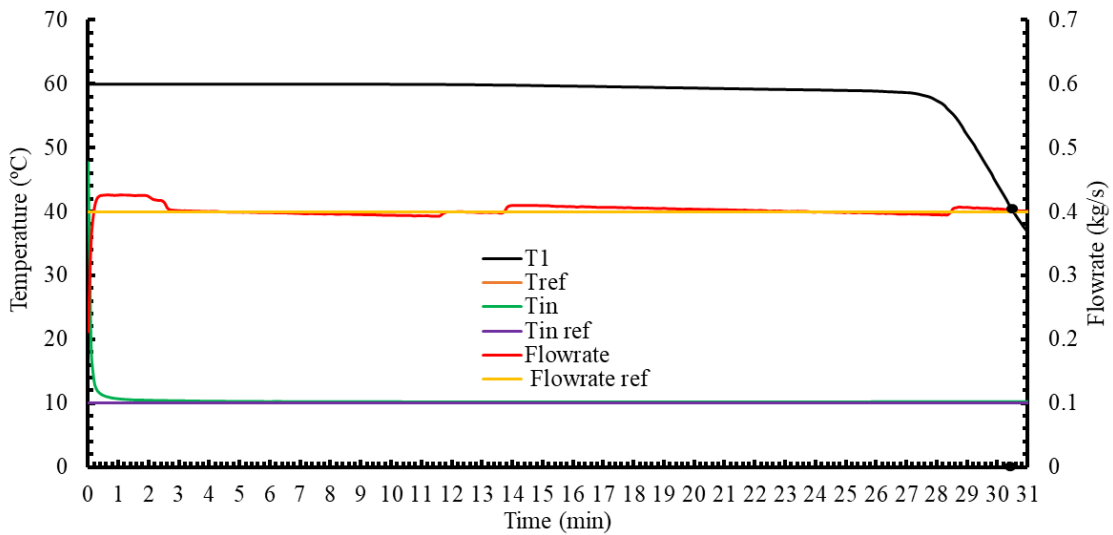


b) Temperature evolution of the highest sensors and the flowrate

Figure III.30: Temperature evolution of the storage tank in function of time of the cooling process (extraction flowrate 0.8 kg·s<sup>-1</sup>)

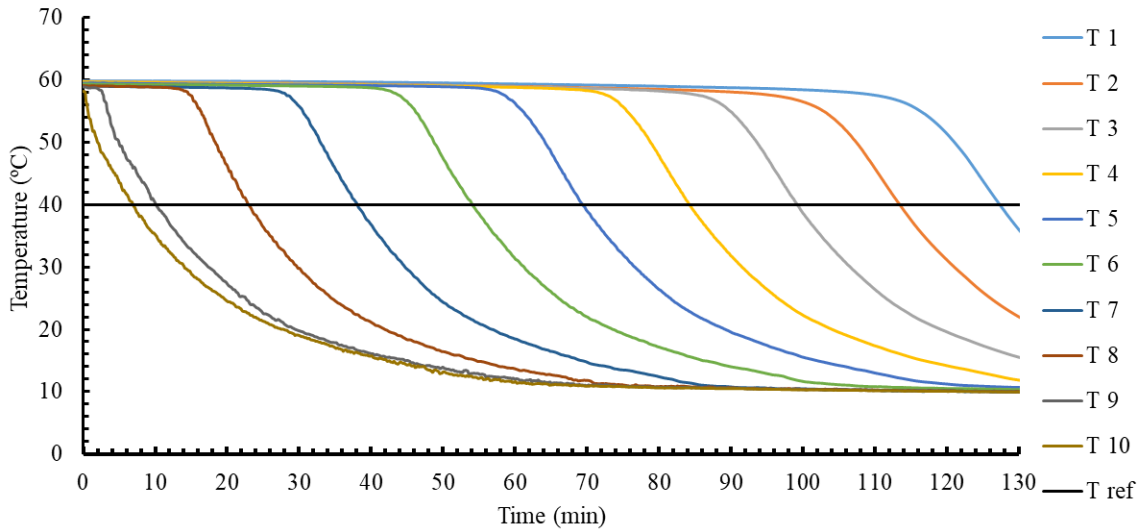


b) Temperature evolution of the 10 RTD sensors in function of time

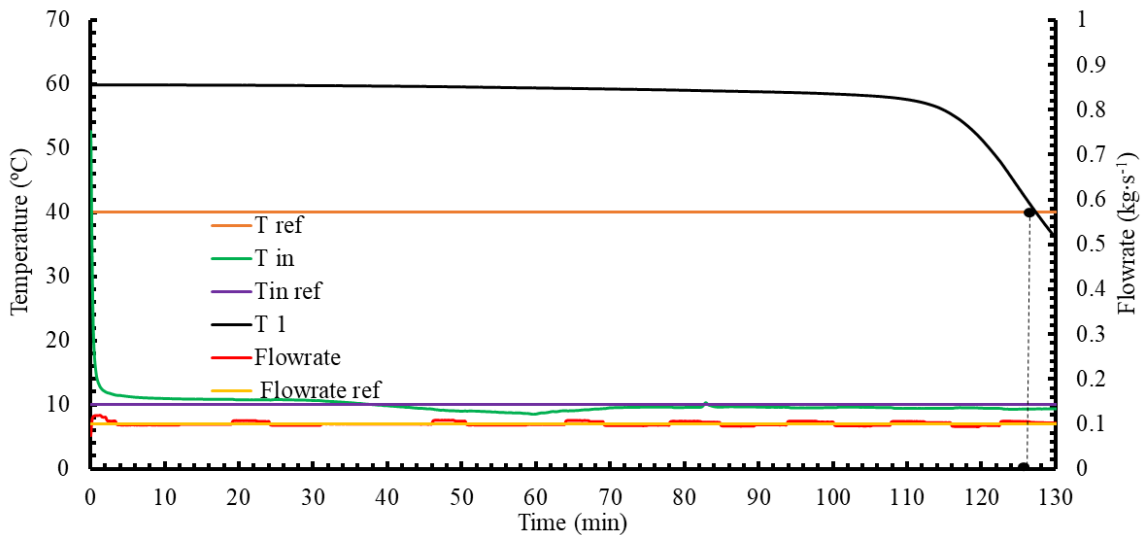


b) Temperature evolution of the highest sensors and the flowrate

Figure III.31: Temperature evolution of the storage tank in function of time of the cooling process (extraction flowrate  $0.4 \text{ kg}\cdot\text{s}^{-1}$ )



b) Temperature evolution of the 10 RTD sensors in function of time



b) Temperature evolution of the highest sensors and the flowrate

Figure III.32: Temperature evolution of the storage tank in function of time of the cooling process (extraction flowrate of  $0.1 \text{ kg}\cdot\text{s}^{-1}$ )

Figures III.30, III.31 and III.32 show the temperature distribution of the cooling process of the 10 RTD sensors in function of time and the extraction flowrate of each case of this process. In figures III.30.a, III.31.a and III.32.a, the temperature evolution in function of time for the 10 RTD sensors during the cooling process, it can be seen that the temperature of the storage tank decreases as the cooling time increases for all extraction flowrate cases. The temperature of the bottom part decreases in the beginning of the

cooling process, as the time increases, the temperature of the storage tank decreases. The decrement of the temperature of each layer is separated by a uniform spaced time for all cases, and this spacing time value represents the velocity of the cold water to travel from the bottom to the top of the storage tank. The temperature of the bottom of the tank reaches the temperature of 10 °C in the case of the extraction flowrate of 0.1 kg·s<sup>-1</sup>, in the other cases, the temperature of this region can't reach the temperature of 10 °C.

Figures III.30.b, III.31.b and III.32.b, illustrate this cooling process, in these figures the extraction flowrates and the inlet temperature of 10 °C and the temperature of the topper sensor of the storage tank are represented.

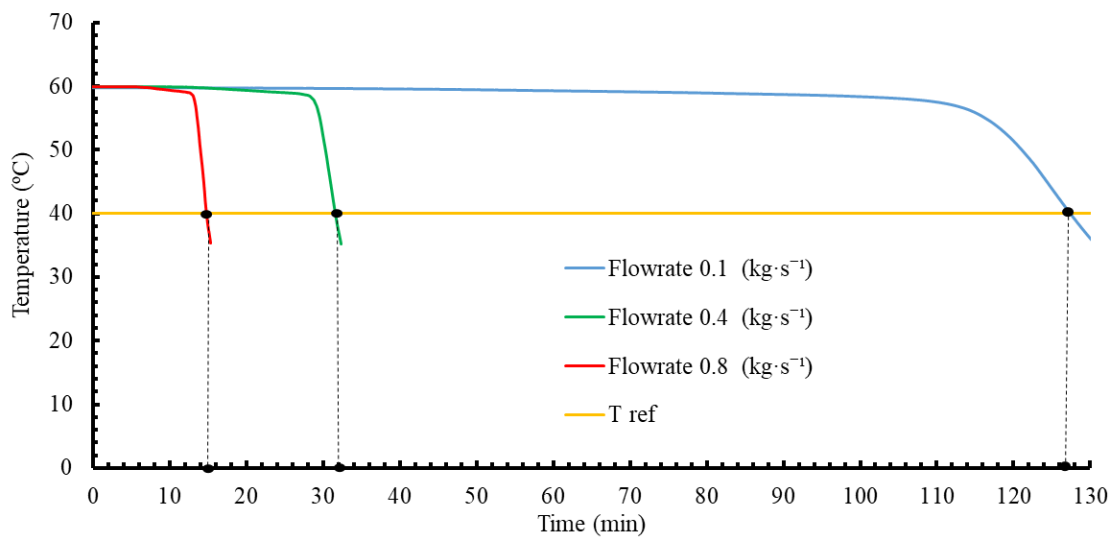


Figure III.33: Temperature evolution highest part of the storage tank in function of time of the cooling process

Figure III.33 shows the temperature evolution of the highest sensor in function of time for all extraction flowrates. The time of the cooling process also is illustrated in this figure and in the table III.4, and it can be seen that as the extraction flowrate increases, the cooling time decreases, and this is due to the traveling water inside the storage tank.

The cooling process take time of 14.7 minutes from the beginning of the cooling process (tank temperature = 60 °C) until the temperature of the topper part reaches 40 °C in the case of 0.8 kg·s<sup>-1</sup>. The cooling time in the extraction flowrate of 0.4 kg·s<sup>-1</sup>, is 30.48 minutes, and the cooling time in the case of 0.1 kg·s<sup>-1</sup> is 127.41.

Table III.4: Cooling process elapsed time.

Flowrate (kg·s <sup>-1</sup> )	0.1	0.4	0.8
Cooling time (min)	127.41	30.48	14.7

# Chapter IV





### I.1. Introduction

Thermal stratification is a natural phenomenon that occurs in thermal storage tanks, and it consists in forming of horizontal layers at different temperatures in such a way that the layer's temperature is always higher than that of the below one. The formation of different layer is due to the density difference of the liquid; hence the cold water has a higher density and the molecule's weight is higher than that of the hot water that has a lower density, and with the intervention of the gravity, this phenomenon is formed.

### I.2. Thermal stratification

The temperature distribution in a stratified storage tank depends mainly on its geometry. In fact, the factor height-width plays an important role in the stratification formation and stability [37,49 and 50]. The form and the disposition are also an important parameter that should be taken in consideration.

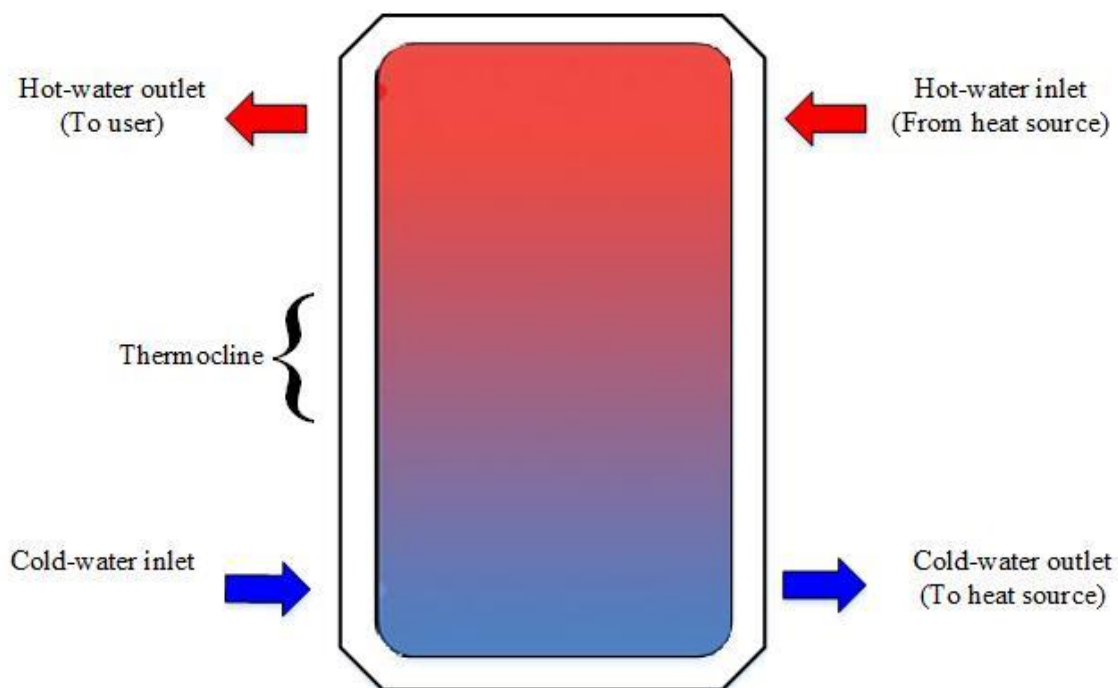


Figure IV.1: Schematic diagram of a stratified storage tank

In a stratified storage tank, it can be found two or more layers at different temperature. A well stratified storage tank has two different layers at two different temperatures named cold and hot region. The cold region is always at the bottom of the tank due to the high density and the hot region at the top, between the two regions a transient layer separates

the cold and hot regions, named thermocline [65-67]. The thermocline has an energetic benefice in thermal storage tank in which avoid liquid mixing of the two regions. The thermocline also has a width and a position, and these parameters depend on the geometry of the tank and the operating conditions. Thermal stratification has a great role for domestic hot water production as it can enhance thermal and energetic efficiency of the whole system. The geometry and the disposition of the tank (vertical or horizontal) also have an important impact in the hot-water stratification, and it can help to maintain the efficiency of the system.

The stratification occurs when the storage tank is at rest, once the liquid begins moving, the stratification formation and the layers disappears slowly until the temperature of the whole storage tank becomes homogenous. There are various parameters that can destroy the thermal stratification in the storage tank. One cause of the stratification destruction is the heat losses to the ambient, to minimize the heat losses and conserve a high thermal quality of water, a good insulation is recommended [68].

During heating or extractions of water, the flowrates must be controlled and optimized, because they also play an important role to avoid water mixing and conserve stratification. Also, the inlet and the outlet of the water during charging and discharging processes have an important impact on the thermal stratification efficiency. Hence, in a stratified storage tank the outlet of the hot water is always at the upper part of the storage tank, and the cold water enters always at the bottom of the tank.

Numerical modeling is an important tool to study the thermal stratification within the storage tank, in the literature, several models are presented. Three dimensional models are widely used in the stratification modelling within the storage tank. CFD is useful tool to show the thermodynamic of the flow inside the storage tank [35-38, 43, 45 and 46].

One dimensional modelling is widely used in thermal stratification within storage tank because the stratification is formed vertically along the vertical axis, and every horizontal layer has the same temperature [69].

Hoseon Yoo and Tong Pak [70] presented analytical solutions to a one-dimensional model for stratified thermal storage tanks. They analyzed the charging process in stratified thermal storage tanks using the semi-infinite assumption.

Nelson et al. [71] presented an analysis of the stratification in thermally stratified vertical cylindrical storage tank using one dimensional conjugate heat conduction model.

In their study, they analysed the impact of the length to diameter ratio, wall thickness to length ratio on thermal stratification degree, also, the thermo-physical properties of the material of the storage tank. The type and thickness of the insulation and the design of the water inlet system for both cold and hot water were also studied. The numerical model used by Nelson et al. is presented in the Figure IV.2.

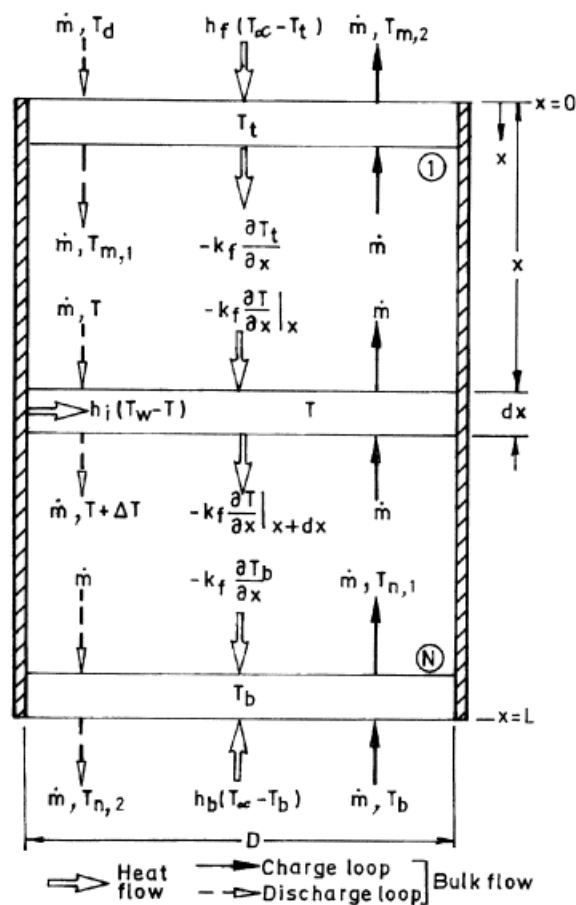


Figure IV.2: Schematic diagram of stratified storage tank model [71].

Mi-Soo Shin et al [72] presented a numerical study on the design of a stratified thermal storage system that sought to determine the optimum design and operating conditions. Also, they proposed for the evaluation of the performance of thermal storage system, to consider and solve the energy equation using the assumptions of the plug-type model.

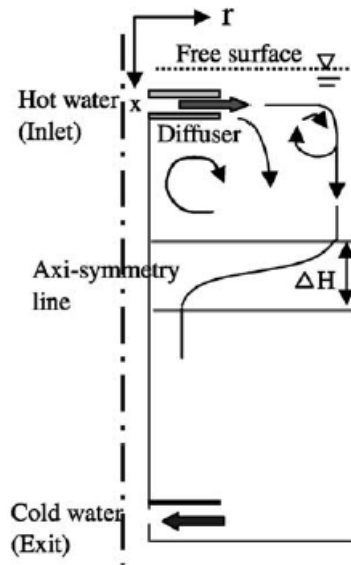


Figure IV.3: Schematic diagram of thermal storage tank [72]

They showed that the plug type model presented, can be used as a suitable tool for the design and evaluation of the thermal storage tank system performance.

Chandra and Tomas [73] presented a review on thermal stratified storage tank for domestic hot water. They categorized several numerical models as multi-node and plug-flow approach, and the temperature distribution models. They also studied the influence of the dynamic and static parameters on the thermocline decay. Some methods of the performance improvement as geometrical parameters, inlet design, tank aspect ratio and wall material specification are presented.

Christopher and Cynthia [74] presented a comparison of the thermal stratified storage tank models of the TRNSYS library (Type 60, Type 534 and Type 4). They found that, the three models predict the identical performance of the tank and there is almost not deviation in tank temperature from one type to another. They also reported that Type 4, Type 60, and Type 534 have the same limitations and can be used interchangeably.

In the TRNSYS library [75], it can be found various numerical models of a stratified storage tank. These models can be either directly heated or can be heated by an additional heat exchanger called auxiliary heater. The auxiliary heaters are used in order to maintain the thermal stratification within the storage tank.

Actually, in TRNSYS library there are several models of thermal storage tank, but there are 3 types that model the thermal stratification (Type 4, Type 39 and Type 60).

### I.3. Stratified storage tank models

#### I.3.1. Stratified fluid storage tank (Type 4)

A multi-node model consists of dividing the tank into  $N$  equally horizontal volume segments (layers or nodes). In the case of  $N=1$ , the storage tank is considered as a fully mixed storage tank and there is no stratification formation. To obtain a high degree of stratification, the  $N$  must have higher values.

The energy balance of this model is as follow

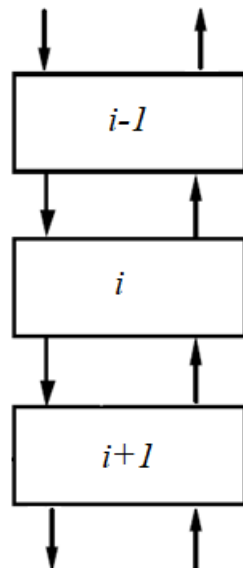


Figure IV.4: Stratified fluid storage tank model [75]

I.3.2. Plug flow Tank (Type 38)

The plug flow model is an algebraic model that simulates the thermal behavior of the thermal stratification inside a storage tank. This model takes in account a variable number and size of segments. In this model the fluid domain of the tank is divided into four segments and each one has a volume  $V_i$  and a temperature  $T_i$ . During the operation of the system, if the heat source has a temperature  $T_h$  which is higher than that of the upper part of the tank then the volume of the tank is shifted downward and the new volume is added above. And at the same time a volume of water is returning from the load at a temperature  $T_L$ . If the load temperature is lower than that of the bottom, a segment is added to the bottom and the tank volume is shifted upward as it seen in the figure.

The energy balance of this model is as follow:

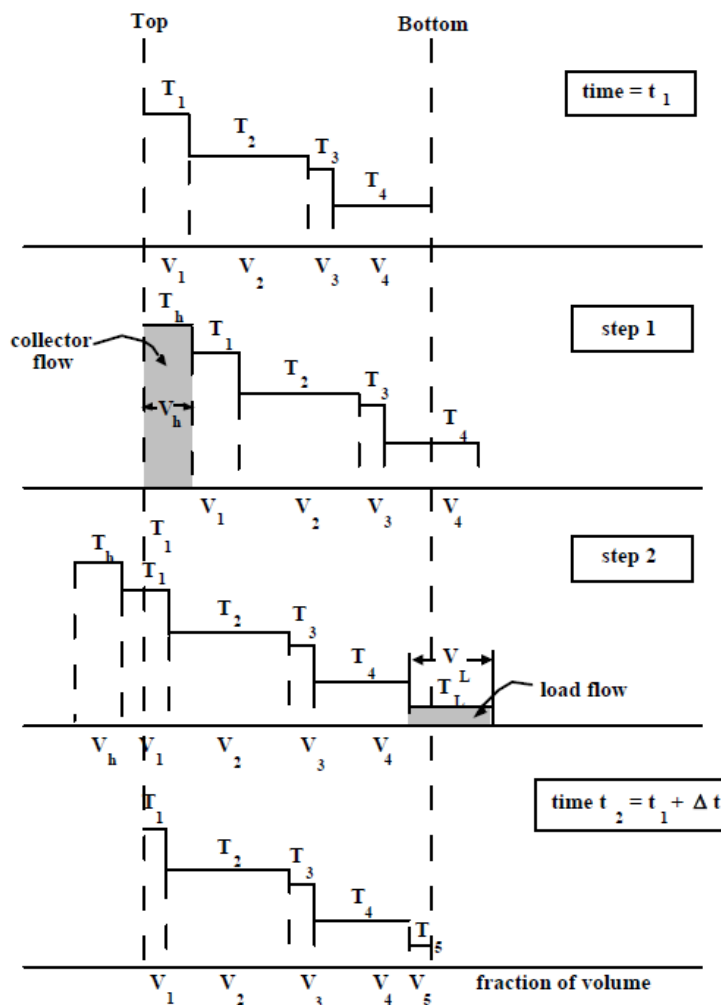


Figure IV.5: Plug flow Tank model [75]

### I.3.3. Stratified storage tank model (Type 60)

This model of storage tank is also named detailed fluid storage tank (type 60), and it simulates the stratification within a storage tank considering that the storage tank is divided into  $N$  fully mixed segments.  $N=1$  means a mixed storage tank and there is no stratification effect in the tank. The stratification degree is depending on the  $N$  value [75].



#### I.4. Development of a new model: Present model (Type 269)

In all of the previous models used in the TRNSYS library, the convective heat losses to the ambient and the convective coefficient inside the storage tank are taken as constant input values. Besides also the thermo-physical properties of the fluid are taken as constant inputs values.

In the present model, thermo-physical properties of the fluid, and the convective heat transfer coefficients are calculated as a function of temperature in each time step iteration. The main idea of this model is to show the thermal stratification phenomenon of the storage tank taking into account the variation of the thermo-physical properties of the fluid as a function of temperature and the heat losses are also calculated in function of the temperature of the storage tank (eq. IV.1- eq. IV.6)

A one-dimensional (1D) numerical model of the hot water storage tank is developed and described in this section. This model is based on the finite difference method to discretize the total volume into volumes segments (figure IV.6).

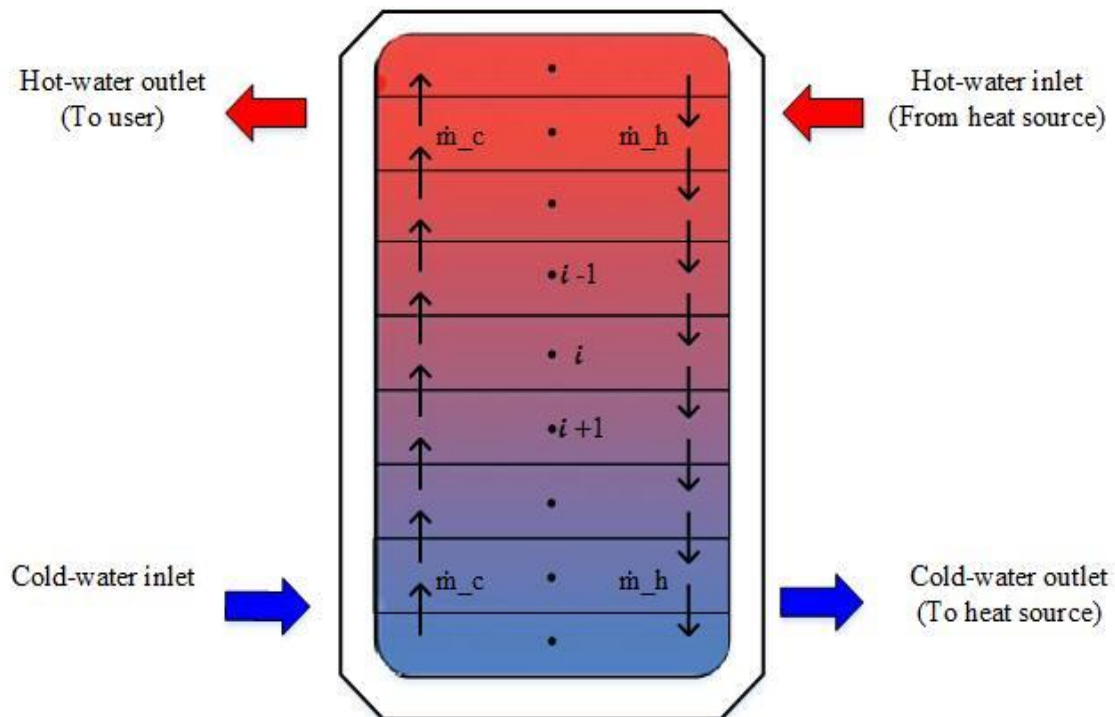


Figure IV.6: Schematic diagram of the present model (Type 269)

The heat transfer phenomena that occur inside and outside the storage tank as the convection and conduction are shown in the figure.

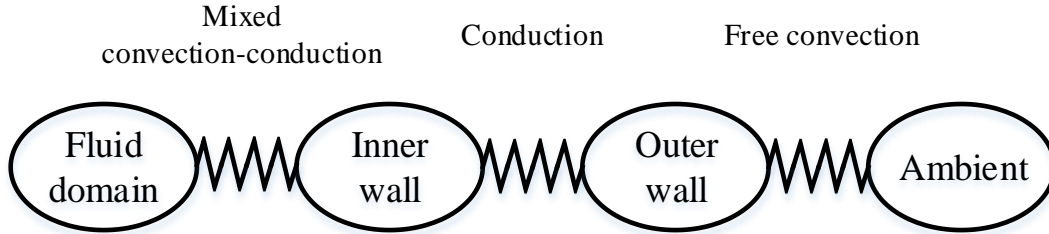


Figure IV.7: Schematic diagram of the heat transfer phenomena based on the thermal resistance of system.

Figure IV.7 shows the schematic diagram of the heat transfer phenomena inside and outside the storage tank. In the present model, it is considered the following heat transfer mechanism:

- \* Molecular conduction inside the storage tank, and this parameter plays an important role in stratification and destratification of the fluid contained in the storage tank, also in the convection heat transfer between the fluid and the inner wall of the storage tank.
- \* Conduction heat transfer between the inner and the outer wall of the storage tank.
- \* Free convection between the outer wall of the tank and the ambient.
- \* Radiation is neglected in this model.

In the model, the convective heat transfer coefficient  $h$  is calculated from Nusselt correlations. Depending on the geometry of the surface and the range of the Rayleigh number, different Nusselt's number correlations are selected [76]

The lateral surface of the tank is a uniform cylinder, and it is treated as a vertical wall since the condition  $D \geq \frac{35L}{Gr^{1/4}}$  is verified.

Where:

$$Gr = \frac{g \beta (T_w - T_{amb}) L_c^3}{\nu} \tag{IV.1}$$

The correlation more accurate of Nusselt number for vertical surfaces is given by [76]:

$$Nu = \left\{ 0.825 + \frac{0.387 Ra_L^{1/6}}{[1 + (0.492/Pr)^{9/16}]^{8/27}} \right\}^2 \quad (IV.2)$$

In the present model, the top and the bottom surface are horizontal discs and are treated as horizontal plate surfaces.

The Nusselt number of the upper surface is given by [76]:

$$Nu \begin{cases} Nu = 0.59 Ra_L^{1/4} 10^4 \leq Ra \leq 10^7 \\ Nu = 0.1 Ra_L^{1/3} 10^7 < Ra \leq 10^{11} \end{cases} \quad (IV.3)$$

The Nusselt number for the bottom surface is given by [76]:

$$Nu = 0.27 Ra_L^{1/4} \quad (IV.4)$$

Where:

$$h = \frac{Nu k}{D} \quad (IV.5)$$

with k the thermal conductivity of the fluid.

The Rayleigh number is given by [76]:

$$Ra = \frac{g \beta (T_m - T_{amb}) L_c^3}{\nu \alpha} \quad (IV.6)$$

where:  $\beta = \frac{1}{T_m}$ ,  $T_m$  is the average temperature of the outer wall surface and  $T_{amb}$  is the ambient temperature out of the thermal boundary layer.  $L_c$  is the characteristic vertical length scale of the problem,  $\mu$  is the dynamic viscosity and  $\alpha$  is the thermal diffusivity of the fluid.

The numerical model of the present study discretizes the hot-water storage tank into  $N$  horizontal segments or nodes. For validation purposes, the centroid of each segment coincides with the location of one of the 10 temperature sensor installed in the axis of the hot-water storage tank of the experimental facility. In order to permit a high stratification degree, the model uses the flow stream assumption. In other words, the model assumes that inlet and outlet the fluid streams flowing up and down during the consumption and filling processes fully mix the fluid mass instantaneously within each node. Thus, based

on the above assumptions, the model considers a mass and energy balance between each segment of the tank, the walls and the tipping.

This information is used in to discretize the unsteady energy conservation equation as shown in the following figure:

**Node1 (top segment):**

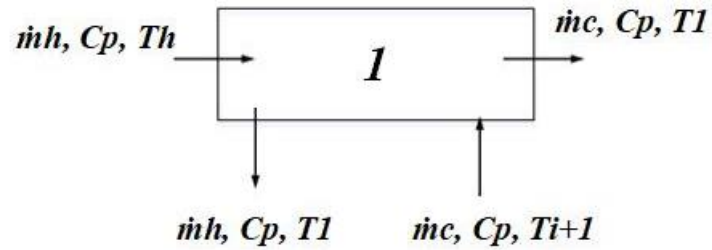


Figure IV.8: Energy balance of the node 1 (top)

$$m * C_p \frac{(T_1^{j+1} - T_1^j)}{\Delta t} = h * S_{1,w} * (T_w^j - T_1^j) + \frac{k * S_{i,i+1}}{\Delta h_i} * (T_{i+1}^j - T_1^j) + \begin{cases} (\dot{m}_h - \dot{m}_c) * (T_{i+1}^j - T_1^j), & \dot{m}_h \geq \dot{m}_c \\ (\dot{m}_c - \dot{m}_h) * (T_h^j - T_1^j), & \dot{m}_h < \dot{m}_c \end{cases} \quad (IV.7)$$

**Nodes 2 to n-1 (middle height segments):**

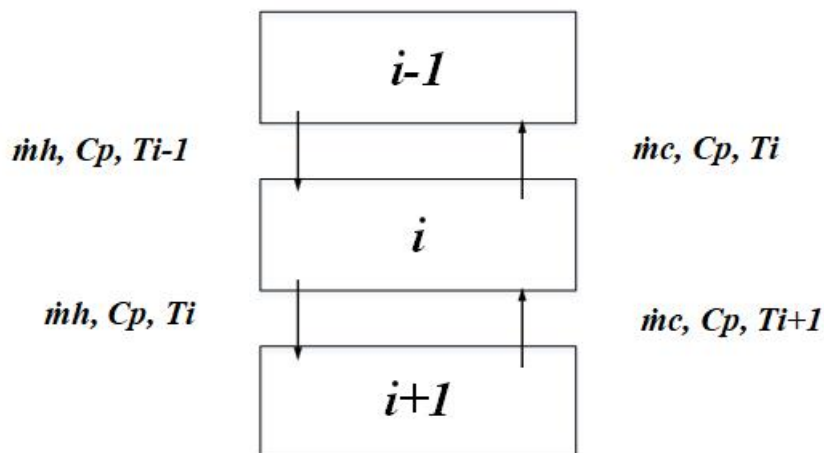


Figure IV.9: Energy balance of the central nodes

$$m * Cp \frac{(T_i^{j+1} - T_i^j)}{\Delta t} = h * S_{i,w} * (T_w^j - T_i^j) + \frac{k * S_{i,i+1}}{\Delta h_i} * (T_{i+1}^j - T_i^j) + \begin{cases} (\dot{m}_h - \dot{m}_c) * (T_{i+1}^j - T_1^j), & \dot{m}_h \geq \dot{m}_c \\ (\dot{m}_c - \dot{m}_h) * (T_{i-1}^j - T_1^j), & \dot{m}_h < \dot{m}_c \end{cases} \quad (IV.8)$$

Node n (bottom segment):

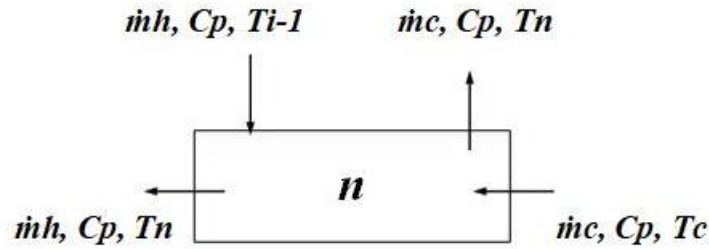


Figure IV.10: Energy balance of the last node (bottom)

$$m * Cp \frac{(T_i^{j+1} - T_i^j)}{\Delta t} = h * S_{1,w} * (T_w^j - T_1^j) + \frac{k * S_{i,i+1}}{\Delta h_i} * (T_{i+1}^j - T_1^j) + \begin{cases} (\dot{m}_h - \dot{m}_c) * (T_c - T_n), & \dot{m}_h \geq \dot{m}_c \\ (\dot{m}_c - \dot{m}_h) * (T_{i-1} - T_1), & \dot{m}_h < \dot{m}_c \end{cases} \quad (IV.9)$$

where  $T_i$  is the water temperature of the node, the superscripts  $j+1$  and  $j$  denote the time steps,  $S_{i,w}$  is the wall surface of the tank in contact with the node  $i$ ,  $T_w$  is the wall temperature in contact with that node.  $C_p$  is the specific heat of the water at constant pressure. Finally,  $\dot{m}_{h\_in}$ ,  $\dot{m}_{c\_in}$  are respectively hot and cold-water mass flowrates entering the hot-water storage tank and,  $\dot{m}_{h\_out}$ ,  $\dot{m}_{c\_out}$  are the hot and cold-water mass flowrates leaving the tank. After doing some algebra with mass conservation equation it is easy to show that, if the characteristic time of the transients is much smaller than the characteristic time of the tests, the steady state assumption can be adopted and  $\dot{m}_{h\_in} = \dot{m}_{h\_out} = \dot{m}_h$ , and  $\dot{m}_{c\_out} = \dot{m}_{c\_in} = \dot{m}_c$ . Please note that, based on the assumption adopted in the model; the energy absorbed by each segment depends on the difference between  $\dot{m}_c$  and  $\dot{m}_h$ .

**I.5. Model validation**

With the aim to show the accuracy of the model, a series of comparisons between the present model and the experimental results are done. For this purpose, the step C and the step E of the test procedure are chosen as a reference. As described above, the step C consists of heating the water stored in the storage tank from 10 °C until the upper sensor of the tank reaches 60 °C, and the step E consists of extract water at the temperature of 60 °C following the extraction profile shown in the table above.

Figure IV.11 shows the TRNSYS program of the numerical simulation of the Type 4, Type 60, and Type 269. Type 269 is the storage tank model developed in our laboratory and the other ones (Type 4 and type 60) are the TRNSYS library models. The input component contains the experimental data of the temperature and the flowrate at the inlet of the gas cooler. In order to perform the numerical simulations, the temperature of the water coming out from the gas cooler towards the inlet of the tank and the flowrate of the experimental results are introduced as input at the inlet of the storage tank.

With the aim to show the accuracy of the model, a series of comparisons between the present model and the experimental results are done. As described above, the step C consists of heating the water stored in the storage tank from 10 °C until the upper sensor of the tank reaches 60 °C. In this case, the test number 1 and 5 from the Table III.1 from the chapter III are taken in consideration.

Figure IV.11 shows the TRNSYS program of the numerical simulation of the Type 4, Type 60, and Type 269.

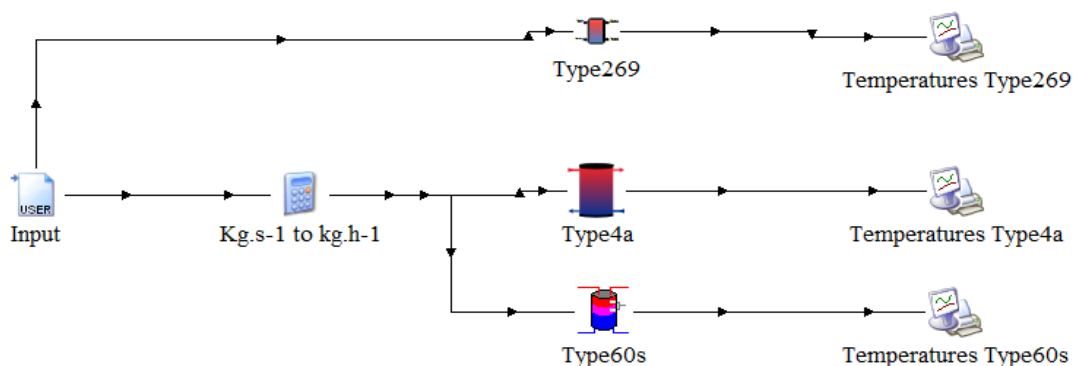
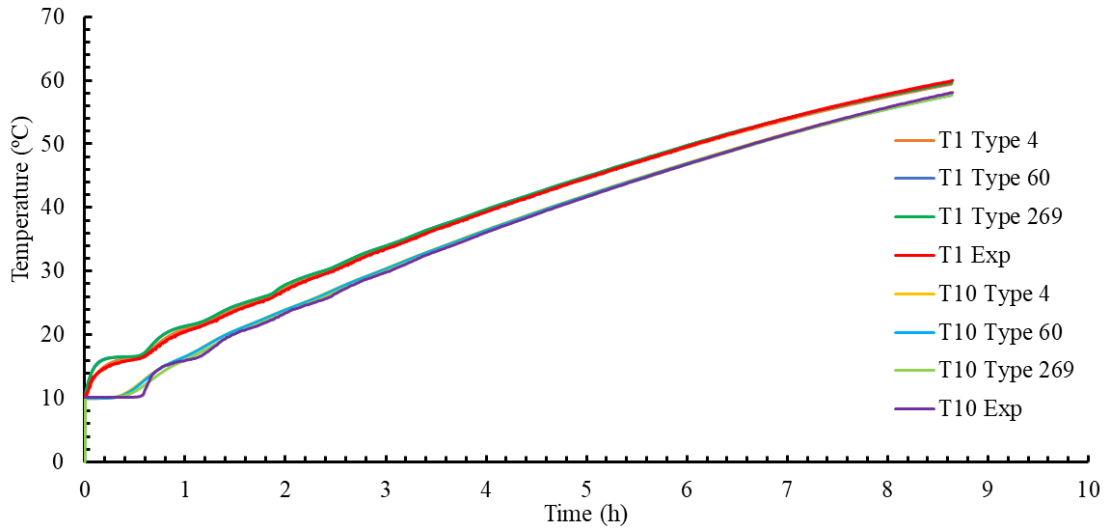
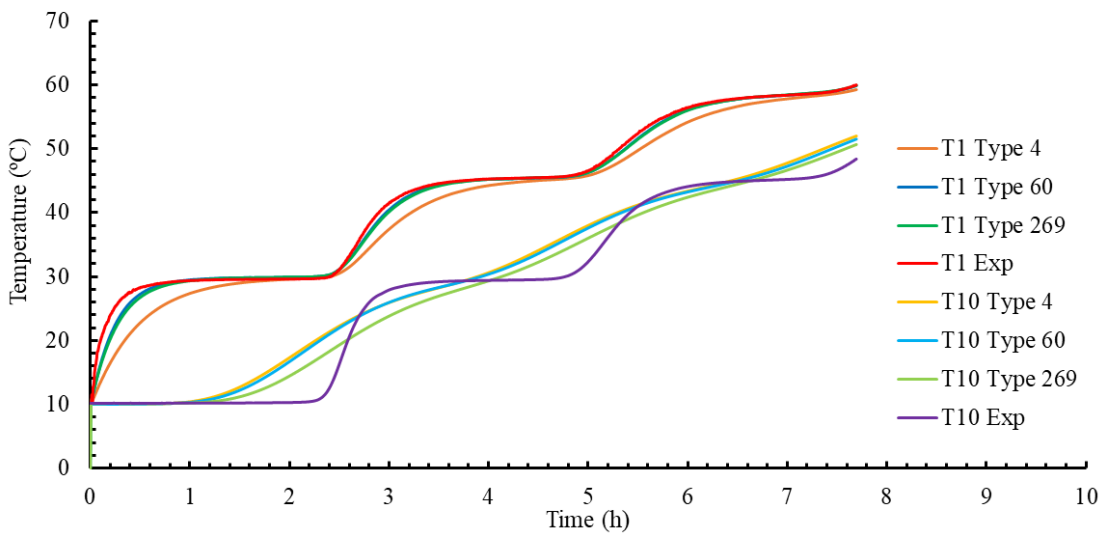


Figure IV.11: TRNSYS program of the Step C



a) Gas cooler flowrate =  $0.305 \text{ kg}\cdot\text{s}^{-1}$



b) Gas cooler flowrate =  $0.083 \text{ kg}\cdot\text{s}^{-1}$

Figure IV.12: Comparison of the temperature evolution of the heating process

Figure IV.12 shows the temperature evolution of the top and the bottom of the storage tank, the comparison between the numerical results of the stratified storage tank of TRNSYS library (Type 4 and Type 60), and the stratified storage tank model developed in our laboratory (Type 269) and the experimental results are presented. Regarding the nodes number inside the storage tank (fluid domain) 10 nodes are taken in this case. The results agree well for all the numerical models in comparison with the experimental results in the case of the high flowrate ( $0.305 \text{ kg}\cdot\text{s}^{-1}$ ) when no stratification phenomenon

effect occurs. On the other hand, in the case of lower flowrates ( $0.083 \text{ kg}\cdot\text{s}^{-1}$ ), the temperature of the bottom of the storage tank of model takes an evolution of a slightly straight line and initially seems not to follow the experimental tendency because of the lack of a correct discretization of the special domain.

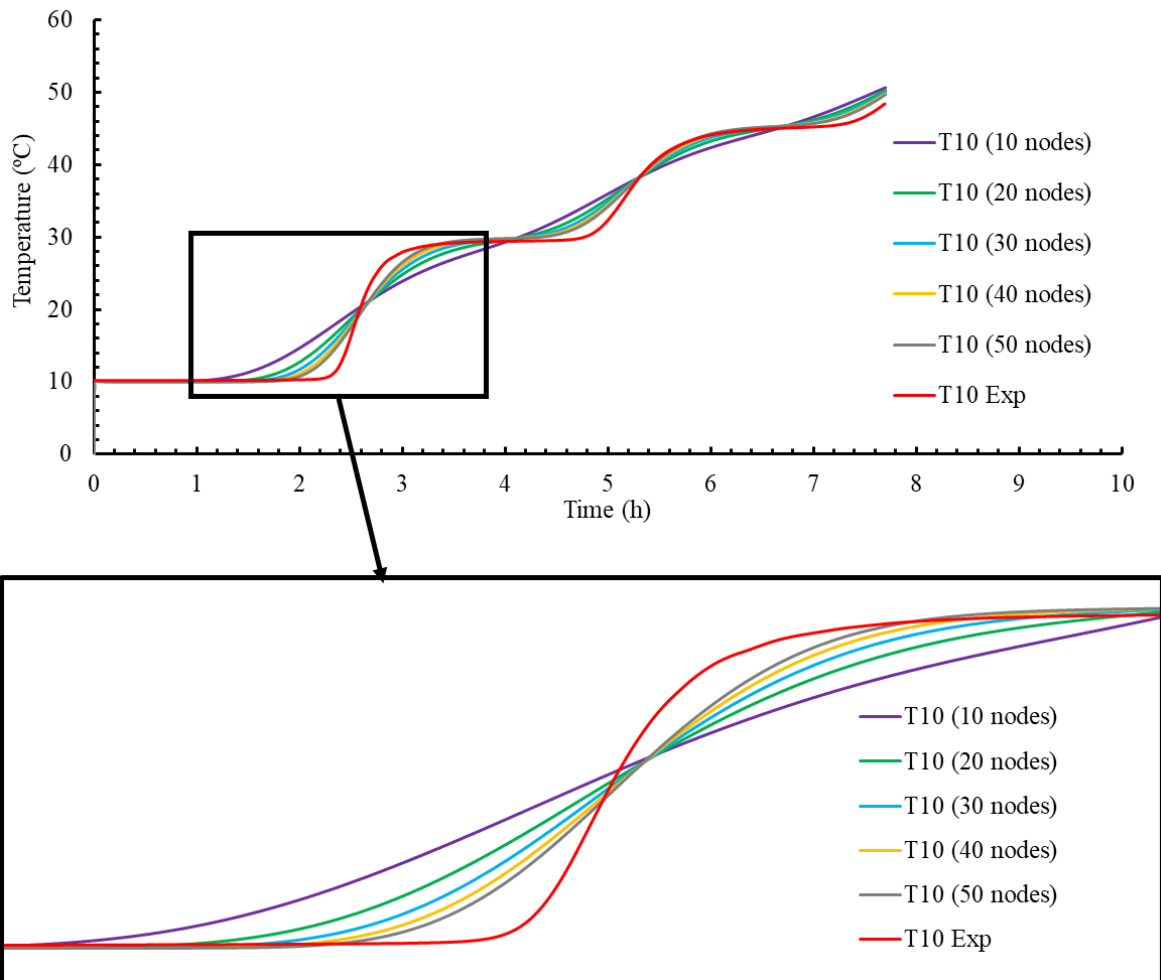


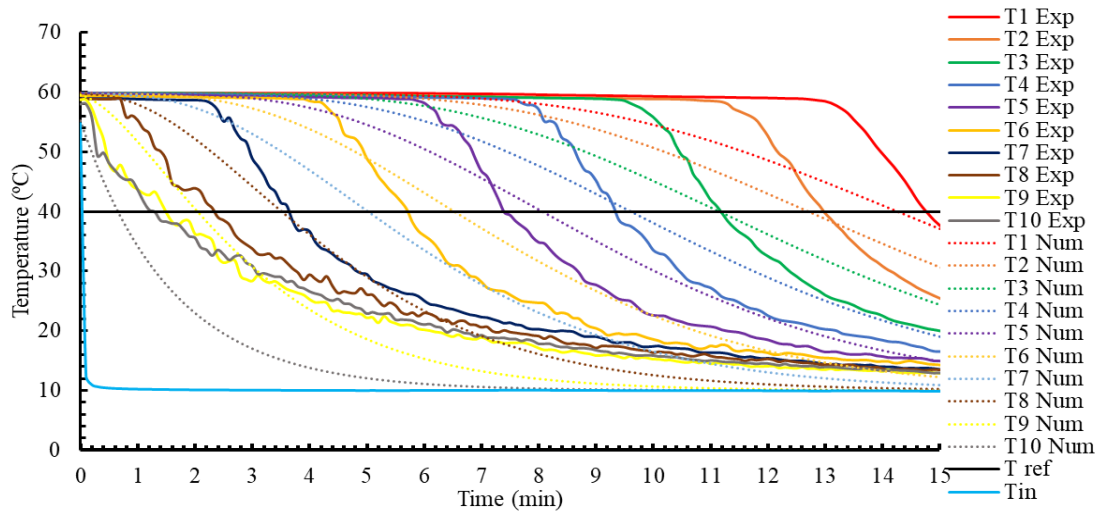
Figure IV.13: Impact of the node number on the stratification formation (Type 269)

Figure IV.13 shows the effect of the nodes number inside the storage tank (fluid domain) in the case of the lower flowrates ( $0.083 \text{ kg}\cdot\text{s}^{-1}$ ) for the model developed in this work (Type 269). In this parametric study the node number are taken as 10, 20, 30, 40 and 50 nodes and results are compared under the same operating conditions. It can be clearly seen that the nodes number has an important effect on the stratification modulization. Also, it can be seen that as the node number increases, the temperature evolution of the numerical model approaches to the experimental results. This means that there is a grid convergence of the results towards the experimental results. In the case of 40 and 50

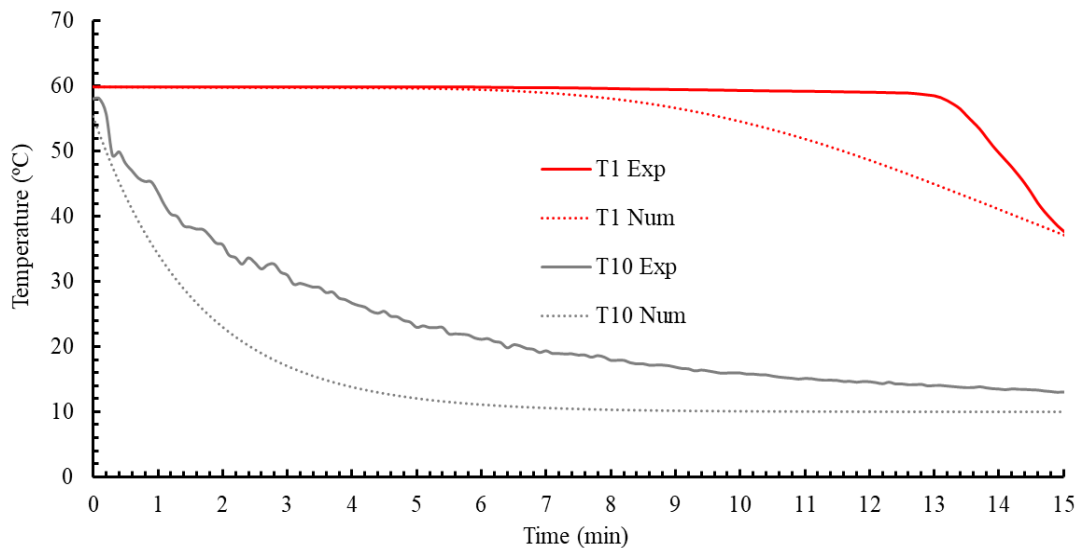


nodes, the results are slightly superimposed, so, for more analysis, the case of 50 nodes is taken into account.

In order to validate the model, the results of the cooling process experiment (step E) also are compared to the results of the numerical model. For this, the inlet flowrate at the storage tank is introduced as input in the stratified storage tank model. In this case, the initial temperature of the storage tank is 60 °C, and the inlet water temperature is 10 °C. Results are shown in the following figures:



a) Comparison of the temperature evolution of the cooling process for 10 layers.



b) Comparison of the temperature evolution of the cooling process for top and bottom temperatures

Figure IV.14: Comparison of the temperature evolution of the cooling process. a) comparison of 10 different layers. b) Top and the bottom temperatures.

## Chapter IV: Numerical model of stratified storage tank

In the experimental results, the temperature remains at the initial temperature of 60 °C then it begins to decrease until about 13 minutes, in the numerical results, the temperature begins to decrease in the 7<sup>th</sup> minute. The cooling time of this step is showed in table IV.1. All in all, the time of the cooling process are similar with a small error of 2.72%.

Table IV.1: Cooling time for both numerical and experimental.

	Experimental result	Numerical model
Cooling time (min)	14.7	14.3

The numerical results of the step E also are introduced to the model in order to show its feasibility. In this stage of the model validation, the temperature distribution inside the storage tank is compared with the experimental results.

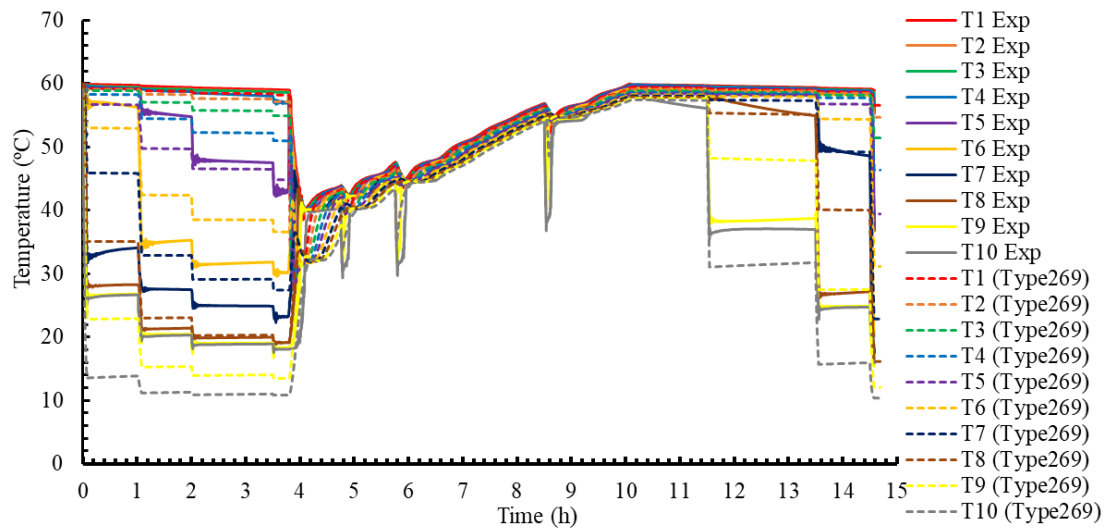
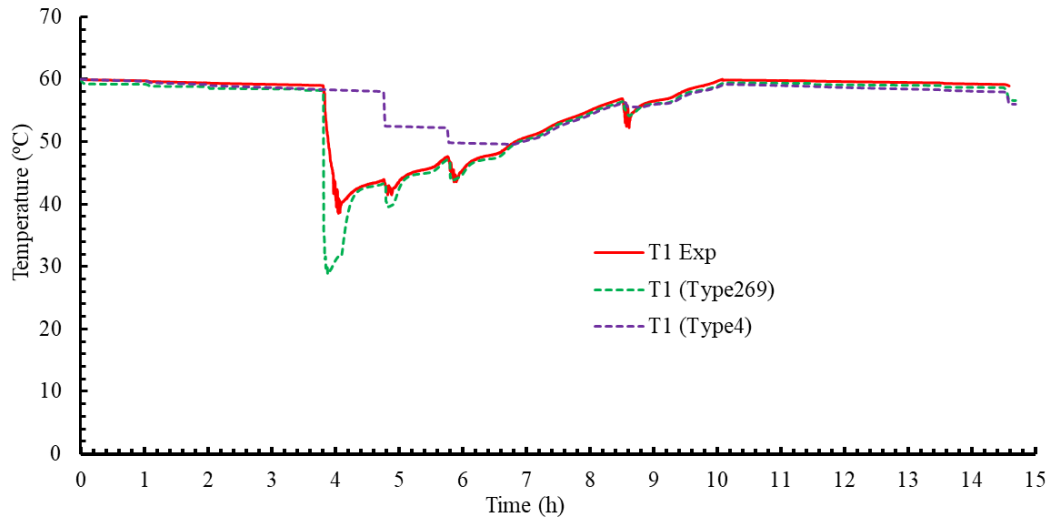
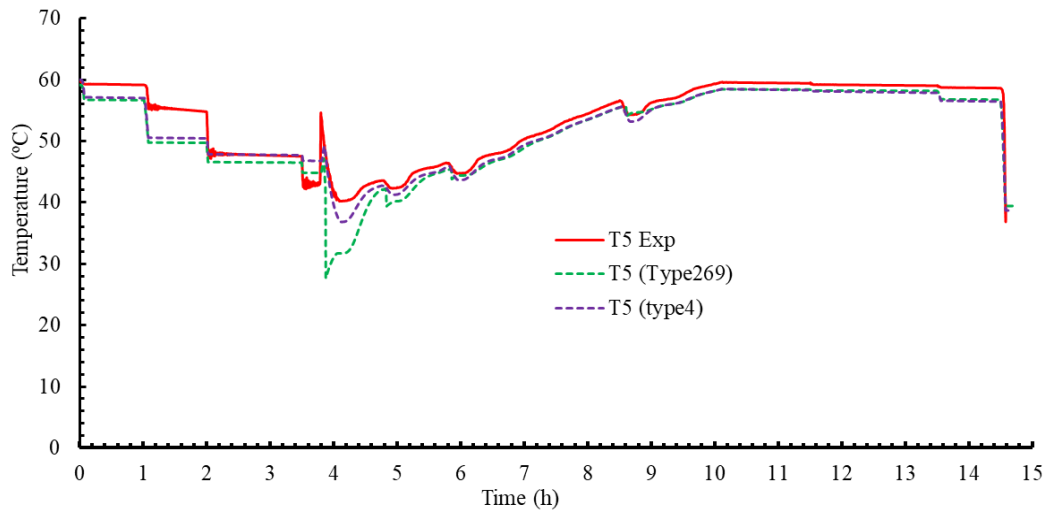


Figure IV.15: Temperature evolution of the step E for both numerical and experimental results.

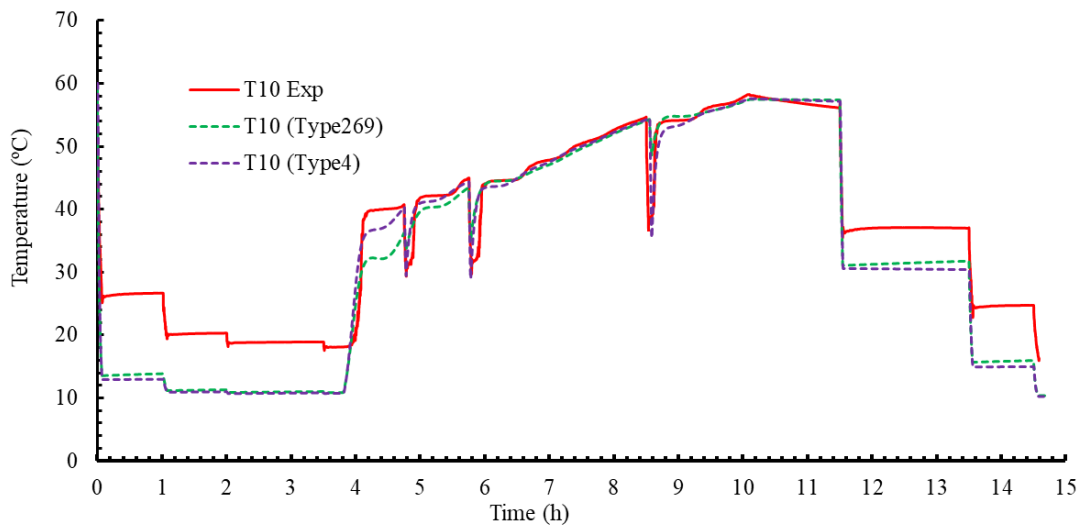
Figure IV.15 shows the comparison of the temperature distribution of the 10 sensors for both numerical and experimental results. To show the results comparison clearly, three regions of the storage tank are taken and compared in Figure IV.16, the top the bottom and the middle of the tank temperature.



a) Top of the storage tank



b) Middle of the storage tank



c) Bottom of the storage tank

Figure IV.16: Temperature evolution of three sensors for Type 4 model and the present model (Type269).

Figure IV.16 presents the comparison of the temperatures evolution as a function of time of the extraction process at the top, the bottom and the middle of the storage tank for the models type 269 and type 4 and the experimental results. It can be seen that the numerical results of the top of the storage tank of the present model (Type 269) agree well with the experimental results with a slight deviation comparing with type 4 (figure IV.16.a). The only deviation of the present model is when the heat pump starts-up, this is due to the mixing inside the storage tank.

Also, the temperature of the storage tank at the middle shows a great coincidence with the results obtained from experiment with the presence of a small error at mixing (Figure IV.16.b).

The bottom of the storage tank also coincides with the experimental results for both models. At the middle and at the bottom of the storage tank the temperature of the storage tank in the case of the numerical results is colder than that of the experimental results, because the inlet temperature of the charging water at every extraction is 10 °C. In the experimental results, the inlet cold water mixes with the warm water contained in the storage tank, thus the temperature of the bottom of the tank is higher than 10 °C.



# Conclusion



The energy efficiency of a DHW production system using trans-critical CO<sub>2</sub> heat pump was analyzed experimentally and numerically under the European standard. For this, a CO<sub>2</sub> heat pump coupled with a stratified storage tank are mounted together to perform the tests.

The DHW system analysis procedure consists of 3 main tests, the heating process, the extraction process and finally a cooling process.

The impact of the IHX is performed comparing two configurations of the heat pump, in the first, a simple cycle without IHX is analyzed, then, the same cycle including an IHX is compared to the simple cycle.

With the aim to perform the heating process and to analyze the energy efficiency of the whole system during this step, various operating conditions were introduced. The impact of the gas cooler flowrate on the heat pump efficiency and the stratification formation was studied. Also, the impact of the evaporator inlet temperature was analyzed to show the energy efficiency of the system under these conditions. The main conclusions are illustrated as follow:

The use of the IHX has a benefit on the thermodynamic performance of the heat pump. The global COP of the cycles with and without IHX has the value of 3.28 and 3.14 respectively, which means that the global COP of the system is enhanced of about 4.42% by adding the IHX.

The choice of the gas cooler flowrate is very important to maintain a good stratification of the storage tank. Low gas cooler flowrates not only give high energetic performance of the heat pump, but also contribute on the stratification of the hot water storage tank. Lower gas cooler flowrates give higher COP. The stratification analysis of the storage tank under various gas cooler flowrates shows that a high temperature gradient between the top and the bottom of the storage tank in the case of the lowest gas cooler flowrate. On the other hand, in the case of the highest gas cooler flowrate, the temperature of the storage tank is quasi homogenous. Notwithstanding, higher gas cooler flowrates result a high energy accumulated in the storage tank.



The evaporator inlet temperature was also analyzed. Results showed that lower evaporator inlet temperature gives lower energetic performance of the heat pump. Also, the heating time increases as the evaporator inlet temperature decreases.

The extraction process was characterized under the 3XL extraction profile conditions. Results of this process shows that the heat pump starts up after the fourth extraction and last 6 hours of heating process. At the extraction moments, the temperature of the storage tank decreases and homogenizes. During the heating process of this step an averaged COP of 2.89 was obtained.

The cooling process of the hot water storage tank was performed under three different extraction flowrates. Results shows that the cooling process has the same behavior, but the cooling time decreases with the increase of the extraction flowrate.

Finally, the stratified storage tank model developed showed a good agreement with the experimental results for all the conditions studied. The new model showed better results compared with the TRNSYS library model (Type 4) especially in the extraction process test.

### **Future works**

The analysis of the stratification within the storage tank and the behavior of the hot water during charging and discharging the storage tank is very interesting. In the near future, we will try to continue the study of the heating process and show the behavior of the stratification phenomena and the thermocline formation under gas cooler flowrate conditions less than  $0.083 \text{ kg}\cdot\text{s}^{-1}$ . As well, the extraction process (Step E) of the test procedure will be realized under different extraction profiles. In addition, the numerical model of the storage tank will be enhanced in the objective of obtain a better accuracy. Also, the numerical model of the whole DHW production system will be performed.

## **Acknowledgements**

This work has been performed in the context of the project “Maximisation of the efficiency and minimisation of the environmental impact of heat pumps for the decarbonisation of heating and domestic hot water production in nearly zero energy buildings” ENE2017-3665-C2-2-P, Funded by the Ministry of Economy and Competitiveness, Spain and the support of the European Regional Development Fund.



h		XXL				3XL				4XL			
		$Q_{sup}$	$f$	$T_m$	$T_p$	$Q_{sup}$	$f$	$T_m$	$T_p$	$Q_{sup}$	$f$	$T_m$	$T_p$
		kWh	l/min	°C	°C	kWh	l/min	°C	°C	kWh	l/min	°C	°C
1	07:00	0,105	3	25		11,2	48	40		22,4	96	40	
2	07:05												
3	07:15	1,82	6	40									
4	07:26	0,105	3	25									
5	07:30												
6	07:45	6,24	16	10	40								
7	08:01	0,105	3	25		5,04	24	25		10,08	48	25	
8	08:05												
9	08:15	0,105	3	25									
10	08:25												
11	08:30	0,105	3	25									
12	08:45	0,105	3	25									
13	09:00	0,105	3	25		1,68	24	25		3,36	48	25	
14	09:30	0,105	3	25									
15	10:00	0,105	3	25									
16	10:30	0,105	3	10	40	0,84	24	10	40	1,68	48	10	40
17	11:00	0,105	3	25									
18	11:30	0,105	3	25									
19	11:45	0,105	3	25		1,68	24	25		3,36	48	25	
20	12:00												
21	12:30												
22	12:45	0,735	4	10	55	2,52	32	10	55	5,04	64	10	55
23	14:30	0,105	3	25									
24	15:00	0,105	3	25									
25	15:30	0,105	3	25		2,52	24	25		5,04	48	25	
26	16:00	0,105	3	25									
27	16:30	0,105	3	25									
28	17:00	0,105	3	25									
29	18:00	0,105	3	25									
30	18:15	0,105	3	40									
31	18:30	0,105	3	40		3,36	24	25		6,72	48	25	
32	19:00	0,105	3	25									
33	19:30												
34	20:00												
35	20:30	0,735	4	10	55	5,88	32	10	55	11,76	64	10	55
36	20:45												
37	20:46	6,24	16	10	40								
38	21:00												
39	21:15	0,105	3	25									
40	21:30	6,24	16	10	40	12,04	48	40		24,08	96	40	
41	21:35												
42	21:45												
43	$Q_{ref}$	24,53				46,76				93,52			



## References:

- [1] K.J. Chua, S.K. Chou, W.M. Yang, Advances in heat pump systems: A review, *Applied Energy* 87 (2010) 3611–3624.
- [2] E.H. Blasco, E.N. Peris, J.M. Corberán, Closing the residential energy loop: Grey-water heat recovery system for domestic hot water production based on heat pumps, *Energy & Buildings* 216 (2020) 109962.
- [3] S. Minetto, Theoretical and experimental analysis of a CO<sub>2</sub> heat pump for domestic hot water, *international journal of refrigeration* 34 (2011) 742-751.
- [4] O. Bamigbetan, T.M. Eikevik, P. Neksa M. Bantle, Review of vapour compression heat pumps for high temperature heating using natural working fluids. *international journal of refrigeration* 80 (2017) 197–211.
- [5] L. Cecchinato, M. Corradi, E. Fornasieri, L. Zamboni, Carbon dioxide as refrigerant for tap water heat pumps: A comparison with the traditional solution, *International Journal of Refrigeration* 28 (2005) 1250–1258.
- [6] F. Illan-Gomez, V.F. Sena-Cuevas, J.R. García-Cascales, F.J.S. Velasco, Analysis of the optimal gas cooler pressure of a CO<sub>2</sub> heat pump with gas bypass for hot water generation, *Applied Thermal Engineering* 182 (2021) 116110.
- [7] L.W. Yang, N. Hua, J.H. Pu, Y. Xia, W.B. Zhou, R.J. Xu, T. Yang, Y. Belyayev, H.S. Wang, Analysis of operation performance of three indirect expansion solar assisted air source heat pumps for domestic heating, *Energy Conversion and Management* 252 (2022) 115061.
- [8] A. Bastani, P. Eslami-Nejad, M. Badache, A.T. Anh Nguyen, Experimental characterization of a transcritical CO<sub>2</sub> direct expansion ground source heat pump for heating applications, *Energy & Buildings* 212 (2020) 109828.
- [9] Y. Wang, D. Wang, B. Yu, J. Shi, J. Chen, Experimental and numerical investigation of a CO<sub>2</sub> heat pump system for electrical vehicle with series gas cooler configuration, *International Journal of Refrigeration* 100 (2019) 156–166.
- [10] J. Stene, Residential CO<sub>2</sub> heat pump system for combined space heating and hot water heating, *International Journal of Refrigeration* 28 (2005) 1259–1265.

- [11] K.J. Chua, S.K. Chou, W.M. Yang, Advances in heat pump systems: A review, *Applied Energy* 87 (2010) 3611–3624.
- [12] Y.P. Chandra, T. Matuska, Stratification analysis of domestic hot water storage tanks: A comprehensive review, *Energy & Buildings* 187 (2019) 110–131.
- [13] M. Liangdong, R. Tixiu, Z. Tianjiao, Z. Tianyi, Z. Jili, Experimental study on effect of operating parameters on performance of serially cascaded wastewater source heat pump, *Journal of Building Engineering* 32 (2020) 101458.
- [14] F. Illan-Gomez, V.F. Sena-Cuevas, J.R. García-Cascales, F.J.S. Velasco, Experimental and numerical study of a CO<sub>2</sub> water-to-water heat pump for hot water generation, *International Journal of Refrigeration* 132 (2021) 30–44.
- [15] Y. Song, F. Cao, The evaluation of optimal discharge pressure in a water-precooler-based transcritical CO<sub>2</sub> heat pump system, *Applied Thermal Engineering* 131 (2018) 8–18.
- [16] E. Brodal, S. Jackson, A comparative study of CO<sub>2</sub> heat pump performance for combined space and hot water heating, *International Journal of Refrigeration* 108 (2019) 234–245.
- [17] J.H. Cheng, Y.J. He, C.L. Zhang, New scenario of CO<sub>2</sub> heat pump for space heating: Automatic mode switch between modified transcritical and cascade cycle in one system, *Applied Thermal Engineering* 191 (2021) 116864.
- [18] B. Daia, H. Qia, W. Doua, S. Liua, D. Zhongb, H. Yanga, V. Niana, Y. Haod, Life cycle energy, emissions and cost evaluation of CO<sub>2</sub> air source heat pump system to replace traditional heating methods for residential heating in China: System configurations, *Energy Conversion and Management* 218 (2020) 112954.
- [19] R. Yokoyama, T. Wakui, J. Kamakari, K. Takemura, Performance analysis of a CO<sub>2</sub> heat pump water heating system under a daily change in a standardized demand, *Energy* 35 (2010) 718–728.
- [20] Z. Wang, F. Wang, Z. Ma, W. Lin, H. Ren, Investigation on the feasibility and performance of transcritical CO<sub>2</sub> heat pump integrated with thermal energy storage for space heating, *Renewable Energy* 134 (2019) 496–508.

- [21] N. Fernandez, Y. Hwang, R. Radermacher, Comparison of CO<sub>2</sub> heat pump water heater performance with baseline cycle and two high COP cycles, *international journal of refrigeration* 33 (2010) 635-644.
- [22] B. Hu, X. Wang, F. Cao, Z. He, Z. Xing, Experimental analysis of an air-source transcritical CO<sub>2</sub> heat pump water heater using the hot gas bypass defrosting method, *Applied Thermal Engineering* 71 (2014) 528-535.
- [23] F. Cao, Z. Ye, Y. Wang, Experimental investigation on the influence of internal heat exchanger in a transcritical CO<sub>2</sub> heat pump water heater, *Applied Thermal Engineering* 168 (2020) 114855.
- [24] S.G. Kim, Y.J. Kim, G. Lee, M.S. Kim, The performance of a transcritical CO<sub>2</sub> cycle with an internal heat exchanger for hot water heating, *International Journal of Refrigeration* 28 (2005) 1064–1072.
- [25] J. Wang, M. Belusko, H. Semsarilar, M. Evans, M. Liu, Frank Bruno, An optimisation study on a real-world transcritical CO<sub>2</sub> heat pump system with a flash gas bypass, *Energy Conversion and Management* 251 (2022) 114995.
- [26] Y. Wang, S. Zong, Y. Song, F. Cao, Y. He, Q. Gao, Experimental and techno-economic analysis of transcritical CO<sub>2</sub> heat pump water heater with fin-and-tube and microchannel heat exchanger, *Applied Thermal Engineering* 199 (2021) 117606.
- [27] K. Nawaz, B. Shen, A. Elatar, V. Baxter, O. Abdelaziz, Performance optimization of CO<sub>2</sub> heat pump water heater, *International Journal of Refrigeration* 85 (2018) 2013-2028.
- [28] F. Liu, W. Zhu, Y. Cai, Experimental Study of a Dual-mode CO<sub>2</sub> Heat Pump System with Thermal Storage, *Energy Procedia* 105 (2017) 4078-4083.
- [29] F. Liu, W. Zhu, J. Zhao, Model-based dynamic optimal control of a CO<sub>2</sub> heat pump coupled with hot and cold thermal storages, *Applied Thermal Engineering* 128 (2018) 1116–1125.
- [30] A. Genkinger, R. Dott, T Afjei, Combining heat pumps with solar energy for domestic hot water production, *Energy Procedia* 30 (2012) 101 – 105.
- [31] R. Majumdar, S.K. Saha, S. Singh, Evaluation of transient characteristics of medium temperature solar thermal systems utilizing thermal stratification, *Applied Energy* 224 (2018) 69–85.

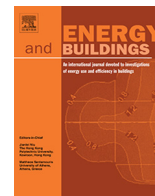


- [32] P. Armstrong, D. Ager, I. Thompson, M. McCulloch, Domestic hot water storage: Balancing thermal and sanitary performance, *Energy Policy* 68 (2014) 334–339.
- [33] P.C. Eames and B. Norton, The effect of tank geometry on thermally stratified sensible heat storage subject to low Reynolds number flows, *Int. J. Heat Mass Transfer*, 41 (1998) 2131-2142.
- [34] S. Alizadeh, An experimental and numerical study of thermal stratification in a horizontal cylindrical solar storage tank, *Solar Energy* 66 (1999) 409–421.
- [35] A. Karim, A. Burnett and S. Fawzia, Investigation of stratified thermal storage tank performance for heating and cooling applications, *Energies* 11 (2018)1049, doi:10.3390/en11051049.
- [36] D.L. Savicki, H.A. Vielmo, A. Krenzinger, Three-dimensional analysis and investigation of the thermal and hydrodynamic behaviors of cylindrical storage tanks, *Renewable Energy* 36 (2011) 1364-1373.
- [37] S. Ievers and W. Lin, Numerical simulation of three-dimensional flow dynamics in a hot water storage tank, *Applied Energy* 86 (2009) 2604–2614.
- [38] L. Gao, H. Lu, B. Sun, D. Che, L. Dong, Numerical and experimental investigation on thermal stratification characteristics affected by the baffle plate in thermal storage tank, *Journal of Energy Storage* 34 (2021) 102117.
- [39] Z. Wang, H. Zhang, H. Huang, Bi. Dou, X. Huang, M.A. Goula, The experimental investigation of the thermal stratification in a solar hot water tank, *Renewable Energy* 134 (2019) 862-874.
- [40] Y.M. Han, R.Z. Wang, Y.J. Dai, Thermal stratification within the water tank, *Renewable and Sustainable Energy Reviews* 13 (2009) 1014–1026.
- [41] Y.P. Chandra, T. Matuska, Stratification analysis of domestic hot water storage tanks: A comprehensive review, *Energy & Buildings* 187 (2019) 110–131.
- [42] D.P Vicente Quiles, *Fundamentos de Energía solar para ACS y Climatización: Buenas prácticas*, (2015) ATECYR AGASTIA 112 A, Madrid.

- [43] Y.P. Chandra, T. Matuska, Numerical prediction of the stratification performance in domestic hot water storage tanks, *Renewable Energy* 154 (2020) 1165-1179.
- [44] S. Fertahi, A. Jamil, A. Benbassou, Review on Solar Thermal Stratified Storage Tanks (STSST): Insight on stratification studies and efficiency indicators, *Solar Energy* 176 (2018) 126–145.
- [45] N. Altuntop, M. Arslan, V. Ozceyhan, M. Kanoglu, Effect of obstacles on thermal stratification in hot water storage tanks, *Applied Thermal Engineering* 25 (2005) 2285–2298.
- [46] D. Erdemir, N. Altuntop, Improved thermal stratification with obstacles placed inside the vertical mantled hot water tanks, *Applied Thermal Engineering* 100 (2016) 20–29.
- [47] A. Li, F. Cao, W. Zhang, B. Shi, H. Li, Effects of different thermal storage tank structures on temperature stratification and thermal efficiency during charging, *Solar Energy* 173 (2018) 882–892.
- [48] Burak Kurşun, Thermal stratification enhancement in cylindrical and rectangular hot water tanks with truncated cone and pyramid shaped insulation geometry, *Solar Energy* 169 (2018) 512–525.
- [49] M. Arslan, A.A. Igci, Thermal performance of a vertical solar hot water storage tank with a mantle heat exchanger depending on the discharging operation parameters, *Solar Energy* 116 (2015) 184–204.
- [50] St. Goppert, R. Lohse, T. Urbaneck, U. Schirmer, B. Platzer, P. Steinert, New computation method for stratification pipes of solar storage tanks, *Solar Energy* 83 (2009) 1578–1587.
- [51] L.J. Shah, E. Andersen, S. Furbo, Theoretical and experimental investigations of inlet stratifiers for solar storage tanks, *Applied Thermal Engineering* 25 (2005) 2086–2099.
- [52] E. García-Marí, M. Gasque, R.P. Gutiérrez-Colomer, F. Ibáñez, P. González-Altozano, A new inlet device that enhances thermal stratification during charging in a hot water storage tank.

- [53] T. Bouhala, S. Fertahi, Y. Agrouaz, T. El Rhafiki, T. Kousksou, A. Jamil, Numerical modeling and optimization of thermal stratification in solar hot water storage tanks for domestic applications: CFD study, *Solar Energy* 157 (2017) 441–455.
- [54] European Committee for Standardization (ECS), EN 16147, heat pump with electrically driven compressor testing, performance rating and requirements for making of domestic hot water units. Spanish standard UNE- EN 16147. December 2017.
- [55] V.F. Sena Cuevas, Experimental and numerical study of a water-to-water heat pump working with CO<sub>2</sub> (2021) doctoral thesis.
- [56] <https://www.dorin.com/>
- [57] <https://www.swep.net/products/b16/>
- [58] <https://www.swep.net/products/bx8t/>
- [59] <https://www.swep.net/products/b17/>
- [60] <https://www.baxi.es/productos/complementos-componentes/circuladores>
- [61] <https://new.siemens.com/global/en/products/automation/process-instrumentation/flow-measurement/electromagnetic/sitrans-f-m-mag-5100-w-for-water-applications.html>
- [62] <https://www.materialescalefaccion.com/acumuladores/1285-acumulador-geiser-inox-gx-800-rb.html>
- [63] National Instruments, Ni-Data Acquisition Ni-DAQ Specifications cDAQ™-9189, 2017
- [64] <https://www.ni.com/>
- [65] L. Gao, H. Lu, B. Sun, D. Che, L. Dong, Numerical and experimental investigation on thermal stratification characteristics affected by the baffle plate in thermal storage tank, *Journal of Energy Storage* 34 (2021) 102117.
- [66] R. Smusz, P. Kielan, D. Mazur, Analysis of thermal stratified storage tank, *archives of electrical engineering* 66 (2017) 631-642.
- [67] M.R.W. Walmsley, M. J. Atkins, J. Riley, Thermocline management of stratified tanks for heat storage, DOI: 10.3303/CET0918036.
- [68] Y. Bai, M. Yang, Z. Wang, X. Li, L. Chen, Thermal stratification in a cylindrical tank due to heat losses while in standby mode, *Solar Energy* 185 (2019) 222–234.
- [69] E.M. Kleinbach, W.A. Beckman, S.A. Klein, Performance study of one-dimensional models for stratified thermal storage tanks, *Solar Energy* 50 (1993) 155-166
- [70] H. Yoo and E.E.-Tong Pak, Analytical solutions to a one-dimensional finite-domain model for stratified thermal storage tanks, *Solar Energy* 56 (1996) 315-322

- [71] J.E.B. Nelson, A.R. Balakrishnan, S.S. Murthy, Parametric studies on thermally stratified chilled water storage systems, *Applied Thermal Engineering* 19 (1999) 89-115
- [72] M.S. Shin, H.S. Kim, D.S. Jang, S.N. Lee, Y.S. Lee, H.G. Yoon, Numerical and experimental study on the design of a stratified thermal storage system, *Applied Thermal Engineering* 24 (2004) 17–27.
- [73] Y.P. Chandra, T. Matuska, Stratification analysis of domestic hot water storage tanks: A comprehensive review, *Energy & Buildings* 187 (2019) 110–131.
- [74] C. Baldwin, C.A. Cruickshank, Using TRNSYS types 4, 60 and 534 to model residential cold thermal storage using water and water/glycol solutions,
- [75] Document transys
- [76] Y.A. Çengel, A.J. Ghajar, *Heat and mass transfer fundamentals & applications*, 5<sup>th</sup> edition, McGraw-Hill Education.



# Experimental characterization of the coupling and heating performance of a CO<sub>2</sub> water-to-water heat pump and a water storage tank for domestic hot water production system



F.J.S. Velasco\*, M.R. Haddouche, F. Illán-Gómez, J.R. García-Cascales

DITEF, Universidad Politécnica de Cartagena, ETSII, Dr. Fleming s/n, 30202 Cartagena, Murcia, Spain

## ARTICLE INFO

### Article history:

Received 28 January 2022

Revised 20 March 2022

Accepted 3 April 2022

Available online 6 April 2022

### Keywords:

Heat pump

Storage tank

Hot water production

CO<sub>2</sub>

## ABSTRACT

This work presents an experimental study of the dynamic performance of a CO<sub>2</sub> water-to-water heat pump in a domestic hot water production system. A facility was developed and used to characterize the time evolution of the COP of this heat pump, the heating and stratification processes of the hot-water storage tank, and the global COP of the system. Results showed that, when heating the water storage tank, strategies based on promoting stratification to reach  $Ri \sim 40$ , such as the use of vertical tank filling velocities  $v \sim 10^{-4} \text{ m}\cdot\text{s}^{-1}$  with low water flow rates between the tank and the heat pump gas cooler, permits an increase of  $\sim 12.4\%$  in the system global COP and a reduction of  $\sim 16\%$  of the compressor energy consumption compared to other strategies. However, strategies based on considering higher water flow rates (i.e.  $Ri \sim 1$ ) increase the thermal energy available in the tank ( $\sim 6\%$  when flow rate and  $v$  increases a factor 3.6) but enhance the water mixing and extend the heating time which reduces the global COP of the system. Besides, an increase of the evaporator inlet water temperature from 5 °C to 20 °C increases the system global COP by 59% and reduces the heating time  $\sim 40\%$ .

© 2022 The Authors. Published by Elsevier B.V. This is an open access article under the CC BY-NC-ND license (<http://creativecommons.org/licenses/by-nc-nd/4.0/>).

## 1. Introduction

Ensuring a reliable, economical, and sustainable energy supply, as well as climate protection, are important global challenges of the 21<sup>st</sup> century. Some international agreements, such as the one committed by the European Union [1], propose to achieve between 80 and 90% reduction of greenhouse gas emissions by 2050 to reach climate neutral countries. The use of renewable energies and the improvement of energy efficiency are some of the most important steps to achieve these energy policy goals. Among others, the building sector is an important consumer where there is a key energy-saving potential. In fact, Heating, Ventilation and Air-Conditioning (HVAC) systems account for 40–60% of the energy consumption in buildings [2]. In Europe, hot water production represents around 15% of the total energy consumption in the household's sector [3]. Nowadays high efficient heat pumps can be considered a solution to replace fossil-fuel boilers, especially in the domestic hot water (DHW) production sector. This can be a

key strategy to decarbonize existing buildings as well as to design carbon-neutral buildings and/or zero-emission buildings.

Among the different applications and technologies used in water-to-water heat pumps [4,5], groundwater or wastewater heat pumps raise as potential candidates for DHW generation and residential heating [6,7]. They use underground or in-house greywater lines as a thermal sink of the system, getting profit of the warmer temperature range of these lines compared to the outdoor ambient temperature to boost its coefficient of performance (COP). Besides, in the case of tertiary buildings, the hot water flow of the cooling towers can be also used in water-to-water heat pumps of hot water generation systems.

Many authors have focused their efforts on water-to-water heat pumps for hot water generation. Among them, Liangdong et al. [8] work stands out. They investigated experimentally the effect of the operating parameters on the heating performance of a cascade, wastewater, heat pump. Their results showed that the COP of the system decreases around 20% with the increase of tap water inlet temperature from 10 °C to 15 °C and about 11–13% with the increase of hot water outlet temperature from 40 °C to 50 °C. They also proved that increasing the flow rate of tap water and greywater can effectively improve the heating performance of the system. Another study interesting to highlight is that of Farzanehkhome-

Abbreviations: DHW, domestic hot water; Ri, Richardson number; COP, Coefficient of Performance.

\* Corresponding author.

E-mail address: [fjavier.sanchez@upct.es](mailto:fjavier.sanchez@upct.es) (F.J.S. Velasco).

## Nomenclature

$c_p$	Specific heat ( $\text{kJ}\cdot\text{kg}^{-1}\cdot\text{K}^{-1}$ )
$D$	Inner diameter of the tank (m)
$dh$	Enthalpy (kJ)
$du$	Internal energy (kJ)
$E$	Energy (kJ)
$g$	Gravity ( $\text{m}\cdot\text{s}^{-2}$ )
$H$	Height (m)
$\dot{m}$	Mass flowrate ( $\text{kg}\cdot\text{s}^{-1}$ )
$m, M$	Mass (kg)
$\dot{Q}$	Thermal power (kW)
$R_i$	Richardson (–)
$t$	Time (s), (h)
$T$	Temperature ( $^{\circ}\text{C}$ )
$V$	Volume ( $\text{m}^3$ )
$v$	Velocity ( $\text{m}\cdot\text{s}^{-1}$ )
$\dot{W}$	Electric power (kW)

### Greek letters

$\beta$	Volume expansion coefficient ( $\text{K}^{-1}$ )
$\Delta$	Temperature difference ( $^{\circ}\text{C}$ )
$\rho$	Density ( $\text{kg}\cdot\text{m}^{-3}$ )
$\tau$	Dimensionless filling time (–)

### Abbreviations

COP	Coefficient Of Performance
DHW	Domestic Hot Water
EEV	Electronic Expansion Valve
GC	Gas Cooler
GWP	Global Warming Potential
HP	Heat pump
HVAC	Heating, Ventilation and Air-Conditioning
IHX	Internal Heat Exchanger
ODP	Ozone Depletion Potential
PCM	Phase Changing Material
RMS	Root Mean Square
RTD	Resistance Temperature Detector

### Subscripts

bottom	Bottom
cw	Cold water
evap	Evaporator
hw	Hot water
in	Inlet
top	Top

neh et al. [9] who made an energy economic assessment of the use of a geothermal heat pump as an air conditioning system for a residential building in a location with a cold semi-arid or steppe climate (BSk) and evaluated the potential reduction of the energy consumption. Their analysis showed that the payback period of the system was about 7.4 years with a low initial cost.

The use of  $\text{CO}_2$  heat pumps for DHW production has a rising interest due to its sustainability and environmental potential, as it permits revaluing this substance in a future circular economy. In addition, the  $\text{CO}_2$  (R744) is a natural refrigerant, non-toxic, non-flammable (i.e. type A1), and cheap. It has a 0 value of Ozone Depletion Potential (ODP) and a Global Warming Potential (GWP) of 1 [10]. For the building sector, low GWP type A1 refrigerants are postulated as highly recommended in future decarbonization policies in this sector. Currently, there are few low-GWP type A1 refrigerants able to compete with  $\text{CO}_2$ . In fact, heat pumps working with  $\text{CO}_2$  are one of the most efficient heating generators for DHW using A1 refrigerants. Due to its low critical point (critical temperature of  $31^{\circ}\text{C}$ ),  $\text{CO}_2$  is mainly used in heat pumps water heaters with *trans*-critical cycles. The use of these types of cycles allows  $\text{CO}_2$  heat pumps to provide high COP values for heating water from very low inlet water temperatures as the heat transfer at the hot sink is performed with sensible energy (not latent energy) also at the refrigerant side of the heat exchanger, what increases its efficiency [11]. In contrast to subcritical cycles, in *trans*-critical cycles, the pressure at which the heat is transferred to the heat sink is not directly conditioned by the temperature of that sink. Thus, there exists an optimal operating pressure that depends on the specific working conditions of the heat pump [12,13]. Many authors have studied the optimal design and configurations to obtain high efficient  $\text{CO}_2$  *trans*-critical heat pumps both experimentally and theoretically [4,14–16]. To assist in the design process of new models, it is a key issue not only to develop numerical models that permit the characterization of this type of hot water production system but also to provide ad-hoc experimental data to validate those models. Wang et al. [17,18] analysed numerically the performance of a  $\text{CO}_2$  heat pump for a residential heating system using TRNSYS. The

results presented for the system proposed therein show that the heating capacity and energy consumption of the proposed system decrease by 21% and 24%, respectively, in comparison with a baseline  $\text{CO}_2$  transcritical simple compression system. Fernandez et al. [19] investigated the effect of the environmental conditions on the COP of a  $\text{CO}_2$  heat pump water heater and they compared a two-stage cycle with an internal heat exchanger and a cycle with a suction line heat exchanger to a basic (i.e. baseline) cycle. They concluded that the overall COP increases when the ambient temperature increases, and by using a suction line heat exchanger they obtained an increase in the COP by up to 7.9 % compared to the baseline cycle under the same conditions. Kim et al. [20] investigated numerically and experimentally the influence of a heat exchanger on the performance of a *trans*-critical  $\text{CO}_2$  cycle. They found that the geometrical parameters of the internal heat exchanger affect the mass flow rate of refrigerant. Moreover, they found that the compressor power consumption decreases with the increase of the length of the heat exchanger whereas the COP of the  $\text{CO}_2$  cycle is improved. Yokoyama et al. [21] analysed numerically the influence of the hot water demand on the performance of a  $\text{CO}_2$  heat pump. They concluded that the daily change in the hot water demand does not significantly affect the daily average system efficiencies. Hu et al. [22] studied experimentally an air-source *trans*-critical  $\text{CO}_2$  heat pump water heater under different working conditions. Their results show that the higher hot water temperature can be reached by decreasing the inlet water flow rate or increasing the water inlet temperature. Among the different technologies available, vapour bypass cycles permit overcoming the traditional limitations found in basic cycles. Indeed, using the vapor bypassed upstream the evaporator has the potential for improving the performance of the system as it permits to decrease the refrigerant's pressure drop of the evaporator of the heat pump. In general, and especially under high heating capacity conditions, the performance of a vapor bypass heat pump is always higher than that of a conventional one].

Besides the heat pump efficiency, other factors influence the energy efficiency of a hot water production system. The thermal

stratification of the hot water storage tank is one of these factors. Thermal stratification is usually employed in DHW storage tanks [23–25], and it is highly recommended for heat pumps water heaters to maintain a high energy performance. Gao et al. [25] studied experimentally and numerically different geometries of a central hole baffle plate to improve and characterize the thermal stratification of a DHW storage tank during the charging process. They performed an optimization process based on the Richardson number of the system as a representative descriptor of the stratification and provided a plate geometry and location as well as an inlet velocity that maximized the tank stratification. Wang et al. [26] experimentally investigated the effect of the inclusion of PCM balls on the thermal stratification of a hot water storage tank. They found that, for a fixed inlet flow rate, an improvement of the thermal stratification was achieved as the positions of the balls became closer to the inlet. Esen and Ayhan [27] developed a model of a cylindrical energy storage tank with PCM packaged in cylinders and the heat transfer fluid (HTF) flowing parallel to it. Their results show that some parameters must be investigated in order to optimize the thermal performance of the storage tank as the PCM properties, cylinder diameter, the mass flow rate, and the inlet temperature of the HTF. Chandra and Matuska [28] presented a numerical study using CFD of the stratification performance in DHW storage tanks. They analyzed the impact that three types of inlet devices (perforated inlet, slotted inlet, and simple inlet) had in the stratification process. They found that all devices performed similarly at low flow rate and high temperature difference between mean storage and water inlet ( $\Delta T$ ), whereas at high flow rate and low  $\Delta T$  (typical conditions in heat pumps application) the slotted inlet performed better than the others.

Despite the abundance of works devoted to both, the study of heat pumps for DHW generation, and the study of the thermal stratification inside a hot water storage tank, there are very few works dedicated to the analysis of the overall performance of the system when a heat pump is coupled with a storage tank together in a DHW production system. Stene [29,30] studied a 6.5 kW CO<sub>2</sub> heat pump for combined space heating and hot water heating coupled with a cylindrical 200-liter DHW storage tank with a movable insulating plate. He performed several tests in hot water heating only mode, in which he studied the influence of several parameters (hot water temperature, evaporation temperature, or compressor discharge pressure). Due to the special characteristics of the storage tank that he used in his tests, hot and cold water never mixed inside the tank and, therefore the water inlet/outlet temperature at the gas cooler was kept constant during his tests and, in fact, water conditions inside the storage tank did not affect to the performance of the heat pump. Tosato et al. [31] also studied a 30 kW CO<sub>2</sub> heat pump for combined space heating, space cooling, and DHW generation, connected in series with two 750-liter storage tanks. During DHW generation tests, they reported an average COP of 5.0 during the first stage of the tank charging process, when the water temperature entering the gas cooler stayed between 10 °C and 14 °C, and an average COP of 4.1 for the total working period, that finished when water temperature entering the gas cooler reached 32 °C. They also performed a numerical study [32] in which they concluded that the higher COP during DHW generation was obtained for the highest water mass flow rate through the gas cooler. It must be taken into account that in their study, the water tank storage was not modeled, and the gas cooler inlet water temperature profile was taken from experimental data collected in [31]. Liu et al. [33] experimentally investigated the performance of a 3 kW CO<sub>2</sub> heat pump system coupled with hot and cold thermal storage. They studied the heating/charging process of the thermal storage tank analysing three parameters: compressor frequency (between 35 and 50 Hz), opening of the expansion valve (i.e. superheating degree) and the flow rates of hot and cold water

loops in the evaporator and gas cooler. For their study, they used a 3 kW CO<sub>2</sub> heat pump with an initial temperature in both tanks of 27 °C. The tests run until the average temperature in the hot tank reached 60 °C. Therefore, Liu's tests were performed under transient conditions in both, evaporator and gas cooler. They concluded that higher compressor frequency (i.e. 50 Hz) provided better thermal stratification and a shorter heating time than a lower one. This also resulted in the better performance of the system. The opening grade of the expansion valve did not have a significant effect on the thermal stratification within the tank but, it affected the superheating degree at the evaporator outlet, influencing the evaporator temperature and this affected the heat pump performance. Sifnaios et al [34] developed a CFD numerical model for an 8.9 kW R600a heat pump connected to a 109.6-liter vertical cylindrical water tank that they validated using their own experimental data. They reported a maximum average COP of 3.23 during the charging process and, according to their conclusions, variations of water flow rates in the range from 0.12 to 0.24 kg·s<sup>-1</sup> did not affect the performance of the system when diffuser plates are used both at the inlet and the outlet of the tank. Aguilar et al. [35] developed their own 1D numerical model to study the charge and discharge process in a compact 1.5 kW nominal heating capacity R134a DHW heat pump integrated in a 190-liter storage tank. In their case, the heat pump condenser coil was made of a 6 mm copper tube that looped 15 times and wrapped around the outside of the bottom of the tank. Therefore, the only water mass flow rate that affected the stratification inside the tank was the water mass flow rate during the tapping cycle. They studied three different tapping cycles (S, M, and L) according to Standard EN 16,147 [36] and found that the different stratification profiles obtained depending on the tapping cycle clearly affected the performance of the system. Li and Hrnjak [37] developed a study in a similar system. They studied a commercial residential R134a heat pump water heater whose condenser had two parallel tubes which were wrapped around a 250-liters (66 gallon) water tank. They simulated the system using a CFD commercial software and focused in the heating-up stage. According to their results, there is an upward flow layer confined in a very thin layer near the tank wall and the flow condition in this layer is critical to the interaction between the vapor compression system and the water tank. During heating-up, the flow filed in the tank would first change dramatically at the beginning and then stabilize.

Other key factors are the hydraulic design of the system and the management and control of the heating, charging, and discharging process of the hot water storage tank. All in all, these key issues define the overall performance of heat pumps as DHW production systems, and it is of utmost importance to assess the influence of these factors on the overall performance of the system. This assessment can be done based on international standards. Specifically, the EN 16,147 [36] is one of the international standards that allow to characterize the performance of these type of systems.

In the open literature, there are many works related to the performance of heat pumps for DHW generation or the filling or stratification of hot water storage tanks. However, there is a lack of studies that analyse the global dynamic performance of both units coupled together in a DHW production system. This work tries to contribute to the gap of knowledge. The objective of this work is to analyse the dynamic performance of DHW production system based on a CO<sub>2</sub> water-to-water heat pump during its operation under standard conditions (i.e. EN 16,147 conditions). Specifically, this work focuses on the evolution of the performance of the DHW production system, including the hot water storage tank, CO<sub>2</sub> heat pump and auxiliary elements, during the heating process of the hot water storage tank. For that purpose, a series of experimental tests have been conducted. The *trans*-critical CO<sub>2</sub> cycle proposed is controlled by electronic back-pressure and thermal expansion valves



and coupled with a high efficient IHX and a stratified water storage tank for improving the efficiency of the DHW generation system. An experimental facility was built and used to evaluate the energy efficiency of the system following the guidelines of the international standard EN 16147. The facility includes a hot water storage tank instrumented with temperature sensors to characterize the heat pump performance and the evolution of the stratification process. During the experimental campaign, the influence of the water flow rate control strategies of the CO<sub>2</sub> water-to-water heat pump on the overall efficiency of the system is analysed, paying attention to the influence of the water flow rate at the gas cooler and the evaporator as well as the inlet water temperature at the evaporator on the performance of the system. Besides, it is also an objective of the work to analyse the influence of the operation mode of the heat pump (i.e. transcritical or subcritical mode) on the performance of the DHW production system. The work is structured as follows: section 2 describes the test procedure followed for the characterization of the DHW generation system. In section 3 it is presented heat pump used and the overall DHW generation system considered in this study. It is also described here the experimental set-up developed, and the test matrix used to characterize the performance of the system. Then, in section 4, the results are analysed and discussed. Finally, in the last section, the most important conclusions are outlined.

## 2. Test methodology used for the characterization of the performance of the DHW production system

The test procedure used in this study for the characterization of the performance of a DHW generation system based on a CO<sub>2</sub> water-to-water heat pump is based on the EN 16147. Following this standard, the characterization process was structured in several temporal stages where the final condition of a stage is the initial condition of the following one. More specifically, the stages considered for the characterization of the water heating process during the test performed in this study were three:

- Stage A: Stabilization
- Stage B: Fill the accumulation tank and prepare the test set-up.
- Stage C: Determination of the water heating time.

Stages A and B correspond to test preparation. Stage A includes the time required for the instrumentation and the system to warm up. During stage B, the storage tank was filled with cold water at 10 °C. During this period, cold water must circulate in the accumulation tank until the outlet temperature is equal to the inlet temperature, within the allowed variation limit of  $\pm 0.2$  K. Stage C seeks to determine the time  $t_h$  necessary to heat the stored water from the initial condition (i.e. temperature of the cold water equal to 10 °C) to the first compressor stop caused by the tank thermostat (which is located at the top of the tank), when the tank temperature reaches 60 °C. This procedure follows the guidelines of the heating process of the EN 16,147 standard (stages A to C).

## 3. Description of the DHW production system and experimental facility

As previously said, the system developed in this work for DHW production consists of a CO<sub>2</sub> trans-critical water-to-water heat pump connected to a hot water storage tank which is fed by the domestic tap water network. Fig. 1a shows a layout of the heat pump developed in this study and the elements and instrumentation used. The heat pump consists of a semi-hermetic reciprocating compressor with a geometrical flow rate of  $1.46 \text{ m}^3 \cdot \text{h}^{-1}$  at 50 Hz (i.e.  $\sim 1.5$  kW of electric power), three brazed plate heat exchangers

working respectively as the evaporator, the gas cooler, and the IHX, a vessel for refrigerant storage, a back-pressure electronic valve (BPV) and an electronic expansion valve (EEV). The back-pressure valve controls the gas cooler pressure, whereas the expansion valve controls the superheat level at the evaporator outlet. The IHX permits reducing the quality of the refrigerant at the evaporator inlet. Table 1 enumerates the main components of the heat pump.

Fig. 1b shows two snapshots of the facility, one of the heat pump (left), and the other of the cold water storage tank used to prepare stage B and of the hot water storage tank (right). As shown in Fig. 1(a & b) the heat pump includes several valves and an IHX which allow the user to modify the operating cycle and test different configurations. In this work, the cycle without gas-bypass is considered (Fig. 1a). Regarding the instrumentation used for the characterization of the performance of the heat pump, it includes RTD temperature sensors, pressure sensors and flowmeters. Table 2 includes some of the specifications of the instrumentation.

Fig. 1c shows a schematic diagram of the hydraulic set-up of the experimental facility developed to afford the experimental characterization of the water heating process of the DHW production system following the procedure described in the previous section. The cold-water tank shown in the figure stores water at 10 °C and simulates the domestic tap water network. It permits feeding the hot water storage tank during DHW consumption process. The hot-water storage tank of the DHW production system is instrumented with RTD probes located in the cylinder axis to measure the water temperature at different heights. The tank is also equipped with valves, pumps, flowmeters, and temperature sensors to simulate the DHW consumption during the tests. This tank has a capacity of  $0.772 \text{ m}^3$  and is connected to the gas cooler of the heat pump. The third tank is the water chiller tank, an auxiliary deposit that provides water to maintain the cold-water storage tank at 10 °C. Finally, the user tank collects the water extracted from the hot-water storage tank during the consumption process and distributes it to the system after the test.

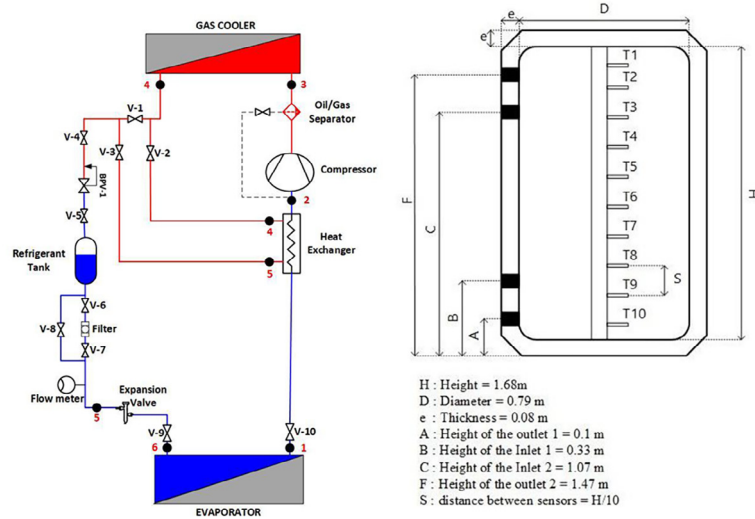
The cold-water storage tank is controlled through a three-way valve and a PID controller and it is also connected to the water chiller tank to maintain it always at a specific temperature of 10 °C. The hot-water storage is one of the most important elements of this study, as its stratification is a key factor in the energy efficiency of the overall DHW production system. Thus, to characterize the stratification within the tank and the temperature transients during the consumption and filling processes, this cylindrical tank was equipped with 10Pt-100 RTD temperature sensors installed along its axis to analyse the behaviour of the water stratification. Note that the hot water storage tank is connected to the gas cooler of the CO<sub>2</sub> heat pump through ports A and C of Fig. 1a(right) which corresponds to ports LC1 and LC2 in Fig. 1c. The parameters of the hot water storage tank are illustrated in Table 3.

The test facility and the DHW production system are controlled through an in-house LabVIEW script whereas the data acquisition is performed via a high sampling frequency data acquisition system type cDAQ 9189 [38] and a low sampling frequency data-logger type Agilent 34970A [39] that scan the variables of the facility at the frequency required by each test. In these tests, data are sampled every 6 or 20 s.

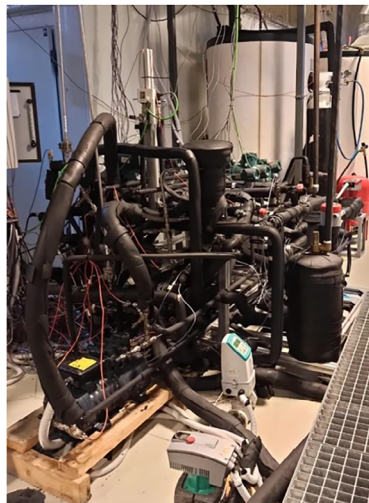
### 3.1. Test matrix and characteristic variables of the test methodology

Table 4 shows the test matrix considered in this work. A total of nine tests were conducted to analyse the energetic performance of the DHW production system developed during the heating process. In all the cases the tests included an IHX. As previously indicated, the tests were designed following the procedure established at the EN 16,147 standard. The tests included different inlet and outlet

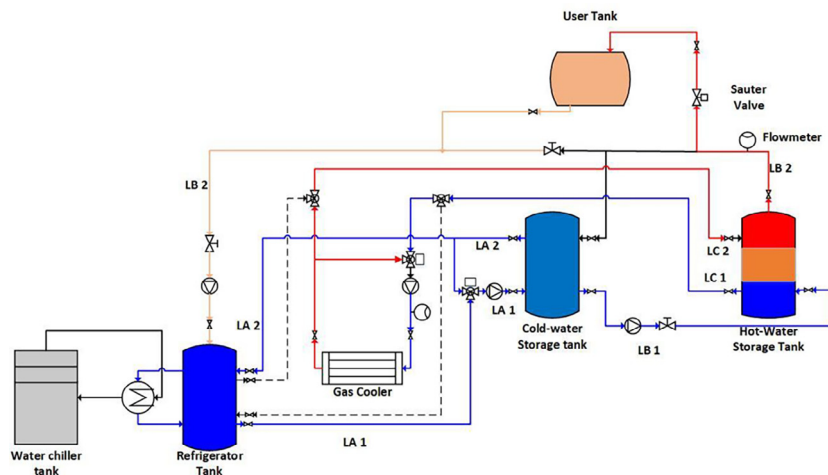




a)



b)



c)

**Fig. 1.** (a) Scheme of the heat pump (left) and hot water storage tank (right). (b) Snapshots of the experimental set-up: CO<sub>2</sub> water-to-water heat pump (left) and cold water and hot water storage tanks (right). (c) Schematic diagram of the hydraulic set-up of the experimental facility.

**Table 1**  
Specifications of the components of the heat pump.

Elements	Manufacturer-Model
Compressor	DORIN CD300H
Evaporator	SWEP BX8T
Gas cooler	SWEP B16
IHXs	SWEP B17
Electronic expansion valve, back-pressure electronic valve	EV CAREL models E2V11CS100 and E2V24CS100

water temperatures and flow rates that were imposed and did not change with time. The inlet water temperature at the gas cooler was always 10 °C at the beginning of the test. There are two main parameters on which this study is focused: the flow rate in the gas cooler and the inlet temperature of the evaporator. The first five rows of the table are the tests where the evaporator conditions were constant, with an inlet and outlet temperature of 10 °C and 7 °C respectively, and the water flow rate at the gas cooler varied between 0.0833 kg·s<sup>-1</sup> and 0.3 kg·s<sup>-1</sup> with an increment of 0.055. Tests 6 to 9 were performed with a fixed gas cooler flow rate of ~ 0.3 kg·s<sup>-1</sup> and a fixed evaporator flow rate of 0.544 kg·s<sup>-1</sup>. These tests were performed at the maximum gas cooler flow rate that can be reached in the facility (0.3055 kg·s<sup>-1</sup>). In this case, the inlet water temperature at the evaporator was imposed between 5 °C and 20 °C. Table 4 shows a summary of the test conditions considered in the evaporator.

During the tests, the heating tests (stage C), started operating and flowing water through the secondary side of the gas cooler to increase the tank water temperature from the initial value of 10 °C up to 60 °C. The tests finish when the temperature at the highest probe of the tank (i. e. T1) reached 60 °C. Based on the data recorded during the test, several characteristic variables were obtained. The global coefficient of performance of the DHW production system (global COP) was defined as the energy of hot water stored in the tank divided by the energy consumed by the compressor. It is worth noting that this definition of the global COP includes the information not only of the COP of the CO<sub>2</sub> heat pump but also of the efficiency in the final energy transfer to the hot water storage tank which is a function of the heating process and the tank insulation and aspect ratio. The energy of the recirculating pumps is neglected and thus:

$$\begin{aligned}
 \text{globalCOP} &= \frac{E_{\text{tank}}}{E_{\text{comp}}} = \frac{\int_0^H \frac{\pi D^2}{4} \cdot \rho \cdot C_p \cdot (T_i(t = t_{\text{tank}}) - T_i(t = 0)) \cdot d\xi}{E_{\text{comp}}} = \\
 &= \frac{\sum_{i=1}^{i=10} C_p \cdot (T_i(t = t_{\text{tank}}) - T_i(t = 0)) \cdot \Delta m}{E_{\text{comp}}} \quad (1)
 \end{aligned}$$

where:

$\rho$  is the water density in kg·m<sup>-3</sup>.

**Table 2**  
Instrumentation characteristics and measurement uncertainty.

Sensor	Characteristics	Measurement accuracy	Range of measurement
Pressure sensors	Absolute sensor: Yokogawa EJX510A ECS	±2.1-kPa //	0 – 5 MPa // 0 – 12 MPa
	// EJX510A ECS JDS	0.04% and 0.05% of the measurement range.	
	Differential pressure sensor: Yokogawa EJX110A JHS	± 260 Pa. 0.26% of the measurement range	0 – 0.1 MPa
Temperature sensors	RTD Pt-100 class A 1/10 DIN	±0.1 K	223–523 K
Compressor electric power measurement sensor	Sineax M563	± 1% of the measured value in W	0 – 2.5 kW
Refrigerant flowmeter (mass flow rate at the refrigerant circuit)	Yokogawa RCCS32	± 5.28·10 <sup>-6</sup> kg·s <sup>-1</sup> ± 0.27% of the measured value in kg·s <sup>-1</sup>	0 – 0.1 kg·s <sup>-1</sup>
Water Flowmeter (flow rate at the water side of the gas cooler)	Siemens fm magflo mag1100 // Sitrans fm mag 5100w.	± 4.91·10 <sup>-7</sup> m <sup>3</sup> ·s <sup>-1</sup> ± 0.2% of the measured value in m <sup>3</sup> ·s <sup>-1</sup>	0 – 0.1111·10 <sup>-2</sup> m <sup>3</sup> ·s <sup>-1</sup>
Clock (time measurement)	Ni-DAQ system	0.001 s	-

**Table 3**  
Hot-water storage tank parameters.

Inner diameter of the tank (D)	0.79	(m)
Inner diameter of the ports (d)	0.034	(m)
Height (H)	1.68	(m)
Aspect ratio (H/D)	2.12	-
Insulation wall thickness	0.08	(m)
Insulation wall conductivity	0.025	(W·m <sup>-1</sup> ·K <sup>-1</sup> )
Insulation wall density	30	(kg·m <sup>-3</sup> )
Insulation wall specific heat	1600	(J·kg <sup>-1</sup> ·K <sup>-1</sup> )

$T_i(t = t_{\text{tank}}) - T_i(t = 0)$  is the temperature variation of the measured water temperature at height level  $i = i \cdot H/10$  of the tank during the heating period.

$\Delta m$ : is one-tenth of the water mass of the tank (M) in kg (i.e. M/10).

$C_p$ : is the specific heat of the hot water, in kJ·kg<sup>-1</sup>·K<sup>-1</sup>.

$t_{\text{tank}}$ : is the heating time, i.e. the duration of the heating process to reach 60 °C at the top of the vessel in s.

$E_{\text{comp}}$  is the electrical energy consumed by the compressor during a test in kJ.

Besides, the instantaneous COP of the system at any time during the heating period can be also obtained based on the formulae:

$$\text{instantaneousCOP} = \frac{dE_{\text{tank}}(t)}{dE_{\text{comp}}(t)} \quad (2)$$

where  $dE_{\text{comp}}$  is the electrical energy absorbed by the compressor during the time lapse  $dt$  in kJ and.

$dE_{\text{tank}}(t)$  in kJ is obtained from:

$$\begin{aligned}
 dE_{\text{tank}}(t) &= \int_0^H \frac{\pi D^2}{4} \cdot \rho \cdot C_p \cdot T_i(t) \cdot d\xi - \int_0^H \frac{\pi D^2}{4} \cdot \rho \cdot C_p \cdot T_i(t - dt) \cdot d\xi \\
 &= \sum_{i=1}^{i=10} C_p \cdot dT_i(t) \cdot \Delta m \quad (3)
 \end{aligned}$$

And  $dT_i(t) = T_i(t) - T_i(t-dt)$  is the temperature variation of the measured water temperature at height level  $i = i \cdot H/10$  of the tank during the heating lapse  $dt$ .

The instantaneous COP is obtained from Equation 2 at each time step of the data acquisition process during the test. Finally, an averaged or accumulated COP can be obtained for each time  $t$  of the heating process by considering the energy consumed by the compressor and the energy accumulated at the tank from the beginning of the test until instant  $t$ :

$$\begin{aligned}
 \text{accumulatedCOP} &= \frac{E_{\text{tank}}(t)}{E_{\text{comp}}(t)} = \frac{\int_0^H \frac{\pi D^2}{4} \cdot \rho \cdot C_p \cdot (T_i(t) - T_i(t = 0)) \cdot d\xi}{E_{\text{comp}}(t)} \\
 &= \frac{\sum_{i=1}^{i=10} C_p \cdot (T_i(t) - T_i(t = 0)) \cdot \Delta m}{E_{\text{comp}}(t)} \quad (4)
 \end{aligned}$$

**Table 4**  
Test conditions considered at the evaporator in the study.

Test N°	Evaporator			Gas Cooler
	Water T inlet (°C)	Water T outlet (°C)	Water flow rate (kg·s <sup>-1</sup> )	Water flow rate (kg·s <sup>-1</sup> )
1	10	7	–	0.0833
2	10	7	–	0.1388
3	10	7	–	0.1944
4	10	7	–	0.25
5 (Reference Test)	10	7	–	0.3055
6	5	–	0.544	0.3055
7	10	–	0.544	0.3055
8	15	–	0.544	0.3055
9	20	–	0.544	0.3055

To characterize the heating process in a hot water storage tank with a water mass of  $M$ , a characteristic time  $t_c$  can be defined from the differential equation of energy conservation applied to the storage tank. Assuming that the water behaves as an incompressible fluid and that the pressure variations in this fluid during the experiments have negligible influence on its enthalpy, thus its internal specific energy and specific enthalpy can be expressed in terms of the water specific heat as  $du = C_p \cdot dT$  and  $dh = C_p \cdot dT$ . In this case, it is also considered that  $C_p$  variations within the temperature range of the experiments have a negligible impact on the results. Neglecting the kinetic and potential energy terms and viscous and radiative process, the energy conservation equation for the hot water storage tank could be expressed as:

$$M \cdot C_p \frac{d}{dt} \iiint_{\text{Tank Volume}} T(x, t) dV = \iiint_{\text{Tank wall}} h(T_w - T(x_{\text{wall}}, t)) dS_w + \dot{m} \cdot C_p \cdot (T_{hw}(t) - T_{cw}(t)) \quad (5)$$

where  $V$  is the tank volume,  $T$  is the local temperature of the water at any point “ $x$ ” within the tank,  $h$  and  $S_w$  are respectively the convective wall heat transfer coefficient and the surface of the walls of the tank,  $T_{hw} - T_{cw}$ , in K, is the temperature difference of the hot water and the cold water at the inlet and the outlet of gas cooler (which are connected to ports A and C of Fig. 1a(right)) and  $\dot{m}$  is the water flow rate at the gas-cooler in kg·s<sup>-1</sup>. Note that in Equation 5 uniform conditions have been considered at the inlet and outlet of the storage tank. Since the first right-hand side term is usually, two orders of magnitude smaller than the second one, the characteristic time of the process can be defined as:

$$t_c = \frac{M}{\dot{m}} \quad (6)$$

this characteristic filling time expresses the time needed by the hot water to flow through a tank of height  $H$ , and reach its bottom taking into account the characteristic vertical velocity of the flow within the tank which is of the order of  $\sim 4\dot{m}/(\rho\pi D^2)$  and the dimensionless filling time is:

$$\tau_{\text{filling}} = \frac{4\dot{m}t_{\text{tank}}}{H\rho\pi D^2} \quad (7)$$

Besides, the dimensionless heating time can be defined based on the nominal power of the heat pump used in the system and the tank capacity. This dimensionless number permits to estimate and compare the efficiency of the DHW production system with other units of different power and/or hot water tank capacity and depends on the heat pump/tank coupling:

$$\tau_{\text{heating HPTank}} = \frac{t_{\text{tank}}}{\frac{M \cdot C_p \cdot (T_{hwr} - T_{cwr})}{Q}} = \frac{t_{\text{tank}}}{M \cdot C_p \cdot (T_{hwr} - T_{cwr})} \cdot \dot{W} \cdot \text{COP}_{\text{ref}} \quad (8)$$

where the heating power transferred at the gas cooler of the CO<sub>2</sub> heat pump is:

$$\dot{Q} = \dot{m} \cdot C_p \cdot (T_{hw} - T_{cw}) \quad (9)$$

In these equations  $\dot{Q}$  is the nominal thermal power of the heat pump,  $\dot{W}$  is the nominal electric power of the heat pump compressor (1.7 kW in our case),  $\text{COP}_{\text{ref}}$  is a reference averaged value of the COP of the heat pump used. In this case, a value of  $\text{COP}_{\text{ref}} = 1$  was adopted in the non-dimensionalization to have a clear basis of comparison with other heat generators (for example, based on Joule effect) and/or with other heat pumps based on the nominal compressor power. Note that this dimensionless parameter could be also defined in terms of a nominal reference COP value (for example  $\text{COP}_{\text{ref}} = 3$ ), or any other nominal performance value of the associated heat pump, to reach values of  $\tau_{\text{heatingHPTank}} \sim 1$  in the design process of a domestic hot water production system.  $T_{hwr}$  and  $T_{cwr}$  are the reference temperatures, in this case, 60 °C and 10 °C respectively.

Regarding the operation mode of the CO<sub>2</sub> heat pump, during the tests it was identified the working cycle of the heat pump by recording the working pressure of the refrigerant at the gas cooler and comparing it with the critical pressure of the CO<sub>2</sub> in order to assess whether the heat pump was working with a subcritical or a transcritical cycle. After this identification of the working cycle was performed online and link to the time during heating process of the hot water storage tank, this way the potential impact of the operation mode on the COP of the DHW production system was analysed.

The uncertainty analysis of the experimental results was performed following the ISO standard [40]. Based on the accuracy of the different sensors and data acquisition systems specified by the manufacturers the “type B uncertainty” of each measured quantity was estimated. Besides, the uncertainty of type A has been calculated based on the standard deviation of the recorded data with respect to the local average value of the variable considered. Error propagation procedure was used to estimate the combined standard uncertainty of the final quantities considered in the study as a function of the measured ones. A confidence level of 95% (i.e.  $k = 2$ ) was used to express the expanded uncertainty of the parameters of interest. Table 5 shows the absolute and relative experimental uncertainty obtained:

## 4. Results and discussion

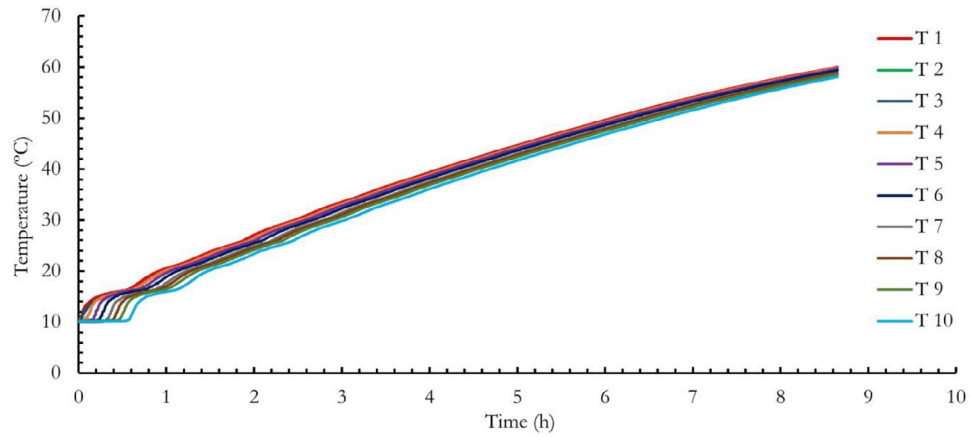
In this section, the experimental results are used to assess the influence of different factors on the performance and efficiency of the DHW production system. First, the results of the experimental tests are described. Later the influence of different key parameters and strategies on the performance of the DHW production system are discussed.

### 4.1. Experimental tests

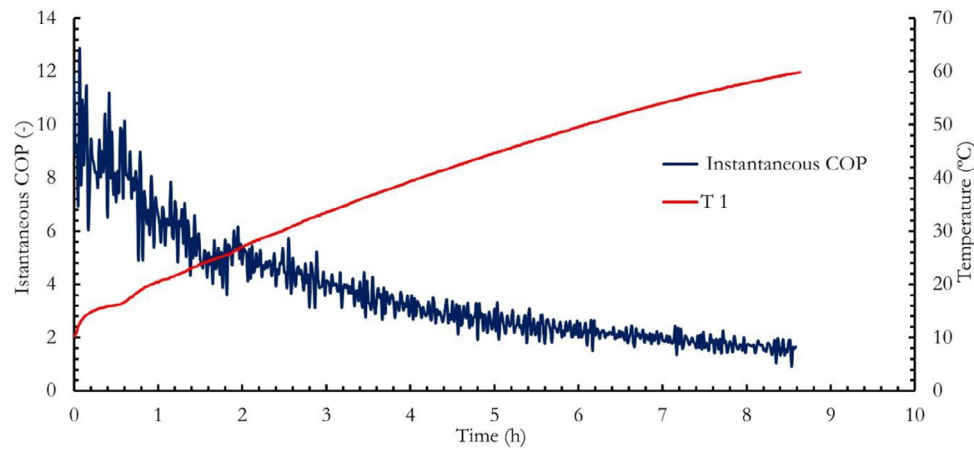
Fig. 2a shows the evolution of the temperature of the hot water storage tank with time during the heating process (stage C) for the

**Table 5**  
Experimental uncertainties obtained in the final quantities during the experiments.

Quantity	Absolute Uncertainty	Range measured	Relative uncertainty measured (%)	Maximum Uncertainty accepted by EN 1647
Temperature (K)	±0.1	273–473	± 0.04 – 0.02	±0.2
Water flow rate (m <sup>3</sup> ·s <sup>-1</sup> )	±0.00153·10 <sup>-3</sup>	0.0830 – 0.306 ·10 <sup>-3</sup>	± 0.5	±1 %
Compressor power (kW)	±0.011 – 0.017	1.1 – 1.7	± 1 %	±1 %
$E_{comp}$ (kJ)	±0.066 – 0.149	39600–63700	less than 0.0004 %	±1 %
$E_{tank}$ (kJ)	±0.156 – 0.255	147500–195300	less than 0.0002 %	±5 %
Global COP	± 0.022 – 0.035	2.49 – 3.97	± 0.87 %	–



a)



b)

**Fig. 2.** (a) Evolution of the tank temperature for the 10 probes inside the tank for test number 5. (b) Evolution of the instantaneous COP of the DHW production system with time and evolution of water temperature at the top of the storage tank (T<sub>1</sub>) for test 5.

temperature probes located at different heights within the tank for test number 5 (reference test) where the heat pump heats up the water of the storage tank (0.772 m<sup>3</sup>) from 10 °C to 60 °C with a gas cooler flow rate of 0.305 kg·s<sup>-1</sup>. As shown, temperature evolution during the initial period of the heating process shows fluctuations that are related to the heating capacity of the heat pump ( $\dot{Q}$ ), but also to the storage tank mass (M). These parameters define the water injection temperature as well as the filling and heating characteristic times. For the conditions of this test, after the first third of the total heating period pass by, the temperature evolution at different heights become self-similar, monotonically increasing

curves that slightly tend to converge due to thermal diffusion. This transport phenomenon reduces the temperature gradient between the top and the bottom of the storage tank and promotes this convergence. Fig. 2b shows the dynamic evolution of the tank temperature and the instantaneous COP of the DHW production system as a function of time during the heating process (stage C). As shown, in this test the heating process last for 8 h and 38 min and has a characteristic time of  $t_c = 2527$  s which corresponds to a dimensionless filling time of  $\tau_{filling} = 12.3$  and a dimensionless heating time of  $\tau_{heatingHPTank} = 0.328$  which shows that the heating process requires ~ 12 times the characteristic time need by the water flow



to traverse the tank height and around  $\sim 1/3$  of the time needed to heat up the tank to the target  $T_{hw}$  by Joule effect. As previously said, the global coefficient of performance of the DHW production system (global COP) is defined as the energy of hot water stored in the tank divided by the energy consumed by the compressor. At the beginning of the process, the instantaneous COP of the system is very high, however, as the temperature of the water in the tank increases, the instantaneous COP of the DHW production system decreases asymptotically. This is due to the performance provided by the CO<sub>2</sub> heat pump (i.e. COP of the heat pump) that shows a similar tendency with time to the one shown by the instantaneous COP of the DHW production system in Fig. 2b. This decreasing tendency with time is due to the fact that a CO<sub>2</sub> heat pump has higher efficiencies for low water inlet temperatures [11]. Since the gas cooler works in counter-flow condition, as the temperature of the water at the bottom of the hot storage tank increases, it also increases the refrigerant temperature at the gas cooler exit and the optimal pressure of the CO<sub>2</sub> cycle. Consequently, the heat pump control system acts increasing the gas cooler pressure seeking to reduce the refrigerant quality at the inlet of the evaporator which also increases the compression work. In other words, as the water at the inlet of the gas cooler increases, the quality of the refrigerant at the exit of the expansion valve as well as the compression work (Fig. 1a) increase reducing the specific heat absorbed at the evaporator and reducing the COP of the heat pump. This increase in the quality of the refrigerant and COP reduction would be higher in the case of a control strategy based on a constant gas cooler pressure. As a result, as the temperature of the water at the bottom of the tank increases during the heating process the COP of the heat pump decreases and the instantaneous COP of the DHW production system decreases with time.

Table 6 shows a summary of the tests results of the experimental campaign (Table 4). The first columns show the time-averaged global COP during the heating period (stage C) and the root mean square (RMS) of the instantaneous COP. It is worth noting that, as the instantaneous COP is a dynamic variable that changes with time, its RMS value was computed based on the dispersion of the sampled data with respect to the moving average of the instantaneous COP with 9 samples (i.e. the time-average of 180 s):

$$RMS_{instantaneousCOP} = \sqrt{\frac{\sum_i^n (x_i - \bar{x}_i)^2}{n^2}} \quad (10)$$

where  $n$  is the number of samples taken,  $x_i$  is the sampled value of the instantaneous COP and  $\bar{x}_i$  is the moving average of the instantaneous COP:

$$\bar{x}_i = \frac{\sum_{j=i-4}^{i+4} x_j}{9} \quad (11)$$

As shown, both the heating time and the global COP of the DHW production system vary with the water flow conditions at both the evaporator and the gas cooler. The CO<sub>2</sub> heat pump COP and the instantaneous COP of the DHW production system show similar dynamic tendencies with time and with the key variables. The difference between both COPs values is due to the losses during the heating process. This difference is of the order of  $\sim 0.35$ . As time pass by, the water at the bottom of the tank heats up and the heat pump COP and the global COP of the DHW production system decreases with time. In general terms, the average of the instantaneous COP at the last third of the heating period is between 2 or 3 times lower than in the first third of the heating period. For fixed evaporator conditions, heating time ( $t_{tank}$ ), accumulated energy ( $E_{tank}$ ), the thermal power transferred by the heat pump to the water (named as “gas cooler thermal power” in Table 6), and global COP depend on the water mass flow rate through the gas cooler. As can be deduced from the values provided in Table 6 for test number 1 to test number 5, this dependency produces a maximum variation of around 13.6 % in the case of  $t_{tank}$ , 6.1 % in the case of  $E_{tank}$ , 9.7 % in the case of gas cooler thermal power and 12.8 % in the case of global COP. The following subsections discuss the results obtained in detail.

#### 4.2. Impact of the gas cooler water flow rate

In tests 1 to 5, the influence of the gas cooler flow rate on the performance of the system is analysed by imposing constant conditions in the evaporator and varying the gas cooler flow rate. These five tests were conducted by varying the flow rate in the gas cooler from 0.0833 kg·s<sup>-1</sup> to 3.055 kg·s<sup>-1</sup> with an increment of 0.055 kg·s<sup>-1</sup> between tests. Fig. 3a shows the temperature evolution of the water storage at the bottom of the tank (probe T<sub>10</sub>) for the different tests. As shown, the temperature fluctuations shown in Fig. 2a are also shown here for different mass flow rates. In the case of Fig. 3a the temperature oscillations change with the flow rate which indicates that these fluctuations are a function of  $T_{hw}$  and  $v$ , the injection velocity of the hot water within the storage tank, which are magnitudes changed during these tests. Since the averaged thermal power transferred by the heat pump in the gas cooler does not vary significantly between tests (less than 10%), the reduction of the gas cooler flow rate to one-third results in a reduction of the characteristic vertical velocity at the storage tank  $v \sim \frac{4\dot{m}}{\rho\pi D^2}$  of the same order and an increase of  $T_{hw}$ . Both tendencies

**Table 6**  
Results of the experimental tests.

Test number	1	2	3	4	5	6	7	8	9
Global COP	3.688	3.487	3.386	3.269	3.280	2.489	3.286	3.867	3.967
RMS instantaneous COP	0.023	0.023	0.024	0.032	0.029	0.019	0.186	0.039	0.057
Heating time $t_{tank}$ (ks)	27.70	29.34	30.35	31.48	31.13	42.75	31.28	26.57	25.93
$t_c$ (s)	9268	5562	3971	3088	2527	2527	2527	2527	2527
$\tau_{filling}$	2.99	5.27	7.64	10.19	12.32	16.92	12.38	10.51	10.26
$\tau_{heating\ HP-Tank}$	0.29	0.31	0.32	0.33	0.33	0.45	0.33	0.28	0.27
Average of the instantaneous COP in the 1st 1/3 of the heating period	5.818	5.990	5.711	6.119	6.215	3.991	6.059	7.304	7.695
Average of the instantaneous COP in the last 1/3 of the heating period	2.442	2.190	2.085	1.945	1.942	1.659	1.756	2.238	2.318
Gas cooler thermal power (kW)	5.617	5.528	5.600	5.120	5.365	4.566	5.470	5.976	5.696
Compressor Power (kW)	1.385	1.447	1.491	1.406	1.516	1.420	1.534	1.486	1.385
$E_{tank}$ (MJ)	149.1	153.1	154.9	157.5	158.2	158.5	158.1	157.6	157.5
$E_{comp}$ (MJ)	40.42	43.91	45.73	48.17	48.24	63.67	48.12	40.75	39.70
Outlet gas cooler Temperature (K)	299	293	290	288	287	287	287	288	288
Tank vertical velocity $\frac{4\dot{m}}{\rho\pi D^2}$ (mm·s <sup>-1</sup> )	0.172	0.286	0.401	0.515	0.630	0.630	0.630	0.630	0.630
Time-averaged COP of the CO <sub>2</sub> heat pump	4.021	3.953	3.944	3.733	3.756	3.155	3.813	4.272	4.249

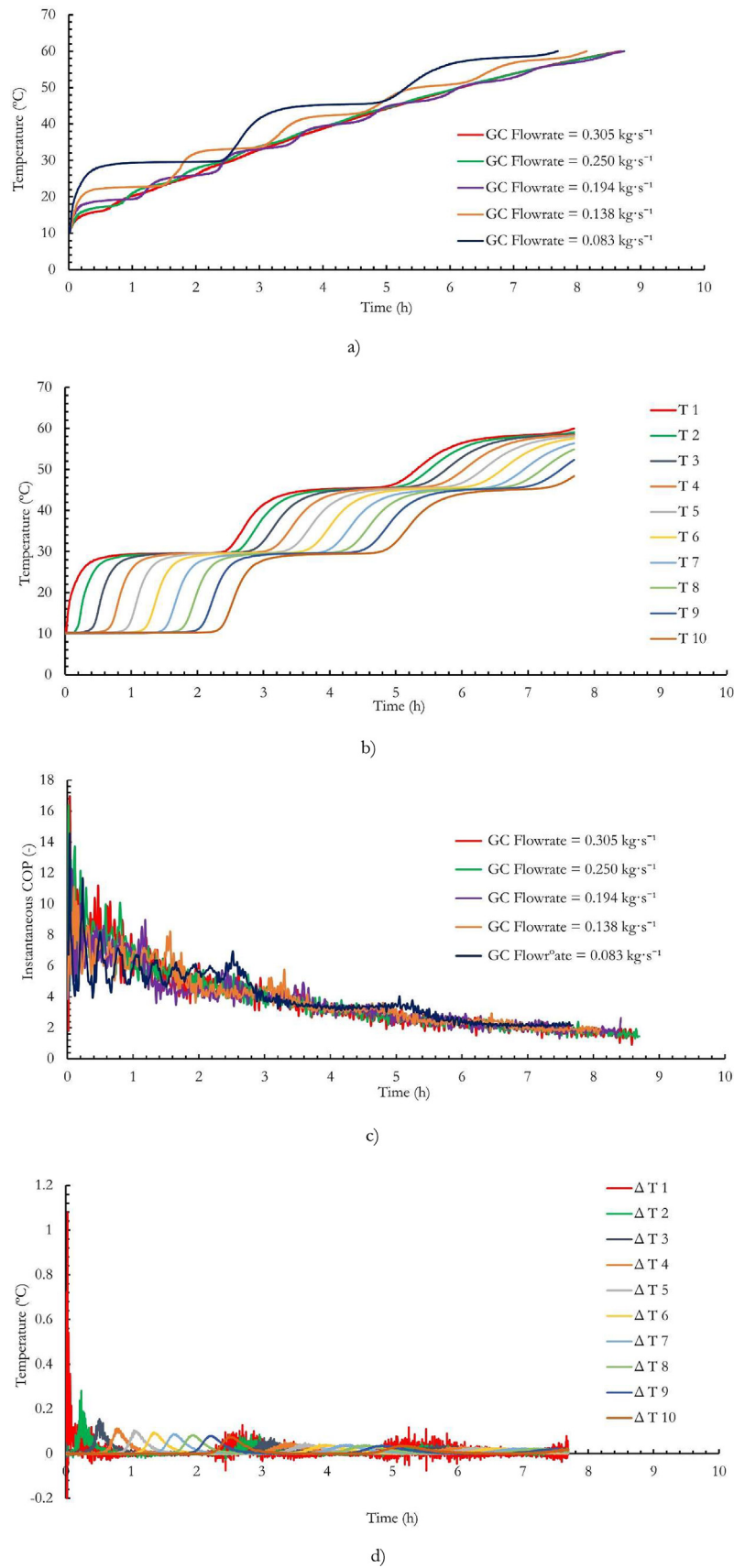


**Fig. 3.** (a) Temperature  $T_{10}$  evolution with time for different water flow rates at the gas cooler. (b) Temperature evolution at different heights of the storage tank for low gas cooler flow rate ( $0.083 \text{ kg}\cdot\text{s}^{-1}$ ). (c) Instantaneous COP evolution with time for different gas cooler flow rate. (d) Evolution with time of the  $\Delta T_i$  at different hot water storage tank heights for the case of  $0.083 \text{ kg}\cdot\text{s}^{-1}$ .

tend to promote water stratification within the tank. As a consequence, as the hot water mass flow rate decreases the amplitude and period of the oscillations measured increases due to the enhancement of the stratification process promoted by the  $T_{hw}$  and  $v$  tendencies of variation. This is somehow expected as the stratification tends to inhibit the water mixing and reduces the intensity of the turbulence mechanism and other transport phenomena that slow down the convective heat transfer. As a result, the thermal inertia of the mass water at the tank increases and the rate of change of water temperature with time decreases.

Fig. 3b helps to clarify these ideas. The figure shows the temperature evolution with time at different heights of the hot water storage tank during the heating process for test 1 (the lowest water flow rate at the gas cooler). As shown, the temperature at different heights shows self-similar profiles. The lower water layer at the bottom of the tank ( $T_{10}$ ) shows a delay in the heating process with respect to  $T_1$  at the top of the tank of the order of  $\sim t_c$  which is due to the time required by the hot water to travel through the water tank height at the vertical characteristic velocity  $v \sim \frac{4\dot{m}}{\rho\pi D^2}$ . Besides, this figure shows that for this test (test 1) the heating process does not follow a continuous increasing tendency as in test 5 (Fig. 2a). On the contrary, in this case, the temperature profiles exhibit several “steps” which are related to the heating capacity of the heat pump used in the DHW production system. These temperature steps are of the order of  $\sim \frac{\dot{Q}}{\dot{m} \cdot c_p} = \frac{\dot{W} \cdot COP}{\dot{m} \cdot c_p}$ . In the first 9200 s, the heat pump is only able to heat up the water within the gas cooler from 10 °C to 22 °C. However, when the temperature of the water at the inlet of the gas cooler ( $T_{10}$ ) starts increasing, also the temperature at the exit of the gas cooler ( $T_1$ ) starts increasing. The height of these “steps” reduces as the water at the bottom of the tank increases ( $T_{10}$ ) because the COP of the heat pump reduces with the increase of the inlet temperature at the gas cooler (Table 6). Moreover, the use of a small gas cooler flow rate in test 1, provides low thermal energy to the hot water storage tank that needs more “steps” to reach the reference  $T_{hwr}$  (60 °C in this case), than in the case of high gas cooler gas flow rate. Note that, in general terms, as the ratio of heat pump heating capacity to the tank mass increased, the number of “steps” would reduce. This clearly shows that when the heating power of a heat pump is limited with respect to the capacity of a hot water storage tank is of major importance to correctly choose the water flow control strategy. In other words, relatively “small” heat pumps coupled with relatively “big” water storage tanks will exhibit different performances and efficiency rates depending on the water flow rate at the gas cooler.

The evolution of the instantaneous COP as a function of time is shown in Fig. 3c. As shown, the instantaneous COP of the system decreases as time evolves and with the increase of the gas cooler flow rate. In the case of lower flow rates, the thermal stratification is formed and maintained (Fig. 3b), and this has an important benefit for the thermodynamic performance of the heat pump and the global COP of the DHW production system (Fig. 3c). However, as the gas cooler flow rate increases, the thermal stratification decreases and the water temperature in the storage tank becomes more homogenous, requiring more working time of the heat pump to reach  $T_{hwr}$  temperature at the top of the tank. As a result, more energy is accumulated in the tank.

Finally, Fig. 3d shows, the instantaneous variation of the water temperature with time ( $dT_i = T_i(t) - T_i(t-dt)$  where  $t$  is the time of the measurement and  $dt$  is the sampling time of the data logger) at different heights of the hot water storage tank during the heating period for the case of low mass flow rate ( $0.083 \text{ kg} \cdot \text{s}^{-1}$ ). As shown, the mass of water in a stratified tank exhibits different temperature heating “jumps” depending on the height within the tank where the temperature is measured. The lower layers of stratified water at the bottom of the tank notice lower heating jumps in a wider

time-lapse than the layers of stratified water at the top of the tank where the heating jumps are sharper in time and more intense in temperature jump. This is due to the diffusion and transport phenomena taking place within the tank that tend to dump these jumps. Note that each temperature sensor measures two temperature heating “jumps” that are related to the regions of maximum temperature slope in Fig. 3b. For example, sensor  $T_1$  notice a jump at the beginning of the heating period and another after a time of the order of  $\sim t_c$ . Thus, the temperature heating “jumps” found in Fig. 3d are related to the moments of the tank heating where a water layer feels the higher heat transfer due to the higher temperature lift at the gas cooler which are the moments when the temperature at the top and the bottom of the tank are similar and/or closer. Thus, the characteristic travel velocity of these heating waves along the tank (from top to bottom) is  $v \sim \frac{4\dot{m}}{\rho\pi D^2}$ . It is worth

noting that these fluctuations in the water temperature at the tank influence very little in the COP of the CO<sub>2</sub> heat pump as the water entering the gas cooler is obtained from port at the bottom of the stratified tank ( $T_{10}$ ) and the temperature variations with time of this tank region are the lowest ones. Table 7 and Fig. 4 show quantitatively the influence of the gas cooler flow rate on the global COP of the DHW production system and on the time-averaged COP of the CO<sub>2</sub> heat pump. The time-averaged COP of the CO<sub>2</sub> heat pump

is defined as:  $COP_{\text{Time averaged}} = \frac{\int_{t=0}^{t=t_{\text{tank}}} \dot{Q} dt}{\int_{t=0}^{t=t_{\text{tank}}} \dot{W} dt}$  where  $t_{\text{tank}}$  is the elapsed

time during each test. It can be seen that the global COP decreases with the increase of the gas cooler flow rate. The highest performance value is given by the lower flow rate of the gas cooler. Again, this is due to the lower inlet temperature of the gas cooler caused by the thermal stratification that enhances the heat pump COP. As previously noticed, the gas cooler mass flow rate also has an influence on the energy storage in the tank. In fact, a reduction in the gas cooler mass flow rate of  $\sim 72\%$  results in a reduction of  $\sim 6\%$  in the overall thermal energy stored in the tank which means a  $dE_{\text{tank}}/d\dot{m} \approx 41 \text{ (kJ} \cdot \text{s} \cdot \text{kg}^{-1})$ .

### 4.3. Impact of the evaporator inlet temperature

To analyse the impact of the inlet temperature of the evaporator ( $T_{in \text{ evap}}$ ), tests 6 to 9 were performed by varying the inlet temperature in the evaporator between 5 °C and 20 °C. Results show that, as  $T_{in \text{ evap}}$  increases, the global COP of the system increases. Table 6 shows a variation of 59% in the global COP of the DHW production system between an inlet evaporator temperature of 5 °C and 20 °C. Fig. 5a shows the evolution of the storage tank temperature as a function of time for different tests. Two effects can be seen, on the one hand, temperature increases with time and, on the other, the heating time decreases as the evaporator inlet temperature increases, which is due to the refrigerant temperature difference between the inlet and the outlet of the evaporator. Also, it is noticeable that the heating time is greater as the water inlet temperature at the evaporator increases. For example, the heating time

**Table 7**

Influence of the gas cooler flow rate on the global COP of the DHW system and the time-averaged COP of the CO<sub>2</sub> heat pump.

Gas cooler flow rate $\text{kg} \cdot \text{s}^{-1}$	Global COP of the DHW production system	Time-averaged COP of the CO <sub>2</sub> heat pump	Thermal energy storage $E_{\text{tank}}$ (kJ)
0.083	3.688	4.021	149.1
0.138	3.486	3.953	153.1
0.194	3.386	3.944	154.9
0.25	3.269	3.733	157.5
0.305	3.280	3.756	158.2

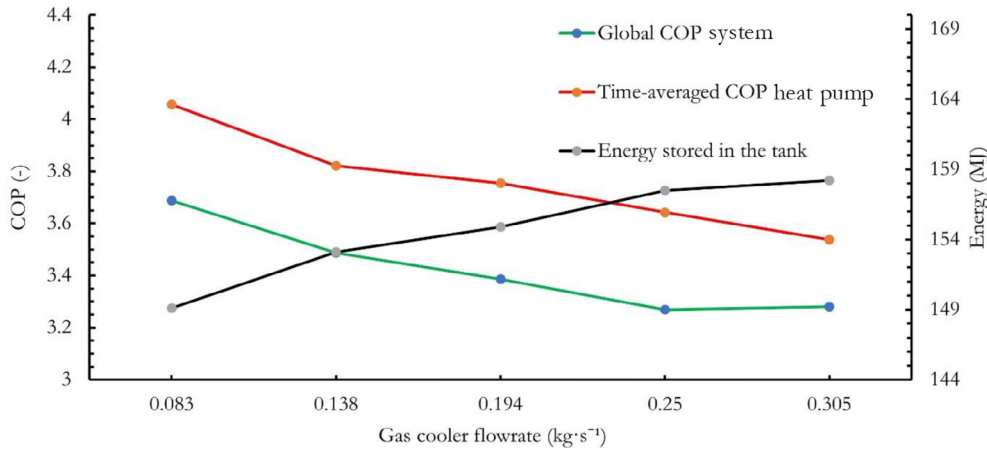


Fig. 4. Evolution of the Global COP of the DHW production system and time-averaged COP of the CO<sub>2</sub> heat pump with gas cooler mass flow rate.

is about 12 h when the water inlet temperature in the evaporator is 5 °C and is about 7 h for the case of an evaporator inlet temperature of 20 °C. This means a total reduction of ~ 40% and reduction of the heating time of 2.7% per degree increased at the inlet evaporator water temperature (i.e.  $dt_{\text{tank}}/dT_{\text{in evap}} \sim 1/3$  (h/ °C)).

The heat pump performance is presented in Fig. 5b. This figure shows the evolution of the instantaneous COP of the system as a function of time. It can be seen that the instantaneous COP decreases with the increase of time, and this is due to the increase of the inlet temperature to the gas cooler, hence, when the storage tank temperature increases, the inlet temperature in the gas cooler increase. Also, the evaporator temperature influences in a negative manner the system performance, so, when the inlet temperature is higher, the system gives higher COP. Fig. 5c shows the evolution of the accumulated COP of the system as a function of the heating time for different water inlet temperatures at the evaporator. As shown, the accumulated COP shows the same decreasing evolution with time as the instantaneous COP, but in this case, the trends are clearer than in the previous case as this variable does not account for the high-frequency fluctuations of the instantaneous COP which are linked to the slight temperature oscillations between each sample during data acquisition. As shown, in the first hour of the heating period, the inlet water temperature at the evaporator has an important impact on the COP of the system. As the evaporator inlet temperature ( $T_{\text{evap,in}}$ ) increases, the accumulated COP also increases gradually, from an initial value of 7 for  $T_{\text{evap,in}} = 5$  °C, to 9 for  $T_{\text{evap,in}} = 10$  °C, 10.5 for  $T_{\text{evap,in}} = 15$  °C, up to 12 for  $T_{\text{evap,in}} = 20$  °C. After the first hour the accumulated COP values tend to slowly converge.

#### 4.4. Discussion on the stratification and the control strategy of the DHW production system

In order to analyse the thermal stratification within the hot water storage tank, two tests are taken into consideration under the same conditions but with the lower and the higher water mass flow rate at the gas cooler (test 1 and test 5). Fig. 6a shows the evolution of the tank temperature at different heights for both tests as a function of time. As shown, the temperature of the storage tank under the low flow rate conditions results in a slower heating process of the different water layers within the tank. These layers maintain a thermal stratification within the storage tank. As a result, the hot water injected from the gas cooler remains at the upper layer of the tank ( $T_1$ ) and this layer reaches the target temperature  $T_{\text{hwr}}$  faster than in the case of test 5, which results in a

shorter global heating time. In contrast, the heating time to reach  $T_{\text{hwr}}$  at the top of the tank with the higher flow rate last more time and the vertical temperature gradient within the tank is smaller during the heating process.

To characterize this stratification, Fig. 6b shows the time-averaged Richardson number during the heating process for different gas cooler mass flow rates and Fig. 6c shows the Ri evolution with time defined as  $Ri = g \cdot \beta \cdot H' \cdot (T_1 - T_{10}) / v_{\text{in}}^2$  during the heating process for different mass flow rates. Ri number describes the ratio of the buoyancy to the mixing force and is a usual descriptor of the stratification. A large Ri indicates a stratified storage tank whereas a small Ri means a mixed storage tank. Note that, we follow the definition of Richardson number of [41,42] where  $H'$  represents the vertical distance between the inlet and outlet water ports of the tank,  $v_{\text{in}}$  is the inlet velocity of the water to the tank. The time-averaged Ri is computed following the mean value theorem as:

$$\text{time - averaged Ri} = \frac{1}{t_{\text{tank}}} \int_{t=0}^{t=t_{\text{tank}}} Ri^* \cdot dt \quad (12)$$

where  $Ri^*$  is the instantaneous value of the Richardson number at the instant “t” of time. As shown in the figures, the time-averaged Ri for the lowest mass flow rate (0.083 kg·s<sup>-1</sup>) is ~ 50 whereas for the case of the highest mass flow rate (0.305 kg·s<sup>-1</sup>) is below 1. In other words, a reduction of a factor of 3.7 in the mass flow rate results in an increase of the stratification in a factor of 50. In fact, in this case, the Ri scales with the inverse of the power of the gas cooler mass flow rate following a potential law:  $Ri = 0.00174/\dot{m}^{3.2}$  (with a fitting  $R^2 = 0.9993$ ). Indeed, due to the heat pump-storage tank coupling, the Ri number can be written as a function of the COP of the CO<sub>2</sub> heat pump as:

$$Ri = \frac{g\beta H'(T_{\text{top}} - T_{\text{bottom}})}{v_{\text{in}}^2} = \frac{g\beta H'(T_{\text{top}} - T_{\text{bottom}})}{\left(\frac{4\dot{m}}{\rho\pi d^2}\right)^2} \approx \frac{\pi^2 d^4 g \cdot H' \cdot \rho^2 \cdot \beta \cdot W \cdot \text{COP}}{16C_p \cdot \dot{m}^3} \quad (13)$$

This way, the stratification reached at the hot water storage tank can be linked with the design and operational parameters of the CO<sub>2</sub> heat pump and its efficiency. Note that, this approximation of the Ri as a function of the COP of the heat pump is valid for the case of negligible thermal losses (i.e. temperature losses  $\Delta T_{\text{losses}}$ ) in the pipes connecting the heat pump and the hot water storage tank



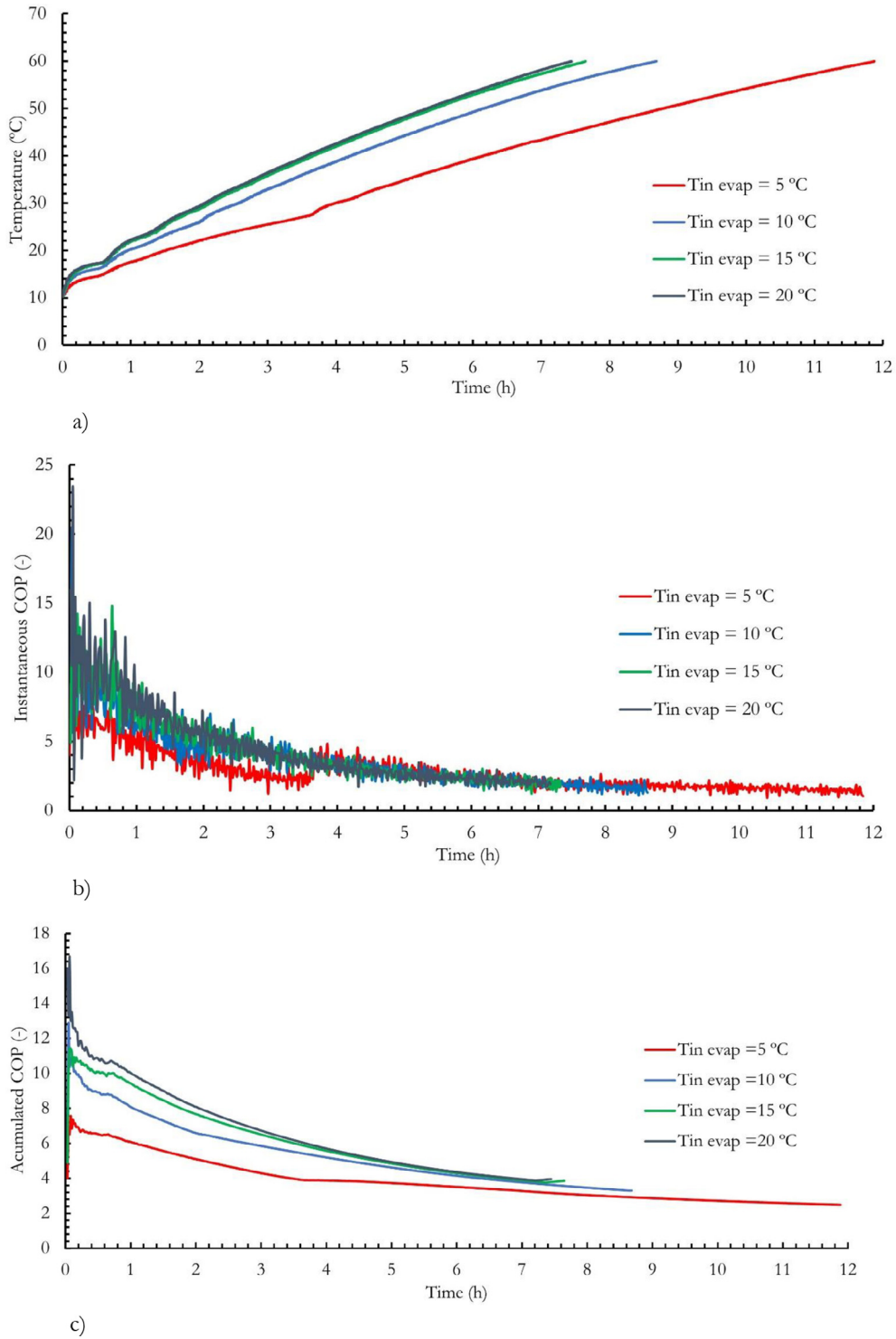


**Fig. 5.** (a) Temperature  $T_1$  evolution with time during the heating process as a function of the evaporator inlet temperature. (b) Instantaneous COP evolution with time. (c) Accumulated COP evolution with time.

as in the present study. In case the thermal losses in the pipes were important they should be taken into account in order to correct the actual temperature difference in Equation 13 by considering:

$$(T_{top} - T_{bottom}) \approx \frac{\dot{Q}}{\dot{m} \cdot C_p} + \Delta T_{losses} = \frac{\dot{W} \cdot COP}{\dot{m} \cdot C_p} + \Delta T_{losses} \quad (14)$$

In light of Equation 13, the potential evolution of averaged Ri with mass flow rate is similar to that found in Fig. 4 for the global COP, and it permits explaining the evolution of global COP found in Fig. 4. As shown in Fig. 4, at high flow rates (0.25 and 0.305 kg·s<sup>-1</sup>) the time-averaged COP of the CO<sub>2</sub> heat pump follows a decreasing trend whereas the global COP of the system does not decrease at high flow rates but, on the contrary, it settles, following a similar

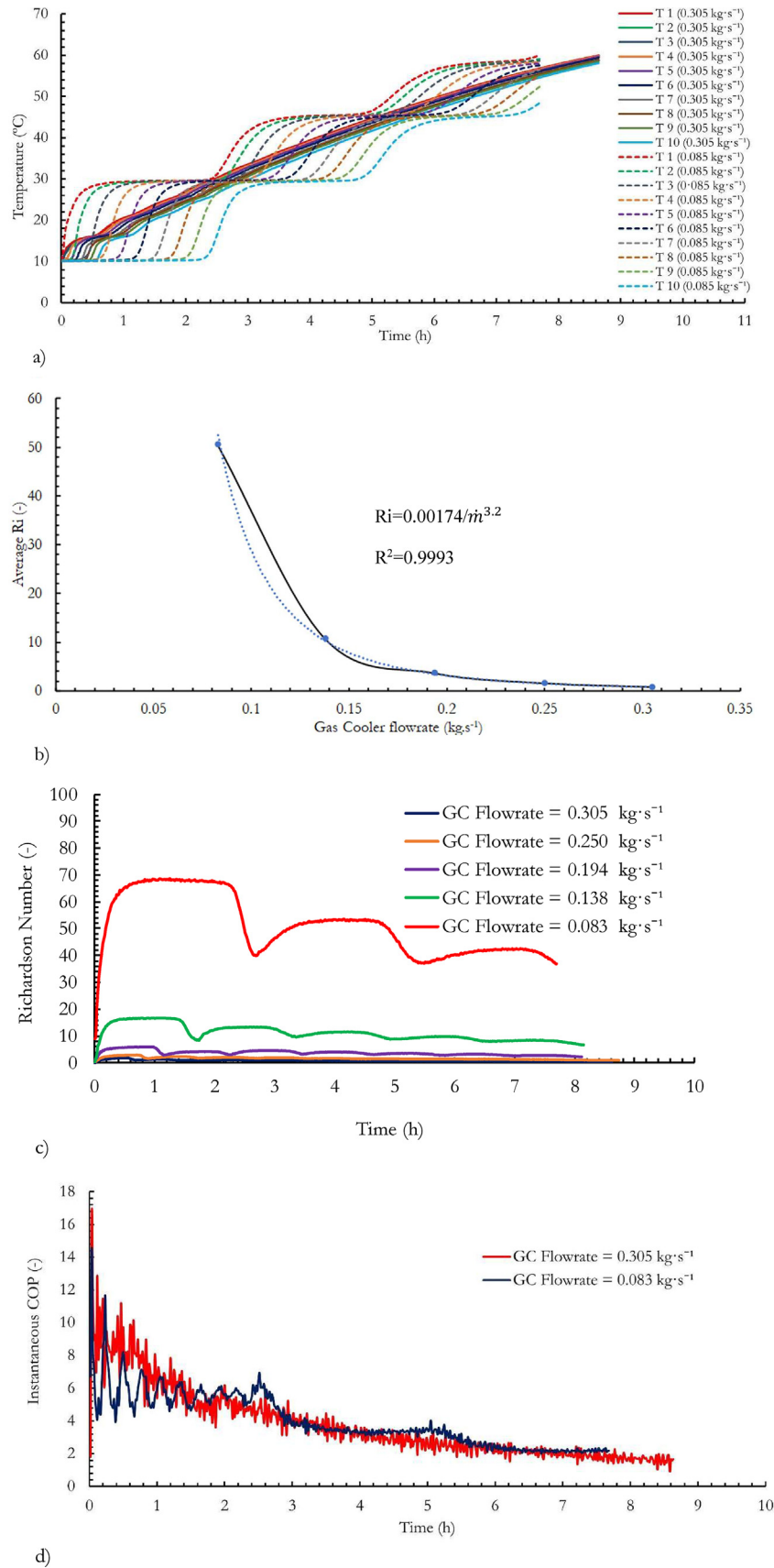


**Fig. 6.** (a) Comparison of temperature evolution at different heights of the hot water storage tank for the case of low and high water mass flow rate at the gas cooler. (b) Maximum Ri vs mass flow rate. (c) Evolution of Ri during the storage tank heating process for different mass flow rates. (d) Evolution of the instantaneous COP during the heating process for low and high mass flow rates at the gas cooler.

tendency of the Ri number of Fig. 6b. As can be inferred from the definition equations of both COPs, this difference in the evolution of both COPs is mainly related to the hot water storage tank regime during the heating process and its stratification. Regarding the time evolution (Fig. 6c), Ri increases from zero to a maximum value, during the heating process of the water of the tank. It is also worth noting that the oscillations in the Ri evolution for low mass flow rates have a period of the order of  $\sim t_c$  and coincide with the time location of the temperature steps (Fig. 6c) which have an amplitude proportional to these temperature steps, i.e.  $\propto \frac{\dot{Q}}{m \cdot c_p}$ . At the end of the heating period, the stratification found with the lowest flow rate is 40 times higher than that found for the highest flow rate. Fig. 6c shows that  $Ri \sim 40$  in the system is enough to ensure tank stratification whereas  $Ri \sim 1$  (i.e. vertical filling velocities at the tank  $v \sim \frac{4\dot{m}}{\rho \pi D^2}$  of the order of  $\sim 0.5\text{--}0.6 \text{ mm}\cdot\text{s}^{-1}$  in tests 4 and 5) inhibit stratification and promote mixing. For the case of a water flow rate of  $0.138 \text{ kg}\cdot\text{s}^{-1}$ , which corresponds to  $Ri \sim 10$  the stratification is deficient (with a temperature gradient of  $\sim 4 \text{ K/m}$ ), whereas for the case of  $0.083 \text{ kg}\cdot\text{s}^{-1}$  i.e.  $Ri \sim 40$  the stratification is better established (with a temperature gradient of  $\sim 8 \text{ K/m}$ ). It is worth remarking that there is not a clear threshold line but a fuzzy band that defines the transition regime between stratified and non-stratified conditions. The region between  $Ri \in [10,40]$  could be considered as a transition region where the flow regime evolves towards a stable, stratified regime. Under this perspective, the value of  $Ri \sim 40$  should be understood as a minimum reference order of magnitude that maintains the stratification in the storage tank. Thus, when coupling a CO<sub>2</sub> heat pump with a hot-water storage tank,  $H'$ ,  $d$ ,  $\dot{m}$ ,  $\dot{W}$  and COP must be selected to ensure a minimum order of magnitude of  $Ri \sim 40$ . Note that, during the estimation of the order of magnitude of the Ri in the design process of a DHW system,  $\dot{W}$  and COP can be obtained from the reference values provided by the manufacturer of the heat pump. Once selected the tank and the heat pump, the gas cooler mass flow rate is the variable that can be changed by the control system and/or the user in order to promote stratification and improve the global COP of the system.

A low flow rate in the gas cooler not only has a great benefit in the thermal stratification but also on the thermal performance of the system. From Fig. 6a can be seen that the temperature of the bottom of the tank in the case of the low flow rate is always lower than that of the higher flow rate. This results in a low inlet temperature to the gas cooler which enhances the efficiency of the heat pump and the whole system. Fig. 6d presents the evolution of the instantaneous COP of the DHW production system as a function of time for both tests. It can be seen that the COP is relatively high in the first third of the heating process and then it decreases with the increase of time for both tests conditions. In the case of a high flow rate in the gas cooler, the instantaneous COP is higher in the first hour than that of the case with low flow rate and then it equals or it is slightly below it. Note that in this last case, the instantaneous COP has three time steps of the order of  $\sim t_c$  which are related to the temperature steps noticed at the bottom of the hot water storage tank due to the tank stratification. Besides, in this case, the instantaneous COP also shows some oscillations within the first 2.5 h (i.e. first time step). This is a general pattern shown at low flow rates. The lower the flow rate, the sharper the oscillations. These are due to the water temperature heating "jumps" found at different heights within the tank (Fig. 3d) and have its characteristic time which of the order of  $\sim H/(10v) \sim \frac{H\rho\pi D^2}{40\dot{m}}$ . As shown in Equation 2, these temperature heating "jumps" at the different water layers of a stratified tank are included on the numerator of the instantaneous COP equation. Consequently, the oscillations presented in Fig. 6d at a low flow

rate corresponds to the curve shape resulting from the sum of the curves shown in Fig. 3d. All in all, as shown in Table 6, the global COP of the system is better in the case of low flow rates than in the case of high flow rates. This variation in the global COP reaches 12.4% when comparing the global COP at the lowest flow rate (test 1) which is 3.688 with the one at the highest flow rate (test 5). In part, this variation is due to the shorter tank heating time of the low flow rate case.

Results showed that, when heating the water storage tank with CO<sub>2</sub> water-to-water heat pumps, strategies based on promoting stratification, such as the use of the minimum possible water flow rate between the tank and the heat pump gas cooler, permits to reduce around 16% the electric power consumption of the compressor during the heating compared to other strategies. However, strategies based on considering higher water flow rates in the gas cooler enhances the water mixing, increase the heating time needed to reach  $T_{\text{hwr}}$  temperature at the top of the storage tank and reduce the global COP of the systems.

In the case of the present study, the difference between the use of low or high mass flow rate strategies (test 1 vs test 5) results in an increase of 19% of energy consumption at the compressor during the heating process and a variation of 25% in the global COP of the system of the last third of the heating period (Table 6). As a result, the operating strategy that maximizes the global COP of the system depends on the specific DHW consumption profile. For the case of small and/or time spaced DHW consumption profiles, the use of low flow rates is recommended as they ensure the maintenance of the stratification and shorter heating periods (and therefore energy consumption) to reach the  $T_{\text{hwr}}$ . However, in cases where high and/or intensive DHW consumption profiles are expected, a strategy based on whether increasing the  $T_{\text{hwr}}$  keeping a low mass flow rate or using high gas cooler water flow rates might be interesting as this strategy provides higher stored thermal energy.

#### 4.5. Comparison of the present results with similar experimental studies

As previously discussed in the introduction section, there are very few experimental works devoted to the analysis of the overall performance of CO<sub>2</sub> heat pumps coupled with a storage tank in a whole DHW production system. One of the few authors that performed experimental tests in a CO<sub>2</sub> heat pump water heater similar to the one tested in this work are Tosato et al. [32]. The comparison of those results with the present work is presented in Table 8. In their work, Tosato et al. reported COP values that ranged from 5.1 in the first period, when the temperature of the water entering the gas cooler reached  $T_{\text{gcin}} \approx 20^\circ\text{C}$ , to an average COP of 4.0 for the whole test, which finished when  $T_{\text{ingc}} = 32^\circ\text{C}$ . As those tests were performed with an evaporator inlet temperature  $T_{\text{mevap}} \approx 15^\circ\text{C}$ , they can be compared to our test number 8, which yields an accumulated COP of 9.7 for the first 80 min, when  $T_{\text{ingc}} \approx 20^\circ\text{C}$ , and an accumulated COP of 7.47 for the first 180 min, when  $T_{\text{ingc}} \approx 32^\circ\text{C}$ . Those important differences can be explained by the differences in the pressure control strategy. Tosato's tests were performed operating the CO<sub>2</sub> heat pump with a constant gas cooler pressure around 105 bar, which means that the system operated following a transcritical cycle. On the contrary, as will be explained in detail in section 4.6, all our tests were performed with a variable (optimal) gas cooler pressure control, that maintains the system operating under subcritical conditions until  $T_{\text{ingc}} \approx 30^\circ\text{C}$  and clearly improves the system's efficiency.

Other authors that present results obtained in a CO<sub>2</sub> heat pump water heater similar to ours are Liu et al. [33], although during their tests the water temperature continuously changed in both,

**Table 8**  
Summary of the comparison of the present results with previous works.

Instantaneous COP			Present work			Accumulated COP			
Liu's work						$T_{in\ evap}$	$T_{in\ gc}$	COP	
$T_{in\ evap}$	$T_{in\ gc}$	COP	$T_{in\ evap}$	$T_{in\ gc}$	COP	(°C)	(°C)	Tosato's work	Present work
(°C)	(°C)		(°C)	(°C)					
27	27	3.65	20	27	6	15	10 → 20	5.1	9.7
27	35	3.05	20	35	4.53				
16	43.5	2.5	16	43.5	3.6	15	10 → 32	4	7.47
10	53.3	2.1	10	53.3	2.6				

the evaporator inlet and the gas cooler inlet, which makes them even more difficult to compare with our results. They provide instantaneous COP values for different compressor frequency ( $f$ ), hot water flow rate ( $V_h$ ), cold water flow rate ( $V_c$ ), or expansion valve opening ( $n$ ) during the whole heating process, that started with both tanks at 27 °C and finished when the hot tank reached 60 °C. Table 8 compares Liu's instantaneous heating COP for  $f = 50$  Hz,  $V_h = 0.4\ m^3 \cdot h^{-1}$ ,  $V_c = 0.2\ m^3 \cdot h^{-1}$  and  $n = 330$ , with those obtained under similar operating conditions in our facility. For this particular case, Liu's instantaneous heating COP varied from COP = 3.65 at the beginning of the process, when the systems had been operated for  $t = 1000$  s (i.e.,  $T_{in\ gc} = T_{in\ evap} = 27\ ^\circ C$ ), to COP = 3.05 when the systems had been operated for  $t = 1000$  s (i.e.,  $T_{in\ gc} \approx 35\ ^\circ C, T_{in\ evap} \approx 27\ ^\circ C$ ), COP = 2.5 for  $t = 4000$  s ( $T_{in\ gc} \approx 43.5\ ^\circ C, T_{in\ evap} \approx 16\ ^\circ C$ ), and COP = 2.1 towards the end of the heating process (i.e.,  $t = 6000$  s,  $T_{in\ gc} \approx 53.3\ ^\circ C, T_{in\ evap} \approx 10\ ^\circ C$ ). In our case, for similar conditions we obtained better COP values (6, 4.53, 3.6, and 2.6 for the corresponding equivalent conditions). Although those differences could be explained by differences in the gas cooler pressure control strategy, Liu does not provide clear information about this point and, therefore, no definitive conclusions can be drawn.

**4.6. Influence of the operation mode of the CO<sub>2</sub> heat pump on the COP of the DHW generation system: transcritical vs subcritical cycle**

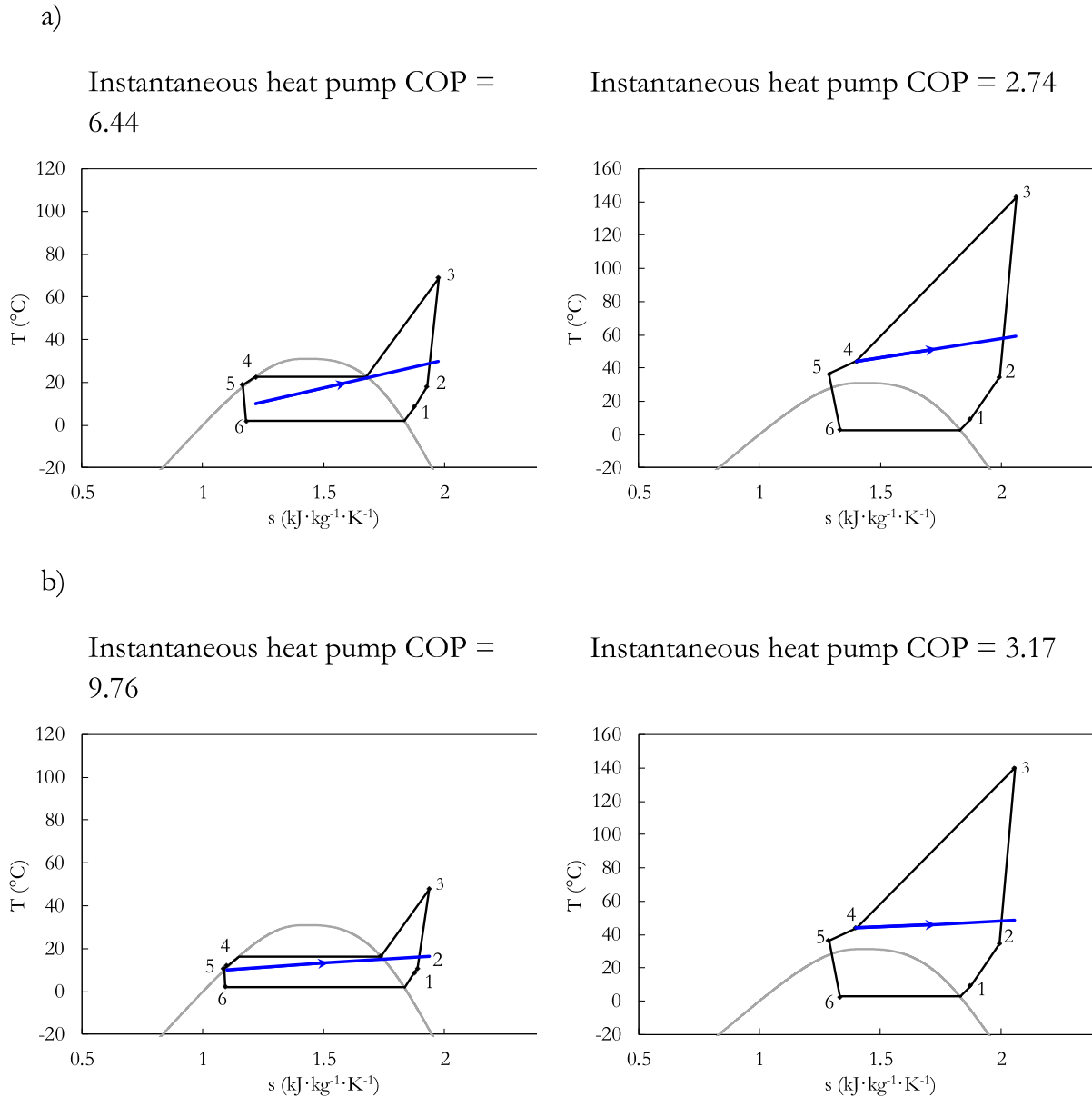
In the case of the CO<sub>2</sub> heat pump used in the present study, the back-pressure electronic valve seeks for the optimal gas cooler pressure in the refrigerant side in order to maximise the COP of the heat pump. This control strategy permits the heat pump to work with a gas cooler pressure over or under the critical pressure of the CO<sub>2</sub>. As indicated in the test methodology section, during the tests it was logged the evolution of the working pressure of the refrigerant at the gas cooler with time, in order to evaluate whether the CO<sub>2</sub> heat pump was working with a transcritical or a subcritical thermodynamic cycle.

Fig. 7 shows the T-s working diagrams of the CO<sub>2</sub> heat pump for the case of test 1 and 5. These tests have a water mass flow rate at the gas cooler of 0.083 kg·s<sup>-1</sup> and 0.305 kg·s<sup>-1</sup>, respectively. In both cases it is shown two representative examples of the working cycle: one at the beginning of the heating test and another at the end of the heating test. In order to properly compare the operation mode of the heat pump, the cases selected for test 5 have a similar water temperature at the gas cooler inlet to that of the test 1. In the figure, the black line represents the thermodynamic states of the refrigerant (i.e. CO<sub>2</sub>) and the blue line represents thermodynamic states of the water at the gas cooler during the heating process. The figure also shows the instantaneous COP of the heat pump for the lapse of time shown in the T-s cycle. As shown, during the beginning of the heating process (left side of the figure), the water temperature at the inlet of the

gas cooler is relatively low and the heat pump works under a subcritical mode with a gas cooler optimal pressure at the refrigerant side below the critical pressure of the CO<sub>2</sub>. In this case there is a phase change of the CO<sub>2</sub> and the gas cooler works as a condenser. This subcritical operational mode at the beginning of the heating process is found for all the water mass flow rate conditions tested. It is also found that the higher the mass flow rate, the lower gas cooler optimal pressure established: In the case of 0.083 kg·s<sup>-1</sup>, it is reached 60 bars, whereas the case of 0.305 kg·s<sup>-1</sup> it is reached 52 bars. This operational mode results in a lower pressure ratio and a lower power consumption at the compressor. As a consequence, there is a "boost" of the instantaneous COP of the heat pump compared to the case of transcritical operation mode when COP reported are between 2 and 3 times lower. Besides, the higher mass flow rate at the gas cooler of test 5 provides a lower gas cooler working pressure and an increase of 50% in the instantaneous heat pump COP when compared with test 1. This explains the lower average COP of the DHW production system in the first third of the heating period reported in Table 6 for test 1 with respect to that of test 5. Thus, in the case of the heat pump working under a subcritical operation mode it is recommended to set high water mass flow rates in order to maximize the COP of the DHW production system.

During the end of the heating process (right side of the figure), the water temperature at the inlet of the gas cooler is higher and the heat pump works under a transcritical mode with a gas cooler pressure at the refrigerant side over the critical pressure of the CO<sub>2</sub>. In this case the optimal working pressure at the gas cooler is much higher (around 105 bars) and the instantaneous COP of the heat pump is drastically reduced when compared to the subcritical operation mode. Moreover, the difference of the gas cooler working pressure between test 1 and 5 is considerably reduced to less than 0.7 bars (it is 105.6 bars in the case of 0.083 kg·s<sup>-1</sup>, and 105.0 bars in the case of 0.305 kg·s<sup>-1</sup>). This shows that the influence of the water mass flow rate at the gas cooler strongly influences the COP of the heat pump when it works under a subcritical cycle (i.e. with low inlet water temperatures at the gas cooler) whereas this influence of the water mass flow rate almost vanishes when the inlet temperature of the water at the gas cooler is relatively high and the heat pump works under a transcritical cycle.

All in all, it is found that in order to maximize the COP of the DHW production system, the heat pump should work with high mass flow rates when it operates under subcritical mode (i.e. at the beginning of the tank heating process when the water temperature at the bottom of the tank is low) and it should "switch" to low mass flow rates when it works under a transcritical operation mode (i.e. during the rest of the tank heating process, when the water temperature at the bottom of the tank is higher). This change in the mass flow rate should be progressive as the heat pump evolves from subcritical towards transcritical operation modes always seeking the maximization of COP of the DHW production system.



**Fig. 7.** Operation mode of the heat pump: T-s cycles of the CO<sub>2</sub> heat pump working at the beginning of the heating process (left) and at the end of the heating process (right). (a) test 1: gas cooler water mass flow rate 0.083 kg·s<sup>-1</sup>. (b) test 5: gas cooler water mass flow rate 0.305 kg·s<sup>-1</sup>.

### 5. Conclusions and future work

This work has focused on the experimental characterization of the dynamic performance of a DHW production system working with CO<sub>2</sub> water-to-water heat pump connected to a hot-water storage tank. By developing an ad-hoc experimental facility, the results of the tests showed that the water control strategy is a key factor in the overall performance of the DHW production system:

- In the case of minimum water flow rate at the gas cooler, results showed that the overall performance of the DHW system increased compared to the case of other flow rates, as the filling process does not induce the mixing of water what promotes that the upper layer of the tank, where the DHW for consumption is obtained, always maintains the highest temperature of the tank. Moreover, the stratification also reduces the heating time. However, very low flow rates also reduce the overall ther-

mal energy stored in the tank. Therefore, there must be a compromise between energy efficiency and capacity to supply the thermal energy demanded by the user.

- Stratification is a key factor in the energy efficiency of the system. Considering a heating strategy where stratification is maintained by establishing the minimum water flow rate at the gas cooler (test 1), the electric consumption of the compressor can be reduced by 25% compared to the case of setting the maximum was flow rate at the gas cooler (test 5).
- Reaching tank Ri numbers  $\sim 40$  during the heating process (i.e. vertical filling velocities at the hot-water storage tank  $v \sim 0.1 \text{ mm}\cdot\text{s}^{-1}$ ) ensures stratification whereas  $Ri \sim 1$  (i.e. velocities  $v \sim 0.5\text{--}0.6 \text{ mm}\cdot\text{s}^{-1}$ ) inhibit stratification and promotes mixing. This means that a reduction of a factor of 3.7 in the mass flow rate results in an increase of the stratification in a factor of 40. Thus, when coupling a CO<sub>2</sub> heat pump with a hot-water storage tank,  $H'$ ,  $d$ ,  $\dot{m}$ ,  $W$  and  $COP$  must be selected to ensure



a minimum order of magnitude of  $Ri \approx \frac{\pi^2 d^4 g H' \rho^2 \beta W_{COP}}{16 C_p m^3} \sim 40$ .

- The use of a heating strategy based on setting high water flow rates at the gas cooler enhances the water mixing, which reduces the global COP of the DHW production system due to three factors: the reduction of the water temperature at the top of the storage tank, the reduction of the COP of the CO<sub>2</sub> heat pump due to the increase of the water temperature at the inlet of the gas cooler and the increase of the heating time and the compressor working time needed to reach the set point temperature at the top of the storage tank. Besides, a reduction in the gas cooler mass flow rate of  $\sim 72\%$  results in a reduction of  $\sim 6\%$  in the overall thermal energy stored in the tank which means a  $dE_{\text{tank}}/dm \approx 41 \text{ kJ}\cdot\text{Kg}^{-1}\cdot\text{s}^{-1}$ .
- The increase of the evaporator inlet water temperature from 5 °C to 20 °C increases the global COP of the DHW production system by 59% during the heating process which means a reduction of  $\sim 3.9\%$  per degree increased at the inlet evaporator water temperature. Besides, it also reduces the heating time by around  $\sim 40\%$  which means a reduction of the heating time of around 2.7% per degree increased at the inlet evaporator water temperature ( $dt_{\text{tank}}/dT_{\text{in evap}} \sim 1/3 \text{ (h/}^\circ\text{C)}$ ).
- In order to maximize the COP of the DHW production system, the heat pump should work with high mass flow rates when it operates under subcritical mode (i.e. at the beginning of the tank heating process when the water temperature at the bottom of the tank low) and it should “switch” to low mass flow rates when it works under a transcritical operation mode (i.e. during the rest the tank heating process when the water temperature at the bottom of the tank is higher).

The methodology followed in the study can be used to assist in the design and dynamic characterization of the behaviour of CO<sub>2</sub> water-to-water heat pumps for DHW production systems. Future work will focus on the development of a numerical model of the hot water storage tank and the use of this experimental data to validate numerical simulations obtained with the numerical model to predict the system behaviour during other stages of the operation of the DHW production system under standard conditions.

## Declaration of Competing Interest

The authors declare that they have no known competing financial interests or personal relationships that could have appeared to influence the work reported in this paper.

## Acknowledgements

This work has been performed in the context of the project in the project “Maximisation of the efficiency and minimisation of the environmental impact of heap pumps for the decarbonisation of heating and domestic hot water production in nearly zero energy buildings” ENE2017- 83665-C2-2-P, Funded by the Ministry of Economy and Competitiveness, Spain and the support of the European Regional Development Fund.

## References

- [1] Communication from the commission to the European parliament, the European council, the council, the European economic and social committee and the committee of the regions The European Green Deal, COM/2019/640 final.
- [2] A. Allouhi, Y. El Fouih, T. Kousksou, A. Jamil, Y. Zeraoui, Y. Mourad, Energy consumption and efficiency in buildings: current status and future trends, *J. Clean Prod.* 109 (2015) 118–130, <https://doi.org/10.1016/j.jclepro.2015.05.139>.

- [3] Eurostat. Energy consumption in households by type of end-use, 2018. [https://ec.europa.eu/eurostat/statistics-explained/index.php?title=Energy\\_consumption\\_in\\_households](https://ec.europa.eu/eurostat/statistics-explained/index.php?title=Energy_consumption_in_households).
- [4] A. Bastani, P. Eslami-Nejad, M. Badache, A.T.A. Nguyen, Experimental characterization of a transcritical CO<sub>2</sub> direct expansion ground source heat pump for heating applications, *Energy Build.* 212 (2020) 109828, <https://doi.org/10.1016/j.enbuild.2020.109828>.
- [5] C. Mateu-Royo, C. Arpagaus, A. Mota-Babiloni, J. Navarro-Esbrí, S.S. Bertsch, Advanced high temperature heat pump configurations using low GWP refrigerants for industrial waste heat recovery: a comprehensive study, *Energy Convers. Manag.* 229 (2021) 113752, <https://doi.org/10.1016/j.enconman.2020.113752>.
- [6] K.J. Chua, S.K. Chou, W.M. Yang, Advances in heat pump systems: A review, *Appl. Energy* 87 (12) (2010) 3611–3624, <https://doi.org/10.1016/j.apenergy.2010.06.014>.
- [7] H. Esen, M. Inalli, M. Esen, K. Pihtili, Energy and exergy analysis of a ground-coupled heat pump system with two horizontal ground heat exchangers, *Build. Environ.* 42 (2007) 3606–3615, <https://doi.org/10.1016/j.buildenv.2006.10.014>.
- [8] M.a. Liangdong, R. Tixiu, Z. Tianjiao, Z. Tianyi, Z. Jili, Experimental study on effect of operating parameters on performance of serially cascaded wastewater source heat pump, *J. Build. Eng.* 32 (2020) 101458, <https://doi.org/10.1016/j.job.2020.101458>.
- [9] P. Farzanehkhameh, M. Soltani, F. Moradi Kashkooli, M. Ziabasharhagh, Optimization and energy-economic assessment of a geothermal heat pump system, *Renew. Sustain. Energy Rev.* 133 (2020) 110282, <https://doi.org/10.1016/j.rser.2020.110282>.
- [10] O. Bamigbetan, T.M. Eikevik, P. Neksa, M. Bantle, Review of vapour compression heat pumps for high temperature heating using natural working fluids, *Internat. J. Refrig.* 80 (2017) 197–211, <https://doi.org/10.1016/j.ijrefrig.2017.04.021>.
- [11] F. Illán-Gómez, V.F. Sena-Cuevas, J.R. García-Cascales, F.J.S. Velasco, Experimental and numerical study of a CO<sub>2</sub> water-to-water heat pump for hot water generation, *Int. J. Refrig.* 132 (2021) 30–44, <https://doi.org/10.1016/j.ijrefrig.2021.09.020>.
- [12] F. Illán-Gómez, V.F. Sena-Cuevas, J.R. García-Cascales, F.J.S. Velasco, Analysis of the optimal gas cooler pressure of a CO<sub>2</sub> heat pump with gas bypass for hot water generation, *Appl. Therm. Eng.* 182 (2021) 116110, <https://doi.org/10.1016/j.applthermaleng.2020.116110>.
- [13] Y. Song, F. Cao, The evaluation of optimal discharge pressure in a water-precooler-based transcritical CO<sub>2</sub> heat pump system, *App Therm Eng.* 131 (2018) 8–18, <https://doi.org/10.1016/j.applthermaleng.2017.11.092>.
- [14] E. Brodal, S. Jackson, A comparative study of CO<sub>2</sub> heat pump performance for combined space and hot water heating, *Internat. J. Refrig.* 108 (2019) 234–245, <https://doi.org/10.1016/j.ijrefrig.2019.08.019>.
- [15] J.-H. Cheng, Y.-J. He, C.-L. Zhang, New scenario of CO<sub>2</sub> heat pump for space heating: Automatic mode switch between modified transcritical and cascade cycle in one system, *Appl. Therm. Eng.* 191 (2021) 116864, <https://doi.org/10.1016/j.applthermaleng.2021.116864>.
- [16] B. Dai, H. Qi, W. Dou, S. Liu, S. Zhong, H. Yang, V. Nian, Y. Hao, Life cycle energy, emissions and cost evaluation of CO<sub>2</sub> air source heat pump system to replace traditional heating methods for residential heating in China: System configurations, *Energy Convers. Manage.* 218 (2020) 112954, <https://doi.org/10.1016/j.enconman.2020.112954>.
- [17] Z. Wang, F. Wang, Z. Ma, W. Lin, H. Ren, Investigation on the feasibility and performance of transcritical CO<sub>2</sub> heat pump integrated with thermal energy storage for space heating, *Renewable Energy* 134 (2019) 496–508, <https://doi.org/10.1016/j.renene.2018.11.035>.
- [18] Z. Wang, Y. Zheng, F. Wang, M. Song, Z. Ma, Study on performance evaluation of CO<sub>2</sub> heat pump system integrated with thermal energy, storage for space heating, *Energy Procedia* 158 (2019) 1380–1387, <https://doi.org/10.1016/j.egypro.2019.01.338>.
- [19] Nicholas Fernandez, Yunho Hwang, Reinhard Radermacher, Comparison of CO<sub>2</sub> heat pump water heater performance with baseline cycle and two high COP cycles, *Int. J. Refrig.* 33 (3) (2010) 635–644, <https://doi.org/10.1016/j.ijrefrig.2009.12.008>.
- [20] Sung Goo Kim, Yoon Jo Kim, Gilbong Lee, Min Soo Kim, The performance of a transcritical CO<sub>2</sub> cycle with an internal heat exchanger for hot water heating, *Int. J. Refrig.* 28 (7) (2005) 1064–1072, <https://doi.org/10.1016/j.ijrefrig.2005.03.004>.
- [21] Ryohei Yokoyama, Tetsuya Wakui, Junya Kamakari, Kazuhisa Takemura, Performance analysis of a CO<sub>2</sub> heat pump water heating system under a daily change in a standardized demand, *Energy* 35 (2) (2010) 718–728, <https://doi.org/10.1016/j.energy.2009.11.008>.
- [22] Bin Hu, Xiaolin Wang, Feng Cao, Zhilong He, Ziwen Xing, Experimental analysis of an air-source transcritical CO<sub>2</sub> heat pump water heater using the hot gas bypass defrosting method, *Appl. Therm. Eng.* 71 (1) (2014) 528–535, <https://doi.org/10.1016/j.applthermaleng.2014.07.017>.
- [23] I.J. Moncho-Estevé, M. Gasque, P. González-Altozano, G. Palau-Salvador, Simple inlet devices and their influence on thermal stratification in a hot water storage tank, *Energy Build.* 150 (2017) 625–638, <https://doi.org/10.1016/j.enbuild.2017.06.012>.
- [24] Zilong Wang, Hua Zhang, Binlin Dou, Huajie Huang, Weidong Wu, Zhiyun Wang, Experimental and numerical research of thermal stratification with a novel inlet in a dynamic hot water storage tank, *Renewable Energy* 111 111 (2017) 353–371, <https://doi.org/10.1016/j.renene.2017.04.007>.

- [25] L. Gao, H. Lu, B. Sun, D. Che, L. Dong, Numerical and experimental investigation on thermal stratification characteristics affected by the baffle plate in the thermal storage tank, *J. Energy Storage* (2021), <https://doi.org/10.1016/j.est.2020.102117> 102117.
- [26] Z. Wang, H. Zhang, H. Huang, B. Dou, X. Huang, M.A. Goula, The experimental investigation of the thermal stratification in a solar hot water tank, *Renewable Energy* 134 (2019) 862–874, <https://doi.org/10.1016/j.renene.2018.11.088>.
- [27] M. Esen, T. Ayhan, development of a model compatible with solar assisted cylindrical energy storage tank and variation of stored energy with time for different phase change materials, *Energy Convers. Mgmt* 37 (1996) 1775–1785.
- [28] Y.P. Chandra, T. Matuska, Numerical prediction of the stratification performance in domestic hot water storage tanks, *Renewable Energy* 154 (2020) 1165–1179, <https://doi.org/10.1016/j.renene.2020.03.090>.
- [29] Jørn Stene, Residential CO<sub>2</sub> heat pump system for combined space heating and hot water heating, *Int. J. Refrig* 28 (8) (2005) 1259–1265, <https://doi.org/10.1016/j.ijrefrig.2005.07.006>.
- [30] Jørn Stene, Residential CO<sub>2</sub> heat pump system for combined space heating and hot water heating. PhD Thesis.
- [31] G. Tosato, P. Artuso, S. Minetto, A. Rossetti, Y. Allouche, K. Banasiak, Experimental and numerical investigation of a transcritical CO<sub>2</sub> air/water reversible heat pump: analysis of domestic hot water production. 14th Gustav Lorentzen Conference, Kyoto, Japan, 6th–9th December 2020.
- [32] G. Tosato, S. Girotto, S. Minetto, A. Rossetti, S. Marinetti, An integrated CO<sub>2</sub> unit for heating, cooling and DHW installed in a hotel. Data from the field. 37th UIT Heat Transfer Conference. 2019. doi:10.1088/1742-6596/1599/1/012058.
- [33] F. Liu, W. Zhu, Y. Cai, E.A. Groll, J. Re, Y. Lei, Experimental performance study on a dual-mode CO<sub>2</sub> heat pump system with thermal storage, *Appl. Therm. Eng.* 115 (2017) 393–405, <https://doi.org/10.1016/j.applthermaleng.2016.12.095>.
- [34] I. Sifnaios, J. Fana, L. Olsenb, C. Madsenb, S. Furbo, Optimization of the coefficient of performance of a heat pump with an integrated storage tank, *Appl. Therm. Eng.* 160 (2019), <https://doi.org/10.1016/j.applthermaleng.2019.114014> 114014.
- [35] F. Aguilar, D. Crespi-Llorens, S. Aledo, P.V. Quiles, One-dimensional model of a compact DHW heat pump with experimental validation, *Energies* 14 (2021) 2991, <https://doi.org/10.3390/en14112991>.
- [36] European Committee for Standardization (ECS), EN 16147, heat pump with electrically driven compressor testing, performance rating and requirements for making of domestic hot water units. Spanish standard UNE- EN 16147. December 2017.
- [37] W. Li, P. Hrnjak, Experimentally validated model of heat pump water heater with a water tank in heating-up transients, *Int. J. Refrig* 88 (2018) 420–431, <https://doi.org/10.1016/j.ijrefrig.2018.01.020>.
- [38] National Instruments, Ni-Data Acquisition Ni-DAQ Specifications cDAQ™-9189, 2017.
- [39] Agilent Technologies, Agilent Datalogger. Agilent 34970A/34972A Data Acquisition / User's Guide, 2012.
- [40] I.S.O. Standard, Guide for Uncertainty Estimation In Measurements, International Standardisation Organization, Switzerland, 1999.
- [41] A. Karim, A. Burnett, S. Fawzia, Investigation of stratified thermal storage tank performance for heating and cooling applications, *Energies* 11 (2018) 1049, <https://doi.org/10.3390/en11051049>.
- [42] Joseph Rendall, Ahmad Abu-Heiba, Kyle Gluesenkamp, Kashif Nawaz, William Worek, Ahmed Elatar, Nondimensional convection numbers modeling thermally stratified storage tanks: Richardson's number and hot-water tanks, *Renew. Sustain. Energy Rev.* 150 (2021) 111471, <https://doi.org/10.1016/j.rser.2021.111471>.

# FE DE ERRATAS

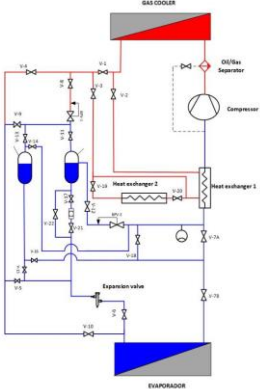
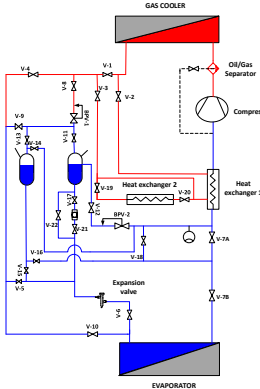
Tesis doctoral:

Caracterización experimental y modelado numérico de una instalación para la generación de ACS con bomba de calor.

PhD Thesis:

Experimental characterization and numerical modelling of an installation for the generation of domestic hot water with heat pump.

Presented by Mohammed Reda Haddouche.

Reference	Origin	Replaced by
Page v, line 3 (Resumen)	Se desarrollado una instalación experimental	Se ha desarrollado una instalación experimental
Page 27, §1, line 6	production has seen an great development	production has seen a great development
Page 31, §4, line 2	it consists in forming of horizontal layers at different temperature such way that	it consists of forming of horizontal layers at different temperatures, in such way that
Page 46, §2, line 3	and it injects the water entering the tank in the layer temperature closest and slowest rate possible	and it injects the water entering the tank in the layer temperature closest and at the slowest flowrate possible
Page 51, §2, line 4	A test series are carried out to investigate the thermodynamic performance	Series of tests are carried out to investigate the thermodynamic performance
Page 52, §3, line 1	As indicated during these tests the facility is prepared for the following steps	As indicated above, these steps are the preparation of the following steps
Page 56	Evaporador 	Evaporator 
Page 62, §1, line 4	Another Baxi Quantum Eco1025 (figure II.9.b) water pumps is a small pump	Another Baxi Quantum Eco1025 (figure II.9.b) water pump is a small pump used for



	used <b>in</b> the recirculation of the cold-water storage tank in order to maintain it at the initial <b>temperatures</b>	the recirculation of the cold-water storage tank in order to maintain it at the initial <b>temperature</b>
Page 64, §1, line 2	The main objective of this valve is open or close to increase or decrease the flow rate at demand.	The main objective of this valve is <b>to</b> open or close <b>in order to</b> increase or decrease the flow rate at demand.
Page 67, §3	<b>The three ways-valve</b> connects <b>between</b> the refrigerator tank and the cold-water storage tank. The RTD sensor measures the temperature of the tank and <b>send a control signal</b> by mean of a control card in order to open the loop or close the loop and <b>recirculate</b> the water in the tank	The <b>three-ways valve</b> connects the refrigerator tank and the cold-water storage tank. The RTD sensor measures the temperature of the tank, and <b>a control signal is sent</b> by mean of a control card in order to open the loop or close the loop and <b>recirculates</b> the water in the tank
Page 70, §1, line 1	<del>In</del> the figure II.22 bellow shows the Data acquisition's LabView program of the temperatures using the DAQ Assistance tool.	The figure II.22 bellow shows the Data acquisition's LabView program of the temperatures using the DAQ Assistance tool.
Page 74, §1, line 7	Once this condition <b>reaches</b> , the water heating step begins	Once this condition <b>is reached</b> , the water heating step begins
Page 74, §3, line 2	For this a sub program (figure II.28) shows the LabView [64] program that controls the temperature of the hot water tank with an <b>indirect—manner</b> . Actually, the <b>temperat64ure</b> of this tank is controlled by means of the highest sensor in the tank	For this, a sub program <b>is used</b> . figure II.28 shows the LabView [64] program that controls the temperature of the hot water tank with. Actually, the <b>temperature</b> of this tank is controlled by means of the highest sensor in the tank
Page 76, §3, line 3	<b>Figure II.230</b> illustrates this process	<b>Figure II.30</b> illustrates this process
Page 77, §1, line 4	and the valves of the tank <b>to close</b> .	and <b>to close</b> the valves of the tank.
Page 80, §4, line 2	at this temperature during <b>all the step periods</b> .	at this temperature during the <b>step</b> .
Page 87, figure III.1	Condenser	Gas cooler
Page 104, figure III.13	The legend colors are upside down ( <b>red for the highest gas cooler flowrate</b> )	The legend colors are upside down ( <b>red for the lowest gas cooler flowrate</b> )
Page 104, §1, line 3	gas cooler <b>mas</b> flow rates	gas cooler <b>mass</b> flow rates
Page 111, §1, line 2	which <b>make</b> the upper part	which <b>makes</b> the upper part

Page 115, §1, line 1	To clarify <del>and</del> —the stratification	To clarify the stratification
Page 118, §1, line 1	To <b>analyses</b> the impact	To <b>analyze</b> the impact
Page 118, §1, line 4	<b>gas</b> flowrate = 0.305 kg·s-1)	<b>Gas cooler</b> flowrate = 0.305 kg·s-1)
Page 124, §1, line 5	and this due to the volume of the cold water entering to the hot water storage tank and also due to the stratification phenomenon	and this <b>is</b> due to the volume of the cold water entering to the hot water storage tank and <b>is</b> also due to the stratification phenomenon
Page 133, §1, line 2	it consists <b>in forming</b> of horizontal layers at different temperatures in such <del>a</del> -way	it consists <b>of the formation</b> of horizontal layers at different temperatures in such way
Page 133, §2, line 3	The form and the disposition are also <b>an important parameter</b> that should be taken in consideration.	The form and the disposition are also <b>important parameters</b> that should be taken in consideration.
Page 147, §1, line 1	On the other hand, in the case of <b>lower flowrates</b> (0.083 kg·s-1)	On the other hand, in the case of <b>the lowest flowrate</b> (0.083 kg·s-1)